

SCHOLARLY PUBLICATIONS

*A CURRENT AWARENESS BULLETIN
OF RESEARCH OUTPUT*

@DTU

(38th Edition)

FEBRUARY 2016

BY: CENTRAL LIBRARY

DELHI TECHNOLOGICAL UNIVERSITY

(FORMERLY *DELHI COLLEGE OF ENGINEERING*)

GOVT. OF N.C.T. OF DELHI

SHAHBAD DAULATPUR, MAIN BAWANA ROAD

DELHI 110042

PREFACE

This is the **Thirty Eight** Issue of Current Awareness Bulletin started by Delhi Technological University, Central Library. The aim of the bulletin is to compile, preserve and disseminate information published by the faculty, students and alumni for mutual benefits. The bulletin also aims to propagate the intellectual contribution of Delhi Technological University (DTU) as a whole to the academia.

The bulletin contains information resources available in the internet in the form of articles, reports, presentations published in international journals, websites, etc. by the faculty and students of DTU. The publications of faculty and student which are not covered in this bulletin may be because of the reason that the full text either was not accessible or could not be searched by the search engine used by the library for this purpose.

The learned faculty and students are requested to provide their uncovered publications to the library either through email or in CD, etc to make the bulletin more comprehensive.

This issue contains the information published during **February 2016**. The arrangement of the contents is alphabetical. The full text of the article which is either subscribed by the university or available in the web is provided in this bulletin.

Central Library

PREFACE

1. A computational pipeline for the prediction of genes associated with age related disorders, **6.Isha Srivastava**, **6.Lokesh Kumar Gahlot**, **6.Pooja Khurana** and **3.Yasha Hasija**, Biotechnology, DTU
2. An Experimental Appraisal on the Efficacy of MWCNT-H₂O Nanofluid on the Performance of Solar Parabolic Trough Collector, **3.Harwinder Singh** and **3.Pushpendra Singh**, Mechanical, Production and Industrial Engineering, DTU
3. Bus Implementation using New Low Power PFSCl Tri-state buffers, **3.Neeta Pandey** and **3.Bharat Choudhry**, Kirti Gupta, Ankit Mital, Electronics and Communication Engineering, DTU
4. Comparative study of thermal stability of filled and un-filled multiwalled carbon nanotubes, **6.Lucky Krishnia**, **6.Reetu Kumari**, **6.Vinay Kumar**, **6.Anshika Singh**, Preeti Garg, Brajesh S. Yadav and **3.Pawan K. Tyagi**, Applied Physics, DTU
5. Database Performance Analyser S/W Test Tool, **3.Dr. Ruchika Malhotra** and **3.Ashish Gupta**, CS, DTU
6. Effects of Sex Appeal in Advertisements on Consumer Buying Behavior in India, **3.Chhavi**, **3.Syed Fazal Karim** and **3.Vipul Jain**, DSM, DTU
7. Electrospun Functional Micro/Nanochannels Embedded in Porous Carbon Electrodes for Microfluidic Biosensing, Kunal Mondal, Azahar Ali, **3.Saurabh Srivastava**, **3.Bansi D. Malhotra**, Ashutosh Sharma, Biotechnology, DTU
8. Environmental Concerns in National Capital Territory of Delhi, India, **3.Shashank Shekhar Singh**, **3.SK Singh** and **3.Shuchita Garg**, Environmental Engineering DTU

9. Gene Prioritization by integrated analysis of protein structural and network topological properties for the protein-protein interaction network of neurological disorders, **3.Yashna Paul** & **3.Yasha Hasija**, Biotechnology, DTU
10. Hybrid Dynamic MCML Style: A High Speed Dynamic MCML Style, **3.Neeta Pandey**, **3.Damini Garg**, Kirti Gupta & **3.Bharat Choudhary**, ECE, DTU
11. IMPACT OF PROMOTIONAL TOOLS ON STUDENTS DECISION-MAKING: STUDY OF PRIVATE ENGINEERING INSTITUTIONS IN DELHI NCR, **6.Antra Singh** & **3.Seema Singh**, Humanities, DTU
12. Mathematical modeling insight of hetero gate dielectric- dual material gate- GAA- tunnel FET for VLSI/analog applications, **3.Jaya Madan**, R. S. Gupta and **3.Rishu Chaujar**, Physics, DTU
13. Mechanical and Thermal Properties of Castor Oil–Based Polyurethane Adhesive: Effect of TiO₂ Filler, **3.Manjeet Malik** and **3.Raminder Kaur**, Polymer Science and Chemical Technology, DTU
14. Mitigating Credit Risk: An Empirical Study Of Indian Public Sector Banks, Renu Arora & **3.Archana Singh**, DSM, DTU
15. Performance Evaluation of Data Mining Techniques for Predicting Software Reliability, **7.1.Pradeep Kumar** & Abdul Wahid, Computer Technology and Applications, DTU
16. Photovoltaic effect in BiFeO₃/BaTiO₃ multilayer structure fabricated by chemical solution deposition technique, **3.Savita Sharma**, Monika Tomar, Ashok Kumar, **3.Nitin K. Puri** & Vinay Gupta, Applied Physics, DTU
17. Quantum dot monolayer for surface Plasmon resonance signal enhancement and DNA hybridization detection, Aditya Sharma Ghrera, Manoj Kumar Pandey & **3.Bansi Dhar Malhotra**, Biotechnology, DTU

18. Rectification of Corrupted Neural Networks, **3.Prakhar Dogra**, Computer Science and Engineering, DTU
19. The Design Of a High Speed Nonlinear Feedback Based Current Comparartor, Veepsa Bhatia, **3.Neeta Pandey, 3.Ranjana Shridhar & 3.Asok Bhattachary**, Electronics and Communication, DTU

1. Vice Chancellor

2. Pro Vice Chancellor

3. Faculty

4. Teaching-cum-Research Fellow

5. Alumni

6. Research Scholar

7. PG Scholar

8. Undergraduate Student

1.1. Ex Vice Chancellor

2.1. Ex Pro Vice Chancellor

3.1. Ex Faculty

6.1. Ex Research Scholar

7.1. Ex PG Scholar

8.1. Ex Undergraduate Student



Contents lists available at ScienceDirect

Journal of Biomedical Informatics

journal homepage: www.elsevier.com/locate/yjbini



dbAARD & AGP: A computational pipeline for the prediction of genes associated with age related disorders

Isha Srivastava, Lokesh Kumar Gahlot, Pooja Khurana, Yasha Hasija *

Department of Biotechnology, Delhi Technological University, Delhi 110042, India

ARTICLE INFO

Article history:

Received 9 March 2015
Revised 11 November 2015
Accepted 12 January 2016
Available online xxxxx

Keywords:

Genome-Wide Association Studies
Age-related disorders
Single nucleotide polymorphisms
Machine learning

ABSTRACT

The atrocious behavioral and physiological shift with aging accelerate occurrence of deleterious disorders. Contemporary research is focused at uncovering the role of genetic associations in age-related disorders (ARDs). While the completion of the Human Genome Project and the HapMap project has generated huge amount of data on genetic variations; Genome-Wide Association Studies (GWAS) have identified genetic variations, essentially SNPs associated with several disorders including ARDs. However, a repository that houses all such ARD associations is lacking. The present work is aimed at filling this void. A database, dbAARD (database of Aging and Age Related Disorders) has been developed which hosts information on more than 3000 genetic variations significantly (p -value < 0.05) associated with 51 ARDs. Furthermore, a machine learning based gene prediction tool AGP (Age Related Disorders Gene Prediction) has been constructed by employing rotation forest algorithm, to prioritize genes associated with ARDs. The tool achieved an overall accuracy in terms of precision 75%, recall 76%, F -measure 76% and AUC 0.85. Both the web resources have been made available online at <http://genomeinformatics.dce.edu/dbAARD/> and <http://genomeinformatics.dce.edu/AGP/> respectively for easy retrieval and usage by the scientific community. We believe that this work may facilitate the analysis of plethora of variants associated with ARDs and provide cues for deciphering the biology of aging.

© 2016 Elsevier Inc. All rights reserved.

1. Introduction

Aging is an inevitable biological phenomenon. The quality of life in old age is usually far worse than in youth, since the elderly often suffer from various age-related disorders (ARDs), like Arteriosclerosis, Diabetes, Dementia, Osteoporosis, Osteoarthritis and Cancer [1]. For those who escape the disease, the cause of death may be traced to subtle tissue atrophies, neuropathies or microvascular leakage [2]. The focus of present day research has shifted from trying to delay aging or achieving immortality, to achieving healthy or successful aging. The inclusions of healthy aging are low probability of disease or disability, high cognitive and physical function capacity and active engagement with life [3].

Research on centenarians has been underway for many years to find out the biological, sociological and psychological factors they possess that enable them to survive longer [4]. Current research on finding out the metabolic signature of extreme longevity centenarians has explored many unresolved factors behind their extreme longevity [5]. A person's genetic make-up plays a crucial

role in the process of aging and determines how successfully an individual reaches old age. However, the role of genetics in aging and longevity is complex.

Several public domain databases like HGMD [6], NHGRI GWAS catalog [7], SNPedia [8], dbGaP [9] and GWAS Central [10] contain information on phenotype associated mutations. In addition to these, locus specific databases focused on a single disease also exist. The AlzGene database for Alzheimer's [11] and the SzGene database for Schizophrenia [12] are collections of GWAS results on these two disorders. However, there is no dedicated database that houses information on all ARDs.

A need was therefore felt for a database to store genetic information on all ARDs. A Graphical User Interface (GUI) has been developed to enable experimental biologists to easily query the database for relevant information. The data collected has been subjected to machine learning analysis. The classifier predicts putative genes involved in age related disorders from all the proteins present in UniProt [13].

2. dbAARD

dbAARD is a manually curated database aimed at providing a freely accessible interactive database of the relationships of human

* Corresponding author at: Department of Biotechnology, Delhi Technological University, Shahbad Daulatpur, Main Bawana Road, Delhi 110042, India.
E-mail address: yashahasija@gmail.com (Y. Hasija).

single nucleotide polymorphisms (SNPs) and age-related disorders along with the supporting evidence. By doing so, dbAARD hopes to facilitate access to and analysis of the relationships asserted between human variation and observed disease conditions. dbAARD collects disease-SNP associations as well as their significance scores in the form of *p*-value and odds ratio.

2.1. Construction and content of dbAARD

The primary data in the dbAARD represents association of SNP with various ARDs. All the complex genetic disorders that are believed to be prevalent in old age have been considered as ARDs for the purpose of this work. The information on ARDs was obtained from the articles published in high-quality journals and various online medical forums discussing aging and associated diseases. All the compiled ARDs were then classified using the classification scheme proposed by Goh et al. for constructing the diseasome [14]. Table 1 lists all the ARDs included in dbAARD along with the supporting evidences [15–24]. The details on these ARDs can be found in our recently accepted review article [25].

The disease-SNP associations for these ARDs were manually curated from the relevant articles published in PubMed extracted using the keywords such as “Disorder name AND Gene AND SNP” or “Disorder name AND SNP” or “Disorder name AND Polymorphisms” and existing databases such as UniProt Humsavar [26], HGMD [6], NHGRI GWAS catalogue [7], SNPedia [8], OMIM [27], and dbGaP [9]. The last access date for these databases is provided in Table 2. The data from the existing databases was carefully assessed and corrected with reference to the original articles. All SNP-disease associations which reached statistical significance ($p < 0.05$) were mined and included in dbAARD. A data model was then created using the free open-source version of the MySQL Workbench to minimize redundancy.

Each entry in dbAARD contains the information on SNP, the associated disease, *p*-value assigned to the association, the odd ratio of the disease-SNP association and the literature reference. It also contains information on ethnicity which describes the ethnic group on which the study was carried out, geographical location in which the study was conducted and if large number of countries were involved in the study then the location has been considered as Mixed. Further, information about gene, chromosome, type of SNP, location of SNP on gene (such as exon, intron, intergenic and untranslated region), reference/mutant nucleotide and amino acid and protein change location has also been included.

2.2. User interface

dbAARD provides a user-friendly interface to query detailed information on each SNP-disease association (Fig. 1A). Users can query the database through disease class, disease, genes or SNP IDs. These categories that can be used to filter the records have been listed in Table 3. Further, dbAARD interface allows for the selection of the attributes, so that only the desired information on SNP-disease association can be viewed without cluttering the screen with data of least importance for the user.

3. Age-Related Disorders Gene Prediction (AGP) tool

The identification of the genetic markers/causative genes have been of paramount importance in the biomedical research as many medical conditions are influenced by human genetic variations. However, the traditional methods of finding genes are time-consuming, expensive and often suffer from the limitation of variable disease penetrance. With lot of data already available in the

Table 1

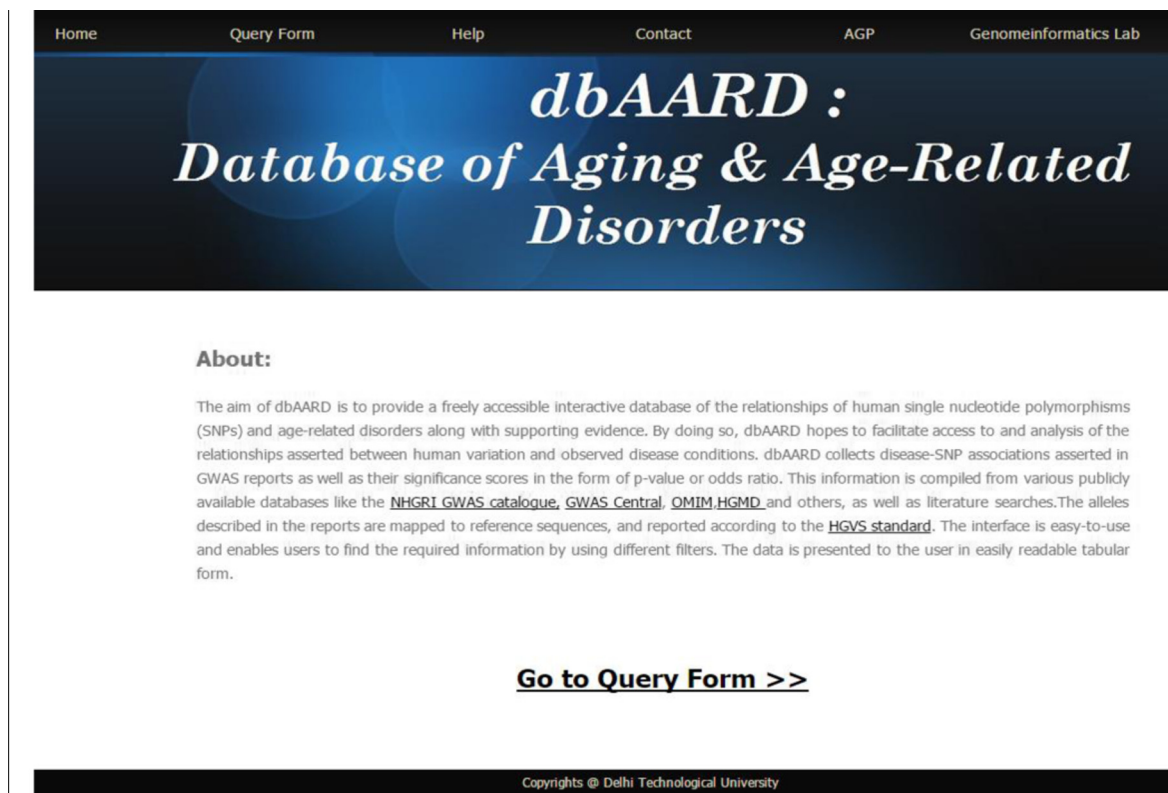
Age-related disorders (ARDs) included in dbAARD.

Disease	Disease class	References
Age-related macular degeneration	Ophthalmological	[15]
Alzheimer's disease	Neurological	[15]
Amyotrophic lateral sclerosis	Neurological	[16]
Atrial fibrillation	Cardiovascular	[15]
Basal cell carcinoma	Cancer	[15]
Bladder cancer	Cancer	[15]
Gastric ulcer	Gastrointestinal	[15]
Breast cancer	Cancer	[15]
Cardiac arrhythmia	Cardiovascular	[15]
Cardiomyopathy	Cardiovascular	[16]
Chronic obstructive pulmonary disease	Pulmonary Disorder	[15]
Colorectal Cancer	Cancer	[15]
Coronary artery disease	Cardiovascular	[15]
Crohn's disease (late-onset)	Gastrointestinal	[17]
Deafness	ENT	[15]
Decreased bone mineral density	Bone	[15]
Dementia	Neurological	[15]
Diabetic retinopathy	Metabolic	[15]
Gastrointestinal cancer	Cancer	[15]
Gaucher disease	Lysosomal storage	[18–20]
Glaucoma	Ophthalmological	[15]
Gout	Bone	[15]
Graves' disease	Metabolic	[15]
Hearing loss	ENT	[15]
Hypercholesterolemia	Metabolic	[16]
Hyperlipidemia	Metabolic	[16]
Hypertension	Cardiovascular	[15]
Insulin resistance	Metabolic	[15]
Lung cancer	Cancer	[15]
Melanoma	Cancer	[15]
Multiple sclerosis	Neurological	[15]
Myocardial infarction	Cardiovascular	[15]
Myopia	Ophthalmological	[15]
Obesity	Metabolic	[15]
Obstructive sleep apnea	Neurological	[15]
Osteoarthritis	Bone	[15]
Osteoporosis	Bone	[15]
Ovarian Cancer	Cancer	[15]
Paget	Bone	[15]
Pancreatic cancer	Cancer	[15]
Parkinson's disease	Neurological	[15]
Presbycusis	ENT	[15]
Prostate Cancer	Cancer	[15]
Pulmonary fibrosis	Pulmonary Disorder	[21]
Restless legs syndrome	Neurological	[15]
Rheumatoid arthritis	Bone	[15]
Schizophrenia (late-onset)	Psychiatric	[22–24]
Stroke	Cardiovascular	[15]
Systemic Lupus Erythematosus	Immunological	[15]
Type-2 Diabetes Mellitus	Metabolic	[15]
Uric acid concentration	Metabolic	[15]

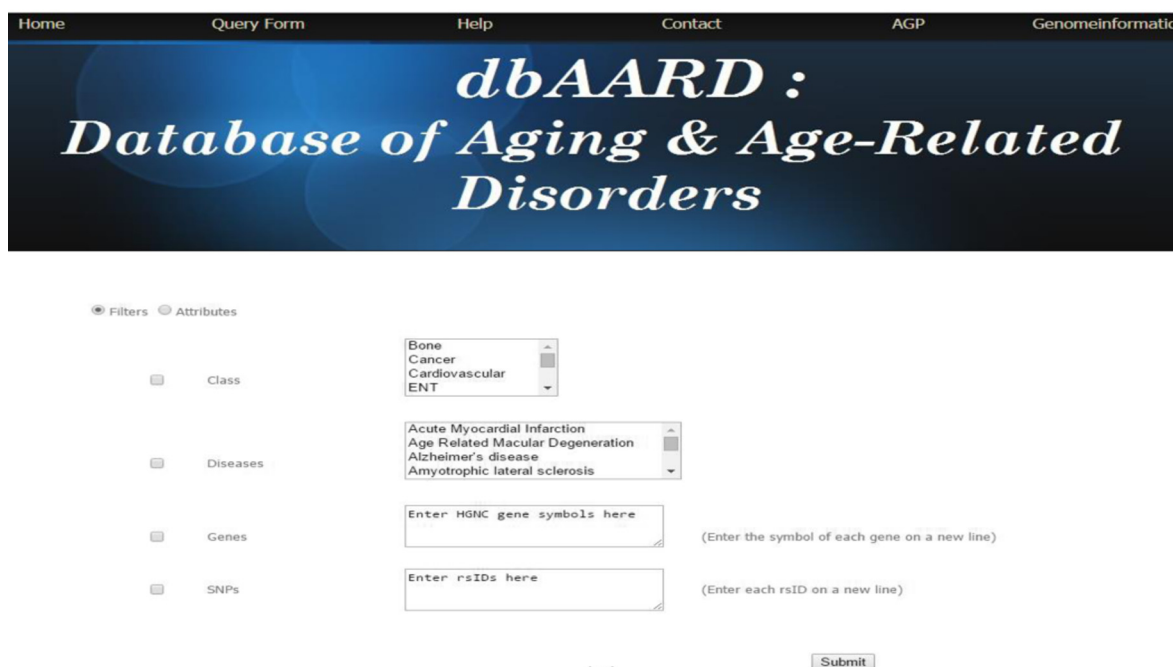
Table 2

Data resources for dbAARD database.

Source	Link	Version/Last Date Accessed
HGMD	http://www.hgmd.cf.ac.uk/ac/index.php	2014.2
OMIM	http://www.ncbi.nlm.nih.gov/omim	Last Accessed in Sep 2014
dbGaP	http://www.ncbi.nlm.nih.gov/gap	Jan 2013
SNPedia	http://www.snpedia.com/index.php/SNPedia	June 2014
NHGRI GWAS central	http://www.genome.gov/gwastudies/	Sep 2014
PubMed	http://www.ncbi.nlm.nih.gov/pubmed	Sep 2014
Uniprot Humsavar	http://www.uniprot.org/docs/humsavar	Sep 2014



(I)



(II)

Fig. 1A. Overview of dbAARD web interface. An example: (I) A screenshot of home page of dbAARD. (II) The query page of dbAARD representing the filters – Class, Disease, Genes and SNPs. (III) The attribute page containing attributes such as Ethnicity, Geographical location, P-Value, Odd Ratio, Chromosome, Variant DNA, Variant RNA, Variant Protein, Types of SNPs, Location of SNPs, Nucleotide/codon change, Amino Acid change, Variant no. (IV) Output page.

databases, computational approaches can thus be exploited to integrate information from these resources and reliably predict disease-genes associations which are yet unknown. Predicting

disease gene is typically a classification problem of distinguishing real disease genes from spurious non-disease genes. Machine learning techniques, have thus been exploited to solve the disease

HomeQuery FormHelpContactAGPGenomeinformatics Lab

dbAARD :
Database of Aging & Age-Related Disorders

FiltersAttributes

EthnicityGeographical Location

p-valueOdds-Ratio

ChromosomeVariantDNAVariantRNAvariantprotein

Type of SNPLocation of SNP

Nucleotide/Codon changeAmino Acid changevariantno.(codonno.)

Submit

(III)

HomeQuery FormHelpContactAGPGenomeinformatics Lab

dbAARD :
Database of Aging & Age-Related Disorders

Result:

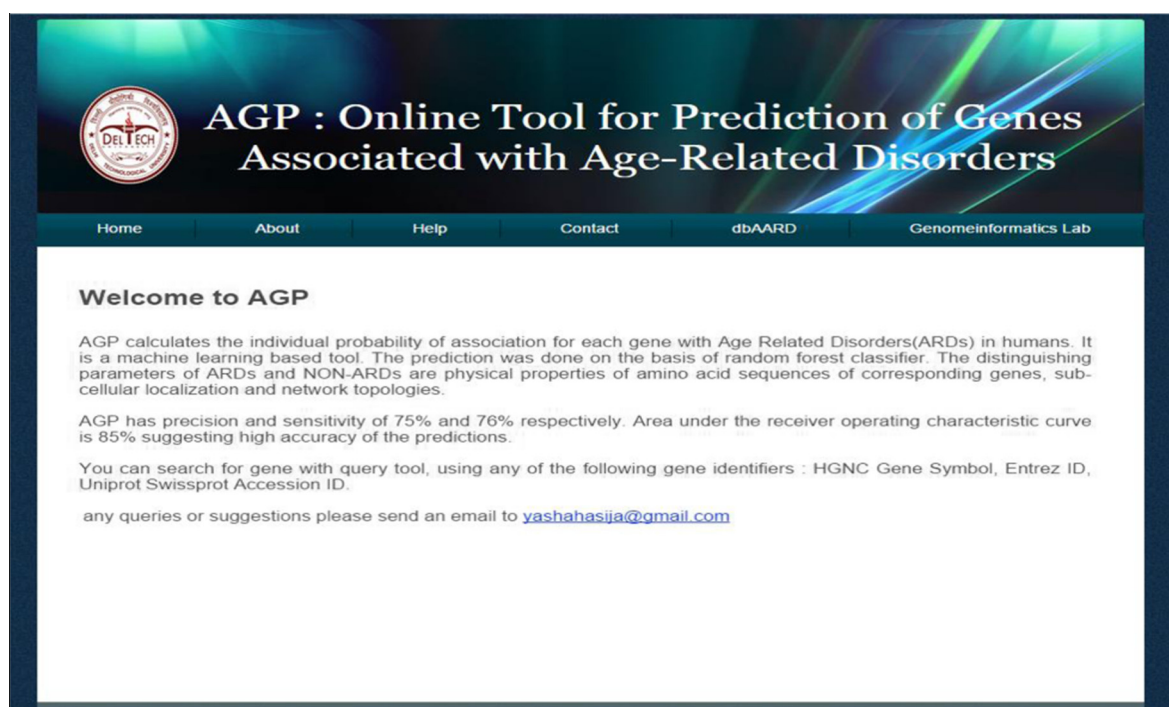
Class	Disease	Gene	RSID	PMID
Cancer	Colon Cancer	This SNP is present in intergenic region of gene	rs10808555	22142333
Cancer	Colon Cancer	This SNP is present in intergenic region of gene	rs17464492	22142333
Cancer	Colon Cancer	This SNP is present in intergenic region of gene	rs2163951	22142333
Cancer	Colon Cancer	This SNP is present in intergenic region of gene	rs6470494	22142333
Cancer	Colon Cancer	This SNP is present in intergenic region of gene	rs6983267	22142333
Cancer	Colon Cancer	This SNP is present in intergenic region of gene	rs7014346	22142333
Cancer	Colon Cancer	This SNP is present in intergenic region of gene	rs7837328	22142333
Cancer	Colon cancer	pml4	rs743582	19728758
Cancer	Colon cancer	serca2b	rs183641769	17116488
Cancer	Colon cancer	GALNT12	rs149726976	19617566
Cancer	Colon cancer	GALNT12	rs267606839	19617566
Cancer	Colon cancer	GALNT12	rs267606840	19617566
Cancer	Colon cancer	MSH3	rs1650697	10944853
Cancer	Colon cancer	PIK3R1	rs3730089	18245521

(IV)

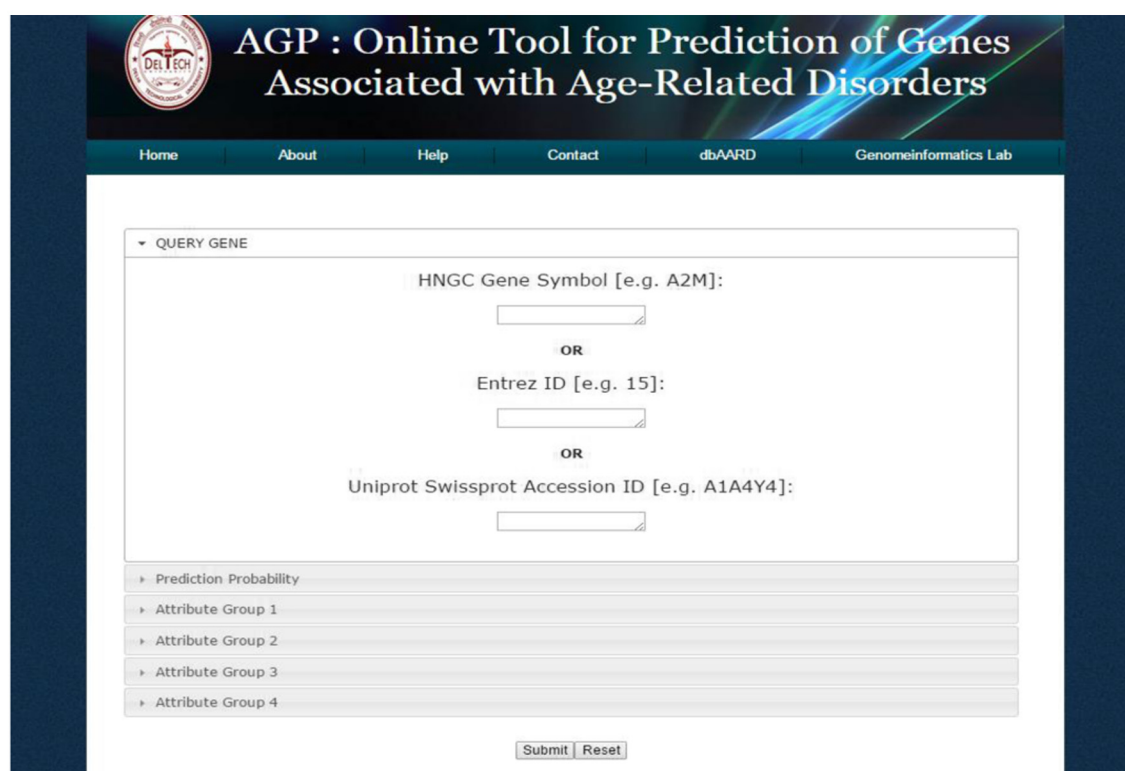
Fig. 1A (continued)

gene classification problem using the confirmed diseases genes as the positive training samples [28–31].
In the network analysis of genes associated with ARDs [25], Srivastava et al. have shown that several genes associated with ARDs are highly interconnected. Similarly, Johnson et al. demonstrated that there are substantial number of GO terms are shared among different age-related diseases classes [34]. Based on the observation that genes associated with similar diseases tend to show

Please cite this article in press as: I. Srivastava et al., dbAARD & AGP: A computational pipeline for the prediction of genes associated with age related disorders, J Biomed Inform (2016), <http://dx.doi.org/10.1016/j.jbi.2016.01.004>

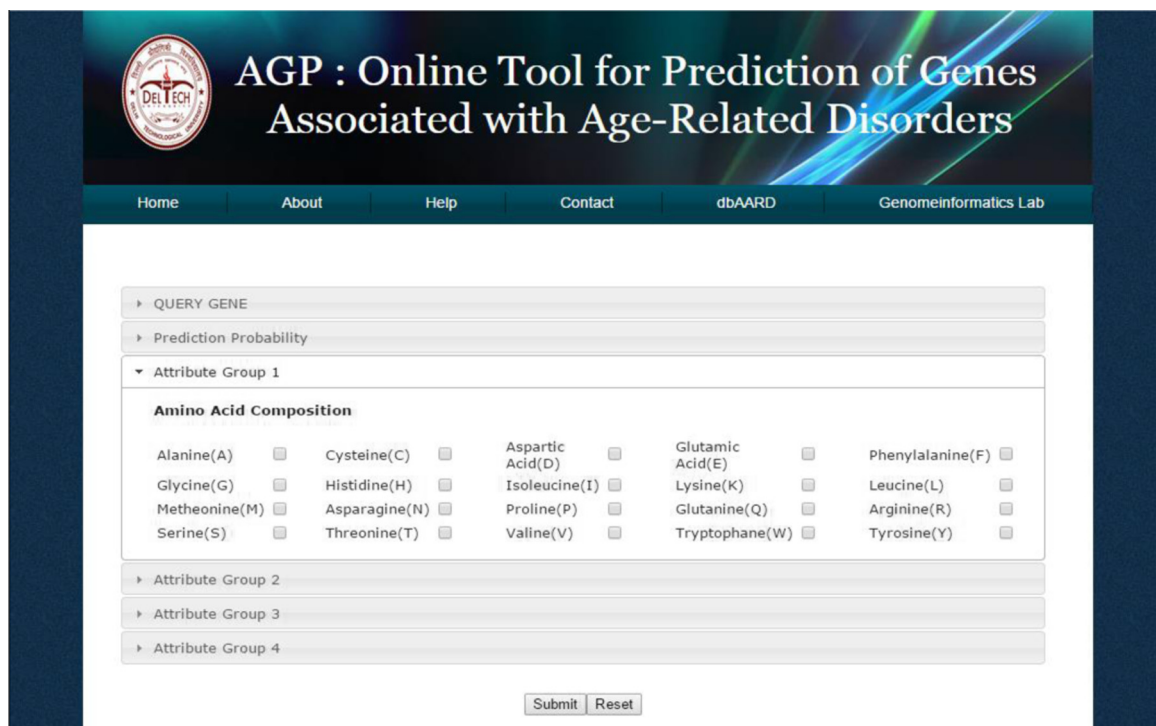


(I)



(II)

Fig. 1B. An overview of AGP web interface: An example: (I) a screenshot of home page of AGP. (II) Query page: input required are HGNC Symbol, entrez ID or uniprot/swissprot accession ID. (III) Attribute group 1: Amino Acid Composition of proteins. (IV) Attribute group 2: Physiochemical properties of proteins. (V) Attribute group 3: Subcellular localization of proteins. (VI) Attribute group 4: Network properties of amino acids. (VII) Output page.



AGP : Online Tool for Prediction of Genes Associated with Age-Related Disorders

Home About Help Contact dbAARD Genomeinformatics Lab

QUERY GENE

Prediction Probability

Attribute Group 1

Amino Acid Composition

Alanine(A) <input type="checkbox"/>	Cysteine(C) <input type="checkbox"/>	Aspartic Acid(D) <input type="checkbox"/>	Glutamic Acid(E) <input type="checkbox"/>	Phenylalanine(F) <input type="checkbox"/>
Glycine(G) <input type="checkbox"/>	Histidine(H) <input type="checkbox"/>	Isoleucine(I) <input type="checkbox"/>	Lysine(K) <input type="checkbox"/>	Leucine(L) <input type="checkbox"/>
Methionine(M) <input type="checkbox"/>	Asparagine(N) <input type="checkbox"/>	Proline(P) <input type="checkbox"/>	Glutamine(Q) <input type="checkbox"/>	Arginine(R) <input type="checkbox"/>
Serine(S) <input type="checkbox"/>	Threonine(T) <input type="checkbox"/>	Valine(V) <input type="checkbox"/>	Tryptophane(W) <input type="checkbox"/>	Tyrosine(Y) <input type="checkbox"/>

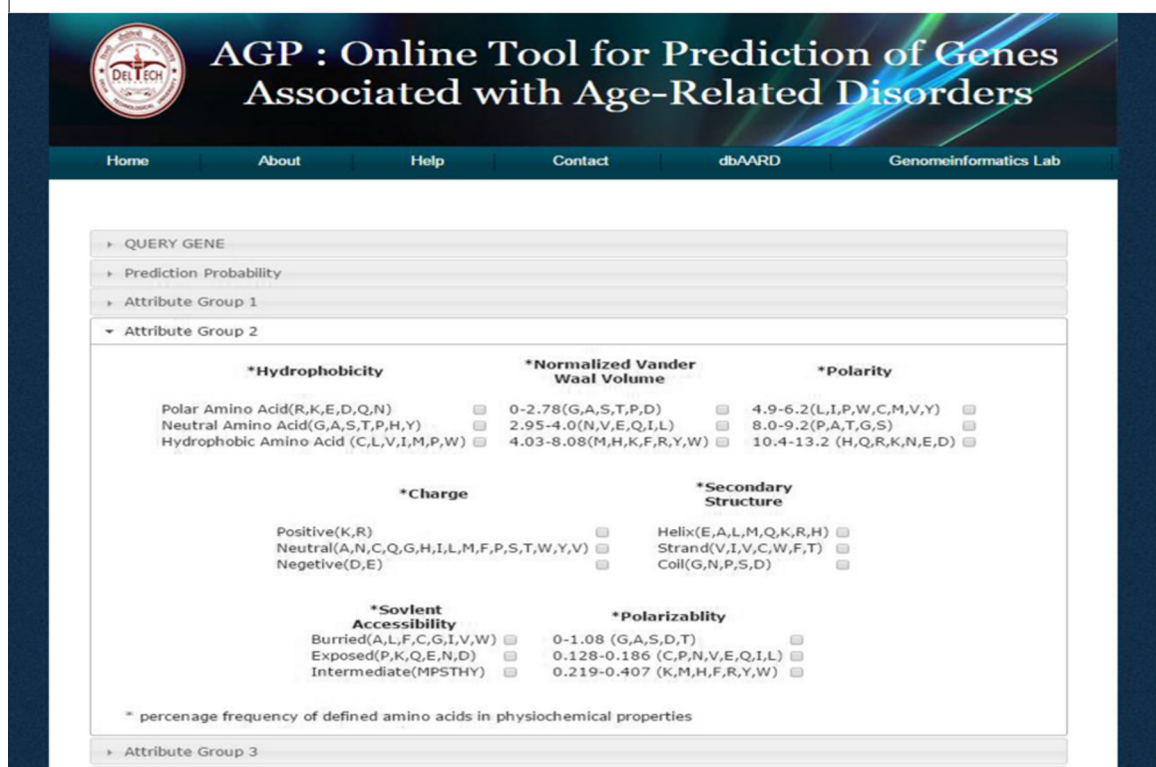
Attribute Group 2

Attribute Group 3

Attribute Group 4

Submit Reset

(III)



AGP : Online Tool for Prediction of Genes Associated with Age-Related Disorders

Home About Help Contact dbAARD Genomeinformatics Lab

QUERY GENE

Prediction Probability

Attribute Group 1

Attribute Group 2

*Hydrophobicity	*Normalized Vander Waal Volume	*Polarity
Polar Amino Acid(R,K,E,D,Q,N) <input type="checkbox"/>	0-2.78(G,A,S,T,P,D) <input type="checkbox"/>	4.9-6.2(L,I,P,W,C,M,V,Y) <input type="checkbox"/>
Neutral Amino Acid(G,A,S,T,P,H,Y) <input type="checkbox"/>	2.95-4.0(N,V,E,Q,I,L) <input type="checkbox"/>	8.0-9.2(P,A,T,G,S) <input type="checkbox"/>
Hydrophobic Amino Acid(C,L,V,I,M,P,W) <input type="checkbox"/>	4.03-8.08(M,H,K,F,R,Y,W) <input type="checkbox"/>	10.4-13.2(H,Q,R,K,N,E,D) <input type="checkbox"/>

*Charge	*Secondary Structure
Positive(K,R) <input type="checkbox"/>	Helix(E,A,L,M,Q,K,R,H) <input type="checkbox"/>
Neutral(A,N,C,Q,G,H,I,L,M,F,P,S,T,W,Y,V) <input type="checkbox"/>	Strand(V,I,V,C,W,F,T) <input type="checkbox"/>
Negative(D,E) <input type="checkbox"/>	Coil(G,N,P,S,D) <input type="checkbox"/>

*Solvent Accessibility	*Polarizability
Buried(A,L,F,C,G,I,V,W) <input type="checkbox"/>	0-1.08(G,A,S,D,T) <input type="checkbox"/>
Exposed(P,K,Q,E,N,D) <input type="checkbox"/>	0.128-0.186(C,P,N,V,E,Q,I,L) <input type="checkbox"/>
Intermediate(MPSTHY) <input type="checkbox"/>	0.219-0.407(K,M,H,F,R,Y,W) <input type="checkbox"/>

* percentage frequency of defined amino acids in physiochemical properties

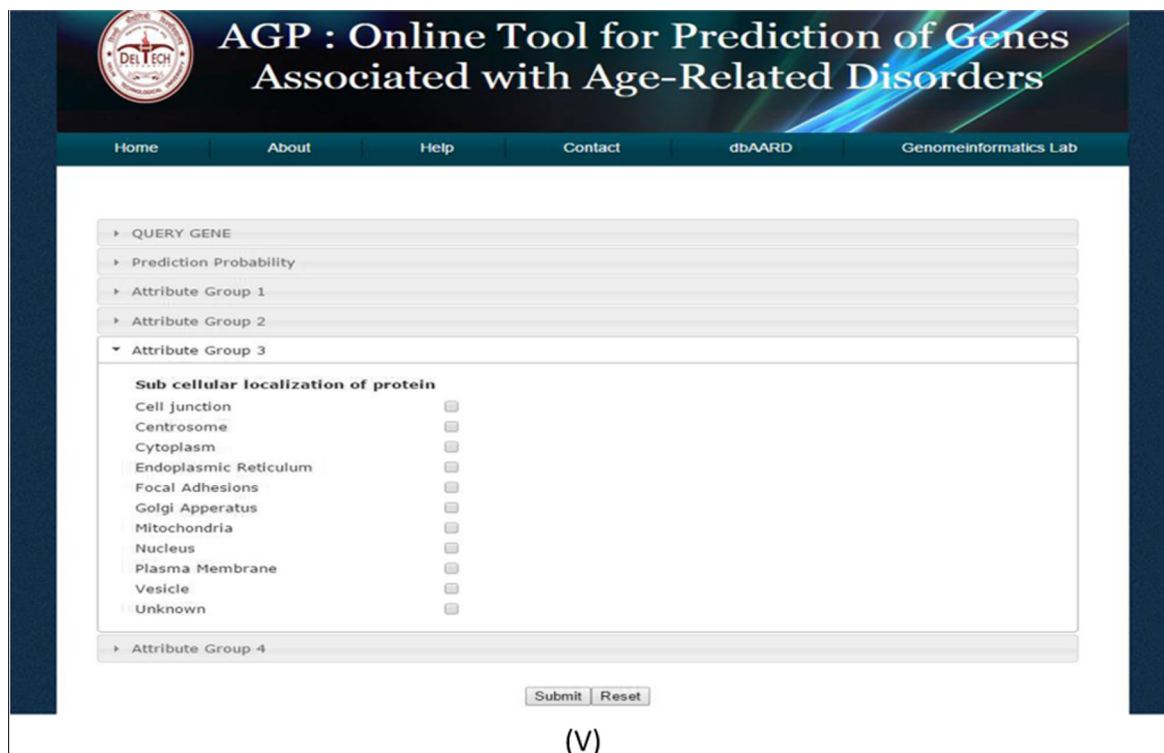
Attribute Group 3

(IV)

Fig. 1B (continued)

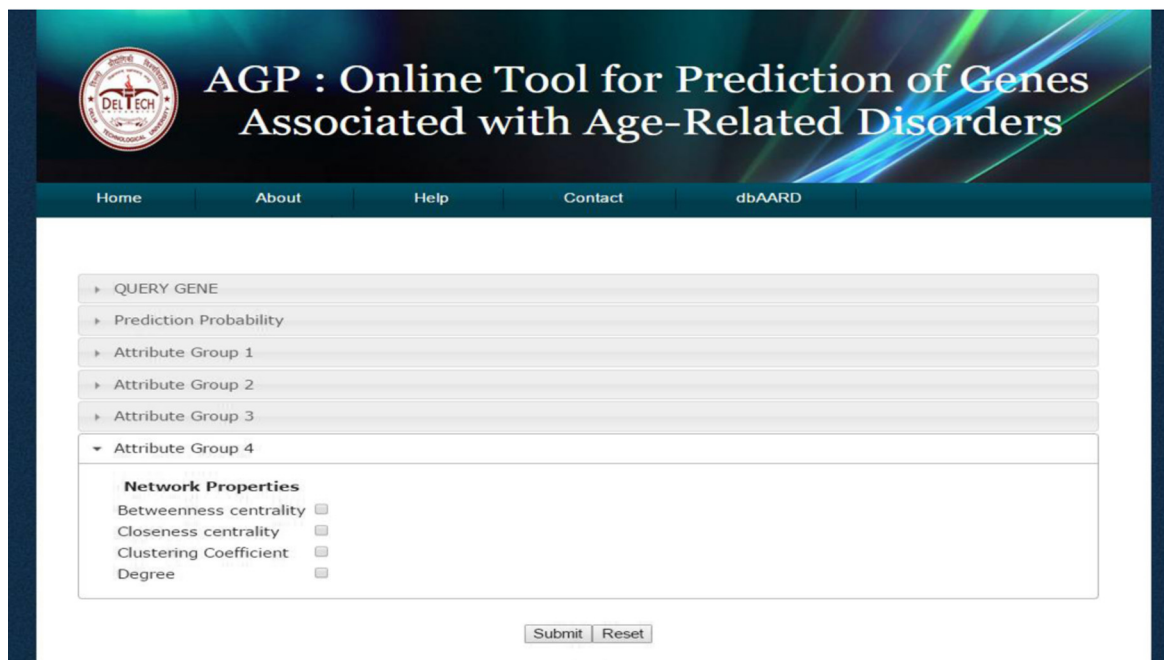
similar biological properties, we have developed a tool AGP that prioritize genes associated with age-related disorder (ARDs). AGP is a machine learning based prediction tool that calculates the

probability of association for each gene with age related disorders (ARDs) in humans. The required input in AGP are HGNC gene symbol, Entrez ID or the UniProt/SwissProt Accession ID and the output



The screenshot shows the AGP web tool interface. The header includes the Delhi Technological University logo and the title "AGP : Online Tool for Prediction of Genes Associated with Age-Related Disorders". The navigation bar contains links: Home, About, Help, Contact, dbAARD, and Genomeinformatics Lab. The main form has several input fields: "QUERY GENE", "Prediction Probability", "Attribute Group 1", "Attribute Group 2", and "Attribute Group 3". Under "Attribute Group 3", there is a section titled "Sub cellular localization of protein" with a list of organelles and their corresponding checkboxes: Cell junction, Centrosome, Cytoplasm, Endoplasmic Reticulum, Focal Adhesions, Golgi Apparatus, Mitochondria, Nucleus, Plasma Membrane, Vesicle, and Unknown. Below the form are "Submit" and "Reset" buttons.

(V)



The screenshot shows the AGP web tool interface. The header and navigation bar are the same as in the previous screenshot. The main form has the same input fields as before. Under "Attribute Group 4", there is a section titled "Network Properties" with a list of network properties and their corresponding checkboxes: Betweenness centrality, Closeness centrality, Clustering Coefficient, and Degree. Below the form are "Submit" and "Reset" buttons.

(VI)

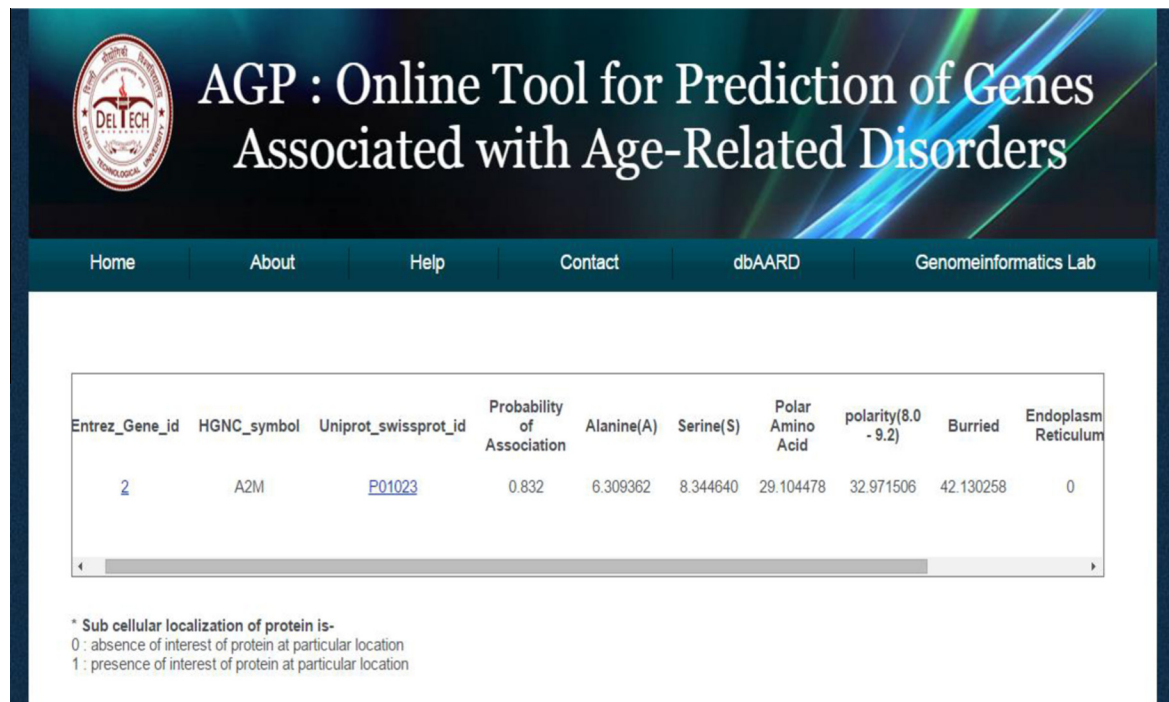
Fig. 1B (continued)

is the probability of association of corresponding gene with age related disorders. This section briefly describes the development of AGP for disease genes prediction.

3.1. Dataset and feature selection

For robust gene prediction, it is desirable to include various biological data sources and it has been found that both sequence based

and topological information are important for evaluating whether unknown gene is disease related or not. Genes associated with similar disorders are usually characterized with high similarity of sequence-based features, functional features and physical interaction between their gene products [29]. Various disease gene prediction tools have been reported in the literature that consider topological features in PPI networks, sequence-derived features, evolutionary age features, etc. for disease gene prediction [29–31].



(VII)

Fig. 1B (continued)

Table 3
Filters used in dbAARD.

Diseases	Select the disease(s) for which you want to know about the SNPs or GWAS
Genes	Filter records based on HGNC gene symbols
SNPs	Filter records based on rsIDs as in dbSNP build 134
Disease Class	You can restrict the records to only the subset that has disease-SNP associations from a particular disease class

2211 positive instances and 2211 randomly selected negative instances from the negative dataset of 25,476 instances. All the 11 training sets were used on previously used state-of-the-art classifiers to find the best performing classifier using 10-fold cross validation in the WEKA Experiment Environment [40].

3.2. Classifier selection and validation

Many different classification techniques have been used and reported in the literature for various machine learning applications. The state-of-the art methods such as Decision Tree, kNN, Naives Bayes, SVM, and Random Forest are known to be used for classification problems including disease gene prediction [30–33]. For the selection of the base classifier for ARD gene prediction we tested known classifiers already known to be used for disease gene prediction along with the ensemble based Rotation Forest algorithm [41]. To the best of our knowledge, this is for the first time that Rotation Forest has been tested for disease gene prediction. For each classifier we used all the training sets created using Cygwin. In order to evaluate these classifying techniques and find the best performing classifier, we employed 10 fold cross validation and measured the performance in terms of Precision, Recall, Area under ROC curve and F-measure which are defined as follows:

- (1) Precision – It is the fraction of retrieved instances that are relevant [42].

$$\text{Precision} = \frac{\text{True Positives}}{\text{True Positives} + \text{False Positives}}$$

- (2) Recall – It is the fraction of relevant instances that are retrieved. Both precision and recall are therefore based on an understanding and measure of relevance [42].

$$\text{Recall} = \frac{\text{True Positives}}{\text{True Positives} + \text{False Negatives}}$$

Therefore, for our model building purpose we included sequence based and physicochemical based features along with the subcellular localization and network topology information of proteins. Protein sequences of all the human proteins were retrieved from UniProt [13]. The sequence based parameters such as amino acid composition and physicochemical properties like hydrophobicity, normalized van der Waals volume, polarity, charge, secondary structure, solvent accessibility, polarizability, etc. were calculated using the PROFEAT program [35]. The information on the subcellular localization of proteins such as cell junction, centrosome, cytoskeleton, mitochondria, golgi body, endoplasmic reticulum, nucleus, lysosome, vesicle was obtained from The Human Protein Atlas [36]. The proteins whose subcellular locations were not defined were categorized as unknown. The information about the various network features of protein–protein interaction network such as betweenness centrality, closeness centrality, degree and cluster coefficient were obtained by building PPI network in Cytoscape [37] using data retrieved from HIPPIE [38].

For building the training set, both positive and negative instances were constructed. All the genes present in dbAARD were mapped to 2211 UniProt IDs using Biomart [39] and were used as positive instances. All those genes that were not present in dbAARD were treated as non-ARD genes and the corresponding 25,476 UniProt entries were used to build negative dataset. The positive and negative dataset were balanced by generating 11 training sets using Cygwin. Each training set was built by including

- (3) Area under ROC curve – Area under ROC (Receiver Operating Characteristic Curve) is a measure of accuracy and is a plot of specificity versus sensitivity at various cut-off values [42].
- (4) *F*-measure – This measure is harmonic mean of precision and recall, so it reflects an average effect of both precision and recall [43].

$$F\text{-measure} = \frac{2 \times \text{Precision} \times \text{Recall}}{\text{Precision} + \text{Recall}}$$

Based on the highest recall, precision, *F*-measure and Area under ROC curve, classifier rotation forest was found to perform well and hence was used to build final model for predictions by integrating base classifier and suitable filters. The ensemble Rotation Forest classifier was then trained further with the training set (the gold standard) consisting of 2211 ARD associated genes and 2211 randomly selected non-ARD genes in the explorer of WEKA.

3.3. Web implementation

For the ease of data retrieval, user-friendly web interface was developed. XHTML and CSS was used for creating presentation layer of dbAARD and AGP, the application server used was Apache. For backend database, MySQL was used and PHP was used as a programming language.

4. Results and discussion

4.1. dbAARD

dbAARD catalogues information about human genetic variants associated with age related disorders like Alzheimers' disease, Parkinson's disease, Diabetes, Cardiovascular disorders and Cancers, etc. (Fig. 1A). The database can be queried individually or in combination of disease class, disease name, gene and rsIDs. dbAARD currently has information on 3197 SNPs across 1297 genes associated with 51 diseases under 12 classes. The distribution of genes and SNPs in various classes of diseases has been represented in Figs. 2 and 3. The associated genes and SNPs can shed light on common pathways associated with these diseases.

Analysis of SNPs associated with ARDs depicted 75.33% as non-coding; 1.02% as coding – synonymous, 20.52% SNPs as missense, and the rest were those SNPs whose locations were unknown in

Distribution of SNPs among various Age Related Disorders

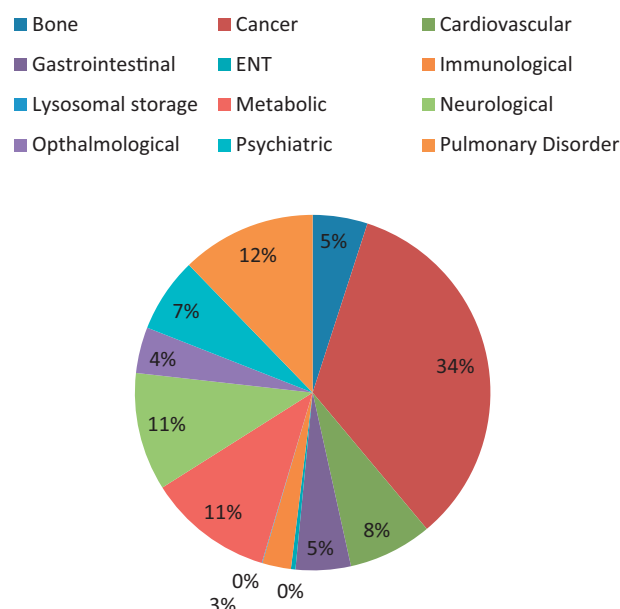


Fig. 3. Pie chart representing the distribution of single nucleotide polymorphisms among various classes of age related disorders.

dbSNP. The data suggests higher contribution of non-coding SNPs in human ARDs risk.

The database comprehensively includes genetic variants across all major populations and ethnicities. This information may therefore be used for associative studies to uncover the role of genetic variants in a particular population that make them more susceptible to an aging disorder. The fact that the genome has been mined for variations at single base resolution may further be used to map age related disorders to their gene loci.

4.2. AGP evaluation

The evaluation of the AGP tool was done on performance measures as defined earlier to select the best classifier. Subsequently, the tool was used to predict ARD associated genes and were biologically validated using Bioinformatics Resources 6.7 [44] and DisGeNET [45].

4.3. Performance comparison of base-classifiers and selection of the best classifier

In order to determine the best performing classifier, we analyzed 7 different classifiers and compared their performances in terms of precision, recall, *F*-measure and Area under the ROC curve (AUC). Fig. 4 shows the performance comparison of all the seven supervised learning algorithms for disease gene prediction. SVM was found to have the highest precision (82%) but the recall was found to be only 31%. On the contrary, Linear Regression was found to have the highest recall (90%), however the precision was found to be only 46%. Since having either too small a precision or too small a recall is unacceptable in disease gene-prediction [30], *F*-measure is generally used to evaluate the performance of classifiers. *F*-measure is the average effect of both precision and recall, and will be large only if both of them are large. Also, it has been suggested that AUC is the better measure of accuracy when comparing the performance of different classifiers [46]. Thus,

Distribution of genes among various classes of Age Related Disorders

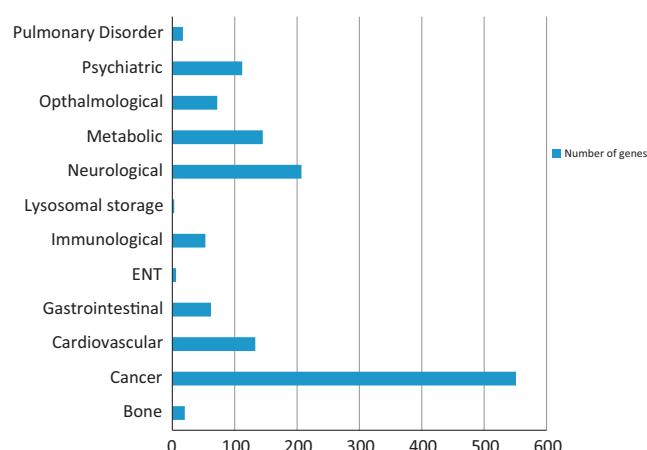


Fig. 2. Distribution of genes among various classes of age related disorders.

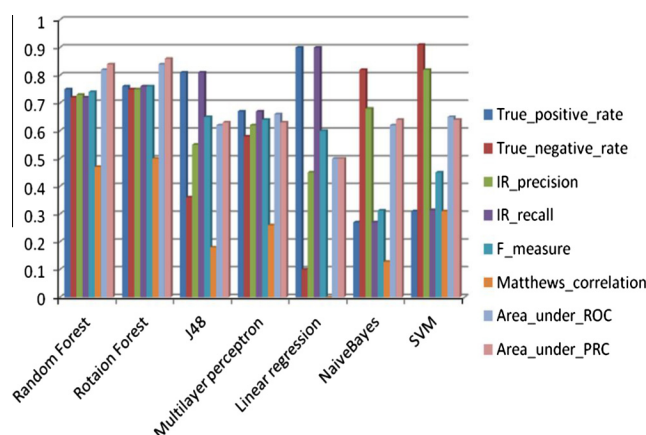


Fig. 4. Bar diagram is representing the True Positive Rate (TPR), True Negative Rate (TNR), Precision, Recall, F-measure and Matthews correlation obtained by various classifiers.

classes is included in Table 4. It can be clearly observed that in terms of precision and F-measure, AGP performed better than PUDI. Thus, we can consider that AGP is robust enough to correctly predict genes associated with ARDs.

4.5. Predicting novel ard genes and biological validation

To evaluate the efficiency of AGP, we carried out analysis of all the genes in the UniProt and determined the ability of AGP in predicting ARD associated genes which are not listed in dbAARD. Subsequently biological evaluation of the predicted ARD genes was carried out using DAVID Bioinformatics Resources 6.7 [44] and DisGeNET [45]. We found 342 UniProt entries to be associated with ARDs with probability greater than 0.7. These entries mapped to 210 genes in humans. 14 predicted ARD associated genes, which were found to have probability of ARD association more than 0.8, were evaluated for their functional significance. The results indicated that 11 of these 14 genes were reported in GAD [48] and 7 in OMIM database [27]. 82% of these genes were associated with age-related diseases included in dbAARD. Some of these include: CEBPA [49] and CREBBP [50] associated with acute myeloid leukemia; HNF4A with type 2 diabetes [51]; NFKB1 with Adenocarcinoma [52], Crohn's disease [53], rheumatoid arthritis [54]; TFAP2A [55] and ERBB3 [56] with schizophrenia (Supplementary Table 2). Further DisGeNET [45] was used to find the evidence for these putative genes for association with various ARDs. DisGeNET [45] integrates information from expert-curated databases with text mined-data on various Mendelian and complex diseases and features a score based on the supporting evidence to prioritize gene-disease association with reference to relevant literature. The results of DisGeNET for 14 predicted ARD genes are attached as Supplementary File and are found to be in accordance with the results from DAVID tool [44].

There is a need to have general applicability that form the basis for the evolving science of biomedical informatics of new methodologies and techniques. Often a large amount of data needs to be collected for biomedical research on human subjects either by personal interviews/internet based questionnaires/lab measurements or by extracting data from literature/electronic health records. Further this data needs to be comprehensively stored in standard format, analyzed and interpreted for addressing wide range of biomedical problems. Our database, dbAARD enhance user's ability to search, locate and evaluate information regarding ARDs in the ever-increasing network of the information search environment. This also calls for user-friendly software tools that can use collected information and quickly and reliably analyze unknown data to allow novel predictions. Although aimed at biomedical research, we are aiming to make the architecture more flexible, so that it may be used on different data for various medical problems such as identification of the genetic markers/causative genes as many medical conditions are influenced by human genetic variations. On the similar lines, our dbAARD database and AGP tool may be further exploited to predict novel diseases' genes and also use the existing information to develop more efficient diagnostic tools and therapies.

An important limitation of the present work is that the current work has only focused on the SNPs in the coding region for building the AGP Tool. As evident, large portion of the SNPs in ARDs are present in the non-coding region and the current approach cannot include the role of these SNPs in prediction of ARD associated genes and the ways by which these SNPs influence various ARDs. Exploiting the information from these regions as knowledge of these non-coding regulatory elements, mechanisms of action, cellular states and processes in which they function remains a challenge. However, integrating information from all the regions (coding and non-coding) may provide holistic view of ARD causation.

considering both F-measure (76%) and AUC (0.85) Rotation Forest performs better than other classifiers. Recent studies have also shown that rotation forest classifier performs better than other non-ensemble based classifiers [47]. Rotation Forest algorithms are fast, scalable and can easily handle high dimensional spaces as well as large number of training examples. Moreover, Rotation Forest algorithm tends to overcome the issue of overfitting in noisy data [41,47]. Hence to exploit the merits of Rotation Forest, we trained it as the base classifier to build the final model for ARD gene prediction (Fig. 1B) and tested it using all the genes in the UniProt.

4.4. Performance comparison with known disease-gene prediction tool

To compare how well our tool performs with respect to other machine learning tools for disease gene prediction, we compared the performance of our tool with one of the known machine learning based tool PUDI [29] for predicting ARD genes. Using training set consisting of 2211 ARD associated genes (POSITIVE DATASET) and randomly selected 2211 NON-ARD genes (NEGATIVE DATASET) and employing 10 fold cross-validation, we measured the performance of AGP and PUDI in terms of F-measure. Our tool achieved 73.6% F-measure which is 2.5% better than PUDI algorithm (71.1%).

We also tested the ability of our tool (AGP) and PUDI to predict genes associated with particular class of ARD. For this study, we included 7 ARD classes and the performance measure on these

Table 4
Performance comparison across different ARD classes.

Disease Class	# Genes	Tool	Precision (%)	Recall (%)	F-measure (%)
Bone	142	AGP	68.5	68.3	68.2
		PUDI	60.2	69.3	64.2
Gastrointestinal	72	AGP	67.4	67.4	67.3
		PUDI	57.6	70	60
Immunological	59	AGP	78	78	78
		PUDI	85.2	64	69.7
Metabolic	150	AGP	61.1	61	60.9
		PUDI	55.3	74	62.3
Neurological	226	AGP	70.6	70.6	70.6
		PUDI	62.7	73.2	67.2
Ophthalmological	83	AGP	65.8	65.7	65.6
		PUDI	50.2	68.7	57.4
Psychiatric	142	AGP	63.9	63.9	63.9
		PUDI	67.5	71.4	69.2

5. Conclusion

In the present work, we have developed a queriable online repository of the genes associated with ARDs, dbAARD, made freely available to the user at <http://genomeinformatics.dce.edu/dbAARD/>. To the best of our knowledge, this is the first resource that hosts genetic association information on human ARDs.

This data allows the user to retrieve genetic information on ARDs at genome-wide systems level. Mining the database for biologically meaningful information keeping these points in mind is likely to reveal hitherto unknown facts about the underlying causes of age-related disorders. This knowledge may eventually be helpful in understanding the biology of aging itself.

Additionally based upon the knowledge of genetic associations of ARDs, we have also developed an online tool, AGP, available at <http://genomeinformatics.dce.edu/AGP/> for the prediction of genes associated with ARDs. The tool obtained an accuracy of 85%, area under ROC curve of 0.85 by rotation forest. AGP predicts association probabilities for the genes on the basis of physiochemical properties of corresponding proteins, sub cellular localization of proteins and protein–protein interaction network features.

The data from dbAARD and AGP may be used to construct networks of Gene–Disease as well as SNP–Disease associations, so as to make it easier to detect genes and SNPs that are significantly involved in different ARDs. These network based studies may provide a deeper insight into how various diseases are associated together and which class of diseases share more common genes and pathways thereby providing a means for better drug repositioning and further progress may be made in the field of personalized medicines. We believe that exploring the role of genes and genetic variations would be helpful in predicting the genes and SNPs which confer susceptibility to various ARDs but are still unknown. Further research on role of non-coding and synonymous SNPs may reveal various unknown molecular mechanisms associated with ARDs. It is believed that the present database and tool may be used to uncover hidden links between aging and various age-related disorders providing valuable perspective to physicians, counsellors and biomedical researchers.

Conflict of interest

The authors declare that they have no conflict of interest.

Funding

The study has been supported by SERB under OYS scheme via project file no. SR/FT/LS-96/2011.

Availability and implementation

The developed database and tool are available as free online resources at <http://genomeinformatics.dce.edu/dbAARD/> and <http://genomeinformatics.dce.edu/AGP/> respectively.

Acknowledgments

Authors acknowledge Gaurav Kandoi for his contribution in annotation, Nitin Thukral and Pooja Khurana for their scientific inputs.

Appendix A. Supplementary material

Supplementary data associated with this article can be found, in the online version, at <http://dx.doi.org/10.1016/j.jbi.2016.01.004>.

References

- [1] R. Holliday, Aging in the 21st century, *Lancet* 354 (Suppl. SIV4) (1999).
- [2] J. Vijg, J. Campisi, Puzzles, promises and a cure for aging, *Nature* 454 (7208) (2008) 1065–1071.
- [3] W.J. Strawbridge, M.I. Wallhagen, R.D. Cohen, Successful aging and well-being: self-rated compared with Rowe and Kahn, *Gerontologist* 42 (6) (2002) 727–733.
- [4] U. Lehr, Centenarian – a contribution to longevity research, *Z. Gerontol.* 24 (5) (1991) 227–232.
- [5] S. Collino, I. Montoliu, F.P. Martin, M. Scherer, D. Mari, S. Salvioli, L. Bucci, R. Ostan, D. Monti, E. Biagi, P. Brigidì, C. Franceschi, S. Rezzì, Metabolic signatures of extreme longevity in northern Italian centenarians reveal a complex remodeling of lipids, amino acids, and gut microbiota metabolism, *PLoS ONE* 8 (8) (2013), <http://dx.doi.org/10.1371/journal.pone.0084306>.
- [6] P.D. Stenson, M. Mort, E.V. Ball, K. Shaw, A. Phillips, D.N. Cooper, The Human Gene Mutation Database: building a comprehensive mutation repository for clinical and molecular genetics, diagnostic testing and personalized genomic medicine, *Hum. Genet.* 133 (1) (2014) 1–9.
- [7] D. Welter, J. Mac Arthur, J. Morales, T. Burdett, P. Hall, H. Junkins, A. Klemm, P. Flicek, T. Manolio, L. Hindorf, H. Parkinson, The NHGRI GWAS Catalog, a curated resource of SNP-trait associations, *Nucleic Acids Res.* 42 (Database issue) (2014) D1001–D1006, <http://dx.doi.org/10.1093/nar/gkt1229>.
- [8] M. Cariaso, G. Lennon, SNPedia: a wiki supporting personal genome, annotation, interpretation and analysis, *Nucleic Acids Res.* 40 (Database issue) (2012) D1308–D1312, <http://dx.doi.org/10.1093/nar/gkr798>.
- [9] L. Walker, H. Starks, K.M. West, S.M. Fullerton, dbGaP data access requests: a call for greater transparency, *Sci. Trans. Med.* 3 (113) (2011) 113–134.
- [10] R.K. Hastings, T. Beck, S. Gollapudi, R.C. Free, A.J. Brookes, GWAS central, *Nucleic Acids Res.* (2009). NAR Molecular Biology Database Collection Entry Number 131.
- [11] L. Bertram, M.B. McQueen, K. Mullin, D. Blacker, R.E. Tanzi, Systematic meta-analyses of Alzheimer disease genetic association studies: the AlzGene database, *Nat. Genet.* 39 (1) (2007) 17–23.
- [12] N.C. Allen, S. Bagade, M.B. McQueen, J.P. Ioannidis, F.K. Kavvoura, M.J. Khoury, R.E. Tanzi, L. Bertram, Systematic meta-analyses and field synopsis of genetic association studies in schizophrenia: the SzGene database, *Nat. Genet.* 40 (7) (2008) 827–834.
- [13] CH. Wu, R. Apweiler, A. Bairoch, DA. Natale, WC. Barker, B. Boeckmann, S. Ferro, E. Gasteiger, H. Huang, R. Lopez, M. Magrane, M.J. Martin, R. Mazumder, C. O'Donovan, N. Redaschi, B. Suzek, The Universal Protein Resource (UniProt): an expanding universe of protein information, *Nucleic Acids Res.* 34 (Database issue) (2006) D187–D191, 2006 Jan 1.
- [14] K. Goh, M.E. Cusick, D. Valle, B. Childs, M. Vidal, A.L. Barabasi, The human disease network, *Proc. Natl. Acad. Sci.* 104 (2007) 8685.
- [15] S.V. Saxon, M.J. Etten, E.A. Perkins, Physical Change and Aging: A Guide for the Helping Professions, Springer Publishing Company, 2014.
- [16] S. Bondy, K. Maiese (Eds.), Aging and Age-Related Disorders, Oxidative Stress in Applied Basic Research and Clinical Practice, vol. 3, Springer Science +Business Media, LLC, 2010.
- [17] C.S. Pitchumoni, T.S. Dharmarajan (Eds.), Geriatric Gastroenterology, Springer, New York, 2012.
- [18] T. Shachar, C.L. Bianco, A. Recchia, C. Wiessner, A. Raas-Rothschild, A.H. Futerman, Lysosomal storage disorders and Parkinson's disease: Gaucher disease and beyond, *Mov. Disord.* 26 (9) (2011) 1593–1604.
- [19] H. Schulze, K. Sandhoff, Lysosomal lipid storage diseases, *Cold Spring Harbor Perspect. Biol.* 3 (6) (2011) a004804.
- [20] J. Guimaraes, O. Amaral, M.S. Miranda, Adult-onset neuronopathic form of Gaucher's disease: a case report, *Parkinsonism Relat. Disorders* 9 (5) (2003) 261–264.
- [21] V.J. Thannickal, Mechanistic links between aging and lung fibrosis, *Biogerontology* 14 (6) (2013), <http://dx.doi.org/10.1007/s10522-013-9451-6>.
- [22] J.E. Maglione, S.E. Thomas, D.V. Jeste, Late-onset schizophrenia: do recent studies support categorizing LOS as a subtype of schizophrenia?, *Curr Opin. Psychiatry* 27 (3) (2014) 173–178, <http://dx.doi.org/10.1097/YCO.0000000000000049>.
- [23] C.I. Cohen (Ed.), Schizophrenia into Later Life: Treatment, Research, and Policy, American Psychiatric Publishing, Inc., Washington, DC, 2003.
- [24] R. Howard, P.V. Rabins, M.V. Seeman, D.V. Jeste, Late-onset schizophrenia and very-late-onset schizophrenia-like psychosis: an international consensus, *Am. J. Psychiatry* (2000).
- [25] I. Srivastava, N. Thukral, Y. Hasija, Genetics of human age related disorders. Advances in gerontology = Uspekhi gerontologii/Rossiiskai akademii nauk, Gerontologicheskoe obshchestvo 28 (2) (2015) 228–247.
- [26] M.L. Famiglietti, A. Estreicher, A. Gos, J. Bolleman, S. Gehant, L. Breuza, A. Bridge, S. Poux, N. Redaschi, L. Bougueleret, I. Xenarios, Genetic variations and diseases in UniProtKB/Swiss-Prot: the ins and outs of expert manual curation, *Hum. Mutat.* 35 (2014) 927–935.
- [27] A. Hamosh, A.F. Scott, J.S. Amberger, C.A. Bocchini, V.A. McKusick, Online Mendelian Inheritance in Man (OMIM), a knowledgebase of human genes and genetic disorders, *Nucleic Acids Res.* 33 (Database issue) (2005) D514–D517, <http://dx.doi.org/10.1093/nar/gki033>.
- [28] F. Mordelet, J.P. Vert, ProDiGe: prioritization of disease genes with multitask machine learning from positive and unlabeled examples, *BMC Bioinformatics* 12 (2011) 389, <http://dx.doi.org/10.1186/1471-2105-12-389>.

- [29] P. Yang, X.L. Li, J.P. Mei, C.K. Kwoh, S.K. Ng, Positive-unlabeled learning for disease gene identification, *Bioinformatics* 28 (20) (2012) 2640–2647.
- [30] E.A. Adie, R.R. Adams, K.L. Evans, D.J. Porteous, B. Pickard, Speeding disease gene discovery by sequence based candidate prioritization, *BMC Bioinformatics* 6 (1) (2005) 55.
- [31] A. Smalter, S.F. Lei, X. Chen, Human Disease-gene Classification with Integrative Sequence-based and Topological Features of Protein-Protein Interaction Networks, *BIBM*, 2007.
- [32] S. Calvo, M. Jain, X. Xie, S.A. Sheth, B. Chang, O.A. Goldberger, V.K. Mootha, Systematic identification of human mitochondrial disease genes through integrative genomics, *Nat. Genet.* 38 (5) (2006) 576–582.
- [33] J. Xu, Y. Li, Discovering disease-genes by topological features in human protein-protein interaction network, *Bioinformatics* 22 (22) (2006) 2800–2805.
- [34] S.C. Johnson, X. Dong, J. Vijg, Y. Suh, Genetic evidence for common pathways in human age-related diseases, *Aging Cell* 14 (5) (2015) 809–817.
- [35] Z.R. Li, H.H. Lin, L.Y. Han, X. Jiang, X. Chen, Y.Z. Chen, PROFEAT: a web server for computing structural and physicochemical features of proteins and peptides from amino acid sequence, *Nucleic Acids Res.* 34 (Web Server issue) (2006) W32–7. Jul 1.
- [36] M. Vivien, Proteomics: an atlas of expression, *Nature* (2014) 645–649.
- [37] M.S. Cline, M. Smoot, E. Cerami, A. Kuchinsky, N. Landys, C. Workman, R. Christmas, I. AvilaCampilo, M. Creech, B. Gross, K. Hanspers, R. Isserlin, R. Kelley, S. Killcoyne, S. Lotia, S. Maere, J. Morris, K. Ono, V. Pavlovic, A.R. Pico, A. Vailaya, P.L. Wang, A. Adler, B.R. Conklin, L. Hood, M. Kuiper, C. Sander, I. Schmulevich, B. Schwikowski, G.J. Warner, T. Ideker, G.D. Bader, Integration of biological networks and gene expression data using Cytoscape, *Nat. Protoc.* 2 (2007) 2366–2382.
- [38] M.H. Schaefer, J.F. Fontaine, A. Vinayagam, P. Porras, E.E. Wanker, M.A. Andrade Navarro, HIPPIE: integrating protein interaction networks with experiment based quality scores, *PLoS ONE* (2012), <http://dx.doi.org/10.1371/journal.pone.0031826>.
- [39] J. Zhang, S. Haider, J. Baran, A. Cros, J.M. Guberman, J. Hsu, A. Kasprzyk, BioMart: a data federation framework for large collaborative projects, *Database: J. Biol. Databases Curation* (2011) bar038, <http://dx.doi.org/10.1093/database/bar038>.
- [40] S. Swasti, J. Monika, A study on WEKA tool for data preprocessing, *IJITEE*, 2278–3075 2 (6) (2013).
- [41] J.J. G. Rodriguez, L.I. Kuncheva, C.J. Alonso, Rotation forest: a new classifier ensemble method, *IEEE Trans. Pattern Anal. Machine Intell.* 28 (10) (2006) 1619–1630.
- [42] D. Jesse, G. Mark, The relationship between precision-recall and ROC curves, in: *Appeared in Proceedings of the 23rd International Conference on Machine Learning*, Pittsburgh, PA, 2006.
- [43] P. Bollmann et al., Restricted evaluation in information retrieval, *ACM SIGIR* (1981) 15–21.
- [44] D.W. Huang, B.T. Sherman, R.A. Lempicki, Systematic and integrative analysis of large gene lists using DAVID bioinformatics resources, *Nat. Protoc.* 4 (1) (2009) 44–57.
- [45] J. Piñero, N. Queralt-Rosinach, À. Bravo, J. Deu-Pons, A. Bauer-Mehren, M. Baron, L. Furlong, DisGeNET: a discovery platform for the dynamical exploration of human diseases and their genes, *Database: J. Biol. Databases Curation* (2015) bav028, <http://dx.doi.org/10.1093/database/bav028>.
- [46] C.X. Ling, J. Huang, H. Zhang, AUC: a better measure than accuracy in comparing learning algorithms, in: *Adv. Artif. Intell.*, Springer, Berlin, Heidelberg, 2003, pp. 329–341.
- [47] A. Dehzangi, S. Phon-Amnuaisuk, M. Manafi, S. Safa, Using rotation forest for protein fold prediction problem: an empirical study, in: *Evolutionary Computation, Machine Learning and Data Mining in Bioinformatics*, Springer, Berlin, Heidelberg, 2010, pp. 217–227.
- [48] K.G. Becker, K.C. Barnes, T.J. Bright, S.A. Wang, The genetic association database, *Nat. Genet.* 36 (5) (2004) 431–432.
- [49] J.M. Hughes, B. Salvatori, F.M. Giorgi, I. Bozzoni, A. Fatica, CEBPA-regulated lncRNAs, new players in the study of acute myeloid leukemia, *J. Hematol. Oncol.* 7 (2014) 69, <http://dx.doi.org/10.1186/s13045-014-0069-1>.
- [50] H.H. Schmidt, MYST3/CREBBP (MOZ/CBP) and CREBBP/MYST3 (CBP/MOZ) transcripts in AML with t(8;16)(p11;p13), *Genes Chromosom. Cancer* 42 (2) (2005) 207–208.
- [51] L. Andrulionyte, O. Laukkanen, J.L. Chiasson, M. Laakso, Single nucleotide polymorphisms of the HNF4alpha gene are associated with the conversion to type 2 diabetes mellitus: the STOP-NIDDM trial, *J. Mol. Med. (Berl.)* 84 (2006) 701–708.
- [52] S. Delhalle, V. Deregowski, V. Benoit, M.P. Merville, V. Bours, NF-kappaB-dependent MnSOD expression protects adenocarcinoma cells from TNF-alpha-induced apoptosis, *Oncogene* 21 (2002) 3917–3924.
- [53] W. Klein, A. Tromm, C. Folwaczny, M. Hagedorn, N. Duerig, J.T. Epplen, H. Wolff, W.H. Schmiegel, T. Griga, A polymorphism of the NFKBIA gene is associated with Crohn's disease patients lacking a predisposing allele of the CARD15 gene, *Int. J. Colorectal Dis.* 19 (2004) 153–156.
- [54] C.H. Lin, T.T. Ou, C.C. Wu, W.C. Tsai, H.W. Liu, J.H. Yen, IkappaBalpha promoter polymorphisms in patients with rheumatoid arthritis, *Int. J. Immunogenet.* 34 (2007) 51–54.
- [55] Y. Kawanishi, S. Harada, H. Tachikawa, T. Okubo, H. Shiraishi, Novel polymorphisms of the AP-2 gene 6p24: analysis of association with schizophrenia, *J. Hum. Genet.* 45 (1) (2000) 24–30.
- [56] D. Li, G. Feng, L. He, Case-control study of association between the functional candidate gene ERBB3 and schizophrenia in Caucasian population, *World J. Biol. Psychiatry* 10 (2009) 595–598.

576
577
578
579
580
581
582
583
584
585
586
587
588
589
590
591
592
593
594
595
596
597
598
599
600
601
602
603
604
605
606
607
608
609
610
611
612
613
614
615
616
617
618
619
620

An Experimental Appraisal on the Efficacy of MWCNT-H₂O Nanofluid on the Performance of Solar Parabolic Trough Collector

Harwinder Singh* and Pushpendra Singh

Department of Mechanical, Production and Industrial Engineering, Delhi Technological University, India

Abstract

An application of MWCNT nanoparticles and distilled water was used to prepare the nanofluid and this type of MWCNT based absorbing medium was found to be highly efficient in investigation of the performance of solar parabolic trough collector due to better thermo physical properties (i.e. thermal conductivity) acquired by the MWCNT based nanofluid. In present research study author decided to take volume concentration 0.01% and 0.02% and high quality surfactant Triton X-100 was used to enhance the dispersion quality of nanoparticles in conventional fluid. The test were performed under different volume flow rate conditions of nanofluid i.e. 160 L/h and 100 L/h. Experimental results show that with an incremental change in volume concentration from 0.01% to 0.02%, there is a substantial increment in efficiency of parabolic collector but observed only at 160 L/h.

Keywords: Parabolic trough collector; MWCNT nanofluid; Triton X-100 surfactant; Collector performance testing

Abbreviations

Q_u : Useful heat gain (Watt); Q_{ut} : Useful heat gain (Watt); \dot{m} : Mass flow rate (Kg/s); C_{nf} : Specific heat of MWCNT nanofluid $\left[\frac{J}{kg-k}\right]$; C : Specific heat of base fluid $\left[\frac{J}{kg-k}\right]$; t : Time interval (half an hour); D_i : Internal diameter (m); U_i : Overall heat loss coefficient; F : Collector efficiency factor; F_R : Collector heat removal factor; G_T : Total solar intensity (W/m^2) $\left(\frac{W}{m^2-k}\right)$; T_{max} : Maximum temperature (K); T_{min} : Minimum temperature (K); T_{out} : Outlet temperature (k); T_{in} : Inlet temperature (k); W : Width of collector (m); L : Length of collector (m); T : Total experimental duration; D_o : Outer diameter (m); C : Concentration ratio; F_R : Collector heat removal factor; h_c : Convective heat loss coefficient; K_{nf} : Thermal conductivity $\left[\frac{W}{m-k}\right]$; S : Absorbed heat flux

Greek symbols

ϕ_p : Weight fraction of MWCNT nano particles in nano fluid; ρ_{nf} : Density of MWCNT nanofluid $\left[\frac{kg}{m^3}\right]$; ρ : Density of base fluid $\left[\frac{kg}{m^3}\right]$; ρ_{np} : Density of nano particles $\left[\frac{kg}{m^3}\right]$; μ_{nf} : Dynamic viscosity of MWCNT nanofluid $\left[\frac{Kg}{m-sec}\right]$; μ : Dynamic Viscosity of base fluid $\left[\frac{Kg}{m-sec}\right]$; ν_{nf} : Kinematic viscosity of MWCNT nanofluid $\left[\frac{m^2}{sec}\right]$; ν : Kinematic viscosity of base fluid $\left[\frac{m^2}{sec}\right]$; E_i : Instantaneous energy production; η_{th} : Thermal efficiency; η_{ot} : Overall thermal efficiency

Introduction

Parabolic trough collector is a prominent way to convert solar radiations into solar thermal energy and transfer this heat or thermal energy to working fluid for purpose of electric power generation. These days solar energy devices are in use widely and enhancement in performance of solar device are very necessary due to purpose of decrease down the effect of environmental pollutants released from conventional methods. From the last two decades scientists gave effort to improve the performance of solar parabolic trough collector and thermal storage systems for achievement of maximum power and there was a performance booster comes after the discovery of nanoparticles. Application of nanoparticles in conventional fluid also become a new approach to enhance the thermo physical properties of working fluid and among other nanoparticles, MWCNTs possess better thermal, mechanical and optical characteristics and MWCNTs based nanofluid

as a working fluid has an capability to enhance the outcome of solar thermal devices. Suspension of metallic and non metallic particles in base fluid is simply known by nanofluid and this term is originated and investigated by Haddad and it has also been seen that nanofluid attain higher dispersion quality as comparison to microfluid [1]. Due to hydrophobic nature, MWCNT nanoparticles have poor dispersion quality in base fluid and stability of nanoparticles in base fluid can be increased with the help of surfactant, which has both hydrophobic and hydrophilic functional groups [2]. Davis et al. evaluate the shear thinning behavior in the viscosity of CNT nanofluid and they found that viscosity of CNTs based nanofluids is function of concentration of nanoparticles in base fluid, He also concluded that with increase in concentration of CNTs, interactions between nanotubes with each other increases and which results in movement between tubes will be stopped [3]. Ding et al. study about the heat transfer process with nano fluid containing CNTs and results concluded that carbon nano tubes enhance the heat convection coefficient as comparison to total enhancement in thermal conductivity. The reason behind more enhancements in heat convection coefficient is high aspect ratio of using CNTs [4]. Lotfi et al. studied experimentally that heat transfer can be enhanced due to presence of MWCNT nanoparticles in water as comparison to simple water and enhanced heat transfer due to MWCNT and water based nano fluids used in horizontal shell and heat exchanger applications [5]. Yousefi et al. evaluate the effect of MWCNT nanofluid on the efficiency of flat plate collector with different mass flow rate of nanofluid 0.0167 to 0.05 kg/s and also with decided weight fraction of CNTs was 0.2% and 0.4%, he concluded an substantial

***Corresponding author:** Harwinder Singh, Department of Mechanical, Production and Industrial Engineering, Delhi Technological University, Delhi College of Engineering, Shahbad Daultpur, Main Bawana Road, Delhi 110042, India, Tel: +91-7503678148; E-mail: harrymehrok14@gmail.com

Received November 25, 2015; **Accepted** December 28, 2015; **Published** January 01, 2016

Citation: Singh H, Singh P (2016) An Experimental Appraisal on the Efficacy of MWCNT-H₂O Nanofluid on the Performance of Solar Parabolic Trough Collector. J Fundam Renewable Energy Appl 6: 200. doi:10.4172/2090-4541.1000200

Copyright: © 2016 Singh H, et al. This is an open-access article distributed under the terms of the Creative Commons Attribution License, which permits unrestricted use, distribution, and reproduction in any medium, provided the original author and source are credited.

increase in efficiency with surfactant at 0.2% MWCNT nanofluid, while an incremental change in efficiency was observed at 0.4% MWCNT nanofluid without surfactant [6]. Kasaeian et al. conducted an experimental study on solar trough collector with the application of MWCNT at decided volume concentration 0.2% to 0.3% in mineral oil and he concluded that 4-5% and 6-7% enhancement in efficiency with MWCNT and mineral oil based nanofluid as comparison to pure oil [7]. Yousefi et al. studied experimentally that effect of Al₂O₃ nanofluid on flat plate collector with different mass flow rates 1, 2 and 3 Lit/min and he concluded that 28.3% enhancement in efficiency at 0.2% weight fraction of nanoparticles along with 15.63% efficiency enhancement with the application of surfactant Triton X-100 due to enhancement in heat transfer [8].

Experimentation & Data Findings

Nanomaterial

In this experimental study high class MWCNT nanoparticles (97% purity) with 20-40nm in diameter were obtained from Nano Green Technologies LLP (India). The Triton X-100 was used to achieve high quality dispersion of MWCNT in distilled water as base fluid for investigation and it is non-ionic natural surfactant (Table 1).

The SEM (Scanning Electron Microscopy) image of MWCNT nanoparticles produced by secondary electron at different resolution and magnification is shown in (Figures 1 and 2).

Preparation of nanofluid

MWCNT with 0.01% and 0.02% volume concentration used in distilled water and Triton X-100 surfactant was used in sufficient amount to avoid aggregation and instability between nanotubes, which results in better dispersion behavior. BRANSON 3510 Sonication device followed by magnetic stirrer was used for homogeneous mixing of MWCNT particles in distilled water. Sonication time also affect to dispersion behavior and corresponding thermal properties of carbon nanotubes and after going through several literature study in this field, the sonication time was decided 45 minutes for mixture amount of 2 liters. Surfactant Triton X-100 due to its non ionic nature showed better dispersion quality for MWCNTs based suspension among other surfactants. Proper dispersion of carbon nanotubes in base fluid is not easy to maintain so that surfactant like Triton X-100 is necessary for better dispersion. It has been seen that Triton X-100 has acquired benzene ring in structure and absorb to graphitic surface in very strong manner due to π - π stacking type interactions [6]. In this experimental study Triton X-100 is used almost same in amount as calculated for MWCNT in base fluid after going through many research discussions. Surfactant is used to bring single phase in solution used as working fluid and fig showed MWCNT based nanofluid contain Triton X-100 with it for proper suspension of MWCNTs throughout experimental span (Figure 3).

Experimental methodology

Item Description (MWCNTs)	
Purity	> 97%
Length of Nanotubes	1-10 micrometer
No. of Walls	3-15
Density	0.15-0.35g/cm ³
Surface Area	350 m ² /g [9]
Specific Heat	630 J/Kg-k [9]
Thermal conductivity	1500 W/m-k [9]

Table 1: Properties of MWCNT nanoparticles.

The parabolic trough collector was experimentally tested at Thapar University (Punjab). The parabolic trough collector has a copper receiver tube in which working fluid is flowing and gets heated at outlet. Temperatures measure at inlet and outlet through thermocouples and flow in piping and receiver was forced convection due to electric pump with 18W capacity used at inlet side. Collector system also has a storage tank with certain 8L capacity and ball valve was used at inlet side after pump to control the volume flow rate of working nanofluid in solar concentrating collector system. Storage tank and piping system was fully insulated through glass wool and aluminium foil insulation to prevent heat loss from the solar system. Total solar heat flux throughout the day was measured by solar power meter (Tenmars TM-207) and also flowing wind speed was measured by CFM/CMM vane anemometer (PRECISE AM804). Temperatures at inlet and outlet was measured after half an hour as decided before initializing the experimental work and experimental readings were taken from forenoon 9:30 am to afternoon 3:00 pm according to Indian standard time (Table 2 and Figure 4).

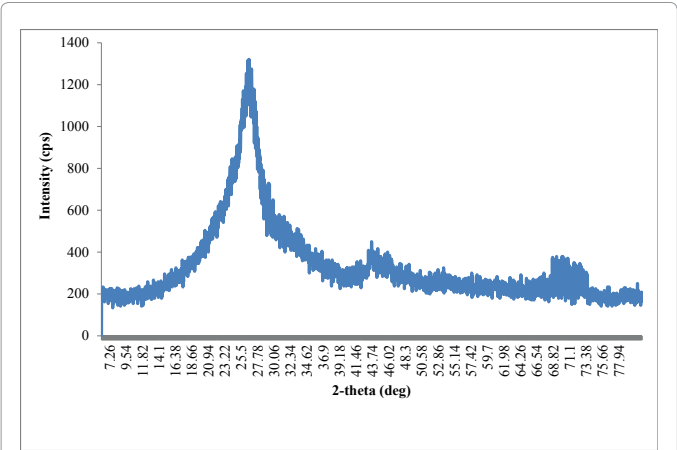


Figure 1: XRD image of MWCNT nanoparticles.

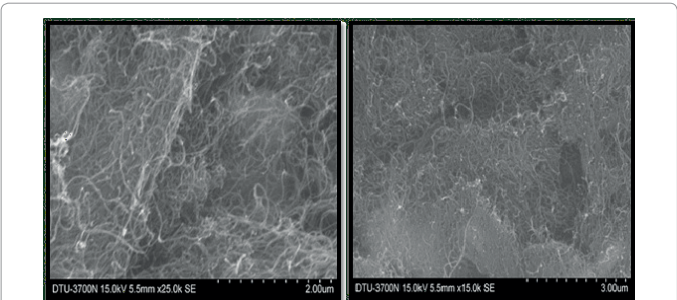


Figure 2: SEM image of MWCNT nanoparticles.



Figure 3: Sample of mixture ($\phi_v = 0.01\%$) and bucket of MWCNT nano fluids at 0.01% and 0.02% volume concentration.

Length of collector	1.2 m
Breadth of collector	0.915 m
Aperture area	1.0188 m ²
Rim angle	90°
Focal length	0.3 m
Inside diameter of receiver tube	0.027 m
Outside diameter of receiver tube	0.028 m
Inside diameter of glass cover	0.064 m
Outside diameter of glass cover	0.066 m
Concentration ratio	9.66

Table 2: The specification of parabolic trough collector [10-13].



Figure 4: Parabolic trough collector (location: Thapar university).

Performance Testing of Parabolic Solar Collector

Thermal steady state analysis was employed to evaluate the performance of solar parabolic collector and further assume piping and storage system was fully insulated. Various experiments were performed on solar collector through different volume flow rate and at certain weight fraction of nanoparticles in distilled water i.e. 6L. Data related to performance of solar parabolic collector was evaluated through efficiency and also useful heat gain as discussed below:

$$Q_u = mC_{nf} (T_{out} - T_{in}) \quad (1)$$

and

$$Q_u = F_R (W - D_o) L \left[S - \frac{U_l}{C} (T_{fi} - T_a) \right] \quad (2)$$

Here \dot{m} is mass flow rate and C_{nf} is specific heat of nanofluid, which is calculated as follow:

$$C_{nf} = \frac{[(1 - \phi_p) \rho_f c_f + \phi_p \rho_{np} c_{np}]}{\rho_{nf}} \quad (3)$$

Here ' c_f ' & ' c_{np} ' is specific heat of base fluid (water) and nanoparticles (MWCNT). Further ' ϕ_p ' is volume concentration of nanoparticles. Density and viscosity of mixture can be calculated through given equations:

$$\rho_{nf} = (1 - \phi_p) \rho_f + \phi_p \rho_{np} \quad (4)$$

$$\mu_{nf} = \mu_f / (1 - \phi_p)^{2.5} \quad (5)$$

Here ' ρ_{nf} ' & ' ρ_{np} ' is the density of nanofluid and nanoparticles. Instantaneous energy production is directly proportional to useful heat gain and is described as below:

$$E_i = \frac{Q_u}{G_T R_b W L} \quad (6)$$

Here ' G_T ' is total solar intensity W/m² and ' R_b ' is bond resistance is taken as constant. Further thermal and overall thermal efficiency of solar parabolic trough collector is discussed in following equations:

$$\eta_{ot} = \frac{mC_{nf}(T_{max} - T_{mini})}{A_{aper} G_{avg} T} \quad (7)$$

Here ' η_{th} ' is thermal efficiency of parabolic collector and further G_T and t is total solar intensity (W/m²) and time interval (half an hour).

$$\eta_{ot} = \frac{mC_{nf}(T_{max} - T_{mini})}{A_{aper} G_{avg} T} \quad (8)$$

Here ' η_{ot} ' is overall thermal efficiency of parabolic collector and further G_{avg} and ' T ' is average solar intensity (W/m²) and total test time period for experimental work.

Also collector efficiency factor (F) and heat removal factor (F_R) of collector system is discussed below:

$$F = \frac{D_i h_f}{D_i h_f + D_o U_l} \quad (9)$$

$$F_R = \frac{\dot{m} C_p}{\delta D_o L U_l} (1 - \exp(-\frac{F \pi D_o U_l L}{\dot{m} C_p})) \quad (10)$$

This equation almost matches with Hottel-Whillier-Bliss equation of flat plate collector. Here ' h ' is convective heat transfer coefficient $[h = N_u \times \frac{K}{D}]$ & ' F_R ' is an important design parameter because it is measure of the thermal resistance comes in the path of absorbed solar radiation in reaching the collector fluid. In equation ' $F_R U_l$ ' is a negative efficiency parameter and it has negative effect on useful heat gain further effect encountered on instantaneous efficiency of collector, which is defined by the ratio of useful heat gain to the incident radiation coming on the solar collector.

Thermophysical properties of MWCNT nanofluid and water

Thermal properties like thermal conductivity and viscosity of water was calculated through various experimental test runs on KD2 Pro conductivity meter and kinematic viscometer with different temperature. Experimentally measured density of water was found almost equivalent to standard density of water, therefore standard value of density was considered for research work. All experimental and standard results were used to calculate the thermophysical properties of MWCNT based nanofluid for both 0.01% and 0.02% weight fraction (Tables 3 and 4).

Results and Discussion

MWCNT based nanofluid used as working fluid

In this present study nanofluid was prepared at 0.01% and 0.02% of MWCNT in distilled water as base fluid with the application of Triton X-100 surfactant in appropriate amount. Prepared nanofluids

Thermal conductivity (K)	$1000 \frac{kg}{m^3}$
Density (ρ)	$1000 \frac{kg}{m^3}$
Dynamic viscosity (μ)	$0.854 * 10^{-3} \frac{Kg}{m-sec}$
Kinematic viscosity (ν)	$0.854 * 10^{-6} \frac{m^2}{sec}$
Specific heat (C_p)	$4.187 \frac{KJ}{kg-k}$

Table 3: Thermophysical properties of water.

Thermo physical Properties	Mixture I ($\phi_p = 0.01\%$) (MWCNT+ Distilled Water)	Mixture II ($\phi_p = 0.02\%$) (MWCNT + Distilled water)
Thermal Conductivity (K_{nf})	$0.617369817 \frac{W}{m-k}$	$0.617369817 \frac{W}{m-k}$
Dynamic viscosity (μ_{nf})	$0.000854213 \frac{Kg}{m-sec}$	$0.000854427 \frac{Kg}{m-sec}$
Kinematic viscosity (ν_{nf})	$0.854 * 10^{-6} \frac{m^2}{sec}$	$0.854 * 10^{-6} \frac{m^2}{sec}$
Specific heat ($C_{p,nf}$)	$4186.91 \frac{J}{kg-k}$	$4186.82 \frac{J}{kg-k}$
Density (ρ_{nf})	$999.925 \frac{kg}{m^3}$	$999.85 \frac{kg}{m^3}$

Table 4: Calculated thermo physical properties of MWCNT nanofluid.

as working fluid was flowing through collector receiver tube at different volume flow rates. It has been seen that overall thermal efficiency outcomes from 0.02% weight fraction MWCNT nanofluid at 160 L/h was 5.45% and higher than as comparison to results found at different fraction and with different flow rates. Figure showed that thermal efficiency of 0.02% weight fraction MWCNT nanofluid at 160 L/h was 12.63% measured, which is greater than other results of thermal efficiency from nanofluid at different weight fraction and volume flow rates. Further this experimental study also include heat losses in collector and it has been seen that $F_R U_i$ has a negative effect on instantaneous efficiency and useful heat gain, further calculated values of $F_R U_i$ in case of MWCNT nanofluid at various flow rates are shown in (Tables 5 and 6). Surfactant Triton X-100 is a non-ionic and high foaming surfactant, which reduces heat transfer b/w water and nanotubes. Surfactant mixed at higher amount with MWCNT nanofluid has also considerable negative effects on performance of solar collector [6]. Overall thermal efficiency of 0.02% MWCNT based nanofluid at 100 L/h showed poor results as comparison to other results outcomes from various experiments conducted

Different volume flow rate	F	F_R	$F_R U_i$
160 L/h	0.9754369	0.97186	12.9063
100 L/h	0.8586555	0.85422	11.3440

Table 5: $F_R U_i$ for parabolic trough collector with 0.01% MWCNT nanofluid.

Different volume flow rate	F	F_R	$F_R U_i$
160 L/h	0.9754437	0.97178	12.9052
100 L/h	0.8586919	0.85426	11.3467

Table 6: $F_R U_i$ for parabolic trough collector with 0.02% MWCNT nanofluid.

through MWCNT nanofluid and decrement in thermal efficiency can be due to higher viscosity of fluid and corresponding pressure drop at 100 L/h. It has also been seen that enhancement in thermal conductivity is dependent upon bulk temperature of nanofluid; Therefore Incremental change in mass flow rate has a considerable effect on bulk temperature and thermal conductivity of MWCNT nanofluid [6]. Further results of Thermal efficiency along with instantaneous energy production are shown graphically as below for different 0.01% & 0.02% volume concentration and at different decided flow rates 160 L/h and 100 L/h (Figures 5-8).

Water as working fluid

Water (base fluid) was used as working fluid in solar parabolic trough collector. Experimental study was done during 9: 00 am to 3: 00 pm and data related to inlet and outlet temperature, temperature difference, useful heat gain and efficiency of collector was measured at various flow rates. (Figures 9 and 10) showed graphical variations in thermal efficiency and instantaneous energy production of collector through water at 160 L/h and 100 L/h. Figure 10 showed maximum thermal efficiency was 7.28% measured during the time interval 11: 00-11: 30 am for water at 160 L/h and further maximum thermal efficiency at 100 L/h was 6.39% measured during the time interval 10: 30-11: 00 am. $F_R U_i$ is a negative efficiency parameter, which account an effect on performance of solar collector as discussed before and (Table 7) showed $F_R U_i$ for water used as working fluid in solar collector device.

Water showed higher value of ' F_R ' at 160L/h as comparison to ' F_R ' at 100 L/h. basically a heat removal factor is defined by the heat lost from the collector system and collector efficiency factor is completely opposite to heat removal factor, it means that how much heat absorbed by the collector system and denoted by ' F '. Thermal losses from the receiver tube can calculate through loss coefficient ' U_L ' and it depends upon area of receiver tube. Collector efficiency factor and loss coefficient can be calculated from similar expression as described for flat plate collector case. Parabolic trough collector is a type of concentrating collector and used to produce high temperature, which means that thermal radiations are important for evaluation of thermal losses and are temperature dependent.

Effect of inlet temperature and mass flow rate

Inlet temperature of fluid has considerable effect on collector performance, when inlet temperature of fluid is increasing results in surface temperature of absorber tube and convective losses from absorber tube are also increases. These losses are increases continuously with change in day time and have a negative effect on collector performance or instantaneous efficiency as shown in graphical results of MWCNT nanofluid and water. Mass flow rate of fluid also showed great effect on system performance because of

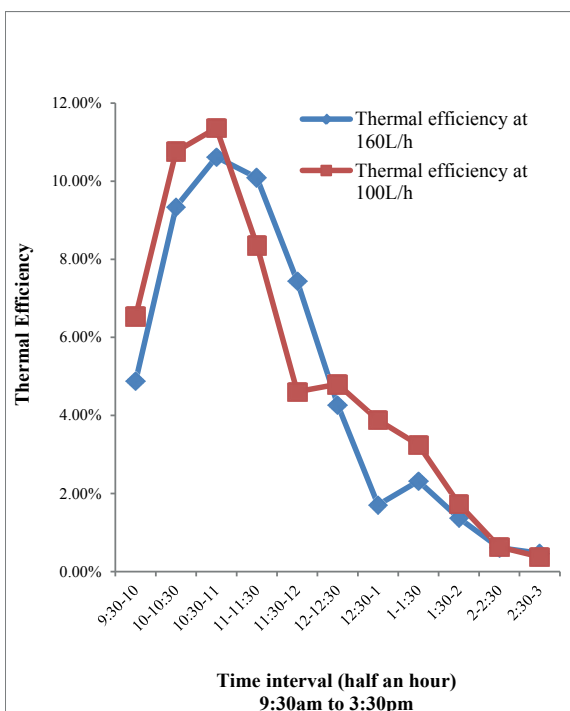


Figure 5: Thermal efficiency of MWCNT nanofluid at 160L/h & 100L/h with 0.01%.

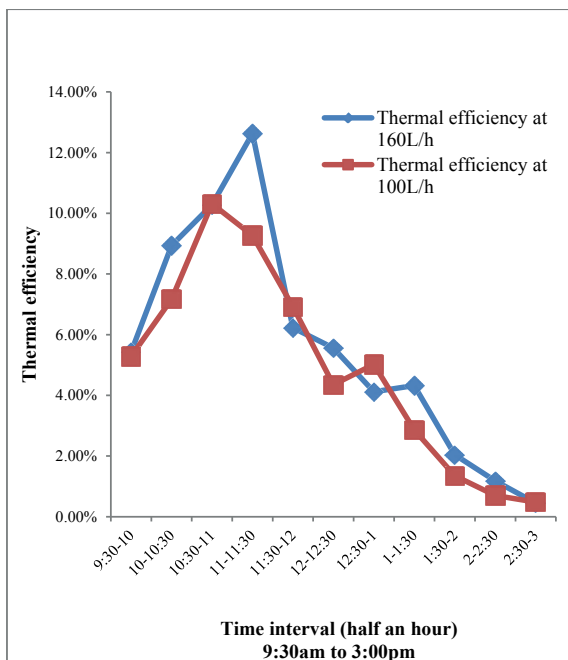


Figure 7: Thermal efficiency of MWCNT nanofluid at 160L/h & 100L/h with 0.02%.

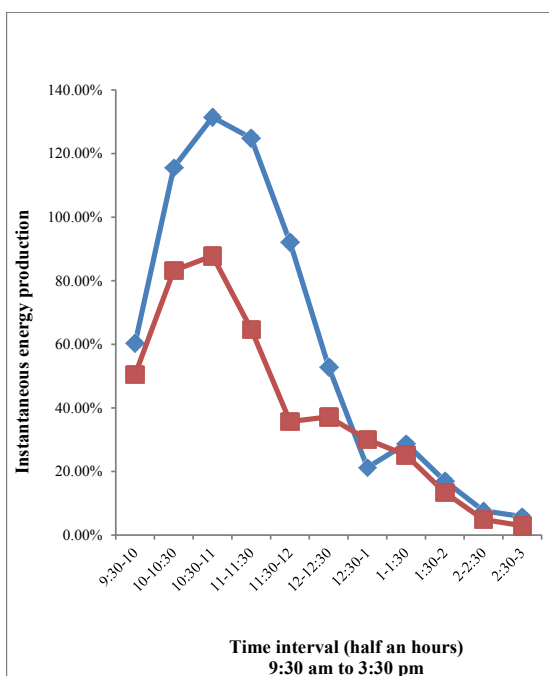


Figure 6: Instantaneous energy production of MWCNT nanofluid at 160L/h & 100L/h with 0.01%.

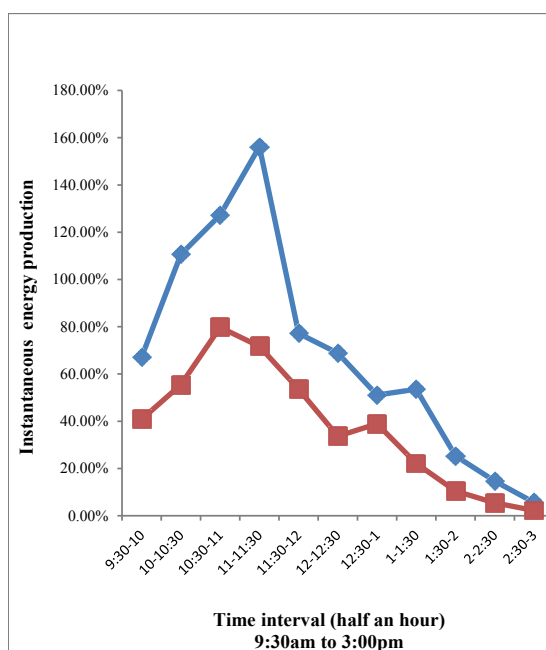


Figure 8: Instantaneous energy production of MWCNT nanofluid at 160L/h & 100L/h with 0.02%.

increasing coefficient of heat transfer increasing, which results in incremental change occur in collector efficiency factor and collector heat removal factor also increased as shown in Tables 5 and 6 for MWCNT nanofluid and also same behavior shown in Table 7 for water.

Conclusion

In this experimental study effect of MWCNT nanofluid on solar parabolic trough collector performance was investigated. The effect of mass flow rate of MWCNT nanofluid mixture containing Triton X-100 at different weight fraction 0.01% and 0.02% was studied. The results showed that 0.02% MWCNT nanofluid possess highest value

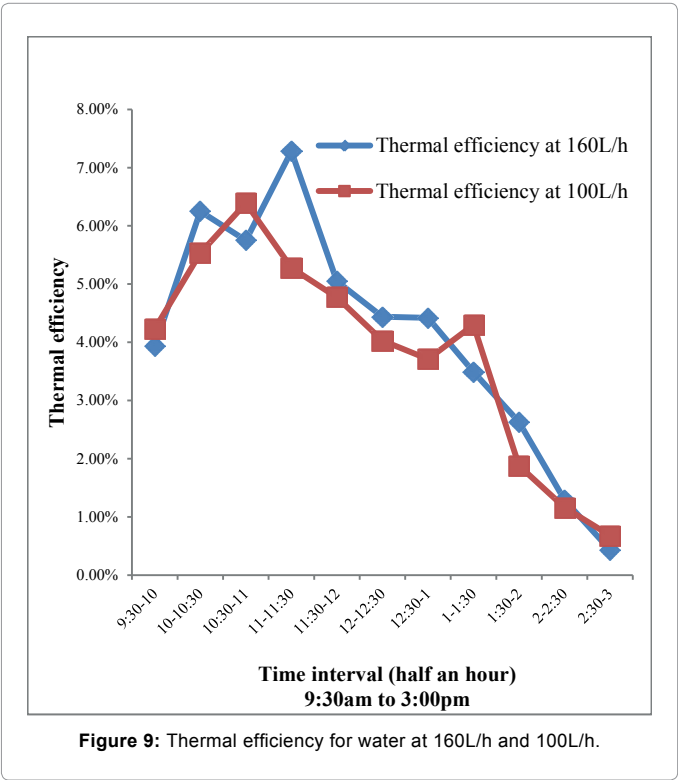


Figure 9: Thermal efficiency for water at 160L/h and 100L/h.

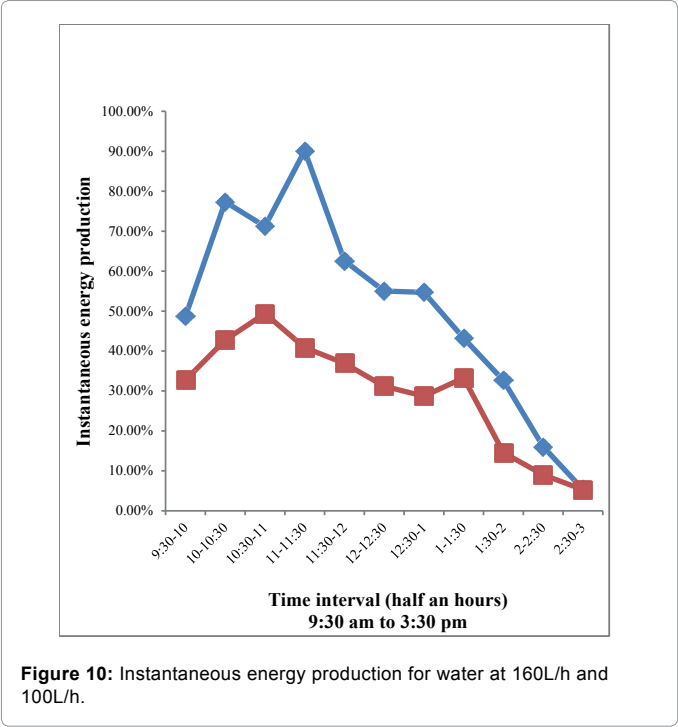


Figure 10: Instantaneous energy production for water at 160L/h and 100L/h.

Different volume flow rate	F	F _R	F _R U _i
160 L/h	0.975429002	0.97185	12.9061
100 L/h	0.858619195	0.85419	11.3436

Table 7: F_RU_i for parabolic trough collector with water as working fluid.

increased by increasing the mass flow rate of fluid was measured in this experimental study, which results in incremental change occur in efficiency.

Acknowledgement

I am very thankful to Mr. Kundan Lal, Assistant professor of Thapar University for allow me to conduct the experimental work on prototype of PTC system and I am also very grateful for his guidance and support enabled throughout my experimental procedure

References

1. Haddad Z, Abid C, Oztop HF, Mataoui A (2004) A review on how the researchers prepare their nanofluids. Int J Thermal Sci 76: 168-189.
2. Rastogi R, Kaushal R, Tripathi SK, Sharma AL, Kaur I, et al. (2008) Comparative study of carbon nanotube dispersion using surfactants. J Colloid Interface Sci 328: 421-428.
3. Davis VA, Ericson LM, Parra-Vasquez ANG, Fan H, Wang Y, et al. (2004) Phase behaviour and rheology of SWNTs in superacids. Macromolecules 37: 154-160.
4. Ding Y, Alias H, Wen D, Williams RA (2006) Heat transfer of aqueous suspension of carbon nanotubes (CNT nanofluids). Int J Heat Mass Transfer 49: 240-250.
5. Lotfi R, Rashidi AM, Amrollahi A (2012) Experimental study on the transfer enhancement of MWNT-water nanofluid in a shell and tube heat exchanger. International Communication in Heat Mass Transfer 39: 108-111.
6. Yousefi T, Veisy F, Shojaeizadeh E, Zinadini S (2012) An experimental investigation on the effect of MWCNT-H₂O nanofluid on the efficiency of flat-plate solar collectors. Exp Thermal Fluid Sci 39: 207-212.
7. Kasaeian A, Daviran S, Azarian RD, Rashidi A (2015) Performance evaluation and nano fluid using capability study of a solar parabolic trough collector. Energy Convers Manag 89: 368-375.
8. Yousefi T, Veisy F, Shojaeizadeh E, Zinadini S (2012) An experimental investigation on the effect of Al₂O₃-H₂O nanofluid on the efficiency of flat-plate solar collectors. Renewable Energy 39: 293-298.
9. Akhavan-Behabadi MA, Shahidi M, Aligoodarz MR (2015) An experimental study on heat transfer and pressure drop of MWCNT-water nano-fluid inside horizontal coiled wire inserted tube. Int Communication Heat Mass Transfer 63: 62-72.
10. Sukhatme SP, Nayak JK (2012) Solar Energy principles of thermal collection and storage. Tata McGraw-Hill Education.
11. Shaker M, Birgersson E, Mujumdar AS (2014) Extended Maxwell model for the thermal conductivity of nanofluids that accounts for nonlocal heat transfer. Int J Thermal Sci 84: 260-266.
12. Esfe MH, Saedodin S (2014) An experimental investigation and new correlation of viscosity of ZnO-EG nanofluid at various temperatures and at various temperatures and different solid fractions. Exp Thermal Fluid Sci 55: 1-5.
13. Sunil K, Kundan L, Sumeet S (2014) Performance evaluation of a nanofluid based parabolic solar collector – an experimental study. Proceedings of Twelveth IRF International Conference.

of thermal, overall thermal and instantaneous energy production among other concentration of nanofluid and water and further also at different flow rates. 0.02% MWCNT nanofluid at 160 L/h showed lowest amount of F_RU_i and highest value for collector efficiency factor among other concentration of fluid. Temperature difference

Bus Implementation using New Low Power PFSCCL Tri-state buffers

Neeta PANDEY¹, Bharat CHOUDHARY¹, Kirti GUPTA², Ankit MITTAL³

¹ Dept. of Electronics and Communication Engineering, Delhi Technological University, Delhi, India

²Dept. of Electronics and Communication Engineering, Bharati Vidyapeeth's College of Engineering, Delhi, India

³Dept. of EEE/E&I, Birla Institute of Technology, Pilani University (K. K. Birla Goa Campus), Goa, India

n66pandey@rediffmail.com, bharatruhela@gmail.com, kirtigupta22@gmail.com, ankitmttl63@gmail.com

Abstract:- This paper proposes new positive feedback source-coupled logic (PFSCCL) tri-state buffers suited to bus applications. The proposed buffers use switch to attain high impedance state and modify the load or the current source section. An interesting consequence of this is overall reduction in the power consumption. The proposed tri-state buffers consume half power than the available switch based counterpart. The issues with available PFSCCL tri-state buffers based bus implementation are identified and benefits of employing the proposed tri-state buffer topologies are put forward. SPICE simulation results using TSMC 180 nm CMOS technology parameters are included to support the theoretical formulations. The performance of proposed tri-state buffer topologies is examined on the basis of propagation delay, output enable time and power consumption. It is found that one of the proposed tri-state buffer topology outperforms in terms of all the performance parameters. An examination of behavior of available and the proposed PFSCCL tri-state buffer topologies under parameter variations and mismatch shows a maximum variation of 14 %.

Keywords

SCL, PFSCCL, Tri-state buffer, Bus

1. Introduction

Conventional CMOS circuits are widely used in digital integrated circuit design due to their design ease, high packing density and negligible static power consumption [1]. The large switching noise generation in CMOS circuits restricts their use in applications pertaining to mixed signal environment [2, 3]. Research efforts are therefore, made towards exploring alternate low-noise logic styles. These logic styles are based on the current steering principle [4-7] and draws a constant current from power supply and generates low switching noise in comparison to CMOS logic style. Positive feedback source coupled logic (PFSCCL) style [6-10] is one among these styles that works on current steering principle and is used in high speed designs.

This paper addresses implementation of PFSCCL busses employed to transfer data between various peripherals inside the microprocessors based systems in mixed-signal environments. A typical bus system has many tri-state buffers attached to a common node. The study of PFSCCL tri-state buffers/inverters reveals that only two topologies are available [11]. These topologies use either a switch or a sleep transistor to attain the tri-state behavior. The suitability of the sleep transistor and the switch transistor based PFSCCL tri-state buffers [11] in bus system implementation is investigated and the drawbacks are identified. New PFSCCL tri-state buffers for this purpose are presented in this work.

The paper is organized in six sections including the introductory one. A brief review of available PFSCCL tri-state buffers is presented in section 2. Design issues in implementing bus system using

the available tri-state buffers are identified in section 3. Thereafter, the new PFSCCL tri-state buffer topologies are presented in section 4. Their performance comparison and suitability in bus implementation are demonstrated through SPICE simulations by using TSMC 180 nm CMOS technology parameters in section 5. The impact of parameter variations and the effect of parameter mismatch are also studied for the proposed topologies. Lastly, the paper is concluded in section 6.

2. Available PFSCCL tri-state buffers

A tri-state gate exhibits a high impedance state in addition to high and low logic levels attained by a regular gate. An additional Enable signal is employed to achieve the desired functionality. In literature, two topologies to implement PFSCCL tri-state buffer are available [11]. These topologies use either a switch or a sleep transistor to attain a high impedance state.

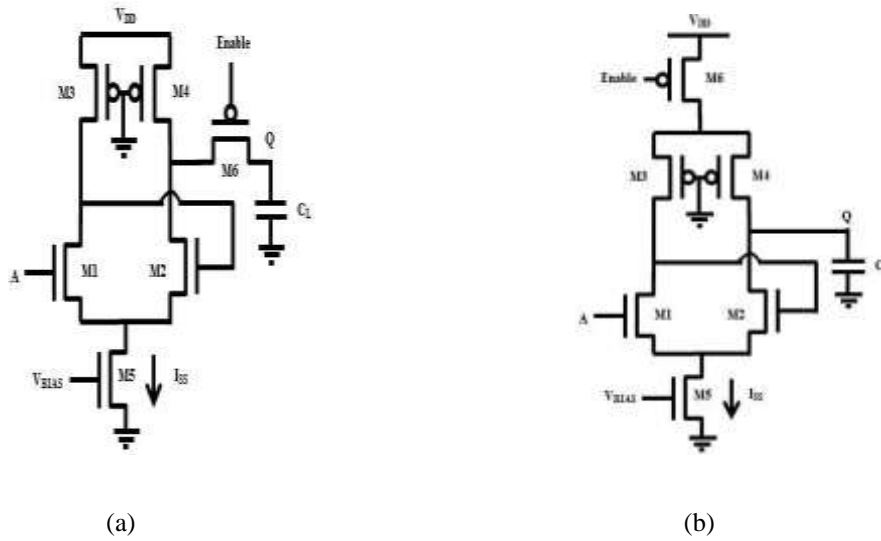


Fig. 1: Available PFSCCL tri-state buffers [11] a) switch based b) sleep based

A switch based PFSCCL tri-state buffer is shown in Fig. 1a. A transistor M6 is added to the output of the regular PFSCCL gate to achieve tri-state operation. For low value of Enable signal, transistor M6 is ON and the circuit acts as a regular buffer. Conversely, a high value of Enable signal turns transistor M6 OFF and provides a high impedance state at the output by disconnecting the regular buffer output to the actual output node Q. Therefore, it can be noted that this tri-state buffer maintains a current in the circuit irrespective of the state of gate.

The other PFSCCL tri-state buffer [11], drawn in Fig. 1b uses a sleep transistor M6 in series to the power supply terminal of the basic PFSCCL buffer. It acts as regular buffer for low value of Enable signal by turning ON transistor M6 while providing a high impedance state at the output, otherwise. The sleep based tri-state buffer is claimed to be more power efficient over the switch based counterpart due to the fact that no current flows in the circuit (Fig. 1b) during high impedance state.

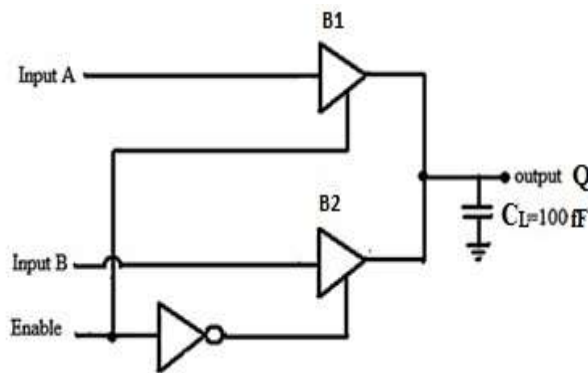
3 Issue in Bus Implementation

The discussion on the available PFSCCL tri-state buffers indicates that the sleep based topology is more power efficient than the switch based counterpart. However, bus implementation using sleep transistor based PFSCCL tri-state buffers suffers a major drawback of incomplete isolation of the common output node from the tri-state disabled buffers.

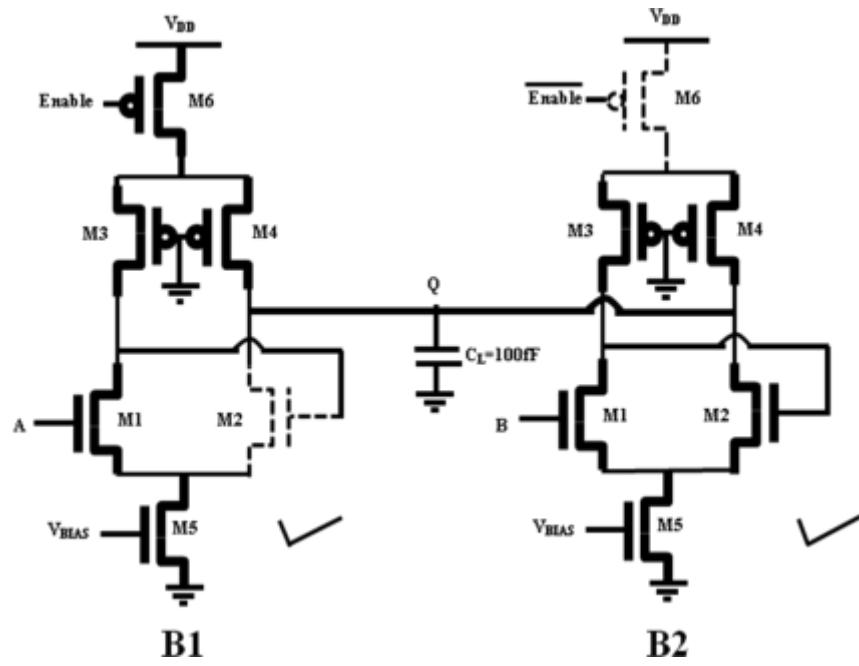
To illustrate this, a typical bus environment consisting of two tri-state buffers driving a common output node is considered. The test bench is shown in Fig. 2a. In this environment, for a low value of Enable signal, B1 is enabled while B2 operates in high impedance state and vice-versa. The test bench is simulated by using the sleep and the switch based tri-state buffers and the corresponding complete MOS based schematics are shown in Fig. 2b and 2c. When the sleep based tri-state buffers are employed (Fig. 2b), a low value of Enable signal enables B1 whereas B2 moves in high impedance state by disconnecting the output node from its power supply. In this condition, on careful examination of the circuit, it is found that as the pull down network (PDN) of B2 is still connected to the output node, a path for the current to flow from the power supply of B1 to ground via the output node Q and B2 still exists. To make this point clear let us consider both inputs A and B as high. In this condition transistor M1 of buffer B1 and both the transistors in PDN of buffer B2 would be ON leading to drawing more bias current from power supply than that of an individual enabled buffer. It is pictorially represented in Fig. 2b by marking ON transistors by bold lines and OFF transistors by dotted lines. The tick mark in the figure signifies a current flow in the current source section. Hence, the isolation of the output node Q from the buffer B2 is not established. This causes malfunctioning of the whole bus system by altering the magnitude of the high and low logic levels. The degradation in the output levels will increase with the increase in number of gates connected to the common node Q. Also the functionality of the device which will be driven by the output of sleep based tri-state buffer may completely be disrupted.

For the switch based tri-state buffer based bus implementation (Fig. 2c), a low value of Enable signal makes switch transistor M6 of buffer B1 ON and that in buffer B2 OFF. The ON and OFF transistors for input A and B high are shown by bold and dotted lines whereas a tick mark represents a current flow in the current source section in the Fig. 2c for the sake of completeness. It is, therefore, clear that the output follows input A and remains unaffected by input B. It, however, lacks in terms of power as both buffers draw current from the power supply irrespective of their state i.e. enabled or disabled.

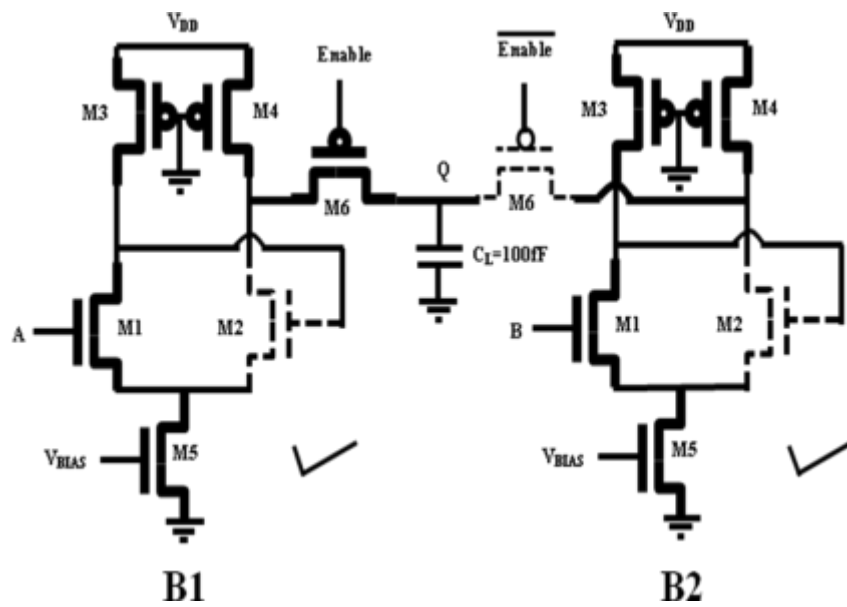
The timing waveforms demonstrating this behavior is shown in Fig. 3. The test bench is simulated with a power supply of 1.8 V and a voltage swing of 400 mV is considered for the inputs. It can be observed that correct voltage levels at the output is achieved for the switch based ones in contrast to the sleep based bus system.



(a)



(b)



(c)

Fig. 2 a) Simulation test bench b) Bus operation by using sleep based tri-state buffers c) Bus operation by using switch based tri-state buffers

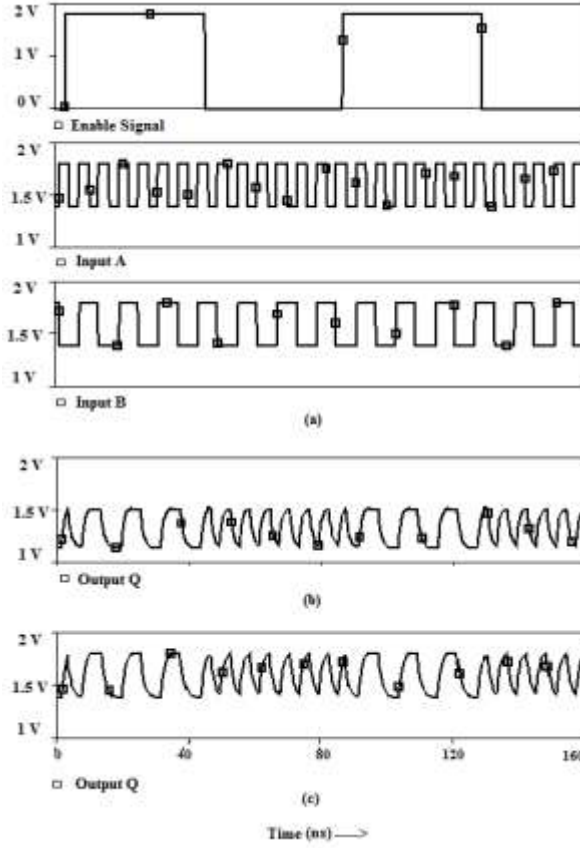


Fig. 3 Timing waveform for bus implementation (a) input signals: Enable, A and B (b) output of sleep transistor based bus (c) output of switch transistor based bus

4. New PFSCCL Tri-state Buffer Topologies

In this section, new PFSCCL tri-state buffer topologies derived from the available switch based tri-state buffer are presented. All the topologies use an output switch to attain the high impedance state and save power by not allowing the current flow in the high impedance state. The current flow is restricted by modifying either the load or the current source section of the PFSCCL switch based tri-state buffer. The resulting topologies are accordingly classified into two categories. The topology with the modified load section are presented first and is followed by the topologies with modified current source section.

4.1. PFSCCL tri-state buffer with modified load section (Proposed Topology 1)

This topology modifies the load by driving the load transistors with an Enable signal instead of a fixed ground potential. The resulting topology is depicted in Fig. 4. For a low value of Enable signal, the circuit behaves as a regular PFSCCL buffer. On the contrary, for high value of Enable signal transistors M3, M4 and M6 are OFF so the buffer enters in the high impedance state and restrict the current flow in the circuit thereby providing overall reduction in power consumption.

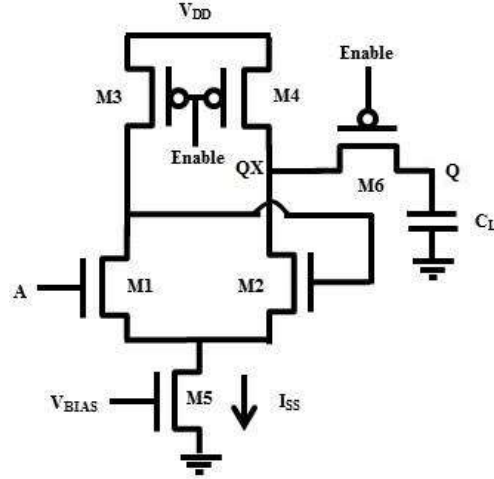


Fig. 4 Proposed Topology 1

4.2. PFSCCL tri-state buffers with modified current source section

4.2.1 Proposed Topology 2

This topology modifies the current source section by adding a PMOS transistor M7 below the current source transistor M5 as shown in Fig. 5a. When Enable signal is low, the circuit behaves as a regular PFSCCL buffer. Conversely, for high value of Enable signal, the transistors M6, M7 are OFF. This allows the circuit to enter high impedance and avoids any current flow in this duration.

4.2.2 Proposed Topology 3

In the proposed topology 2, the addition of the PMOS transistor below the current source requires a higher value of bias voltage (V_{BIAS}) in comparison to the one required in conventional PFSCCL buffer in order to maintain the same current value (I_{SS}). This situation can be addressed by altering the placement of the transistors M5 and M7 as shown in Fig. 5b. A low value of Enable signal allows normal operation by providing a path to ground via transistor M7. Analogously, for a high value of Enable signal the path to ground is disconnected by turning OFF the said transistor. At this point, the transistor M6 is OFF therefore the circuit enters the high impedance state and does not consume power.

4.2.3 Proposed Topology 4

The proposed topologies 2 and 3 use stacking of the transistors in the current source section to reduce power consumption. In proposed topology 4, an alternate approach to avoid current flow in the circuit is presented. The availability of bias voltage to the current source is made dependent on Enable signal by using a PMOS transistor M7 and an NMOS transistor M8 as shown in Fig. 5c. For a low value of Enable signal, the transistor M5 receives the necessary biasing through transistor M7. At this point the transistor M6 is ON and the topology behaves as a regular buffer. Conversely, when Enable signal is high, the transistor M7 is OFF and the transistor M8 is ON. This discharges the potential of node X to the ground potential and consequently disables the current source. Therefore the buffer does not consume power and high impedance state is achieved as transistor M6 is turned OFF.

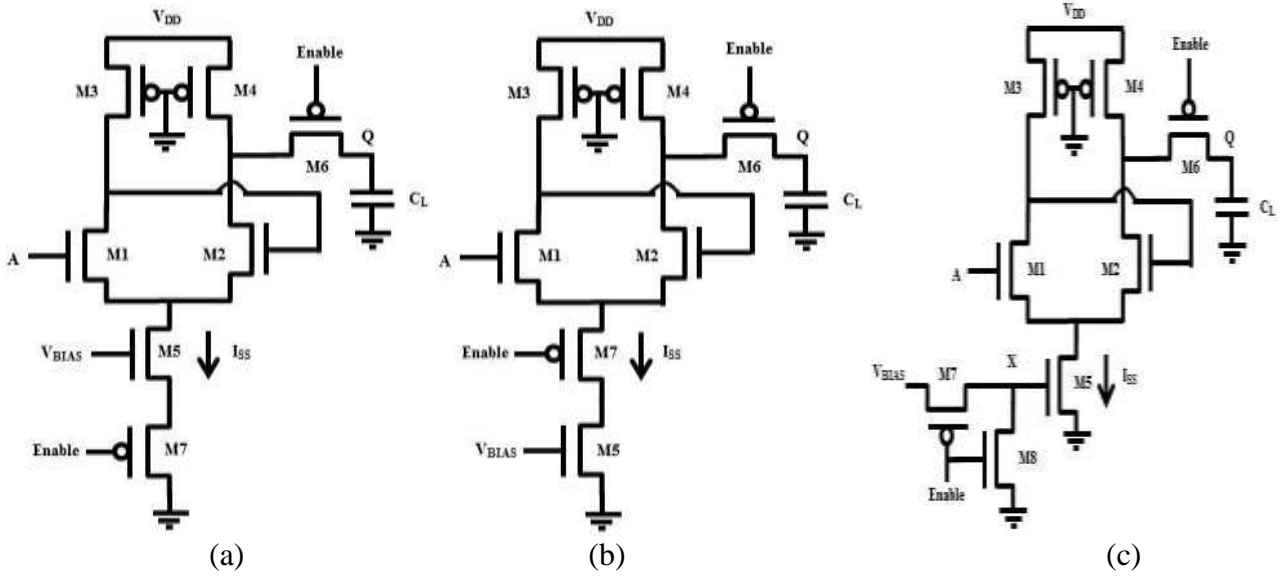


Fig. 5 Proposed PFSCCL tri-state buffer a) Topology 2 b) Topology 3 c) Topology 4

5. Simulation Results and Discussion

The section first compares performance of proposed PFSCCL tri-state buffers and thereafter verifies their suitability for bus system implementations through simulations. The TSMC 180 nm CMOS technology parameters and power supply of 1.8 V are taken in all the SPICE simulations. The bias current and voltage swing of 50 μ A and 400 mV respectively are considered **for all PFSCCL tri-state buffers** uniformly.

5.1. Performance Comparison

The proposed PFSCCL tri-state buffer topologies 1-4 (Fig. 4 and 5) and available switch based PFSCCL tri-state buffer (Fig. 1a) are simulated with a load capacitance of 50 fF. The performance is compared in terms of propagation delay, output enable time, power consumption and power delay product. The simulation results are summarized in Table 1.

It is found that all the proposed topologies consume half the power than the available switch based PFSCCL tri-state buffer [11] due to the fact that they all possess the provision of disabling the current flow in the high impedance state. In terms of propagation delay, it can be observed that all the topologies have almost equal delays since all of these possess similar loads and maintains same bias current in the enabled state. These two factors account for the low power-delay product values for the proposed topologies in comparison to the available one. A maximum reduction of 47 % in the power delay product is obtained in proposed topologies.

There is a variation in the output enable time of the tri-state buffers which, therefore, needs little more investigation on the behavior during high impedance state.

- For proposed topology 1 (Fig. 4), wherein the load is modified, it is to be noted that, transistors in the pull down network (M1-M2) and current source (M5) sections are ON. This condition leads to discharging of node QX to the ground potential. Subsequently, when the gate is enabled, the node QX will attain the valid low or high voltage levels depending upon the applied input. This explains longer output enable time in proposed topology 1.
- For the proposed topologies 2-4 (Fig. 5), current source section is modified. Out of these

three, the topology-4 (Fig. 5c) shows the longest output enable time. It can be attributed to the fact that a proper V_{BIAS} , at node X, will be established through M7 whereas in the remaining two topologies, the path from common source coupled point to the ground is instantly established the moment the buffer is enabled. The topology 2 uses larger bias voltage than topology 3 explains its longer output enable time.

- The proposed topology 3 shows the best output enable time among the available and the proposed topologies which is due to interaction of internal node capacitances.

Tab.1: Summary of performance parameters for proposed and available PFSCCL tri-state buffers

Parameter Tri-state Buffer	Propagation Delay (ps)	Output Enable Time (ps)	Power (μW)	Power Delay Product (fJ)
Proposed Topology 1	425	553	45	19.125
Proposed Topology 2	419	348	45	18.855
Proposed Topology 3	408	132	45	18.360
Proposed Topology 4	428	438	45	19.260
Switch based buffer [11]	430	182	90	38.700

The impact of parameter variations is also examined for all proposed and available switch based PFSCCL tri-state buffers at different design corners and are plotted in Fig. 6. It is observed that the proposed tri-state buffer topologies show maximum variations in the propagation delay, the output enable time, the power consumption and the power delay product by a factor of 1.3, 4.35, 1.8 and 1.31 between the best/worst and typical cases respectively. Similarly, the available switch based PFSCCL tri-state buffer shows maximum variations by a factor of 1.08, 3.14, 1.55 and 1.14 for all above performance parameters respectively.

The effect of width mismatch is also studied for all proposed and available switch based PFSCCL tri-state buffer topologies. The widths of the transistors are varied by 10% corresponding to which a maximum change of 11% is observed in propagation delay, 14% in output enable time and 8% in power consumption.

Further, to explore the feasibility of working of proposed topologies at lower potential, it is necessary to compute minimum power supply requirement. Using the method outlined in [12] it is found that the minimum power supply requirement for topologies 1 - 4 is respectively given as

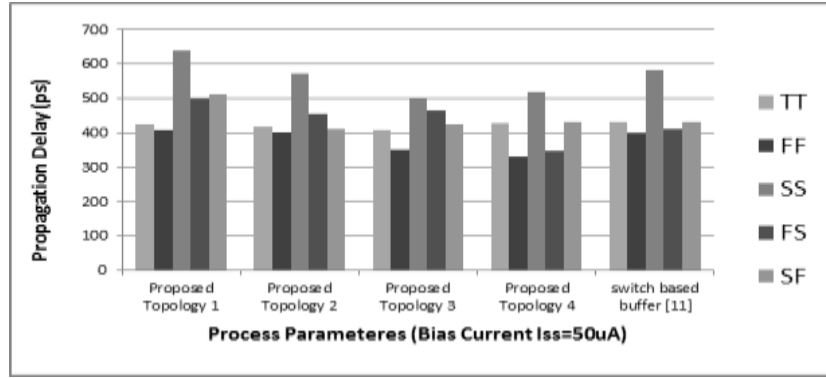
$$V_{DD_MIN_topology1} = 2V_{BIAS} - V_T \quad (1)$$

$$V_{DD_MIN_topology2} = 2V_{BIAS} - V_T + |V_{TP}| \quad (2)$$

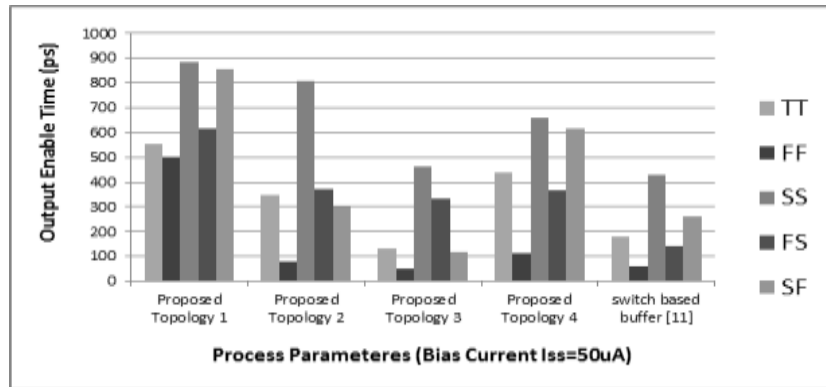
$$V_{DD_MIN_topology3} = 2V_{BIAS} - V_T + I_{BIAS}R_P \quad (3)$$

$$V_{DD_MIN_topology4} = 2V_{BIAS} - V_T \quad (4)$$

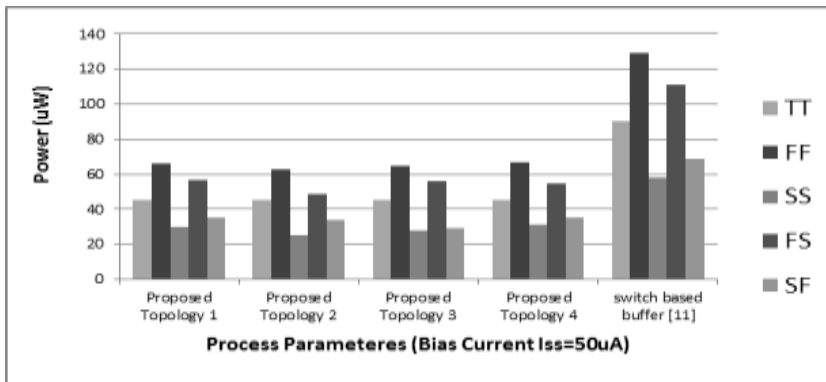
where V_T and V_{TP} is threshold voltages of NMOS and PMOS transistors. The V_{BIAS} is the biasing voltage of transistor M5 and R_P is resistance of PMOS transistor. Assuming V_{BIAS} of 0.8 V, the minimum supply voltage for topology 1 and 4 is 1.1V. It is equal to 1.6 V for topology 2 and slightly larger than 1.1 V for topology 3 as $I_{BIAS}R_P$ is very small in comparison to other terms in the expression.



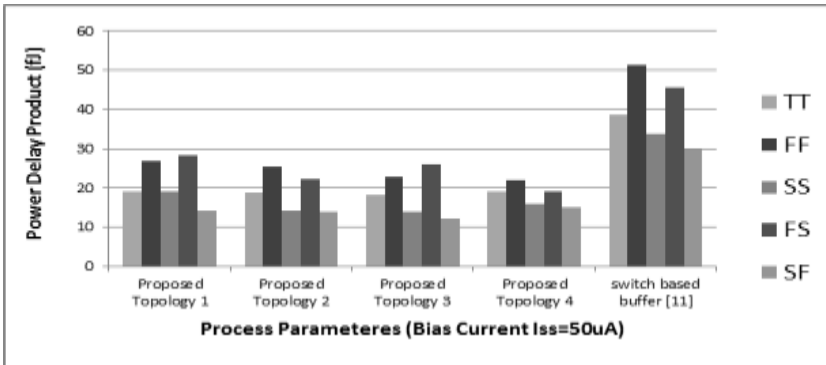
(a)



(b)



(c)



(d)

Fig. 6 Impact of parameter variations on (a) propagation delay (b) output enable time (c) power (d) power delay product at different design corners

5.2. Bus system implementation

After performance comparison of the PFSCCL tri-state buffers, their suitability in bus system implementation is now explored. The test bench shown in Fig. 2a is considered and is simulated with all proposed and available PFSCCL tri-state buffer topologies. The simulation waveforms are shown in Fig. 7. It is found that all proposed tri-state buffers maintain the same voltage levels as the available one. Also, none of the proposed tri-state buffers exhibits the variation in the voltage levels as observed in the case of the sleep based PFSCCL tri-state buffers. Hence, it can be stated that proposed tri-state PFSCCL buffers conform to the functionality.

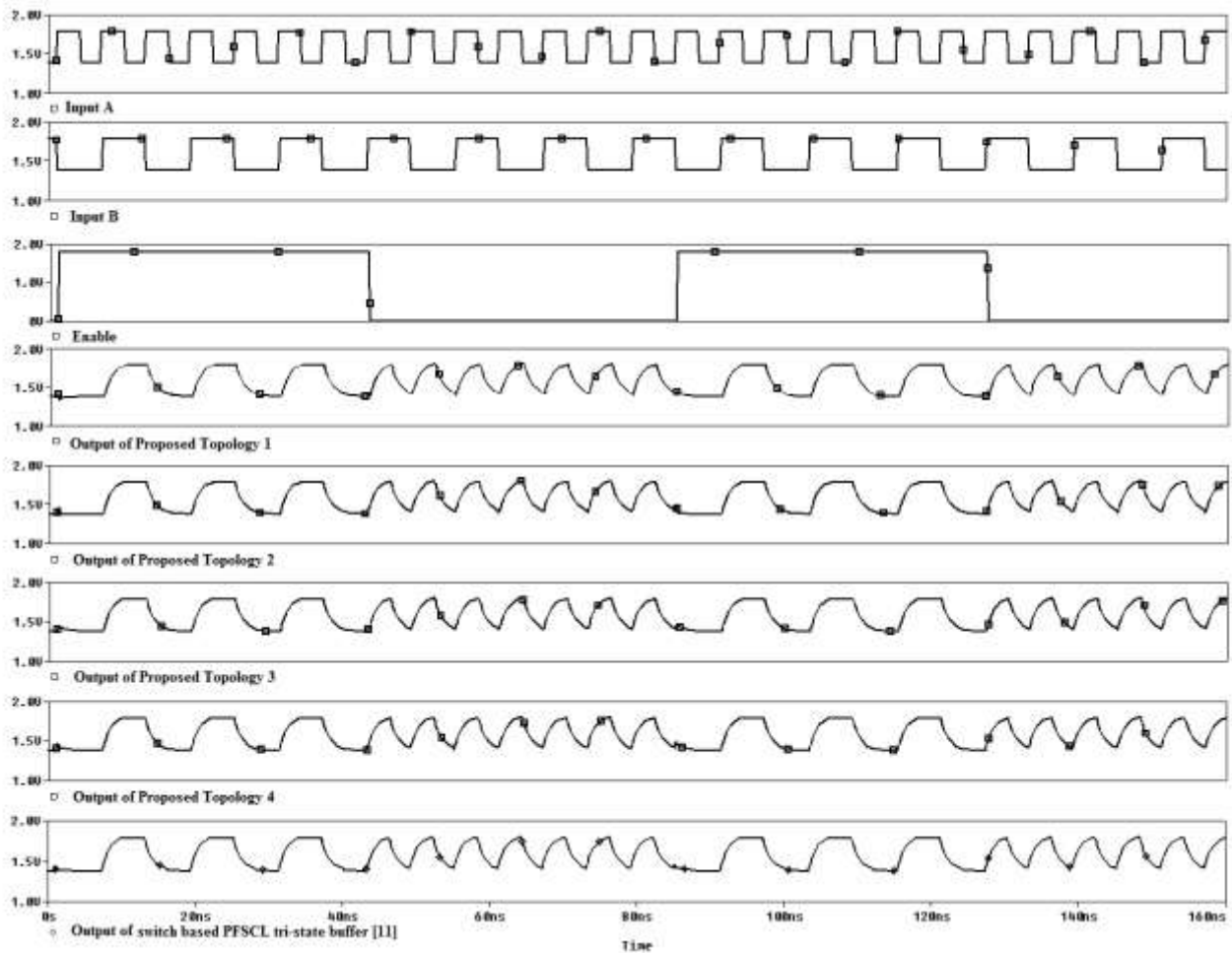


Fig. 7. Simulation waveforms of the proposed and available switch based [11] PFSCCL tri-state buffer topologies.

6. Conclusion

In this paper, implementation of a bus employing tri-state PFSCCL buffers is presented. The drawbacks in the bus realization using the available PFSCCL tri-state buffers are put forward and different switch based PFSCCL tri-state buffer topologies are proposed. The load or the current source sections of the available switch based PFSCCL tri-state buffer are modified which culminate in reduced power consumption. The performance of proposed buffer topologies is compared through simulations by using 180 nm TSMC CMOS technology parameters. The results indicate that one of the proposed buffer topology outperforms the others in terms of the propagation delay,

the output enable time and the power consumption. The impact of parameter variations and the effect of parameter mismatch are also included for completeness.

References

- [1] WESTE, N. and K. ESHRAGHIAN. *Principles of CMOS VLSI Design: A System Perspective*. Boston (USA): Addison-Wesley, 1993.
- [2] KIAEI, S., CHEE and D. ALLSTOT. CMOS source-coupled logic for mixed-mode VLSI, In: *Proceedings of International Symposium on Circuits and Systems*.1990, p. 1608–1611.
- [3] MALEKI, M. and S. KIAEI. Enhancement source-coupled logic for mixed-mode VLSI circuits. *IEEE Transactions on Circuits and Systems-II*.1992, vol. 39, pp. 399-402.
- [4] ALLSTOT, D., S. CHEE, S. KIAEI, and M. SHRISTAWA. Folded source-coupled logic vs. CMOS static logic for low-noise mixed-signal ICs. *IEEE Transactions on Circuits and Systems-I*.1993, vol. 40, pp. 553–563.
- [5] YAMASHINA, M. and H. YAMADA. An MOS current mode logic (MCML) circuit for low-power sub-GHz processors. *IEICE Transactions*, October 1992, E75-C.
- [6] ALIOTO, M., L. PANCIONI, S. ROCCHI and V. VIGNOLI. Modeling and evaluation of positive-feedback source-coupled logic. *IEEE Transactions on Circuits and Systems.-I*. Regular Papers, 2004, vol. 51, pp. 2345–2355.
- [7] GUPTA, K., R. SRIDHAR, J. CHAUDHARY, N. PANDEY and M. GUPTA. Performance Comparison of MCML and PFSC L Gates in 0.18 μm CMOS Technology. In: *Proceedings of IEEE ICCCT*.2011.
- [8] PANDEY, N., K. GUPTA, and M. GUPTA. An Efficient triple-tail cell based PFSC L D Latch. *Microelectronics Journal*. 2014, vol. 45, pp. 1001-1007.
- [9] ALIOTO, M., A. FORT, L. PANCIONI, S. ROCCHI and V. VIGNOLI. An approach to the design of PFSC L gates. In: *Proceedings of IEEE Symposium on Circuits and Systems*.2005, pp. 2437–2440.
- [10] ALIOTO, M., L. PANCIONI, S. ROCCHI and V. VIGNOLI. Power-Delay-Area-Noise Margin Trade-offs in Positive-Feedback MOS Current-Mode Logic, *IEEE Transactions on Circuits and Systems.-I*, Regular Papers, **54** (2007), pp. 1916-1928.
- [11] GUPTA, K., R. SRIDHAR, J. CHAUDHARY, N. PANDEY and M. GUPTA. New Low-Power Tri-state Circuits in Positive Feedback Source-Coupled Logic. *Journal of Electrical and Computer Engineering*. Volume 2011, Article ID 670508, 6 pages.
- [12] HASSAN, H., ANIS, M., ELMASRY, M. Analysis and Design of Low-Power Multi-Threshold MCML, in: *Proceedings of the IEEE International Conference on System-on-Chip*. 2004, pp. 25-29.

Comparative study of thermal stability of filled and un-filled multiwalled carbon nanotubes

Lucky Krishnia¹, Reetu Kumari¹, Vinay Kumar¹, Anshika Singh¹, Preeti Garg²,
Brajesh S. Yadav², Pawan K. Tyagi^{1*}

¹Department of Applied Physics, Delhi Technological University, Bawana Road, Delhi 110042, India

²Solid State Physics Laboratory, Lucknow Road, Timarpur, Delhi 110054, India

*Corresponding author. Tel: (+91) 11-27852212; Fax: (+91) 11- 27871023; E-mail: pawan.phy@dce.edu

Received: 09 September 2015, Revised: 30 November 2015 and Accepted: 03 January 2016

ABSTRACT

Filled or un-filled multiwalled carbon nanotubes (CNTs) used in this study have been synthesized by the floating catalyst method and fixed catalyst method, respectively. The thermal stability of filled/un-filled carbon nanotubes has been investigated by using Thermogravimetric analysis (TGA) and Derivative thermogravimetric (DTG) analysis. In this report, we have developed a methodology to distinguish between filled and un-filled carbon nanotubes. Filled-CNTs are found to be more resistant to oxidation than the un-filled carbon nanotubes. The calculated activation energy of as-grown filled CNTs, by using differential method, determined to be 3.29 ± 0.04 eV, which is higher than that of highly ordered pyrolytic graphite (HOPG). Carbonaceous impurities; amorphous carbon, catalyst and CNT of different diameter, which are structurally different, are identified by their reactivity and the resistance to oxidation. Copyright © 2016 VBRI Press.

Keywords: Carbon nanotubes; thermogravimetric analysis; derivative thermogravimetric analysis; highly ordered pyrolytic graphite.

Introduction

Carbon nanotubes since their discovery in 1991 [1] owing to their distinctive electronic and mechanical properties have raised much interest. Their astonishing properties: electrical conduction beyond copper, thermal conduction beyond diamond, tougher than diamond, and stronger than steel, etc. have generated a huge interest and engendered innumerable potential applications in various fields [2–6]. Besides these well-known applications recently much research interest has been shifted to 3D carbon nano-network [7], where CNT are connected through either by coating of amorphous carbon [8] or reduced graphene [9]. Recently this network has been envisioned as a superior architecture for lithium ion battery [7]. Further, development of carbon based 3D materials include aerographite [10] as well as 3D graphene networks [9] have been demonstrated their utilization in flexible magnetic aerogels [11], stiff magnetic nanopaper [11], ultralight and flexible supercapacitor electrodes [12], Li batteries [7, 13], conducting composite materials for sensor and photonic applications [14]. Most promising application of CNTs is reported by Mecklenburg Matthias *et al.* [10]. They have reported the synthesis of 3D interconnected structure of carbon microtube called as aerographite of remarkable enhanced mechanical strength and conductivity. In order to further explore the applications CNTs possess high thermal stability, high mechanical strength, electrical or thermal conductivity as well as purity are prerequisite. Thus, many research groups have used various methods for the synthesis of CNTs, for example, thermal chemical

vapor deposition [15–17], plasma enhanced chemical vapor deposition [18, 19], laser ablation [20] and arc discharge [21]. But, so far, synthesis of CNTs having quality and purity as needed for specific application is still a challenge. So, we need a simple method not only for synthesis but also to ensure the purity and quality of carbon nanotubes.

Carbon nanotubes grown by using either physical or chemical routes have mainly two kinds of impurities one being the metallic impurities and the other being carbonaceous impurities [22]. Carbonaceous impurities include graphitic particles, amorphous carbon and CNT of different wall numbers. From the existing methods of analysis Thermogravimetric analysis (TGA) technique seems to be the most promising technique as it gives information about the presence of the metallic impurities, amorphous carbon and other carbonaceous structures and even the defect contents in carbon nanotubes. Thermogravimetric technique not only provides the metal contents, but also thermal stability of the contents can be studied in detail. However, oxidation temperature and thermal stability of un-filled CNTs have been studied in many reports [23–29]. Among all the reports to date, no reports have been published on how to identify the carbon impurities present in the as-grown CNT sample by using TGA. Furthermore, thermal stability of filled-CNT is also not much explored [30]. In filled-CNT, concave geometry of hollow core with confined space offers the tremendous possibility to generate the nanomaterial of superior electronic, physical or chemical properties [31]. This has been attributed to the fact that in filled-CNT, tube-walls not only protect the filled nanomagnets against harsh

environment but also prohibit coalescence. In previous reports [32,33], CNTs filled with ferromagnetic materials have been proposed as a novel material and have numerous potential applications such as biomedicine [34], spintronics [35], magnetic recording media [36] and magnetic force microscopy (MFM) [37]. Hence comparative study of thermal stability of filled as well as un-filled CNTs is desirable.

In this work, we report a simple procedure to identify the crystallinity as well as purity of the plethora of CNT by merely studying the thermal stability and differentiating the activation energy of oxidation for various carbonaceous structures present in sample. In presented study we have identified the type of impurities present in the sample and activated energy was calculated for the different variants of MWCNTs. The calculated values of activation energy of filled-CNTs have been compared with activation energy for the oxidation of highly oriented pyrolytic graphite (HOPG) [38]. Here HOPG is used as reference to access the crystallinity of CNT because HOPG possess high crystallinity as well as low defect concentration. If the activation energy of CNTs is found to be of the order of HOPG, then one can claim that the CNTs are of high purity and have low defect concentration. Furthermore, present work intend to confirm that thermogravimetric analysis (TGA) could be considered as a reliable technique to identify the crystallinity and purity of the plethora of CNT unlike Raman spectroscopy and high resolution transmission electron microscopy (HRTEM) which only probe the individual CNT.

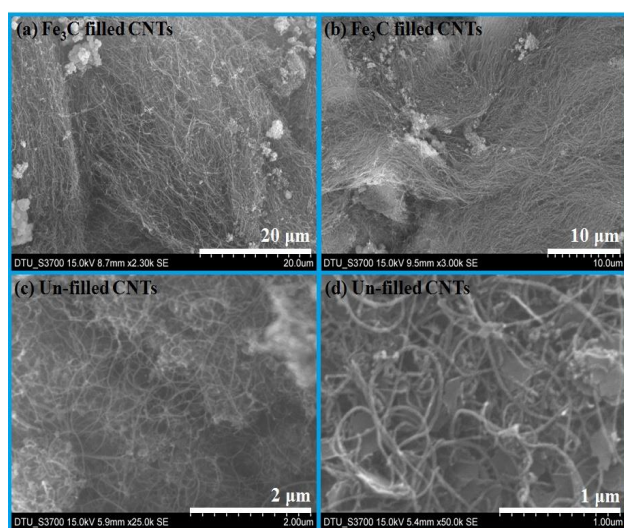


Fig. 1. SEM images (a) & (b) for Fe_3C filled CNTs synthesized by floating catalyst method, (c) and (d) un-filled CNTs synthesized by fixed catalyst method.

Experimental

The Fe_3C filled as well as un-filled CNTs were grown by thermal chemical vapor deposition method. The Fe_3C filled CNTs were synthesized using ferrocene as a floating catalyst. The precursor solution of ferrocene/toluene was made to flow in the system's pre heating zone with argon as a carrier gas. The temperature of the heating zone is kept 825°C . More details are given in [39]. The un-filled CNTs

were grown by using Fe: Mo: MgO (1:1.5:10) as a catalyst. Ethanol was used as carbon precursor. Synthesis temperature for un-filled CNT is 840°C . To carry the vapors of ethanol, argon gas of optimized flow rate 150 sccm was used. The morphology and structure of CNTs were analyzed by XRD (Bruker D8 – Advance) and SEM (Hitachi S-3700N).

Results and discussion

Microstructural analysis

SEM micrographs of Fe_3C filled CNTs and un-filled CNTs have shown in **Fig. 1**, where plenty of CNTs can be clearly seen. CNTs in **Fig. 1(a, b)** are found to be straight in comparison to that in (c) and (d) in which the CNTs are twisted. This may be due to the fact that either CNTs are un-filled or are of lower diameter. The quality of CNT depends upon the growth parameters (temperature, precursor and catalyst).

Structural analysis

In order to confirm the crystallinity of both CNT as well as filled nanocrystal, XRD was performed. Peaks shown in XRD pattern (**Fig. 2**) are originating only from two components which are MWCNT and iron carbide. The peak which corresponds to the (002) crystallographic plane of graphitic structure of MWCNT (PCPDF: 89-8487), was observed at 26.2° .

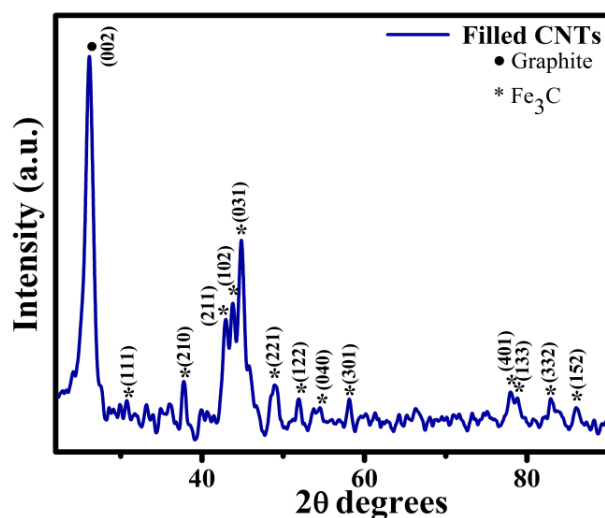


Fig. 2. X-ray diffraction pattern of Fe_3C filled CNTs collected from the inner walls of the quartz tube. (Orthorhombic structure of Fe_3C (PCPDF: 89-7271)).

This peak is known as the characteristic peak of MWCNTs. The diffraction peaks at 2θ position of 30.2° , 37.72° , 42.82° , 43.61° , 45.01° , 49.04° , 51.87° , 54.42° , 58.00° , 77.86° , 78.79° , 83.04° and 85.96° identified and found corresponding to the planes (111), (210), (211), (102), (031), (221), (122), (040), (301), (401), (133), (332) and (152) respectively of orthorhombic structure of Fe_3C (PCPDF: 89-7271) are associated with Fe_3C (indexed in **Fig. 2**). Hence, presence of Fe_3C is clearly confirmed. No other peaks related to other phases of carbide and iron was

found. This confirms that MWCNT are filled with pure Fe_3C .

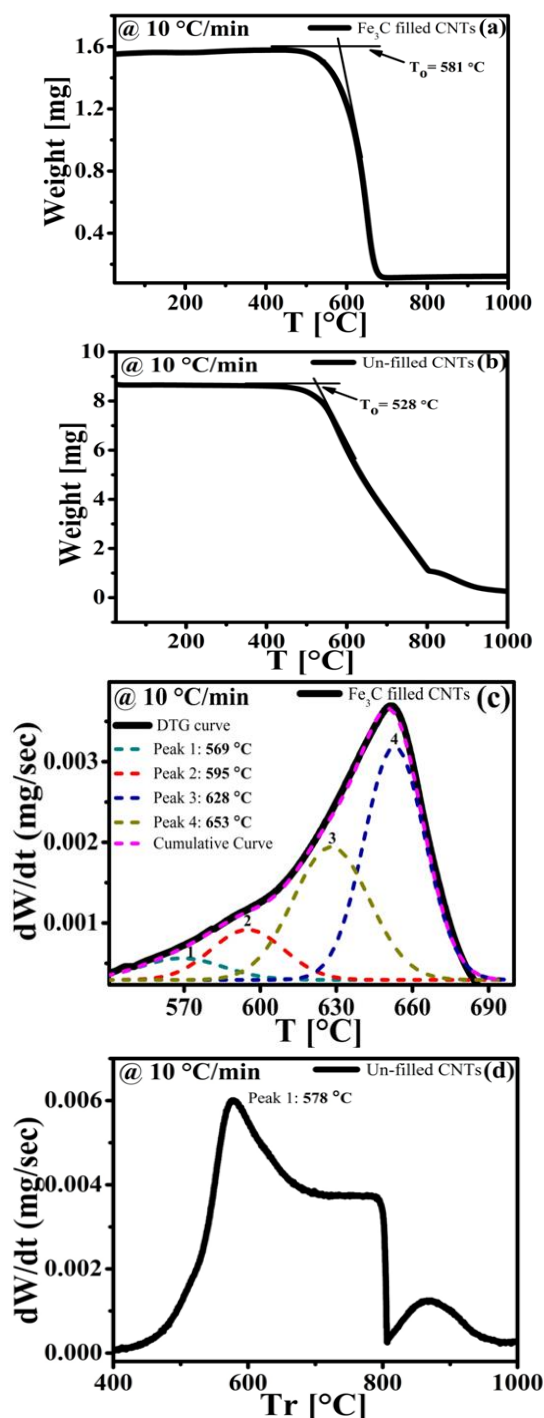


Fig. 3. TGA curves (a) Fe_3C filled CNTs (b) Un-filled CNTs; (c) and (d) DTG curve for Fe_3C filled CNTs and un-filled CNTs.

Thermal analysis

The thermogravimetric analysis on both filled and un-filled CNTs sample was performed at a constant heating rate ($10^\circ\text{C}/\text{min}$) and has plotted in **Fig. 3** (a) and (b). From the TGA curves it is clearly depicted that oxidation process for both filled and un-filled CNTs is a single step process. The onset temperatures (T_0) were found to be 581°C and

528°C for filled and un-filled CNTs respectively. With consideration of the onset temperatures, it can be confirmed that un-filled CNTs are less thermally stable because they started to oxidize early at 528°C as compared to filled CNTs which start to oxidize at 581°C . The DTG curve of the Fe_3C filled sample is plotted in **Fig. 3**(c), it features four stepwise weight-losses which correspond to the peak oxidation temperatures for each sample fraction. Analysis of the DTG curve can be done by considering two temperatures being initialization temperature and oxidation/peak temperature. The peak temperature is the oxidation temperature and the initialization temperature is the temperature at which carbonaceous impurities start to decompose. Gaussian fitting was applied to do the quantitative analysis of each part. Peak 1 at 569°C corresponds to the oxidation temperature of amorphous carbon. The other peaks were found to correspond to the different types of CNTs present in the sample: peak 2 at 595°C of SWCNTs, peak 3 at 628°C of thin-MWCNTs (TWCNT) and peak 4 at 653°C of MWCNTs. Higher thermal stability for MWCNT may be due to the presence of low defects or low curvature i.e. to pure sp^2 structure. The DTG curve for un-filled CNTs is shown in **Fig. 3** (d) in which there is only one peak at 578°C corresponding to the un-filled CNTs.

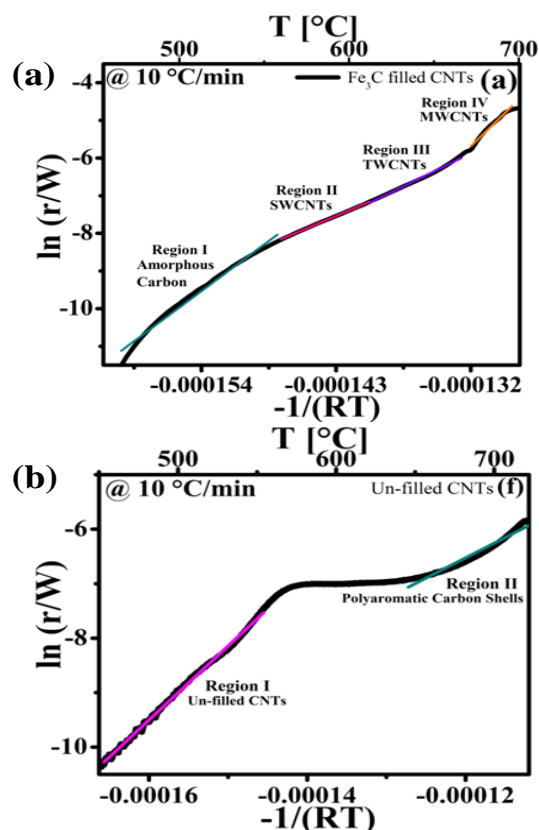


Fig. 4. The $\ln(r/W)$ vs. $(1/RT)$ and T) curve at heating rate $10^\circ\text{C}/\text{min}$ (a) The regions I, II, III, and IV represents the dominating oxidation of amorphous carbon, SWCNTs, TWCNTs and MWCNTs (b) The region I represent oxidation of un-filled CNTs and region II of polyaromatic carbon shells.

A $\ln(r/W)$ vs. $1/RT$ curve is plotted (as shown in **Fig. 4**) for determining the activation energies for the oxidation of

un-filled and filled CNTs together with the impurities of amorphous carbon, SWCNTs, TWCNTs as shown in **Fig. 4(a)**. By using equation (1) (differential method) [40] the activation energies can be calculated for both Fe₃C filled CNTs and un-filled CNTs.

$$\ln\left(\frac{r}{W}\right) = E\left(-\frac{1}{RT}\right) + \ln A \quad (1)$$

where, W: Weight, R: rate of change of weight with respect to time, A: constant

Table 1. Determined values of activation energy for filled as well unfilled CNT by using differential method.

Type of Sample	Regions in the Curve	Activation Energy (eV)
Fe ₃ C Filled CNTs	Amorphous Carbon	2.50 ± 0.019
	SWCNTs	1.42 ± 0.002
	TWCNTs	1.65 ± 0.009
	MWCNTs	3.29 ± 0.04
Un-filled MWCNTs	Un-filled MWCNTs	1.41 ± 0.002
	Polyaromatic Carbon Shells	0.77 ± 0.005

For Fe₃C filled CNTs curve can be fitted with four regions representing region I for amorphous carbon, region II for SWCNTs, region III for TWCNTs and region IV for MWCNTs similarly, for un-filled CNTs the curve is fitted with two regions: region I for un-filled CNTs and region II for polyaromatic carbon shells [41]. The calculated activation energies are tabulated in **Table 1**. However, the calculated activation energies for filled CNTs are very high and not comparable to HOPG. Therefore, in order to calculate the accurate values of activation energy differential method have to be improvised to integral method [42]. An integral method cannot be applied to this data because it comprises only of one heating rate (10 °C/min) and for better studies it is required to employ it for various heating rates.

The comparative study of Fe₃C filled CNTs and un-filled CNTs confirmed that the filled CNTs have a higher oxidation temperature than un-filled CNTs so it can be stated that the filled CNTs are more thermally stable. Un-filled CNTs presumed to have one open-end while another may be open or have a carbon cap at the tip [43]. Tip of CNT or open-end are reported to be energetically favored to initiate the oxidation [28, 44-47]. This may be a possible cause of low thermal stability in comparing to filled CNTs. In filled-CNT the open end is blocked by the filler and has minimum possibility of shortening the tubes at higher temperature. This possibility is high for un-filled CNTs. We believe that factors discussed above mainly affect the thermal stability of filled/un-filled CNTs.

Conclusion

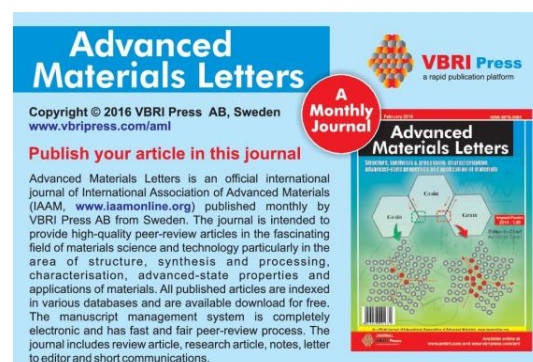
A comparative TGA and DTG study on both filled and un-filled CNTs has been made. Filled CNTs are found to be more thermally stable and have high resistance to oxidation. This study reveals that different variant of MWCNTs do not exhibit same thermal stability but nearly same activation energy. This activation energy is found comparable to reported values of activation energy for HOPG. Detailed analysis of the DTG profile for the plethora of filled-CNTs reveals that different carbonaceous

structures can be identified. These structures have followed systematic order of the thermal stability. We have demonstrated that TGA/DTG technique can be used to identify the nature of different variants of MWCNTs.

Reference

- Iijima, S., *Nature*, **1991**, 354, 56.
DOI: [10.1038/354056a0](https://doi.org/10.1038/354056a0).
- Tans, S. J.; Vershueren, A. R. M.; Dekker, C., *Nature*, **1998**, 393, 49.
DOI: [10.1038/29954](https://doi.org/10.1038/29954).
- Yakobson, B. I.; Smalley, R. E., *Am Sci*, **1997**, 85, 324-37.
- Qian, D.; Dicke, E. C.; Andrews, R.; Rantell, T., *Appl Phys Lett*, **2000**, 76, 2868.
DOI: [10.1063/1.126500](https://doi.org/10.1063/1.126500).
- Wagner, H. D.; Lourie, O.; Feldman, Y.; Tenne, R., *Appl Phys Lett*, **1998**, 72, 188.
DOI: [10.1063/1.120680](https://doi.org/10.1063/1.120680).
- Dai, H., *Surf Sci*, **2002**, 500, 218.
DOI: [10.1016/S0039-6028\(01\)01558-8](https://doi.org/10.1016/S0039-6028(01)01558-8).
- Tian, M.; Wang, W.; Liu, Y.; Jungjohann, K.L.; Harris, C.T.; Lee, Y. C.; Yang, R., *Nano Energy*, **2015**, 11, 500.
DOI: [10.1016/j.nanoen.2014.11.006](https://doi.org/10.1016/j.nanoen.2014.11.006).
- Bi, H.; Chen, I. W.; Lin, T.; Huang, F., *Adv. Mater.*, **2015**, 27, 5943.
DOI: [10.1002/adma.201502682](https://doi.org/10.1002/adma.201502682).
- Lin, Z.; Gui, X.; Gan, Q.; Chen, W.; Cheng, X.; Liu, M.; Zhu, Y.; Yang, Y.; Cao, A.; Tang, Z., *Scientific Reports*, **2015**, 5, 11336.
DOI: [10.1038/srep11336](https://doi.org/10.1038/srep11336).
- Mecklenburg, M.; Schuchardt, A.; Mishra, Y. K.; Kaps, S.; Adelung, R.; Lotnyk, A.; Kienle, L.; Schulte, K., *Adv. Mater.*, **2012**, 24, 3486.
DOI: [10.1002/adma.201200491](https://doi.org/10.1002/adma.201200491).
- Olsson, R. T.; Samir, M. A. S. A.; Salazar-Alvarez, G.; Belova, L.; Ström, V.; Berglund, L. A.; Ikkala, O.; Nogués, J.; Gedde U. W., *Nat. Nanotechnol.*, **2010**, 5, 584.
DOI: [10.1038/nnano.2010.155](https://doi.org/10.1038/nnano.2010.155).
- He, Y.; Chen, W.; Li, X.; Zhang, Z.; Fu, J.; Zhao, C.; Xie, E., *ACS Nano*, **2012**, 174.
DOI: [10.1021/nn304833s](https://doi.org/10.1021/nn304833s).
- Shi, J.L.; Tang, C.; Peng, H.J.; Zhu, L.; Cheng, X.B.; Huang, J. Q.; Zhu, W.; Zhang, Q., *Small*, **2015**, 11, 5243.
DOI: [10.1002/sml.201501467](https://doi.org/10.1002/sml.201501467).
- Schuchardt, A.; Braniste, T.; Mishra, Y.K.; Deng, M.; Mecklenburg, M.; Stevens-Kalceff, M. A.; Raevschi, S.; Schulte, K.; Kienle, L.; Adelung, R.; Tiginyanu, I., *Scientific Reports*, **2015**, 5, 8839.
DOI: [10.1038/srep08839](https://doi.org/10.1038/srep08839).
- Amelincx, S.; Zhang, X. B.; Bernaerts, D.; Zhang, X. F.; Ivanov, V.; Nagy, J. B., *Science*, **1994**, 265, 635.
DOI: [10.1126/science.265.5172.635](https://doi.org/10.1126/science.265.5172.635).
- Journet, C.; Bernier, P., *App. Phys. A: Mater. Sci. Process*, **1998**, 67, 1.
DOI: [10.1007/s003390050731](https://doi.org/10.1007/s003390050731).
- Huczko, A., *App. Phys. A: Mater. Sci. Process*, **2002**, 74, 617.
DOI: [10.1007/s003390100929](https://doi.org/10.1007/s003390100929).
- Chen, M.; Chen, C. M.; Chen, C. F., *J. Mater. Sci.*, **2002**, 37, 3561.
DOI: [10.1023/A:1016544001173](https://doi.org/10.1023/A:1016544001173).
- Wang, H.; Ren, Z. F., *Nanotechnology*, **2011**, 22, 405601.
DOI: [10.1088/0957-4484/22/40/405601](https://doi.org/10.1088/0957-4484/22/40/405601).
- Thess, A.; Lee, R.; Nikolaev, P.; Dai, H.; Petit, P.; Robert, J.; Xu, C.; Kim, S. G.; Rinzler, A.G.; Colbert, D.T.; Scuseria, G.E.; Tománek, D.; Fisher, J. E.; Smalley, R.E., *Science*, **1996**, 273, 483.
DOI: [10.1126/science.273.5274.483](https://doi.org/10.1126/science.273.5274.483).
- Ebbesen, T. W.; Ajayan, P. M., *Nature*, **1992**, 358, 220.
DOI: [10.1038/358220a0](https://doi.org/10.1038/358220a0).
- Lehman, J. H.; Terrones, M.; Mansfield, E.; Hurst, K. E.; Meunier V., *Carbon*, **2011**, 49, 2581.
DOI: [10.1016/j.carbon.2011.03.028](https://doi.org/10.1016/j.carbon.2011.03.028).
- Bom, D.; Andrews, R.; Jacques, D.; Anthony, J.; Chen, B.; Meier, M.S.; Selegue, J. P., *Nano. Lett.*, **2002**, 2, 615.
DOI: [10.1021/nl020297u](https://doi.org/10.1021/nl020297u).
- Saxby, J. D.; Chatfield, S. P.; Palmisano, A. J.; Vassallo, A. M.; Wilson, M. A.; Pang, L. S. K., *J. Phys. Chem.*, **1992**, 96, 17.
DOI: [10.1021/j100180a007](https://doi.org/10.1021/j100180a007).
- Pang, L.S.K.; Saxby, J.D.; Chatfield, S. P., *J. Phys. Chem.*, **1993**, 97, 6941.

- DOI: [10.1021/j100129a001](https://doi.org/10.1021/j100129a001)
26. Chiang, I.W.; Brinson, B.E.; Huang, A.Y.; Willis, P.A.; Bronikowski, M.J.; Margrave, J.L.; Smalley, R.E.; Hauge, R. H., *J. Phys. Chem., B* **2001**, *105*, 8297.
DOI: [10.1021/jp0114891](https://doi.org/10.1021/jp0114891)
 27. Lee, C. J.; Park, J.; Huh, Y.; Lee, J. Y., *Chem. Phys. Lett.*, **2001**, *343*, 33.
DOI: [10.1016/S0009-2614\(01\)00680-7](https://doi.org/10.1016/S0009-2614(01)00680-7)
 28. Murphy, R.; Coleman, J. N.; Cadek, M.; McCarthy, B.; Bent, M.; Drury, A.; Barklie, R. C.; Blau, W. J., *J. Phys. Chem. B*, **2002**, *106*, 3087.
DOI: [10.1021/jp0132836](https://doi.org/10.1021/jp0132836)
 29. Ajayan, P.M.; Ebbesen, T.W.; Ichihashi, T.; Iijima, S.; Tanigaki, K.; Hiura H., *Nature*, **1993**, *362*, 522.
DOI: [10.1038/362522a0](https://doi.org/10.1038/362522a0)
 30. Rinzler, A.G.; Liu, J.; Dai, H.; Nikolaev, P.; Huffman, C.B.; Rodriguez- Macias, F.J.; Boul, P.J.; Lu, A. H.; Heymann, D.; Colbert, D.T.; Lee, R.S.; Fischer, J.E.; Rao, A. M.; Eklund, P.C.; Smalley, R.E., *Appl. Phys. A*, **1998**, *67*, 29.
DOI: [10.1007/s003390050734](https://doi.org/10.1007/s003390050734)
 31. Qiang, F. U.; Weinberg, G.; Dang-sheng, S. U., *New Carbon Mater*, **2008**, *23*, 17.
DOI: [10.1016/S1872-5805\(08\)60008-6](https://doi.org/10.1016/S1872-5805(08)60008-6)
 32. Weissker, U.; Hampel, S.; Leonhardt, A.; Buchner, B., *Materials*, **2010**, *3*, 4387.
DOI: [10.3390/ma3084387](https://doi.org/10.3390/ma3084387)
 33. Leonhardt, A.; Hampel, S.; Müller, C.; Mönch, I.; Koseva, R.; Ritschel, M.; Elefant, D.; Biedermann, K.; Bernd Buchner, B., *Chem. Vap. Deposition*, **2006**, *12*, 380.
DOI: [10.1002/cvde.200506441](https://doi.org/10.1002/cvde.200506441)
 34. Martincic M, Tobias G., *Expert Opinion on Drug Delivery*, **2015**, *12*, 563.
DOI: [10.1517/17425247.2015.971751](https://doi.org/10.1517/17425247.2015.971751)
 35. Rossella, F.; Soldano, C.; Onorato, P.; Bellani, V., *Nanoscale*, **2014**, *6*, 788.
DOI: [10.1039/C3NR03856D](https://doi.org/10.1039/C3NR03856D)
 36. Chou, S.Y.; Wei, M. S.; Peter R. Krauss, P. R.; Fischer, P. B., *Appl. Phys.*, **1994**, *76*, 6673.
DOI: [10.1063/1.358164](https://doi.org/10.1063/1.358164)
 37. Wolny, F.; Weissker, U.; Mühl, T.; Lutz, M. U.; Müller, C.; Leonhardt, A.; Buchner, B., *J. of Physics Conference Series*, **2010**, *200*, 112011.
DOI: [10.1088/1742-6596/200/11/112011](https://doi.org/10.1088/1742-6596/200/11/112011)
 38. Ramesh, B. P.; Blau, W. J.; Tyagi, P. K.; Misra, D. S.; Ali, N.; Gracio, J.; Cabral, G.; Titus, E., *Thin Solid Films*, **2006**, *494*, 128.
DOI: [10.1016/j.tsf.2005.08.220](https://doi.org/10.1016/j.tsf.2005.08.220)
 39. Stevens, F.; Kolodny, L. A.; Beebe, T. P., *J. Phys. Chem.*, **1998**, *102*, 10799.
DOI: [10.1021/jp982025e](https://doi.org/10.1021/jp982025e)
 40. Kumari, R.; Krishnia, L.; Kumar, V.; Singh, S.; Singh, H. K.; Kotnala, R.K.; Juluri, R.R.; Bhatta, U. M.; Satyam, P. V.; Yadav, B.S.; Tyagi, P. K.; *Article in communication*.
 41. Chan, J. H.; Balke, S. T., *Polymer Degradation and Stability*, **1997**, *57*, 135.
DOI: [10.1016/S0141-3910\(96\)00160-7](https://doi.org/10.1016/S0141-3910(96)00160-7)
 42. Luxembourg, D.; Flamant, G.; Laplaze, D., *Carbon*, **2005**, *43*, 2302.
DOI: [10.1016/j.carbon.2005.04.010](https://doi.org/10.1016/j.carbon.2005.04.010)
 43. Krishnia, L.; Kumar, V.; Kumari, R.; Garg, P.; Yadav, B.S.; Ghosh, A.; Sinha, R. K.; Singh, M. K.; Tyagi, P. K., *Article in preparation*.
 44. Tessonnier, J.P.; Su, D. S., *Chem Sus Chem*, **2011**, *4*, 824.
DOI: [10.1002/cssc.201100175](https://doi.org/10.1002/cssc.201100175)
 45. Singh, A. K.; Hou, X. M.; Chou, K. C., *Corrosion Science*, **2010**, *52*, 1771.
DOI: [10.1016/j.corsci.2010.01.029](https://doi.org/10.1016/j.corsci.2010.01.029)
 46. Tsang, S.C.; Harris, P.J.F.; Green, M. L. H., *Nature*, **1993**, *362*, 520.
DOI: [10.1038/362520a0](https://doi.org/10.1038/362520a0)
 47. Geng, H.Z.; Zhang, X. B.; Mao, S. H.; Kleinhammes, A.; Shimoda, H.; Wu, Y.; Zhou, O., *Chem. Phys. Lett.*, **2004**, *399*, 109.
DOI: [10.1016/j.cplett.2004.09.150](https://doi.org/10.1016/j.cplett.2004.09.150)



Database Performance Analyser S/W Test Tool

Dr. Ruchika Malhotra, Assistant Professor

CS Dept., Delhi Technological University (DTU) (DCE)
Main Bawana Road, Delhi 1100 42, India
ruchikamalhotra@dce.edu

Ashish Gupta

CS Dept., Delhi Technological University (DTU) (DCE)
Main Bawana Road, Delhi 1100 42, India
connect.ashishgupta@gmail.com

Abstract— The role of a database is indispensable in the successful running of any business. The advent of the internet has totally changed the business scenario and how industries operate which has led to the growing popularity of online database. There are many scenarios in which there are multiple DB queries fired at a single point on time as multiple clients can access database at the same time. It may be possible that thousands of clients are accessing same table using same stored procedure. So it is important to check database capabilities/performance and its stored procedures in multi threaded environment before launching it into real world. DB_Performance_Analyser_Software_Test_Tool is a tool that helps to simulate multiple clients' environment and generate logs that can be use to analyze the capability of stored procedures created and database selected. This tool gives user a freedom to create as many clients as he wants that will interact with the database at the same time. By creation of this tool, we try to approach to non- functional quality attributes of DataBase (DB) like reliability, robustness, etc. In this paper , we are focusing only on creating a simulated environment in which, multiple queries will be fired on DB for simultaneous updation / deletion / addition of DB rows. There will be a possibility of some queries not entertained by DB because DB handling other query at that particular time. So , an error log will be generated which will depict total queries fired in a give span of time , total successful queries fired , total unsuccessful queries. The purpose of this paper is to run simulation and share the performance of the DB_Performance_Analyser_Software_Test_Tool.

Keywords— DataBase (DB), Software Testing (ST).

I. INTRODUCTION

Reliability has been prominently impacting human life ever since we learned to form the groups/societies among themselves. Societies reflect the interdependence; and reliability is at the core of interdependence. Today, softwares have become the indistinguishable parts of our lives. Measuring or predicting reliability has always been an intuitive task. In case of softwares, researches have been done to make this task more scientific rather than intuitive. The present thesis adds a bit in this series of researches. For critical business applications, continuous availability is a requirement, and software reliability is an important component of continuous application availability [1-7].

1) Reliability:

The probability of failure-free system operation over a specified time in a given environment for a given purpose is called the Reliability [1-7].

2) Availability:

The probability that a system, at a point in time, will be operational and able to deliver the requested services is called the availability.

It is sometimes possible to subsume system availability under system reliability. Obviously if a system is unavailable it is not delivering the specified system services. However, it is possible to have systems with low reliability that must be available [1-7].

3) Software reliability engineering:

Software reliability engineering is the application of statistical techniques to data collected during system development and operation to specify, predict, estimate and assess the software reliability of software-based systems.

The three major classes of software reliability assessment are:

a) Black box reliability analysis:

Estimation of the software reliability based on failure observations from testing or operation. These approaches are called black box approaches because internal details of the software are not considered.

b) Software metric based reliability analysis:

Reliability evaluation based on the static analysis of the software (e.g., lines of code, number of statements, complexity) or its development process and conditions (e.g., developer experience, applied testing methods).

c) Architecture-based reliability analysis:

Evaluation of the software system reliability from software component reliabilities and the system architecture (the way the system is composed out of the components[1-7].

B. Scope & Limitations

DB_Performance_Analyser_Software_Test_Tool is a be tightly coupled with the DB and this tool currently will only capture logs in multithreaded environment . The logs show the the queries which are successful and the queries which are not successful. Error handling is not part of current tool . Only error logging and checking is performed [1-7].

II. PURPOSE OF TOOL

In order to scale successfully and handle a large number of concurrent users, database has to provide support for Multithreaded environment. In a heavy usage situation, many client requests may arrive at the DataBase simultaneously. The question is to check whether or not the client query will receive a response, also to check the time of response; will the response time be acceptable to the user? That's where threading comes into the picture. In a single-threaded model, any DB can response very quickly, but all the clients must "pipeline" one behind the other. If you are the fifth client to make a request, you must wait for clients one through four to be served first. This process is surprising quick and not as bad as it sounds. In fact, unless our queries are really complex, this model will deliver the best performance for most applications. But what happens when you are tenth in line, and the second client in line has made a time-consuming request? That is when multi-threading delivers [1-7].

1) Example 1 :

One of the leading retail outlets of India has organized biggest sale day all over India. This company has thousands of retail out let across the India. On the day of sale customer count, get increased by 200% as compare to normal days. Many of the customers pay via electronics card. This causes huge traffic on payment gateway that result in failure of payment server [1-7].

Reason: Payment server database was not designed in a way that can handle this much of transition at single instance of time. Later on the whole Database design has been analyzed and modification done to handle this kind of situation [1-7].

2) Example 2:

When India govt. has increased petrol prices. The prices was to be applicable by the mid of that night. This news leads to huge customer rush on fuel outlets. Some of these outlets are automated in order to provide best services to their customer. This automation system record each and every transaction done on each bay and later on these transactions are used to generate reports to check whether there is some false bulk receipt or not. On that evening due to huge rush on fuel outlets some of the transactions cannot be recorded because the database was not designed to handle multiple transaction insertion at single instance of time. This result in error in reports and Fule Company were not able to check for false bulk receipt [1-7].

Reason: Transaction record server database was not designed in a way that can handle this much of Transaction at single instance of time. Later on, the changes are made to handle this kind of situation in database [1-7].

All these examples show those databases are installed in real world without proper testing in multi-threaded environment. To ensure this kind of situation will not occur during business all the database must be tested properly for

multi threading operations. To facilitate this we have developed on tool called DB performance analyzer [1-7].

III. DESIGN & IMPLEMENTATION OF TOOL

The design and implementation of the DB_Performance_Analyser_Software_Test_Tool is described below [1-7]:

A. Architecture Diagram

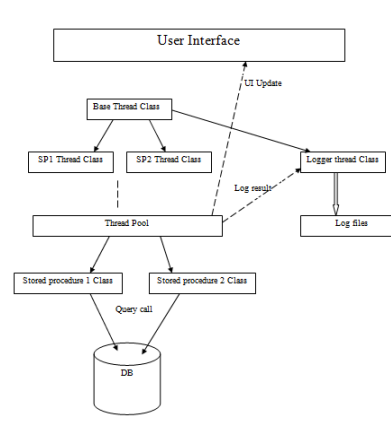


Figure: Architecture Diagram

B. Class Diagram

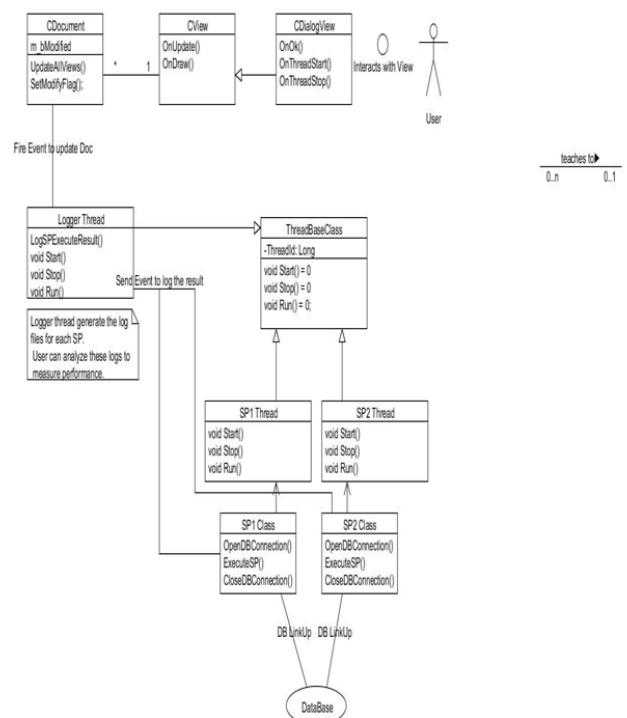


Figure: Class Diagram

C. Use Case Diagram

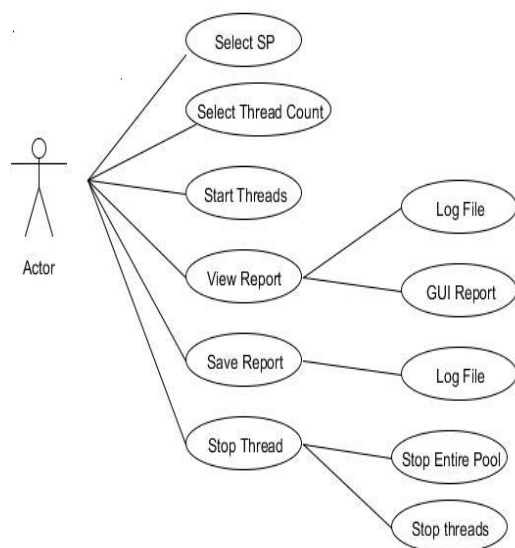


Figure: Use Case Diagram

D. File Logger Thread Class

This class is derived from thread class explained above. The purpose of this class is to create a log file in which all the operations are registered in order to do analysis. All the messages are stored in list and operations on that list are managed by mutex in order to maintain the consistency in multi-threaded application [1-7].

E. Table Operation Class

This class act as a client for operation on table. This class is also derived from thread class. User can create as many instance of this class as he wants. We maintain a list of all the clients to manage them while start and stop of client. Run function is override in this class to call the stored procedure of the database to perform operation on the table. This will also report all the results of operation to the logger thread so that logging can be done [1-7].

IV. HOW TO USE TOOL

Below are some screen shots of this tool along with the details:

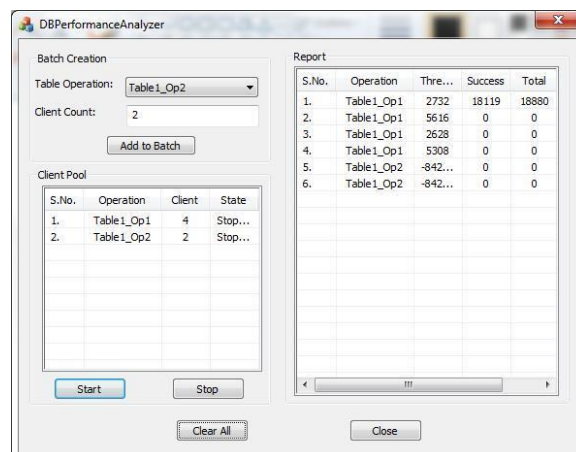


Figure: Analyzer Diagram

A. Steps to use

1) Add to Batch

Step 1:- Select the table operation, which you want to perform.

Step 2:- Enter client count (number of client that will operate on table simultaneously)



Figure: Batch Diagram

Step 3:- Press Add to batch button this will create the client pool for the table operation.

Note: - user can add more than one table operation.

2) Client Pool

This will show the client pool created by the user

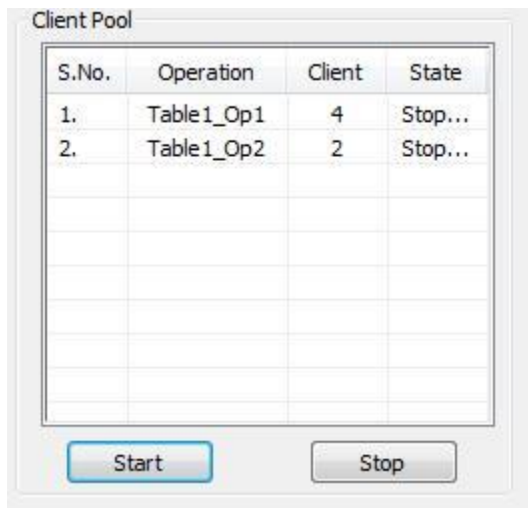


Figure: Client Pool

Step 4:- User can press start button that will run all the client thread and start performing operation on table.

Step 5:- User can press stop button that will stop all the client thread.

B. Report

Report will show the status of the table operations done by clients

S.No.	Operation	Thre...	Success	Total
1.	Table1_Op1	2732	18119	18880
2.	Table1_Op1	5616	0	0
3.	Table1_Op1	2628	0	0
4.	Table1_Op1	5308	0	0
5.	Table1_Op2	-842...	0	0
6.	Table1_Op2	-842...	0	0

Figure: Report Diagram

1) Report understanding

Operation :- operation that will be done on table.

Thread :- the client ID

Success :- Is the success rate of any operation performed.

Total :- Is the total operation performed on that table by that client.

Failure :- No of fail case.

V. CONCLUSION

DB_Performance_Analyser_Software_Test_Tool has shown that, we can test various scenarios of multi client and database interaction. Using this tool we can reduce the real world failure as most of the scenarios can be produce using DB_Performance_Analyser_Software_Test_Tool. This also helps to reduce the cost of testing the database application and facilitate us to test the application in real world like scenarios with in a lab. Or org. Enhancement of this tool can be extensive logs inclusion, time based client database testing and variation of number of client during that period of time. Variation on number of client during certain time will be helpful to test sales application that are using database as sales may vary during different hours of sale. For example, sale will be low during morning and night while the number of clients will be high during evening etc. We can enhance DB_Performance_Analyser_Software_Test_Tool in a way that it will work as a varying sale terminal throughout the day and record performances of inserting record in best and worst cases.

VI. ACKNOWLEDGMENT

This paper is specifically meant for educational purpose for completing M.Tech. degree with Delhi Technological University (DTU), Delhi India. This paper is prepared for submission for publication as a part of M.Tech. course work. The authors are very much thankful to Samsung Electronics India and Delhi Technological University (DTU) (DCE).

VII. REFERENCES

- [1] Bergsten, B., Couprie, M., and Valduriez, E', "Overview of Parallel Architecture for Databases", The Computer Journal, vol. 36, no. 8, pp. 734-740, 1993.
- [2] Cattell, R.G.G. (editor), The Object Database Standard ODMG-93, Release 1.1, Morgan Kaufmann Publishers, 1994
- [3] K. K. Aggarwal, Yogesh Singh, and Arvinder Kaur "code Coverage Based Techniques for Prioritizing Test Cases for Regression Testing", ACM SIGSOFT Software Engineering Notes, vol. 29, no. 5, September, 2004.
- [4] K. K. Aggarwal and Yogesh Singh "Software Engineering: Programs, Documentation, Operating Procedures", New Age International Publishers, New Delhi, India, 2008.
- [5] Yogesh Singh "Software Testing", Cambridge University Press, New Delhi 2012.
- [6] W. M. McKeeman, "Differential testing for software," Digital Technical Journal, vol. 10(1), pp. 100-107, 1998.

Effects of Sex Appeal in Advertisements on Consumer Buying Behavior in India

Chhavi¹, Syed Fazal Karim² and Vipul Jain³

^{1,2,3}Delhi School of Management Delhi Technological University

Abstract—In recent years, it is evidently seen that the use of erotic stimuli and sexual themes have increased in advertising methods. In India also where showing sexual content publically is a taboo, this increase is significant. Despite the common intolerance in society for these practices, such kinds of advertisements are huge successes on social platforms. There have been a lot of studies on effect of using sexual appeal in advertisements on consumer behavior. However, little research has been done on what exactly consumer thinks about such kind of advertisements and why such kind of advertising practices are gaining popularity in a country like India, where there is an overall negative attitude towards this topic. The aim of this paper is to identify whether there is a change in thinking of Indian consumer towards sexual content or the perspective of consumer has changed when it comes to viewing an advertisement

1. INTRODUCTION

Sex in Advertising is basically the use of sex appeal to sell a particular product or service. The use of sexual content in any advertisement can vary from highly overt to extremely subtle. Initially illustrations of attractive women were used on the posters of tobacco, tonics and saloons. Pearl tobacco in 1871 featured a naked maiden on its package cover. This was the first known use of sexual content in advertising.

Early twentieth century was the era of mass media and modern society was involved in consumption of goods opposite to production. Middle class people pursued materialistic pleasures and goods with an aim of owning an item. Consensus of public on nature of shopping slowly and gradually shifted from “need driven activity” to “an intrinsic feature of standard urban living”. The advertising industry grew manifolds.

“People are curious about sexuality”, this is the hypothesis on which sex in advertising is built on. Today’s consumer is more exposed to sexual content in advertisements than ever before. Generally nudity, romantic themes and attractive women are used in broadcast advertisements to draw the attention of consumers. In a country like India, where public consensus on this topic is negative yet advertisers seems to be in no mood to rectify erotic stimuli from the advertisements. Surprisingly this practice followed by the advertising and marketing experts seems to be apt and absolutely right in lieu to the success of such kind of advertisements.

There are numerous examples in Indian advertising industry which prove that “sex sells”. Slice Aamsutra, despite being a mango drink uses this practice in its each and every advertising campaign. It is a well-known fact that a mango drink has nothing to do with sex. The question is why this practice is so evident? Then again, the advertisements for men’s underwear beg a very similar question. VIP, Rupa and Amul Macho rule this department. All their advertising campaigns use sexual content or messages in one way or the other. An example without which this list of examples would be incomplete is Indian advertising’s favorite product in the world: AXE. With time we’ve grown immune to ads that abandon logic for the sake of that historic formula – empty a can of AXE onto your shaved torso and the hottest women within a 100-mile radius will fly at you from every direction.

Despite there is a common unacceptance of society for these practices yet such kind of advertisements are huge successes on social platforms. There have been a lot of studies on effect of using sexual appeal in advertisements on consumer behavior. The aim of this paper is to identify whether there is a change in thinking of Indian consumer towards sexual content or the perspective of consumer has changed when it comes to viewing an advertisement.

2. LITERATURE REVIEW

There have been several researches ascertaining that advertisement with sexual appeal can increase consumers’ congeniality. A strong affirmative correlation is also found between the degree of how well an advertisement is liked with the amiability to the brand advertised [1, 2, 3, 4]. In short, adding sexual aspects can increase one’s likability of an advertisement and ultimately escalate liking to the brand advertised.

Advertising aims to persuade the way customers ponder themselves and how purchasing particular products can turn out to be helpful for them. The message expressed through advertising effects the buying decisions of customers [5]. Nonetheless, the advertising plea which has generated universal censure, and which has been stated as most unethical, is sex appeal. Belch and Belch (2004) [6] notes: the advertising appeals that have got the most reproach for being

in poor tang are those using sexual appeals or nudity. These methods are time and again used to get consumers' attention and may not even be appropriate to the product being advertised. Even if the sexual appeal connects with the product, people may be affronted by it. Sometimes people complain about both nudity in advertisements and sexually reminiscent advertisements (p.755).

According to Wikipedia, sex appeal refers to a person's ability to entice the sexual or erotic curiosity of another individual. The attraction can be physical or to such qualities in the environment in which they appear. The attraction may be to somebody looks, movements or to their voice or smell, above and beyond other factors. The attraction can be enhanced by a person's embellishments, attire, cologne, hair stylishness and whatsoever which can appeal the sexual interest of another individual. The competence of a person's corporeal and other capabilities to create a sexual curiosity in others is the base of their usage in advertising.

There are several discrepancies regarding what is being considered as sex appeal. Sex appeal in advertising is the usage of sexual or sensual descriptions to draw curiosity to a specific product, for purpose of sale. A study was performed and discovered four features of sexy commercials: bodily features of models, comportment/movement, closeness between models, and circumstantial features such as camera effects (p.267) [7]. They strived to find to find what people thought as sexy in advertising and the most generic referent was physical features (66%), followed by a model's actions and verbal and nonverbal communication (39%), relative features (26%), and proxemics (15%). They made an imperative note that what people stated as sexy differed gender to gender (p.269).

In an effort to attract customers, some advertisers have consistently pushed the boundaries of what is morally and socially tolerable. It line with this that, it was suggested that the increasing gathering in the advertising environment has made advertisers to endure to use sexual appeals and other methods that affront many people but catch the contemplation of customers and may even create advertising for their businesses [8]. Since the commencement of advertisements, sex appeal has often been exploited. The earliest forms of sex appeal in marketing are wood carvings and artworks of attractive women (often unclothed from the waist up), decorated posters, signs, and commercials for saloons, tonics, and tobacco. Sex appeals in advertising are used commonly and with cumulative explicitness. While the use of such explicit sex was improbable not many years ago, it now exemplifies part of the advertising landscape [9]. It is supposed that this form of appeal goes a long way in aiding advertisers accomplish their aims, "advertising research reveals that sexual requests are attention receiving, arousing, touching, persuading and notable" [10].

3. RESEARCH METHODOLOGY

The paper is based on an empirical study of effects of sexual advertisements on consumers' buying behavior. The paper takes into consideration the positive as well as negative aspects of using sexual advertisements over normal advertisements. Primarily, the focus is on recognizing the influential reasons that affects the consumer buying behavior following sexual advertisements.

The data was collected through the source directly, i.e., Primary Data Collection was done. The data that has been collected directly from the source for a study purpose is called Primary Data. The data collected through the source was via a questionnaire or survey format. The questionnaire is one of the most significant and widely used data collection methods. A questionnaire is set of questions used for gathering information and data from individuals. The questionnaire has been designed keeping in view the general views and perceptions that a consumer has while watching sexual advertisements. The survey was specifically focused on respondents who are much into advertisements and are frequent buyers. Demographic factors such as age, income level, gender and profession have also been considered.

The questionnaire was based on a 5-Point Likert Scale. Likert Scale is a highly common and widely used scale for questionnaires that encourage the respondents to rank the options / quality from either high to low or low to high [11]. The 5-Point Likert Scale chosen for the study has labels attached to each point on the mentioned scale and the mid-point of the scale has been set as the point of neutrality. The label are as follows : 1 : Strongly Disagree ; 2 : Disagree ; 3 : Neutral ; 4 : Agree ; 5 : Strongly Agree.

The questionnaire was tested through a pilot study on 40 consumers. The pilot study helped in making the needed changes in the questionnaire and allowed the researchers to have a more clear knowledge of what consumers' perception is towards the usage of plastic money, thereby, leading to an improved questionnaire. The refined questionnaire was then sent to 300 eligible respondents out of which only 219 responses came back. Out of the received 219 responses, 19 responses had missing data. Therefore, only 200 responses qualified for the data analysis done. Therefore, overall response rate was 66.6%.

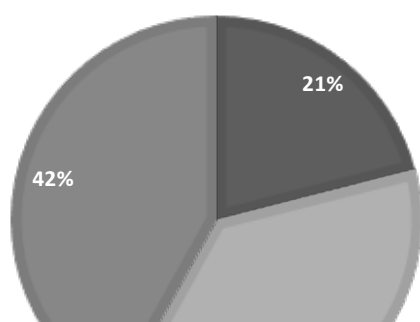
4. DATA REPORTING AND ANALYSIS

Among 200 qualified respondents, 68% were male and 32% were female. Our sample was spread across different age groups. 63% belong to the age group of 20-30 years, 22% belong to the age group 30-40 years and the remaining 15% are from the age group of 40+ years. We did not question/consider responses from people belonging to the age group below 20 years, due to the nature of our topic.

Now, we questioned our respondents on certain factors such as viewing habits, behavioral aspects and more. When the respondents were asked about their preferred mode of entertainment, 21% answered FM Radio, 37% responded with Television and the remaining majority of 42% chose Internet (Laptop/Mobile).

MODE OF ENTERTAINMENT

■ FM Radio ■ TV ■ Internet (Laptop/Mobil



The sample was also questioned about their viewing timings in two ways – the preferred time to view and the amount of time spent in viewing. When asked about the preferred timing, a mere 7.5% answered morning, a substantial 22.5% chose the afternoon, surprisingly just 11% chose the evening time and a whopping 59% answered the night time. Regarding the second part i.e. the amount of time spent viewing their mode of entertainment, 28% replied 0-1 hours, 39% answered 1-3 hours and the remaining 33% chose 3+ hours.

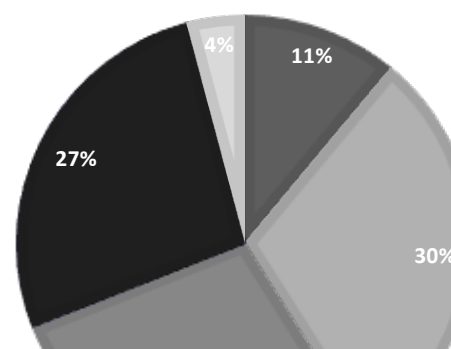
Getting on topic, we asked whether people switch channels when such advertisements play. 83% responded with a yes and only 17% said no. Next we asked that, whether people feel that the nature of advertisements has grown to be more sexual/erotic in nature. As expected 71% said yes and 29% thought that it hadn't. As a follow up question, we asked on a scale of 1-5, how uncomfortable it made them. 11% chose very uncomfortable, 30% chose uncomfortable, 27% felt comfortable watching such ads, 4% were very comfortable and 28% weren't affected and felt neutral about such advertisements. Moving on to content, we asked how relevant they felt this content was to the product/service being marketed. This was again done on a scale of 1-5, 1 being very irrelevant and 5 being very relevant. Only 3% thought it was very irrelevant, 19% felt that it was irrelevant, 23% were indifferent, 39% thought that it was relevant and the remaining 16% thought that the advertisement really needed that nature of the content.

In addition to this we asked whether the same advertisement could have been done without using sexual content or innuendos. To this 69.6% said that it could have been done and 30.4% said it was essential. Moving on to the relation

between such content and the buying behavior, we categorized our question in 2 parts. We noticed that a majority of such advertisements were deodorant and perfume ads and the others were a smaller part. So we asked whether the sex appeal in deodorant advertisements attracted our respondents and gives the product an edge over others. To this a huge majority of 88.2% replied that it does and only 11.8% people said that they're unaffected. In the next part we asked the same question but in context of retail and FMCG (fast moving consumer goods). We asked whether the sex appeal in advertisements about clothing, food, drinks etc. were more attractive as compared to normal ads. To this an equally opposite response was gathered with 75.5% responding with a no, and 24.5% replying as a yes.

COMFORT LEVEL

■ Very Uncomfortable ■ Uncomfortable ■ Neutral
■ Comfortable ■ Very Comfortable



5. CONCLUSION

From the data analysis done on the respondents' answers, we found out that people of India have actually broadened their mindsets. With a majority of people feeling comfortable with erotic advertisements, the times have really changed. Our assumptions about the consumers, that they are still shy and do not accept of such advertisements, were shattered with these findings. But a change in mindset does not give a reason to exploit the consumer's desires. As our respondents replied too, that these sexual innuendos were not essential and the advertisements can be made without them too. So, we conclude that the effect of sex appeal in advertisements, neither has a negative effect (as we assumed), but nor it has a positive effect (as the advertisers feel), barring only one category i.e. the deodorants and perfumes. In this sector, the sex appeal in advertisements does seem to work for the benefit of the companies.

REFERENCES

- [1] Gelb, B. D., & Pickett, C. M. (1983). Attitude toward the ad: Links to humor and to advertising effectiveness. *Journal of Advertising*, 12, 34-42.
- [2] Haley, Russell I.; Baldinger, Allan L. (1991) *The ARF Copy Research Validity Project*, *Journal of Advertising Research*, Vol.31, April/May, p.11-32.
- [3] Weinberger, Marc G. and Leland Campbell (1991). "The Use and Impact of Humor in Radio Advertising," *Journal of Advertising Research*, 30(6), 44-52.
- [4] Zhang, Y. (1996), The effect of humor in advertising: An individual-difference perspective. *Psychol. Mark.*, 13: 531-545. doi: 10.1002/(SICI)1520-6793(199609)13:6<531::AID-MAR1>3.0.CO;2-9.
- [5] Ashwini Ambekar. (2009). *Advertising appeals*. Retrieved on May 2, 2012 from <http://www.articleswave.com/advertising-articles/types-of-advertising-appeals.html>.
- [6] Belch, G., and Belch, M. (2004). *Advertising and promotion: An integrated marketing communication perspective*. Sixth edition.
- [7] Reichert, T. and Ramirez, A. (2000). *Defining Sexually Oriented Appeals in Advertising: a Grounded Theory*
- [8] Belch, G., and Belch, M. (2004). *Advertising and promotion: An integrated marketing communication perspective*. Sixth edition.
- [9] Shimp, T. A. (2003). *Advertising, promotion and supplemental aspects of integrated marketing communication*. Sixth edition.
- [10] Traudt, P. J. (2005). *Media, audiences, effects: An introduction to the study of media content and audience analysis*. Pearson Education, Inc.
- [11] Shimp, T. A. (2003). *Advertising, promotion and supplemental aspects of integrated marketing communication*. Sixth edition.
- [12] Albaum, G. The Likert scale revisited: An alternate version. *Journal of the Market Research Society*, 1997, 39, 331-349

See discussions, stats, and author profiles for this publication at: <https://www.researchgate.net/publication/291830173>

Electrospun Functional Micro/Nanochannels Embedded in Porous Carbon Electrodes for Microfluidic Biosensing

ARTICLE *in* SENSORS AND ACTUATORS B CHEMICAL · JANUARY 2016

Impact Factor: 4.1 · DOI: 10.1016/j.snb.2015.12.108

READS

70

5 AUTHORS, INCLUDING:



Kunal Mondal

North Carolina State University

19 PUBLICATIONS 58 CITATIONS

SEE PROFILE



Md Azahar Ali

Iowa State University

38 PUBLICATIONS 356 CITATIONS

SEE PROFILE



Bansi Malhotra

Delhi Technological University

327 PUBLICATIONS 9,386 CITATIONS

SEE PROFILE



Ashutosh Sharma IITK

Indian Institute of Technology Kanpur

336 PUBLICATIONS 7,416 CITATIONS

SEE PROFILE

Accepted Manuscript

Title: Electrospun Functional Micro/Nanochannels Embedded in Porous Carbon Electrodes for Microfluidic Biosensing

Author: Kunal Mondal Azahar Ali Saurabh Srivastava Bansi D. Malhotra Ashutosh Sharma



PII: S0925-4005(15)30768-1
DOI: <http://dx.doi.org/doi:10.1016/j.snb.2015.12.108>
Reference: SNB 19617

To appear in: *Sensors and Actuators B*

Received date: 22-10-2015
Revised date: 9-12-2015
Accepted date: 12-12-2015

Please cite this article as: Kunal Mondal, Azahar Ali, Saurabh Srivastava, Bansi D. Malhotra, Ashutosh Sharma, Electrospun Functional Micro/Nanochannels Embedded in Porous Carbon Electrodes for Microfluidic Biosensing, *Sensors and Actuators B: Chemical* <http://dx.doi.org/10.1016/j.snb.2015.12.108>

This is a PDF file of an unedited manuscript that has been accepted for publication. As a service to our customers we are providing this early version of the manuscript. The manuscript will undergo copyediting, typesetting, and review of the resulting proof before it is published in its final form. Please note that during the production process errors may be discovered which could affect the content, and all legal disclaimers that apply to the journal pertain.

Electrospun Functional Micro/Nanochannels Embedded in Porous Carbon Electrodes for Microfluidic Biosensing

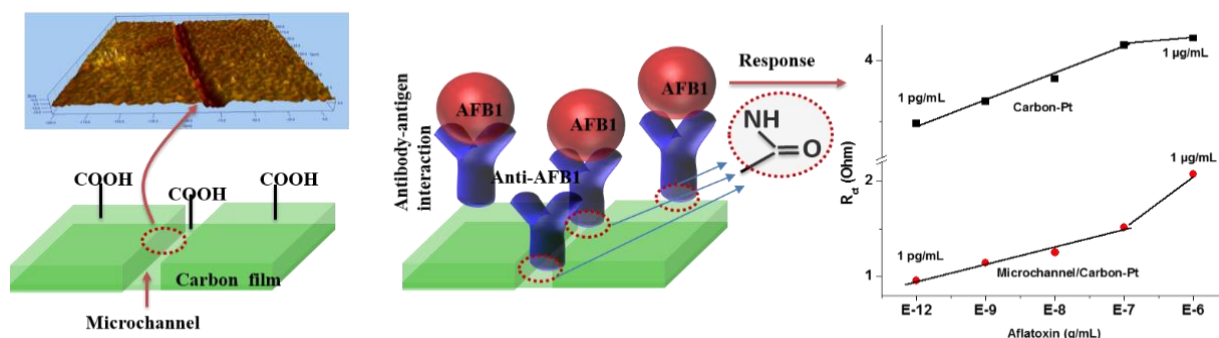
Kunal Mondal^a, Md. Azahar Ali^a, Saurabh Srivastava^b, Bansi D Malhotra^{b*}
bansi.malhotra@gmail.com, Ashutosh Sharma^{a*} ashutos@iitk.ac.in

^aDepartment of Chemical Engineering, Indian Institute of Technology Kanpur, India

^bDepartment of Biotechnology, Delhi Technological University, Delhi, India

*Corresponding authors.

Graphical Abstract



We present a straightforward method to fabricate functional micron, submicron and nano-channels embedded in a porous carbon film and the use of this microfluidic platform for electrochemical sensing. Carbonization of a composite of electrospun PMMA nanofibers embedded in in a PAN film produces microchannels in the PAN derived amorphous monolithic carbon electrode. The platinum nanoparticles decorated carbon micro-channels are used to detect aflatoxin B1 (AFB1; food toxin) by surface biofunctionalization of antibody of AFB1 (anti-AFB1) via electrochemical impedance technique. The fabricated immunsensor is found to be highly sensitive to 1 pg/mL of AFB1 concentration with a range of 10^{-12} g/mL to 10^{-7} g/mL.

ABSTRACT

We present a straightforward method for fabricating functional micro-, submicro-, and nano-channels embedded in a porous carbon film and the application of this microfluidic platform for electrochemical sensing. A skin layer of poly(methyl methacrylate) (PMMA) fibers was first electrospun on a thoroughly cleaned Si wafer substrate, followed by spin coating of a polyacrylonitrile (PAN) film on top of the skin. High-temperature carbonization of the composite film decomposed the PMMA fibers and produced embedded microchannels in the PAN-derived amorphous monolithic carbon electrode. The channels were decorated with Pt nanoparticles by *in situ* thermal decomposition of a precursor metal salt to enhance functionality of the carbon electrode. Carbon electrodes decorated with Pt nanoparticles (carbon-Pt), with and without embedded microchannels, were used to detect the food toxin aflatoxin B1 (AFB1) by surface biofunctionalization with the antibodies of AFB1 (anti-AFB1) *via* an electrochemical impedance technique. The aligned nanochannels in the porous carbon film act as a reaction chamber for antigen–antibody interactions and provide channels for fast electron transport toward the electrode from the electrolyte, resulting in improved electrochemical performance of the biosensor. The fabricated immunosensor is highly sensitive to 1 pg/mL of AFB1 with a concentration range of 10^{-12} to 10^{-7} g/mL.

Keywords: Microchannel fabrication; Spin coating; Porous carbon film; Electrospinning; aflatoxin B1 detection.

1. INTRODUCTION

There is increased demand in the biomedical field for the integration of smart nanomaterials with functional microfluidic devices [1, 2]. The fabrication of micro/nanochannels is an important issue in the development of state-of-the-art microfluidic devices. A number of lithography-based microfabrication methods have been used for many applications, in which the shape, size, and structure of a microchannel can be varied [3-5]. The microchannels can be used for processes such as the separation, sorting, and counting of biological samples or assays. However, the microfabrication of channels in porous carbon and surface functionalization of microchannels are still challenging [3, 4]. Much work has centered on microchannel fabrication in polydimethylsiloxane (PDMS) [5, 6]. PDMS-based replica molding and near-field electrospinning have expanded micro/nanochannel fabrication by enabling fast, simple, cost-effective prototyping, and direct transfer of microfluidic patterns into the elastomer [7, 8]. However, solvent compatibility is a major concern with materials that swell in the presence of non-polar solvents such as hydrocarbons, toluene, and dichloromethane [9]. The lithography-free production of microchannels using electrochemically stable carbon materials can be useful in overcoming some of these limitations [10]. The fabrication of micro/nanochannels based on electrospun micro/nanofibers without lithography has recently been used for development of nanoelectronic devices [11]. The desired shape and size of microchannels can be achieved by controlling the electrospinning parameters [12]. This technique is a suitable method for long microchannel fabrication without diffusion of etchants into long and narrow channels.

Carbon materials such as carbon films, nanofibers, nanotubes, and graphene sheets have been explored for the development of point-of-care biosensors, and in other fields, including bioimaging, conjugated materials, and nanoelectronics [13-15]. Carbon films, in particular, have

good electrochemical activity/stability and are excellent biomolecule absorbents for biosensor fabrication [16]. Metallic nanoparticles can be used to enhance the electrochemical activity of a biosensor [17]. Hrapovic *et al.* explored the use of carbon tubes decorated with Pt nanoparticles (Pt NPs) as an electrochemical glucose biosensor with a detection time and limit of 3 s and 5 μ M, respectively [17]. Ha *et al.* fabricated an array of ordered mesoporous carbon nanochannels with cobalt nanoparticles, which can be regarded as a nanochannel reactor for high-performance Fischer–Tropsch synthesis [18]. The scanned coaxial electrospinning of silica nanochannels (20 nm) was used for single-molecule detection by Wang *et al* [19].

The integration of microfluidic channels into a porous carbon film may improve the surface functionality for biomolecule immobilization, resulting in enhanced stability, reproducibility, and sensitivity, as a result of improved hydrophilicity. A network of microfluidic channels in a porous carbon film provides greater binding affinity (such as rapid attachment of enzyme molecules) than in a planar dense carbon film [20, 21]. In this context, a nanochannel decorated with Pt NPs can act as a reaction chamber for antigen–antibody interactions and provide a conducting channel for electron transport from the electrolyte to the electrode, resulting in improved electrochemical performance of the biosensor. Catalytic micro/nanochannels in a porous carbon film are, therefore, suitable platforms for the development of point-of-care microdevices, an example of which we have developed in this study, as discussed below.

The aflatoxins (B1, B2, G1 and G2) are toxic, mutagenic, and carcinogenic substances; they are produced by *Aspergillus flavus* and *A. parasiticus* under certain conditions [18, 22]. Aflatoxins can be present in cereal grains, dried fruits, corn, nuts, oil seeds, wine, apple juice, and meat products, and they pose a risk to human health [23]. AFB1 is the most toxic aflatoxin

and can cause human hepatocellular carcinoma. A number of techniques have been developed for the quantification of aflatoxins in foods and feed [24]. Thin-layer chromatography, liquid chromatography, and enzyme-linked immunosorbent methods have been used for the detection of aflatoxins for the past two decades [25]. However, these methods have long detection times and require costly instruments [26]. User-friendly, low-cost, and environmentally friendly point-of-care devices may overcome these limitations and provide alternative methods for the detection of food contaminants. There is thus an urgent need to develop rapid and sensitive point-of-care devices for AFB1 detection.

We developed an easy and lithography-free fabrication of aligned micro/nanochannels embedded within highly macroporous Pt-decorated carbon (carbon-Pt) electrodes. We fabricated microchannels by placing electrospun poly (methyl methacrylate) (PMMA) fibers directly on a Si wafer, followed by spin coating of polyacrylonitrile (PAN) films. We exploit different thermal stabilities of PAN and PMMA polymers which allow their different roles in electrode fabrication [27]. Pyrolysis of the fiber-templated composite film created continuous channels by sacrificial removal of polymer fibers by thermal decomposition. Carbon electrodes decorated with Pt NPs, with and without embedded microchannels, were used for the detection of aflatoxin B1 (AFB1) *via* antigen–antibody interactions. Covalent interactions between antibodies (amino terminal) and the carbon electrode exposed to plasma treatment were achieved *via* 1-ethyl-3-(3-dimethylaminopropyl) carbodiimide (EDC)–*N*-hydroxysuccinimide (NHS) coupling, resulting in the formation of a stable amide bond on the transducer surface. This method is simpler and more economical than other conventional techniques. This method enables efficient and label-free detection of AFB1 using a Pt-NP-decorated porous microchannel-based microfluidic biosensing platform.

2. Experimental

2.1 Materials. Polyacrylonitrile (PAN; MW = 150,000), poly (methyl methacrylate) (PMMA; MW= 120,000), and chloroplatinic acid hexahydrate salt were obtained from Sigma–Aldrich Inc., USA. N, N-dimethyl formamide (DMF), acetone were obtained from Fischer Scientific, India. HPLC grade water was supplied by Merck Pvt. Ltd., India. All reagents were of analytical grade. Aflatoxin B1 (AFB1), monoclonal anti-aflatoxin B1 (anti-AFB1) antibody, N-ethyl-N-(3-dimethylaminopropyl) carbodiimide (EDC), N-hydroxysuccinimide (NHS) and bovin serum albumin (BSA) were purchased from Sigma-Aldrich, USA.

2.2 Synthesis of porous carbon films with impregnated Pt NPs. Three Pt/carbon hybrid films were prepared, using a similar strategy as that used for the PAN film, but with addition of chloroplatinic acid hexahydrate salt (0.25 equiv with respect to the PAN monomer) during preparation of the PAN:DMF solution. The PMMA fibers were synthesized using an electrospinning technique, as described in the literature [28]. Briefly, 30 wt% PMMA ($M_w = 120\,000$, Sigma-Aldrich Inc., USA) solution was prepared by dissolving PMMA in DMF in a capped bottle; magnetic stirring was performed for 4 h to ensure uniform mixing. This precursor solution was transferred to a plastic syringe, which was connected to a high-voltage DC power source (Gamma High Voltage, Inc., High Bridge, NJ, USA) by a metallic needle tip. A stainless-steel rotating electrode with attached Si wafers was used as the collector for the electrospun fibers. The distance between the needle tip and collector was 7 cm, and a solution flow rate of 80 $\mu\text{L}/\text{min}$ was maintained using a syringe pump (Harvard Apparatus, Holliston, MA, USA), with a constant high voltage of 14 kV. The collection time and collector speed were optimized so that the minimum number of fibers was deposited on the Si wafer. The electrospun PMMA fibers were stabilized in air at 150 °C.

After electrospinning the PMMA fibers on the Si wafer, spin coating was used to deposit PAN ($M_w = 150\,000$, Sigma-Aldrich Inc., USA) films on top of the fibers, using a previously reported standard protocol.[29, 30] Briefly, an 8 wt% solution of PAN:DMF was prepared by dissolving a known quantity of PAN in DMF, and heating at 65 °C with constant stirring for 45 min to obtain a transparent viscous solution. This polymer solution (200 μ L) was spin coated at 5000 rpm for 40 s on a thoroughly cleaned Si wafer (1.5 cm \times 1.5 cm). After covering the electrospun PMMA fibers with a PAN film, the composite film (Si wafer/PMMA fibers/PAN film) was stabilized in air at 200 °C for 1 h. The thickness of the spin-coated films was varied from micrometers to a few hundred nanometers by simply varying the PAN polymer concentration and the speed of the spin coater.

2.3 Fabrication of microchannel-embedded electrodes. Scheme 1 shows the concept of micro/nanochannel fabrication. Among the various fiber preparation procedures, electrospinning has attracted much interest because it is a high throughput, continuous process and the fiber diameter can be controlled from the nanometer to micrometer scale.

The use of electrospun fibers has mainly focused on biomedical uses such as drug delivery and tissue-engineering scaffolds, and as substrates for functionalizing the channels of microfluidic devices. Spin-coating techniques are used to deposit uniform thin films on flat substrates, and are extensively used in the microfabrication of metal oxides using polymeric blend precursors, and in photolithography for photoresist coatings. Here, we used this technique to create a polymeric thin film on a substrate containing pre-deposited sacrificial fibrous layers. Channel widths ranging from a few micrometers to a few hundred nanometers were attained by simply varying the sacrificial electrospun fiber diameter; the channel height could therefore be controlled by controlling the thickness of the deposited film. The channels were cleaned and

residual polymer debris was removed by washing in acetone and deionized water. The channel functionality was enhanced by decorating the channels or nearby films with Pt NPs, which were deposited during electrospinning using chloroplatinic acid hexahydrate salt as the precursor. This method was successful for micro/submicro/nanochannel networks and straight channel fabrication. It is important to note that the functional platinum nanoparticles are uniformly deposited over the porous carbon electrode when PAN/chloroplatinic acid blend is used for spin coating and it is only present in the channels when the PMMA/chloroplatinic acid is used for electrospinning.

2.4 Biosensing platform. The fabricated electrodes consisting of porous carbon on a steel substrate, with and without microchannels, were exposed to oxygen plasma treatment to create –COOH groups on their surfaces. The oxygen plasma treatment was performed in a vacuum pressure of 0.005 mbar and the oxidation voltage was kept at 450 V for 0.5 h. Prior to covalent surface functionalization, the –COOH groups of the porous carbon were activated using EDC as the coupling agent and NHS as the activator. A monoclonal antibody (anti-AFB1) solution was prepared in phosphate buffer (pH 7.4). The anti-AFB1 solution (10 μ L) was spread on the porous carbon surface and incubated in a humid chamber for about 4 h at 25 °C. The –COOH groups on the carbon surface and –NH₂ groups of the anti-AFB1 interacted covalently to form strong amide bonds (C–N). BSA (1 mg/mL) solution was used to block the non-specific active sites on the antibody-functionalized carbon electrode. The antibody-functionalized electrode was then washed with phosphate-buffered saline and stored at 4 °C when not in use.

2.5 Characterization. The field emission scanning electron microscopy (FESEM, Quanta 200, Zeiss, Germany) was utilized to characterize the surface morphologies of microchannels on porous carbon film decorated with platinum nanoparticles.

EDX (Oxford Instruments, England) was performed for elemental analysis of the carbon and platinum nanoparticles decorated within the microchannels. The powder X-ray diffraction (XRD) measurements were conducted on an X'Pert Pro, PAN-analytical, Netherlands, X-ray system with Cu K α radiation to get the structural information of the pure component and the Pt hybrid films. Raman spectral analysis was performed on WiTec, Germany using laser light of 543 nm wavelength to characterize the graphitic nature of the carbon material. The surface topography of the carbon film was further established by the atomic force microscopy (AFM) using an Agilent Technologies atomic force microscope (Model 5500) operating in the non-contact/ACAFM mode. Micro-fabricated silicon nitride cantilevers with a spring constant (C) of 50 N/m and resonant frequency (f) of 175 kHz were used. The average thickness (T), width (W), and length (L) of the cantilever were approximately 700, 38, and 225 μ m, respectively. Data acquisition and analysis were carried out using PicoView 1.4 and Pico Image Basic software, respectively. Surface profiling and the thicknesses of the PAN film were analyzed using an optical profiling system (Nano Map-D, AepTechnology, USA). The electrochemical investigations of the fabricated biosensors were carried out via Autolab Potentiostat/Galvanostat (Model AUT-84275) in a three electrode electrochemical cell system consisting of a working electrode, Ag/AgCl as a reference electrode and platinum as a counter electrode.

3. RESULTS AND DISCUSSION

3.1 Fabrication and characterization of micro/nano channels. The thermal stabilities of PMMA and PAN were investigated using thermal gravimetric analysis (TGA); the results are shown in Figure 1a. TGA of PMMA shows that there is a gradual decrease in weight with increasing temperature, reaching a weight loss of 98.5%. The remaining 1.5% is char. TGA of

PAN shows that a weight loss of 50% occurs upto 700 °C, after which there is no further loss. This is because PAN is converted to amorphous carbon at that temperature. The thermograms of the polymers show that there are two weight-loss steps. Stage 1 involves the decomposition of residual *N*, *N*-dimethylformamide (DMF) solvent, and polymer degradation occurs at stage 2. The temperature at which 50% weight loss occurred ($T_{50\%}$) is 364 °C for PMMA and 648 °C for PAN; these results show that PAN has good thermal stability. On the basis of this difference between the thermal stabilities, we chose PMMA fibers as a sacrificial template for making channels underneath PAN-derived carbon films.

Figure 1b shows field-emission scanning electron microscopy (FESEM) image of submicrometer PMMA fibers after electrospinning. The fiber diameter was varied from several micrometers to a few hundred nanometers by simply varying the solution viscosity, applied electric field strength, and solution flow rate during electrospinning. The FESEM images (Figure 1c, 1d) show PAN films of thicknesses of 2 μm and 700 nm, respectively, produced by varying the rotation speed of the spin coater.

A low-viscosity polymer solution and high spin coater rotation speed produce thinner films, and the thickness increases with increasing viscosity and decreasing rotation speed [29]. The PAN film porosity can be optimized by optimizing parameters such as viscosity of the polymer solution, spin coater rotation speed, nature of the solvent for the polymer, and humidity [29, 30]. Figure 1e shows a few submicron electrospun fibers covered with a PAN film of thickness 500 nm. The composite film was placed in a tubular furnace for carbonization.

The samples were carbonized for 1 h in an argon gas atmosphere with a constant flow rate of 0.15 L/min; the heating rate was maintained at 5 °C/min up to 900 °C, followed by ambient cooling to form micro/submicro/nanometer channels embedded in the porous carbon

film. TGA analysis shows that PMMA is thermally stable up to 300 °C and then undergoes rapid decomposition, but PAN is stable and converted to carbon. Figure 1f shows decomposed PMMA fibers within the PAN film (the decomposed fiber track is indicated by a red dashed line). Finally, after 400 °C, the PMMA fibers are removed, leaving behind voids, which create channels embedded in the PAN-derived carbon film. Carbonization at 900 °C produces amorphous macroporous carbon films.

We carbonized the PMMA/PAN composite at 900 °C to ensure complete removal of PMMA and to obtain a good-quality carbon film by PAN carbonization. Figure 1g shows the parallel microchannels fabricated on the Si substrate. After carbonization at high temperature, sacrificial PMMA polymer fibers were preferentially decomposed, but debris was produced (Figure 1h) because of the carbon residue. This debris (indicated by an arrow in Figure 1h) was easily removed by cleaning the channels with acetone and deionized water. Figure 1i shows completely clean channels after debris removal (the arrow in Figure 1i indicates a debris-free channel).

The channel alignment was controlled by alignment of the electrospun fibers. Random unaligned channels were created by electrospinning of PMMA fibers on a static collector (Figure 2a shows randomly oriented channels). Partially aligned electrospinning fibers are obtained using a rotating collector, which produces highly aligned parallel microchannels, (Figure 2b). In this spinning procedure, the electrospun fibers undergo alignment and undergo mechanical stretching because of the high-speed rotating cylindrical electrode [31, 32].

We believe that these features distinguish our method for fabrication of the micro/nanochannels from the existing techniques [33, 34]. The width and number density of the channels can be easily controlled by optimizing the electrospun PMMA fiber diameter and

deposition time. The channel number density increased with increasing electrospinning time. The calculated channel densities were $\sim 1 \times 10^8$, 2×10^8 , and 8×10^8 per square meter for electrospun fiber deposition times of 1, 2, and 5 min, respectively.

After prolonged electrospinning, the fibers overlapped and stuck together, leading to non-uniform, broken, short channels, or even no channel formation. The carbon film porosity can be varied by varying the spin coating speed and polymer concentration, as previously reported [29, 30]. Figure 2c shows the microchannels embedded in a thick (thickness $\sim 1.2 \mu\text{m}$), non-porous carbon film, formed by spin coating a 16 wt% PAN film at 1000 rpm. However, a 4 wt% PAN film (Figure 2d) spin coated at 10 000 rpm produced a thin macroporous (thickness $\sim 150 \text{ nm}$) carbon film. We also varied the channel width (the width was estimated using optical profilometry, as discussed later) from a few hundred nanometers to tens of micrometers; the FESEM images in Figure 2e, f, and g show the fabricated channels.

The minimum channel diameter obtained was $\sim 200 \text{ nm}$ (Figure 2g); this required careful control of the fiber diameter and thickness of the deposited film. However, fabrication of the microchannels was relatively easy.

The fabrication technique proposed here is not only a proficient method for the synthesis of micro/submicro/nanochannels, but can also be used to enhance the functionalities of the channels and/or the films. For example, we easily decorated the microchannels with Pt NPs (Figure 2h) by modifying the sacrificial electrospun PMMA fibers with chloroplatinic hexahydrate salt, which is used as a precursor for Pt NPs. Chloroplatinic hexahydrate salt undergoes thermal decomposition during high-temperature carbonization and produces Pt NPs [29, 35]. The channels in the carbon films can also be modified. In this case, the Pt NP precursor was introduced directly during spin coating of PAN (Figure 2i). This method is highly

reproducible as we can easily control the electrospinning and spin-coating technique along with the carbonization process.

The amorphous nature of the porous carbon films was investigated using Raman spectroscopy. The Raman spectra obtained from the porous carbon films are shown in Figure 3a; they consist of two major peaks, at 1350 and 1595 cm^{-1} , corresponding to the fundamental D and G bands, respectively, for sp^2 carbon. The intensity ratio of the D band to the G band (I_D/I_G) can be used to determine the degree of disorder in carbon films [29, 30]. The calculated intensity ratio is 0.94; this indicates that the film is amorphous.

The porous morphology and film thickness were determined using atomic force microscopy (AFM); the results are shown in Figure 3b. The AFM analysis confirms the presence of macropores in the film. The height profile analysis shows (in Figure 3b) that the pore size is $\sim 2 \mu\text{m}$.

The microchannel filled with Pt NPs was examined using energy-dispersive X-ray spectroscopy (Figure 3c); the spectrum, along with the quantitative data listed in Table 1, confirms the presence of spherical Pt NPs in the microchannels.

The widths and thicknesses of the microchannels and the thicknesses of the carbon films were measured using an optical profiler in non-contact mode (Figure 3d). Figure 3d(i) shows an array of parallel microchannels on the carbon film. Figure 3d(ii) shows an optical three-dimensional profiling image of the carbon film containing microchannels of average width and depth $\sim 20 \pm 1.5 \mu\text{m}$ and $550 \pm 30 \text{ nm}$, respectively. A single microchannel within the porous carbon film is shown in Figure 3d(iii). The optical micrograph in Figure 3d(iv) shows the D topography of Figure 3d(iii), which can be used to estimate the channel width and depth.

The hydrophilic nature of the functionalized carbon films was investigated using contact angle measurements (Figure 4). The porous carbon-Pt film has a contact angle of 68.5° , and this decreases to 46° after plasma treatment. This may be caused by the introduction of hydrophilic functional groups (*e.g.*, $-\text{COOH}$, $-\text{OH}$, $-\text{CHO}$) on the carbon-Pt film surface. The hydrophilicity of the carbon-Pt film increased more when a surface-embedded network of microchannels was present (contact angle: 20.1°). A carbon-Pt film with a microchannel network has superior hydrophilicity, which helps antibody immobilization on its surface.

3.2 Electrochemical properties. Figure 5 shows the impedance spectra (Nyquist plots) obtained by measuring the charge-transfer resistance (R_{ct}), constant phase element at the electrode/electrolyte interface, and heterogeneous electron transfer (HET) rate constant. The carbon electrode decorated with Pt NPs has a larger semicircle diameter, leading to a higher R_{ct} ($173.0 \Omega \times \text{cm}^2$) compared with a carbon electrode with embedded microchannels. The R_{ct} of the carbon-Pt electrode with embedded microchannels is lower ($139.7 \Omega \times \text{cm}^2$) than that of the bare carbon-Pt electrode. Perhaps the microchannels embedded in the carbon electrode act as conduction paths for the flow of electrons generated from oxidation/reduction of the $[\text{Fe}(\text{CN})_6]^{3-/4-}$ redox probe, resulting in enhanced electrochemical reactivity. The enhanced electrochemical reactivity in the case of the microchannel-embedded carbon electrode is caused by a higher HET rate constant ($3.05 \times 10^{-4} \text{ cm/s}$) and the lower time constant (99.5), resulting in a lower R_{ct} compared with that of a carbon-Pt electrode without microchannels integrated on its surface. Anti-AFB1 immobilization on the carbon-Pt electrode increases the R_{ct} value (7.8 k Ω), because of the higher HET ($0.26 \times 10^{-4} \text{ cm/s}$) rate constant toward the current collector, compared with that of the bare carbon-Pt electrode. The antibodies may establish an insulating layer on the carbon-Pt electrode surface, which enhances the impedance signal, resulting in a

higher R_{ct} . However, the time constant for a carbon-Pt electrode with immobilized anti-AFB1 was higher than those for other fabricated electrodes (Table 1), because of the slow diffusion of electrons *via* oxidation/reduction of the $[\text{Fe}(\text{CN})_6]^{3-/4-}$ redox probe at the electrode/solution interface. The R_{ct} value for the anti-AFB1/carbon-Pt electrode with integrated microchannels (4.7 k Ω) is higher than that of the anti-AFB1/carbon-Pt electrode. The microchannels embedded in the carbon film therefore enhance the electrochemical conductivity and HET rate constant.

3.3 AFB1 detection. Electrochemical impedance spectroscopy (EIS) was used to determine the AFB1 concentrations on fabricated immunoelectrodes with and without integrated microchannels. The impedance response of the immunoelectrode (anti-AFB1/carbon-Pt) was investigated (Figure 6i) as a function of AFB1 concentration (1 pg/mL to 0.1 $\mu\text{g/mL}$). The corresponding impedance spectra (or Nyquist plots), and sensor calibration plot for the immunoelectrode as a function of AFB1 concentration, are shown in Figure 6(ii). The impedance response curves and sensor calibration plots for anti-AFB1/carbon-Pt with integrated microchannels are shown in Figure 6(iii) and (iv). In both cases, R_{ct} increased with increase in AFB1 concentration from 10^{-12} g/mL to 10^{-7} g/mL. The R_{ct} value is proportional to the AFB1 concentration. The antigen–antibody interactions on the functionalized electrode surface may create a capacitive layer, which is in series with a double-layer capacitance. This capacitive layer acts as a barrier to electron transfer on the electrode surface, resulting in an enhanced impedance signal. The impedance signal was higher at higher concentrations of AFB1. The electrode response became saturated at an AFB1 concentration of 10^{-7} ng/mL for the carbon-Pt electrode. However, the impedance signal did not become saturated for the carbon-Pt electrode with microchannels; this is probably because of the higher loading of anti-AFB1. Within the testing range of 10^{-12} – 10^{-7} g/mL, these proposed immunosensors do not show an equilibrium adsorption

of AFB1. Compared to previous reported literature [Table 2], the proposed immunosensors thus have a higher detection range. The sensitivities of the fabricated immunoelectrodes for AFB1 detection are comparable, as shown in Figure 6.

The slightly better sensitivity of the microchannel/carbon-Pt electrode-based immunosensor is due to the presence of microchannels in the carbon surface; these provide an electrochemical conduction path for better transport of electrons from the bulk solution compared with that in the bare carbon-Pt electrode, as shown by the impedance studies (Figure 6ii and iv). This immunosensor can detect both high (0.1 $\mu\text{g/mL}$) and low (1 pg/mL) AFB1 concentrations, with a wide detection range. The reproducibilities of the results obtained using the fabricated immunosensors were investigated by EIS using different working electrodes at an AFB1 concentration of 1 ng/dL (Figure 6i). The immunosensors with and without microchannels provided good reproducibilities for five different electrodes, as shown by their low relative standard deviations (RSDs), namely, 2.32% and 5.32%, respectively. The low RSD value of the fabricated immunosensor with microchannels indicates good precision. The stabilities of the immunosensors were monitored at regular time intervals for 50 d. The impedance responses of the immunoelectrodes with and without microchannels at 40 d decreased by 5.3% and 8.9% from their initial values, indicating good stability after incorporation of microchannels on the carbon film. Table 2 shows the AFB1-sensing characteristics of the fabricated immunoelectrodes and those reported in the literature.

The selectivities of the immunosensors were investigated in the presence of ochratoxin A (1.0 ng/dL) using EIS. We did not observe any significant change in the current response, as shown by the very low RSDs of 2.1% for microchannel/carbon-Pt and 2.2% for carbon-Pt. These results indicate that the immunosensors are highly selective. The selectivity is derived from the

presence of adsorbed bovine serum albumin (BSA) molecules, which block non-specific sites, and specific recognition of the antibody and antigen of AFB1.

4. CONCLUSIONS

We developed a novel, simple, and easy method for the lithography-free fabrication of aligned micro/nanometer functionalized channels on porous carbon films using eletrospinning and spin-coating techniques. PMMA fibers acted as a sacrificial polymer for the creation of channels embedded in a PAN-derived porous carbon film. The alignment of the fabricated microchannels on the carbon film was controlled by electrospinning on a rotating collector. The channel width was varied by changing the diameter of the electrospun fibers. Channels of widths in the range 200 nm to tens of micrometers were fabricated. We improved the channel functionality by modification with preloaded Pt NPs. The microchannels decorated with Pt NPs gave an electrochemical biosensor with improved electrocatalytic properties. The electrochemical activity of the carbon-Pt electrode with microchannels showed excellent conductivity, because of the higher diffusivity and HET constant, compared with the carbon-Pt electrode without microchannels. Anti-AFB1 functionalization of the carbon-Pt films with and without microchannels was performed using conjugation chemistry (EDC–NHS) *via* oxygen plasma treatment, for AFB1 detection. The higher electrochemical conductivity of the carbon-Pt electrode with integrated microchannels had lower impedimetric sensitivity compared with that of the bare carbon-Pt electrode for AFB1 detection. The performances of these biosensors are highly reproducible, and the biosensors are stable and capable of detecting picomolar concentrations of AFB1 in foods. Efforts should be made to extend this microfluidic platform for the development of pressure-driven and electric-field-driven fluid flows for catalytic, photocatalytic, drug-delivery, and diagnostic devices.

ASSOCIATED CONTENT**AUTHOR INFORMATION****Author Contributions**

The manuscript was written through contributions of all authors. All authors have given approval to the final version of the manuscript.

Notes

The authors declare no competing financial interest.

Acknowledgements

This work was supported by the DST Unit of Excellence on Soft Nanofabrication at Indian Institute of Technology Kanpur from the Department of Science and Technology, New Delhi, India. KM wants to acknowledge Sandhya Kumari for her B.Tech project report, (2012) at IIT Kanpur and interesting discussions.

Biographies



Kunal Mondal is a Post-doctoral Research Associate at the North Carolina State University, USA, in the Department of Chemical and Biomolecular Engineering. He received his Ph.D from the Indian Institute of Technology Kanpur, India (2015) and both of his M.Sc and M.Tech from the Indian Institute of Engineering Science and Technology, Shibpur, India (2006-2010). Kunal's research interests are in micro/nano fabrication of functional materials, colloids and interfaces of soft nanostructures, self and directed assembly, nano/micro-electronics, microfluidics, photovoltaics, polymer thin-films, carbon nanomaterials, carbon composites, carbon MEMS/NEMS in health, energy and environmental applications. He has published 12 papers in peer-reviewed journals, authored in a book chapter and filed 2 patents.



Md. Azahar Ali received his PhD degree from Biomedical Engineering Department at Indian Institute of Technology Hyderabad, India in collaboration with Biomedical Instrumentation Section at National Physical Laboratory, New Delhi, India. He also received his Master of Technology degree from Department of Electronics Engineering, Tezpur University, Assam in 2009. Currently, he is doing Post-Doctoral Associate at Electrical and Computer Engineering, Iowa State University, USA. He is actively engaged in the area of microfluidic based multiplex biochips for biomolecules detection.



Saurabh Srivastava received his Ph.D. in Physics from Banaras Hindu University (BHU), India in 2015. He is presently a DST-INSPIRE Faculty at Department of Applied Physics, Delhi Technological University, Delhi, India. He is actively engaged in the area of development of graphene based immunosensor for cancer detection.



B. D. Malhotra received his Ph.D. degree from the University of Delhi, Delhi, India in 1980. He has published more than 270 papers in peer-reviewed journals, filed 10 patents, and edited/co-edited books on biosensors and polymer electronics. After his stint as Chief Scientist and Head of the DST Centre on Biomolecular Electronics at the CSIR-National Physical Laboratory, New Delhi, India, he moved to Delhi Technological University (DTU), India. He has nearly 30 years of research experience in the field of biomolecular electronics and has guided 25 Ph.D. students to date. His current activities include biosensors, nanobiomaterials, conducting polymers, and ordered molecular assemblies including Langmuir–Blodgett films and self-assembled monolayers among others. Dr. Malhotra is a Fellow of the Indian National Science Academy (INSA), the National Academy of Sciences, India (NASI) and an Academician of the Asia-Pacific Academy of Materials (APAM).



Ashutosh Sharma is a Chair Professor in Chemical Engineering at the Indian Institute of Technology at Kanpur (IITK). Ashutosh received his PhD from the State University of

New York at Buffalo (1987), MS from the Pennsylvania State University (1984) and B. Tech. from IITK (1982). Ashutosh's research interests are in soft functional interfaces, micro/nano-mechanics of confined soft matter, self-organized patterning, soft nanofabrication, colloid and interfacial engineering, carbon nanocomposites and carbon MEMS/NEMS in energy, health and environmental applications, and membranes. He is currently Secretary to the Government of India, Department of Science and Technology starting January 2015.

REFERENCES

- [1] A.C. Ferrari, F. Bonaccorso, V. Falko, K.S. Novoselov, S. Roche, P. Boggild, et al., Science and technology roadmap for graphene, related two-dimensional crystals, and hybrid systems, *Nanoscale*, (2014).
- [2] [Y. Lu, J. Liu, Functional DNA nanotechnology: emerging applications of DNAzymes and aptamers, *Current Opinion in Biotechnol*, 17\(2006\) 580-8.](#)
- [3] [D.J. Beebe, G.A. Mensing, G.M. Walker, Physics and applications of microfluidics in biology, *Annual Rev, Biomed Eng*, 4\(2002\) 261-86.](#)
- [4] [G.M. Whitesides, The origins and the future of microfluidics, *Nature*, 442\(2006\) 368-73.](#)
- [5] [Y. Hongbin, Z. Guangya, C.F. Siong, W. Shouhua, L. Feiwen, Novel polydimethylsiloxane \(PDMS\) based microchannel fabrication method for lab-on-a-chip application, *Sensors and Actuators B: Chemical*, 137\(2009\) 754-61.](#)
- [6] [C.-C. Chang, Z.-X. Huang, R.-J. Yang, Three-dimensional hydrodynamic focusing in two-layer polydimethylsiloxane \(PDMS\) microchannels *J Micromech Microeng*, 17\(2007\) 1479–86.](#)
- [7] [H. Yongfang, Z. Gaofeng, W. Xiang, S. Daoheng, Fabrication of micro/nanometer-channel by near-field electrospinning, *Nano/Micro Eng Molecul Syst \(NEMS\)*, 2011 IEEE Int Conference 2011, pp. 877-80.](#)
- [8] [Y. Xia, J.J. McClelland, R. Gupta, D. Qin, X.-M. Zhao, L.L. Sohn, et al., Replica molding using polymeric materials: A practical step toward nanomanufacturing, *Adv Mater*, 9\(1997\) 147-9.](#)
- [9] [J.N. Lee, C. Park, G.M. Whitesides, Solvent compatibility of poly\(dimethylsiloxane\)-based microfluidic devices, *Anal Chem*, 75\(2003\) 6544-54.](#)
- [10] [E. Jo, M.-C. Lim, H.-N. Kim, H.-J. Paik, Y.-R. Kim, U. Jeong, Microfluidic channels fabricated on mesoporous electrospun fiber mats: A facile route to microfluidic chips, *J Polymer Sci B: Polymer Phys*, 49\(2011\) 89-95.](#)
- [11] [E.M. Jeffries, Y. Wang, Biomimetic micropatterned multi-channel nerve guides by templated electrospinning, *Biotechnol Bioeng*, 109\(2012\) 1571-82.](#)

- [12] A. Ali, K. Mondal, C. Singh, B.D. Malhotra, A. Sharma, Anti-epidermal growth factor receptor conjugated mesoporous zinc oxide nanofibers for breast cancer diagnostics, Nanoscale, (2015).
- [13] V. Vamvakaki, M. Hatzimarinaki, N. Chaniotakis, Biomimetically synthesized silica-carbon nanofiber architectures for the development of highly stable electrochemical biosensor systems, Anal Chem, 80(2008) 5970-5.
- [14] H.-M. So, K. Won, Y.H. Kim, B.-K. Kim, B.H. Ryu, P.S. Na, et al., Single-walled carbon nanotube biosensors using aptamers as molecular recognition elements, J Am Chem Soc, 127(2005) 11906-7.
- [15] M. Pumera, Graphene in biosensing, Mater Today, 14(2011) 308-15.
- [16] J. Xu, M.C. Granger, Q. Chen, J.W. Strojek, T.E. Lister, G.M. Swain, Peer reviewed: Boron-doped diamond thin-film electrodes, Anal Chem, 69(1997) 591A-7A.
- [17] S. Hrapovic, Y. Liu, K.B. Male, J.H.T. Luong, Electrochemical biosensing platforms using platinum nanoparticles and carbon nanotubes, Anal Chem, 76(2003) 1083-8.
- [18] S. Srivastava, V. Kumar, M.A. Ali, P.R. Solanki, A. Srivastava, G. Sumana, et al., Electrophoretically deposited reduced graphene oxide platform for food toxin detection, Nanoscale, 5(2013) 3043-51.
- [19] M. Wang, N. Jing, C.B. Su, J. Kameoka, C.-K. Chou, M.-C. Hung, et al., Electrospinning of silica nanochannels for single molecule detection, Appl Phys Lett, 88(2006) -.
- [20] R.A. Vijayendran, K.M. Motsegood, D.J. Beebe, D.E. Leckband, Evaluation of a Three-Dimensional Micromixer in a Surface-Based Biosensor, Langmuir, 19(2003) 1824-8.
- [21] R.B. Schoch, L.F. Cheow, J. Han, Electrical Detection of Fast Reaction Kinetics in Nanochannels with an Induced Flow, Nano Letters, 7(2007) 3895-900.
- [22] G. Bacher, S. Pal, L. Kanungo, S. Bhand, A label-free silver wire based impedimetric immunosensor for detection of aflatoxin M1 in milk, Sens Actuators, B: Chem, 168(2012) 223-30.
- [23] P.P. Maia, M.E.P.B.d. Siqueira, Occurrence of aflatoxins B1, B2, G1 and G2 in some Brazilian pet foods, Food Additives Contaminants, 19(2002) 1180-3.

- [24] [A.P. Wacoo, D. Wendi, P.C. Vuzi, J.F. Hawumba, Methods for detection of aflatoxins in agricultural food crops, J Appl Chem, Vol-2014\(2014\) 1-15.](#)
- [25] [N. Paniel, A. Radoi, J.-L. Marty, Development of an electrochemical biosensor for the detection of aflatoxin M\(1\) in milk, Sensors \(Basel\), 10\(2010\) 9439-48.](#)
- [26] [N.H.S. Ammida, L. Micheli, G. Palleschi, Electrochemical immunosensor for determination of aflatoxin B1 in barley, Anal Chim Acta, 520\(2004\) 159-64.](#)
- [27] [N.C. Abeykoon, J.S. Bonso, J.P. Ferraris, Supercapacitor performance of carbon nanofiber electrodes derived from immiscible PAN/PMMA polymer blends, RSC Advances, 5 19865-73.](#)
- [28] [K. Nayani, H. Katepalli, C.S. Sharma, A. Sharma, S. Patil, R. Venkataraghavan, Electrospinning combined with nonsolvent-induced phase separation to fabricate highly porous and hollow submicrometer polymer fibers, Ind Eng Chem Res, 51\(2012\) 1761-6.](#)
- [29] [K. Mondal, J. Kumar, A. Sharma, Self-organized macroporous thin carbon films for supported metal catalysis, Colloids Surfaces A: Physicochem Eng Aspects, 427\(2013\) 83-94.](#)
- [30] [K. Mondal, J. Kumar, A. Sharma, TiO₂-nanoparticles-impregnated photocatalytic macroporous carbon films by spin coating, Nanomater Energy, 2\(2013\) 121-33.](#)
- [31] [H. Lee, H. Yoon, G. Kim, Highly oriented electrospun polycaprolactone micro/nanofibers prepared by a field-controllable electrode and rotating collector, Applied Physics A, 97\(2009\) 559-65.](#)
- [32] [K. Mondal, M.A. Ali, V.V. Agrawal, B.D. Malhotra, A. Sharma, Highly Sensitive Biofunctionalized Mesoporous Electrospun TiO₂ Nanofiber Based Interface for Biosensing, ACS Appl Mater Interfaces, 6 2516-27.](#)
- [33] [Y. Huang, G. Zheng, X. Wang, D. Sun, Fabrication of micro/nanometer-channel by near-field electrospinning Proc 2011 6th IEEE Int Conference Nano/Micro Eng Molecul Syst, Taiwan, February 20-23\(2011\).](#)
- [34] [Y.-J. Chuang, F.-G. Tseng, J.-H. Cheng, W.-K. Lin, A novel fabrication method of embedded micro-channels by using SU-8 thick-film photoresists, Sensors Actuators A: Phys, 103\(2003\) 64-9.](#)
- [35] [W. Chen, J. Zhang, Ag nanoparticles hosted in monolithic mesoporous silica by thermal decomposition method, Scripta Mater, 49\(2003\) 321-5.](#)

- [36] P. Kalita, J. Singh, M. Kumar Singh, P.R. Solanki, G. Sumana, B.D. Malhotra, Ring like self assembled Ni nanoparticles based biosensor for food toxin detection, *Appl Phys Lett*, 100(2012) -.
- [37] S. Piermarini, L. Micheli, N.H.S. Ammida, G. Palleschi, D. Moscone, Electrochemical immunosensor array using a 96-well screen-printed microplate for aflatoxin B1 detection, *Biosen Bioelectron*, 22(2007) 1434-40.
- [38] Y. Liu, Z. Qin, X. Wu, H. Jiang, Immune-biosensor for aflatoxin B1 based bio-electrocatalytic reaction on micro-comb electrode, *Biochem Eng J*, 32(2006) 211-7.
- [39] J.H.O. Owino, O.A. Arotiba, N. Hendricks, E.A. Songa, N. Jahed, T.T. Waryo, et al., Electrochemical immunosensor based on polythionine/gold nanoparticles for the determination of Aflatoxin B1 Sensors, 8(2008) 8262-74.
- [40] D. Tang, Z. Zhong, R. Niessner, D. Knopp, Multifunctional magnetic bead-based electrochemical immunoassay for the detection of aflatoxin B1 in food, *Analyst*, 134(2009) 1554-60.
- [41] A.-L. Sun, Q.-A. Qi, Z.-L. Dong, K.Z. Liang, An electrochemical enzyme immunoassay for aflatoxin B1 based on bio-electrocatalytic reaction with room-temperature ionic liquid and nanoparticle-modified electrodes, *Sens & Instrument Food Qual*, 2(2008) 43–50.
- [42] A. Sharma, Z. Matharu, G. Sumana, P.R. Solanki, C.G. Kim, B.D. Malhotra, Antibody immobilized cysteamine functionalized-gold nanoparticles for aflatoxin detection, *Thin Solid Films*, 519(2010) 1213-8.
- [43] C. Singh, S. Srivastava, M.A. Ali, T.K. Gupta, G. Sumana, A. Srivastava, et al., Carboxylated multiwalled carbon nanotubes based biosensor for aflatoxin detection, *Sens Actuators B: Chem*, 185(2013) 258-64.
- [44] J.H.O. Owino, A. Ignaszak, A. Al-Ahmed, P.G.L. Baker, H. Alemu, J.C. Ngila, et al., Modelling of the impedimetric responses of an aflatoxin B1 immunosensor prepared on an electrosynthetic polyaniline platform, *Anal Bioanal Chem*, 388(2007) 1069-74.
- [45] S. Srivastava, M.A. Ali, S. Umrao, U.K. Parashar, A. Srivastava, G. Sumana, et al., Graphene oxide-based biosensor for food toxin detection, *Appl Biochem Biotechnol*, 174(2014) 960–70.

Figure Captions

Figure 1. (a) TGA curves of PMMA and PAN shows the stability of polymers against temperature, (b) partially aligned PMMA fibers electrospun at 80 $\mu\text{L}/\text{min}$ flow rate, (c) a 2 μm thick, and (d) a 150 nm thin PAN film deposited on a Si wafer. Electrospun PMMA fibers covered by PAN film, (e) after stabilization at 150 $^{\circ}\text{C}$, and (f) pyrolysis at 400 $^{\circ}\text{C}$. Array of parallel microchannels embedded in porous carbon film, (g) parallel microchannels within porous carbon film, (h) a single microchannel with residue debris, and (h) a clean channel after removal of debris.

Figure 2. FESEM image of (a) unaligned micro channels while sacrificial PMMA fibers were electrospun on a static collector, (b) highly parallel micro channel array, (c) parallel micro channel array with decomposed PMMA derived residue, (d) parallel micro channels after cleaning. (e) A micrometer, (f) a submicrometer, and (g) a nanometer size clean embedded channel within the porous carbon film. (h) A micro channel loaded with functional platinum nanoparticles delivered during electrospinning of PMMA fibers, and (i) porous carbon film impregnated by platinum nanoparticles delivered during the time of spin coating of PAN polymer.

Figure 3. (a) Raman spectra confirm the amorphous nature of the carbon film. (b) AFM micrograph with height profile analysis of the thin porous carbon film. (c) EDX spectra for the elemental analysis of platinum nanoparticles decorated microchannels. (d) [i] Optical profilometry image showing parallel microchannel array within carbon film, [ii] 3D micrograph of 'i' shows the estimation of the channel width and depth, [iii] a single micro channel within the porous carbon film, and [iv] 3D micrograph of 'iii' estimate the channel width and depth.

Figure 4. (a) Porous carbon-Pt film, (b) plasma treated porous carbon-Pt film, (c) porous carbon-Pt film with microchannels.

Figure 5. Impedance spectra of various electrodes.

Figure 6. (i) Impedance spectra of the prepared immunosensor (anti-AFB1/Carbon-Pt) as a function aflatoxin concentration (1pg/mL-1 μ g/mL) and (ii) the corresponding Rct value and concentration plot. (iii) Impedance spectra of the prepared immunosensor (anti-AFB1/ μ channel/Carbon-Pt) as a function aflatoxin concentration (1pg/mL-1 μ g/mL) and (iv) the corresponding Rct value and concentration plot to the evaluation of sensor parameters.

Scheme 1. Schematic shows the fabrication of micro/nano channels on carbon-platinum electrode.

Figures

Figure 1

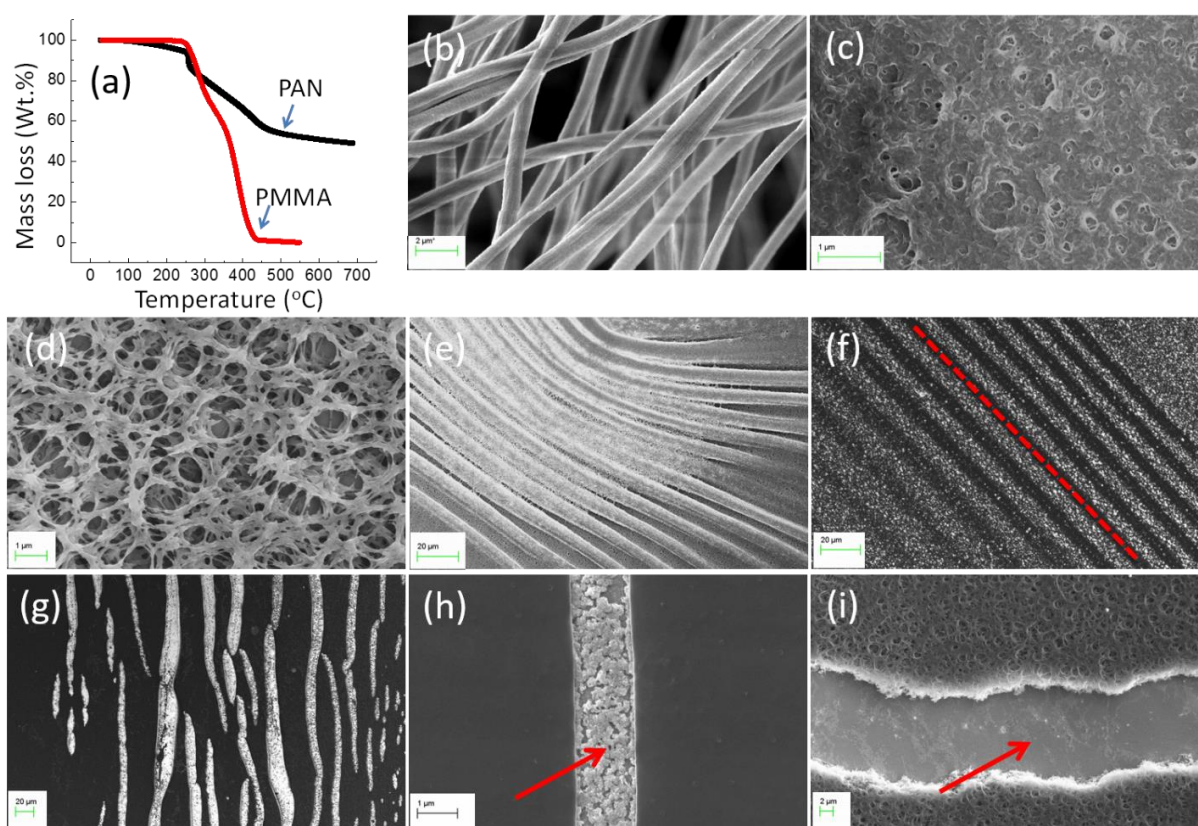


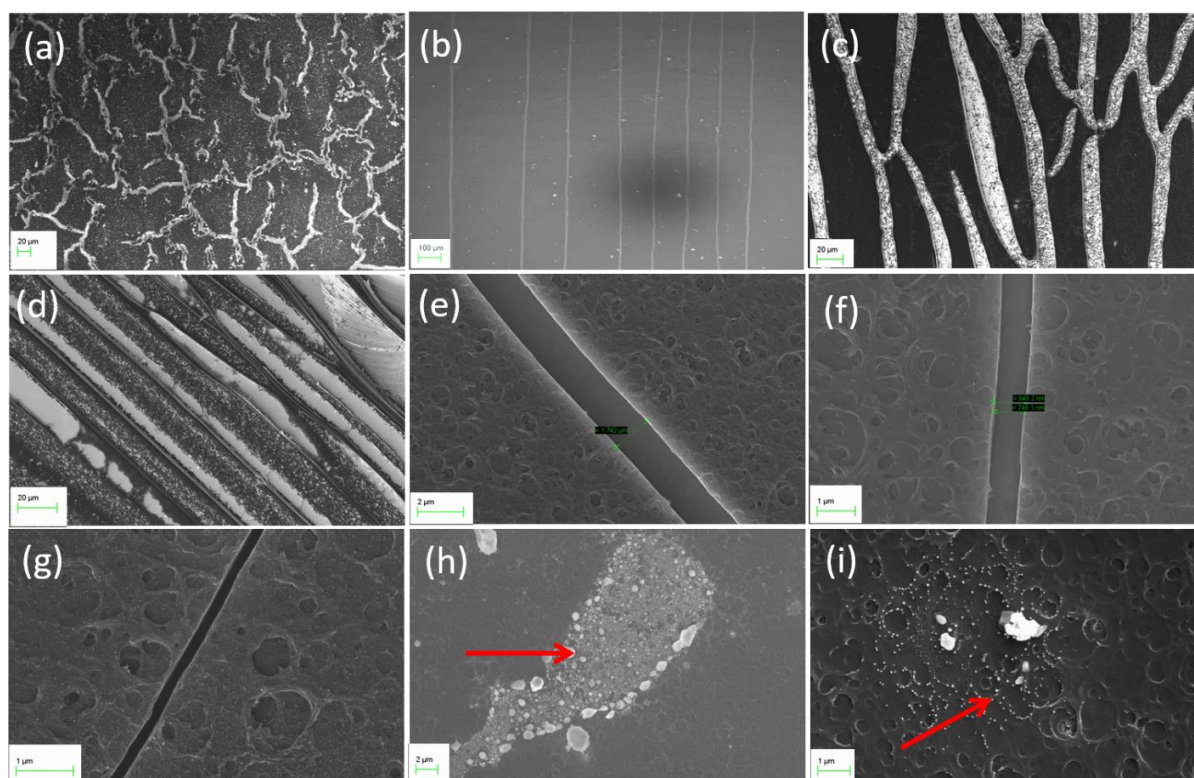
Figure 2

Figure 3

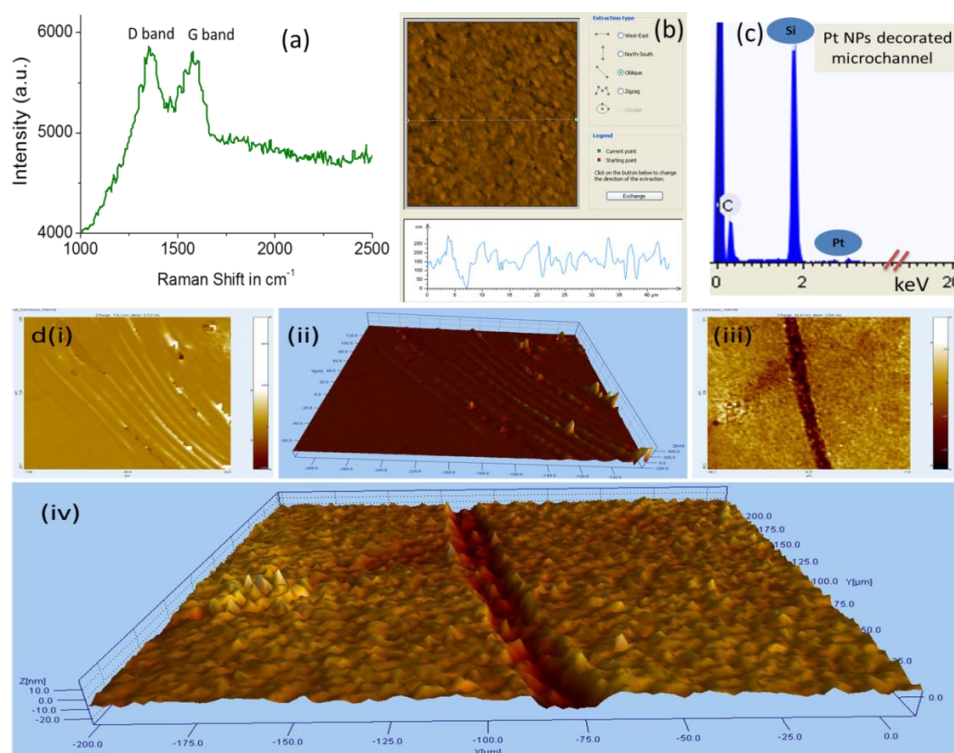


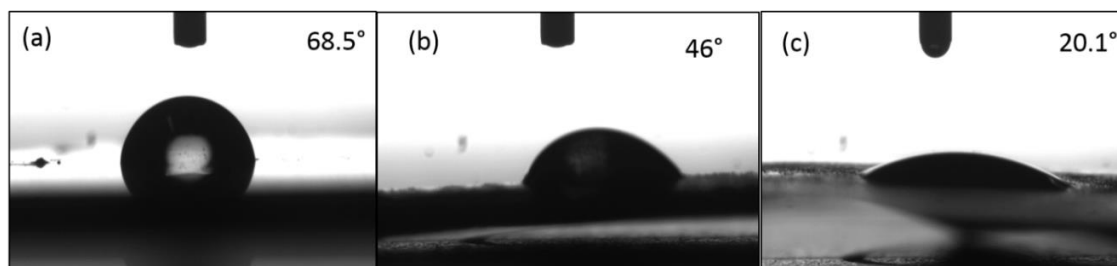
Figure 4

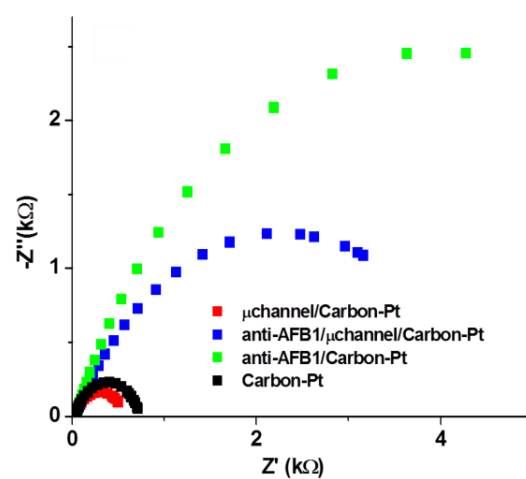
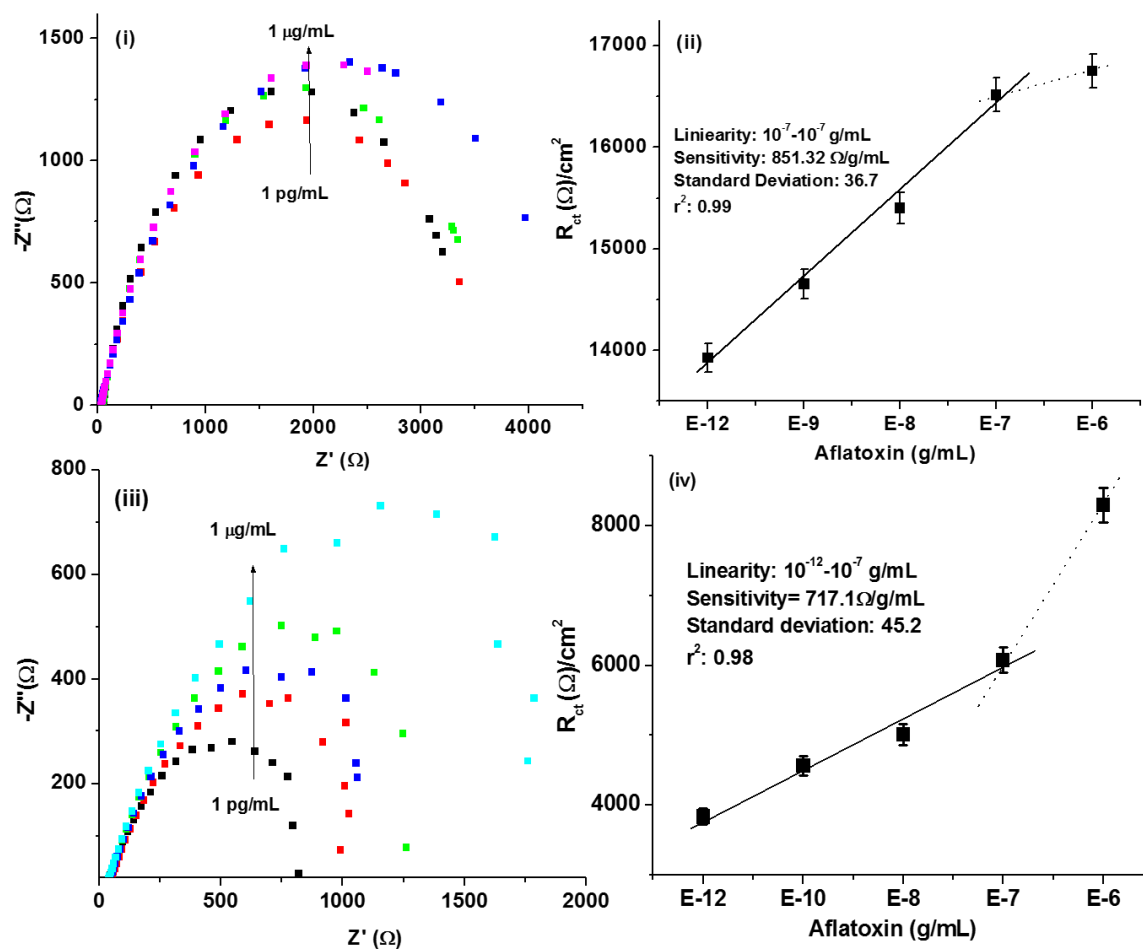
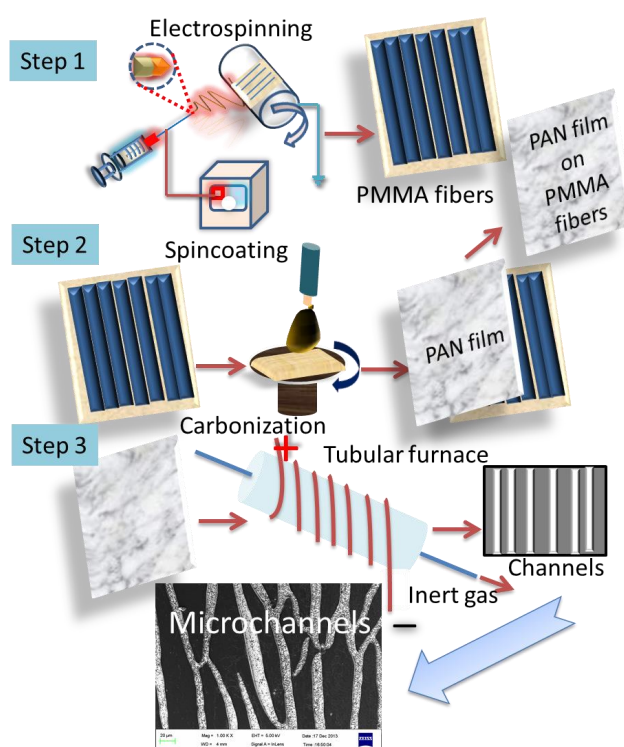
Figure 5

Figure 6:



Scheme 1



Tables

Table 1. Quantitative EDX data for the elemental analysis of platinum nanoparticles decorated microchannels with porous carbon electrode.

Element	Weight %	Weight % σ	Atomic %
Carbon	43.919	1.130	65.769
Silicon	52.525	1.093	33.638
Platinum	3.556	0.634	0.593

Table 2: Sensing characteristics of the proposed BSA/anti-AFB1/ μ channel/Carbon-Pt immunosensor, summarized along with some result reported in literature.

Electrode	Sensitivity μ A/(ng/mL)	Detection Limit (ng/mL)	Detection range (ng/ml)	Stability (days)	References
Ni-ITO	59	0.327	0.05-1	60	Kalita <i>et al.</i> [36]
SPCE		0.15	0.05-2	30	Piermarini <i>et al.</i> [37]
Au NPs	1.4	0.1	0.5-10	12	Liu <i>et al.</i> [38]
Au Nps/PTH-GCE	1.23	0.07	0.6-2.4		Owino <i>et al.</i> [39]
MMB	0.046	0.006	0.05-12	17	Tang <i>et al.</i> [40]
Nano Au/TiO ₂ /RTIL/Nafion	0.12	0.05	0.1-12	19	Sun <i>et al.</i> [41]
BSA/aAFB1-C- AuNP/MBA/Au	45	0.18	0.1-1	-	Sharma <i>et al.</i> [42]
MWCNTs/ITO	95	0.08	0.25-1.375	42	Singh <i>et al.</i> [43]
RGO/ITO	68	0.15	0.125-1.5	45	Srivastava <i>et al.</i> [18]
Pt/PANi-PSSA	869.6 Ω /ng/mL	100	1-6	56	Owino <i>et al.</i> [44]
GO/Au	639 Ω /ng/mL	0.23	0.5-5	35	Srivastava <i>et al.</i> [45]
BSA/anti- AFB1/ μ channel/Carbon- Pt	717.1 Ω /g/mL	1 pg/ml	1 pg/ml ⁻¹ - μ g/L	40	Present work

Environmental Concerns in National Capital Territory of Delhi, India

Shashank Shekhar Singh*, Singh SK and Shuchita Garg

Environmental Engineering Department, Delhi Technological University, Delhi, India

Abstract

After Independence, the city of Delhi became a major center of commerce, industry and education. The rapid urbanization of Delhi along with the level of growth in economic activities in the city and its surrounding areas stressed the natural environment significantly. Among the environmental problems, air pollution, water pollution, loss of biodiversity, municipal waste and noise pollution are major environmental challenges that the city is facing. The city suffers from air pollution caused by transportation, road dust, industries and pollutant emissions. Noise pollution comes mainly from industries, transportation, aircraft etc. Water pollution and lack of adequate solid waste treatment facilities have caused serious damage to the river on whose banks Delhi grew, the Yamuna. Several steps have been taken in the recent past to improve the environment condition which includes massive focus on afforestation, universal use of CNG by commercial vehicles, ban on plastic use, better management of solid waste, treatment of waste water and improvement of sewage system etc. But still many challenges remain to contain the environmental pollution. This paper summarizes the major environmental concerns and the present status of pollution in NCT of Delhi.

Keywords: Environmental concerns; Pollution; Atmosphere; Hazardous wastes

Introduction

Environment of any city is the asset of that city and for a city like Delhi-NCR, the significance of a clean and pleasing environment is as beneficial as it can be. Delhi being hub of political, social, economic and other national/international affairs of India portrays the image of India to the world. Being the national capital, plethora of national and international migration takes place from and to Delhi resulting in increasing pollution stress on natural resources viz. Air Water and Land. The overutilization of these resources makes Delhi prone to all types of pollution making lives of people difficult here. With Delhi expanding its boundaries each day and National Capital Region (NCR) getting to nearby states, the whole effect is quite evident in this area. Proper water use techniques need to be brought in place to make Delhi efficient and making water available to its masses. First step in this direction can be controlling water pollution levels. Similar stress needs to be made to control rising air pollution levels. Noise pollution and Land degradation too makes Delhi unviable and unsustainable. Delhi as a sustainable city needs proper planning and operation to make it as pleasing as cities of the world.

Air environment

The air pollution levels in Delhi are strikingly high and the transport sector is a major contributor. Besides the transport sector, domestic and power sectors are also major sources of air pollution in the capital. Nearly 421.84 tons of CO, 110.45 tons NO_x, 184.37 tons HC and 12.77 tons particulate matter is released in Delhi's atmosphere per day (Department of Environment and Forests, 2010).

The CO emission has dipped drastically post-CNG use [1]; SPM and RSPM have increased, SO₂ has declined marginally and NO₂ is still high over 1997-2011 [2]. The composition of pollutants have changed with the introduction of CNG, new pollution standards and phasing out of old vehicles. The concentration of CO, SO₂ and PAHs has declined, while NO_x and SPM increased [3-5]. The rise in NO_x is attributed to CNG use and SPM to the diesel vehicles' growth.

The Central Pollution Control Board has been monitoring ambient air quality at six locations in Delhi under NAAMP for the past many

years. (Figures 1-4) Year-wise annual mean ambient air quality levels in Delhi during 1997 to 2014 is presented in the following table: (Table 1) The values for 1997 to 2010 are of the monitoring stations of CPCB while the values of 2011 to 2014 are of the monitoring station network developed by Delhi Pollution Control Committee. DPCC presently monitors air quality through six online continuous ambient air quality monitoring stations at 6 locations. The stations can be classified in two categories i.e. residential Puram RK, Mandir Marg & Punjabi Bagh and hot spots I.G.I Airport and Anand Vihar. Civil Lines is also influenced by traffic emissions [6] (Table 2).

Increasing levels of air pollution are responsible for higher incidence rate of respiratory diseases, cancer, and heart diseases in the capital. Various studies carried out for Delhi reflect the correlation between air pollution and health impacts. A study by AIIMS reconfirmed the point that respiratory symptoms are more frequent amongst people residing in highly polluted areas. To tackle the problem of air pollution, a number of measures have been taken in the past, such as switching to cleaner fuels, tightening vehicular emission limits, phasing out of old vehicles and maintenance of in-use vehicles, closing or relocating polluting industries, plantation activities etc. However, a lot more still needs to be done if the capital desires to breathe clean air.

Water environment

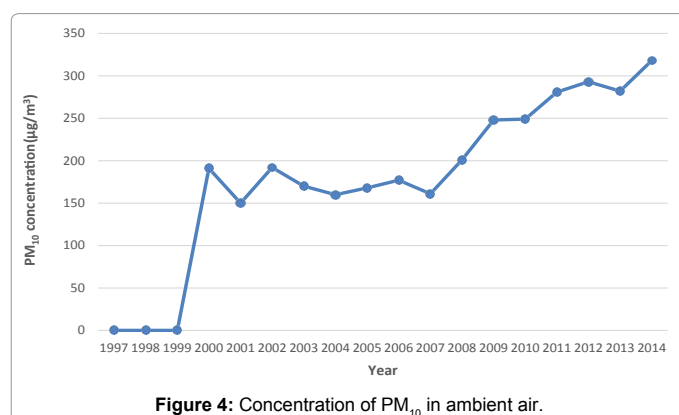
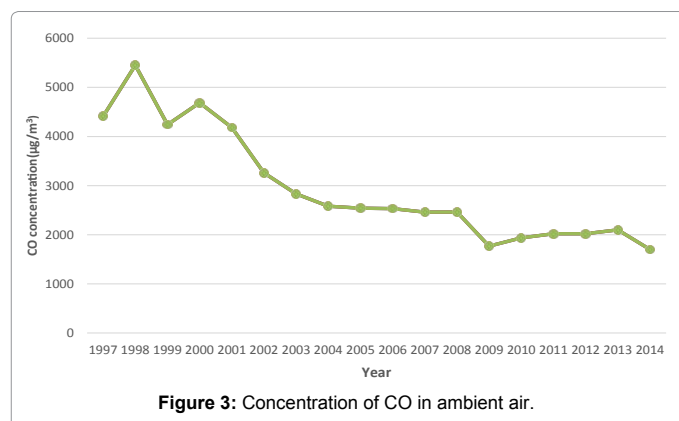
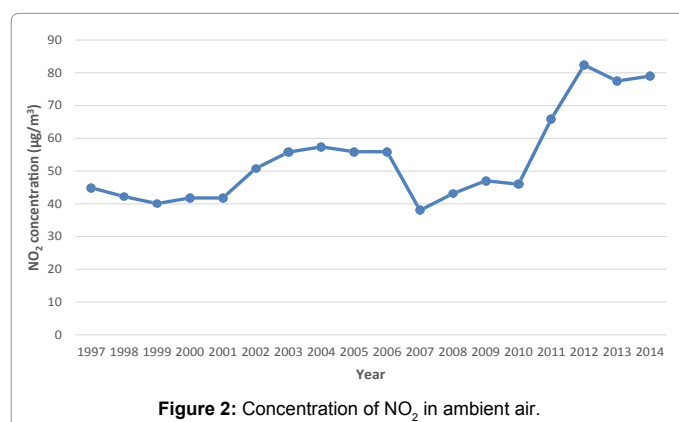
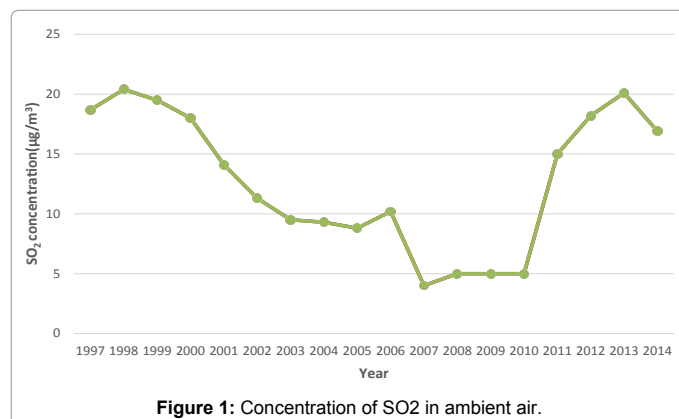
With the population of Delhi increasing from 0.4 million in 1911 to 18.24 million in 2015, there is an ever increasing pressure on the water resources. Improvement in living standards and access to sanitation

***Corresponding author:** Shashank Shekhar Singh, Research Scholar, Environmental Engineering Department, Delhi Technological University, Delhi, India, Tel: +91-11-27871018; E-mail: sssinghdtu@gmail.com

Received November 27, 2015; **Accepted** December 14, 2015; **Published** December 21, 2015

Citation: Singh SS, Singh SK, Garg S (2015) Environmental Concerns in National Capital Territory of Delhi, India. J Climatol Weather Forecasting 3: 147. doi:[10.4172/2332-2594.1000147](https://doi.org/10.4172/2332-2594.1000147)

Copyright: © 2015 Singh SS, et al. This is an open-access article distributed under the terms of the Creative Commons Attribution License, which permits unrestricted use, distribution, and reproduction in any medium, provided the original author and source are credited.



S. No	Years	Ambient Air Quality (µg/M ³)			
		So ₂	No ₂	Co	Rspm (Pm ₁₀)
1	1997	18.7	44.9	4410	--
2	1998	20.4	42.2	5450	--
3	1999	19.5	40.1	4241	--
4	2000	18.0	41.8	4686	191
5	2001	14.1	41.8	4183	150
6	2002	11.3	50.8	3258	192
7	2003	9.5	55.8	2831	170
8	2004	9.3	57.4	2581	160
9	2005	8.8	55.9	2541	168
10	2006	10.2	55.9	2531	177
11	2007	4.0	38.0	2460	161
12	2008	5.0	43.1	2461	201
13	2009	5.0	47.03	1768	248
14	2010	5.0	46.0	1937	249
15	2011	15.0	66.0	2020	281
16	2012	18.2	82.4	2020	293
17	2013	20.1	77.5	2100	282
18	2014	16.9	79.0	1700	318
Standard		50	40	2000	60

Table 1: Year-Wise Annual Mean Ambient Air Quality Levels in Delhi During 1997 To 2014.

R. K. Puram	13.6	51.6	263	140	41	1.45
Mandirmarg	12.5	87.4	203	125	51	1.28
Punjabi Bagh	17.3	106.4	248	139	39	1.86
Igi Airport	17.7	66.8	289	176	85	1.48
Anandvihar	20.4	84.5	583	191	32	1.73
Civil Lines	19.7	79.4	318	141	96	2.64

Table 2: Annual Average of Critical Pollutants at Six Stations in Delhi (In µg/M³) For the Year 2014.

facilities increases the per capita water demand levels. For sustainable development of Delhi, it is essential to ensure adequate supply of water in terms of reliability, quality and quantity. Although Delhi has an average water availability of 225 lpcd, the distribution is not uniform. Some areas get 24 hrs. Water supplies, whereas some get hardly 1-2 hr. water supply in a day.

Delhi depends on river Yamuna and partially on river Ganga for its share of raw water. Surface water contributes to over 86% of Delhi's total water supply. Yamuna, a perennial river, provides the major share of this water supply. Urban agglomeration of NCT Delhi is the major contributor of pollution load in Yamuna followed by Agra and Mathura. The stretch between Wazirabad Barrage and Chambal River confluence is critically polluted and there is significant fluctuation in dissolved oxygen level from nil to critically low levels. This reflects presence of organic pollution load and persistence of eutrophic conditions in the river. Pollution load in the river Yamuna added from various sources like industries and domestic and long dry season, has virtually converted it into a nala. Najafgarh drain along with its 70 sub-drains is the biggest polluter of the river.

DPCC has been conducting monthly water quality monitoring of river Yamuna (at 9 locations) and major drains (24 drains) falling into river Yamuna. Recent water quality monitoring reports of river Yamuna indicate that the water quality parameters, BOD & DO, are in the desirable/prescribed norms, with respect to Water Quality criteria of "C" class, at Palla, which is upstream of Wazirabad Barrage.

However, the water quality of River Yamuna at the downstream of Wazirabad barrage after confluence of Nazafgarh Drain is not meeting the desirable/prescribed norms.

The annual average of DO has ranged from 0.20 mg/l at Shahdara (Downstream) to 8.48 mg/l at Palla. The annual average of BOD has ranged from 1.99 mg/l at Palla to 60.33 mg/l at KhajuriPantoolpul. The water quality standards for DO and BOD as per CPCB norms are 4 mg/l and 3 mg/l respectively for class 'C' of river water. The water quality monitoring results in Delhi stretch clearly indicates river water is grossly polluted (Table 3).

Water quality monitoring results of the drains indicate that most of the drains are not meeting the standards with respect to Bio-chemical Oxygen Demand (BOD), Chemical Oxygen Demand (COD) and Total Suspended Solids (TSS) (Table 4).

S. No.	Locations	Ph (Mg/L)	Cod (Mg/L)	Bod (Mg/L)	Do (Mg/L)
	Water Quality Criteria	6.0- 9.0		3 (Max)	4 (Min)
1	Palla	7.63	14	1.99	8.48
2	Surghat	7.5	22.66	4.51	5.78
3	Khajuri Pantool Pool	7.40	200.33	60.33	Nil
4	Kudesia Ghat	7.45	125.67	37.00	Nil
5	Ito Bridge	7.53	100.67	31.80	Nil
6	Nizamudin Bridge	7.30	88.70	27.10	1.00
7	Agra Canal Okhla	7.50	96.20	29.90	0.90
8	Shahdara (Down Stream)	7.45	138.67	38.80	0.20
9	Agra Canal Jaitpur	7.45	108.83	28.83	0.60

Table 3: Annual Average Water Quality of River Yamuna at Different Locations: April 2014 to March 2015.

S. No	Drains	Ph	Tss (Mg/L)	Cod (Mg/L)	Bod (Mg/L)
1	Najafgarh Drain	7.39	269.67	241.00	70.75
2	Metcalfe House Drain	7.53	113.17	85.58	24.00
3	Khyber Pass Drain	7.51	40.17	42	10.30
4	Sweeper Colony Drain	7.33	55.83	100.83	27.42
5	Magazine Road Drain	7.39	212.83	298.33	87.92
6	Isbt Drain	7.40	148.00	283.33	87.92
7	Tonga Stand Drain	7.55	161.33	333.50	114.17
8	Moat Drain	No Flow	No Flow	No Flow	No Flow
9	Civil Mill Drain	7.42	167	302	94.42
10	Power House Drain	7.43	268.33	350.17	117.83
11	Sen Nursing Home Drain	7.48	302	389.33	132.08
12	Drain No. 12a	No Flow	No Flow	No Flow	No Flow
13	Drain No. 14	7.54	58.67	45.67	11.97
14	Barapulla Drain	7.37	163.67	164.50	49.08
15	Maharani Bagh Drain	7.25	454.67	395.50	135
16	Kalkaji Drain	No Flow	No Flow	No Flow	No Flow
17	Saritavihar Drain (Mathura Road)	7.34	272.00	438.00	146.67
18	Tehkhand Drain	7.34	289.67	470.08	150
19	Tuglakabad Drain	7.34	265.67	314.75	98.83
20	Drain Near Lpg Bottling Plant	No Flow	No Flow	No Flow	No Flow
21	Drain Near Saritavihar Bridge	7.43	102.00	130.17	39
22	Shahdara Drain	7.44	376.33	509.67	151.67
23	Sahibabad Drain	7.31	606.33	817.58	271.67
24	Indrapuri Drain	7.42	355.33	476.33	128.42

Table 4: Annual Average Water Quality of Drains at Different Locations in Delhi: April 2014 To March 2015.

As per CPCB, the contribution of pollution load from NCR & non-NCR states are in the proportion of 80:20, i.e. over 3/4th of the pollution load in River Yamuna is contributed by the NCR [7].

Besides surface water sources, groundwater contributes a substantial quantity of water supply in Delhi. Inadequate and intermittent supply of piped water has led to unchecked exploitation of the groundwater resource. A comparison of existing groundwater levels in different administrative blocks with levels in 1960 shows a decline of 2-30 m. Levels in Alipur and Kanjhawala blocks have declined 2-6 m, in the Najafgarh block by 10m, and in the Mehrauli block by 20 m. In addition to quantity, the quality of groundwater is also deteriorating and in several places it has been found to be unfit for human consumption.

Municipal and hazardous wastes

Solid waste includes commercial and residential waste generated in municipal or notified areas. As per the data available with DPCC records, solid waste generation in Delhi was around 8360 MTD. This is expected to increase due to economic and population growth. 700 MGD sewage is also generated, which generates organic sludge. Municipal waste of Delhi is disposed in three landfill sites namely Bhalswa GT Road, Ghazipur and Okhla.

Hazardous waste means any waste which by reason of any of its physical, chemical, reactive, toxic, flammable, explosive or corrosive characteristics causes danger or is likely to cause danger to health or environment. The most critical hazardous waste generated in Delhi is from small-scale enterprises such as pickling units, electroplating units, anodizing units, and sludge from CETPs.

Bio-Medical Waste (BMW) means any waste, which generated during the diagnosis, treatment or immunization of human being or animals or in research activities. With the increase in the number of hospitals and nursing homes in Delhi, hospital waste has become another area of concern. This waste is sent to common biomedical waste facilities in the city. Delhi is having 3 CBWTF operators who collect the waste from HCEs of Delhi and dispose the BMW after its treatment.

Electronic Waste, means any waste, which is generated due to product obsolescence and discarded electronic items, and may include data processing, telecommunications or entertainment in private households and businesses. The quantity of e-waste generated in the city is going to be much higher than hazardous waste and healthcare waste and thus requires proper management.

The most acceptable strategy for solid waste management in Delhi would be to categorize waste streams as biodegradable, recyclables, and inert matter to maximize recovery and minimize the quantity of waste generation. Efforts should also be made towards reclaiming and redeveloping the abandoned and filled landfill sites.

Forest

The vegetation cover is imperative for balanced atmospheric temperature and sustenance of life. As per the reports of Forests Survey of India (2011), total area of forest and tree cover was 40 and 111 km² respectively in 2001 that increased to 120 and 176.2 km² in 2011 [8]. Total vegetative cover doubled in a decade from 10% to 19.97% on account of substantial increase in tree cover under the Green Action Plan of Delhi Government. Open forests have coverage share of 119.96 km² and dense forests are merely 6 km² [9]. The National Forest Policy, 1988 provides that a minimum of 1/3rd of the total land area of the country should be under forest or tree cover. Taking this into view, the

Govt. of NCT of Delhi is making all endeavors to meet the national goal as set by the Central Govt. and is constantly adding to the green cover of the State [8] (Table 5).

The forest and tree cover area increased to 297.81 km² in 2013 increasing thereby the share of forests in the total area to 20.08 per cent. Of the total 297.81 km² of forest area in NCT of Delhi, nearly 272 km² has been added during the period 1999 to 2013 [8] (Table 6).

South Delhi district has the highest forest cover area at 79.02 sq. km, South West Delhi has 44.63 sq. km, that of North West Delhi is 16.50 sq. km and New Delhi has 16.31 sq. km. The lowest forest cover is in North West Delhi of 3.75 sq. Km.

Composition of forests in terms of its density is shown in Chart. Out of the total geographical area of NCT of Delhi, very dense forest is spread over 0.45 percent, moderately dense forest is spread over 3.33 percent, open forest is spread over 8.34 percent and scrub is spread over 0.15%, which is almost negligible [8] (Figure 5).

Delhi has 42 city forests. Fifteen city forests are in South-West district, Ten in North-West district, five each are in North-East and South districts, three each in East and North districts and one in West district.

Noise environment

The major contributors to noise pollution are industries, vehicular traffic, festivals, construction activities, diesel generating sets etc. Use of high sound loudspeakers during festivals and many social gatherings in public place directly increases the noise pollution in the affected areas.

Noise levels in Delhi exceed permissible levels in all areas except industrial areas according to a study by Delhi Pollution Control Committee in 1996. Another study carried out by CPCB in Delhi during 2006 revealed that during daytime ambient noise levels exceeded the prescribed residential area standard at all the locations. The ambient

noise levels in commercial and industrial locations were below their respective standard values.

The ambient noise levels permitted by Central Pollution Control Board for different areas:-

(Table 7) [10-14]. Noise levels observed at 40 different residential locations have been tabulated below. The data shows ambient noise levels being exceeded in all the selected residential areas. (Day time standard for residential area 55dB (A), Night time standard for residential area 45dB (A), All values in Leq dB (A)) [14-17] (Table 8).

Discussion and Recommendations

Growing urbanization and migration of population in search for better employment opportunities to Delhi is constantly putting pressure on city's limited environmental resources. Though the green cover has increased in past several years due to massive plantation drives and awareness schemes, other assets like lakes, groundwater, river etc. are under constant threat due to their over exploitation. To make an informed, scientific decision about saving these natural and environmental resources and to retain them to their closest pristine form, urgent measures are required. Measures like easing out transportation services are needed to deal with problems pertaining to air pollution. Initiatives by government of Delhi to only ply those private vehicles on road which have even numbers on dates having even count and same with odd is a noble step which needs to be executed with few exceptions. Waste management is one such area which needs to be dealt with care and urgency. Segregation while collection should be the desired practice for municipal authorities. Different colour bags should be assigned for different kind of wastes which can be directly sent to processing plants. Principle of Recycle and Reuse should be adopted which can help Delhi get rid of tons of pollutants. Zero net waste should be the objective which can only be attained if proper care is taken of the waste. For increasing and maintaining the forest cover, the horticulture department should make proper road map. Large scale plantation drive and maintenance of existing plants should be done. This can be helpful in dealing with the menace of Air pollution. To deal with pollution of river Yamuna in Delhi, one needs to take care of all

S. No.	Year	Forest and Tree Cover	Absolute Increase in Area	% of Total Area
1.	1993	22	--	1.48
2.	1995	26	4	1.75
3.	1997	26	--	1.75
4.	1999	88	62	5.93
5.	2001	151	63	10.2
6.	2003	268	117	18.07
7.	2005	283	15	19.09
8.	2009	299.58	16.58	20.20
9.	2011	296.20	-3.38	19.97
10.	2013	297.81	1.61	20.08

Table 5: Forest and Tree Cover Area of Delhi 1993-2013.

Sl. No.	Districts	Geographical Area	Forest Cover Area	% of Geographical Area
1.	Central Delhi	25	5.05	20.20
2.	East Delhi	64	3.05	04.77
3.	New Delhi	35	16.31	46.60
4.	North Delhi	59	4.81	8.15
5.	North East Delhi	60	4.02	6.70
6.	North West Delhi	440	16.50	3.75
7.	South Delhi	250	79.02	31.61
8.	South-West Delhi	421	44.63	10.60
9.	West Delhi	129	6.42	04.98
	Total	1483	179.81	12.12

Table 6: District-Wise Forest Cover in Delhi-2013 (Sq. Km).

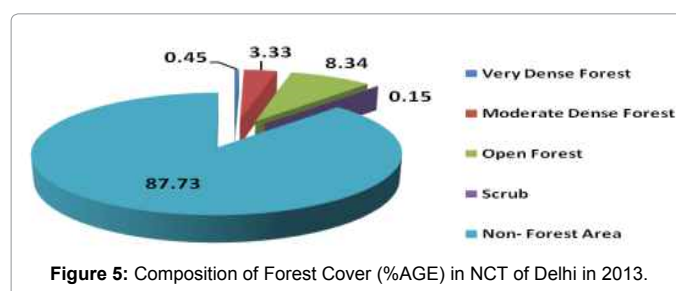


Figure 5: Composition of Forest Cover (%AGE) in NCT of Delhi in 2013.

S. No.	Area	Leq/Db (A)	
		Day Time *	Night Time **
1.	Industrial Area	75	70
2.	Commercial Area	65	55
3.	Residential Area	55	45
4.	Silence Zone***	50	40

Notes: *Day Time-6 Am To 10 Pm

**Night Time-10 Pm to 6 Am

*** Silence Zone is an Area Comprising Not Less Than 100 Meters around Hospitals, Educational Institutions, Courts, Religious Places or Any Other Areas Which Is Declared as Such by Competent Authority.

Table 7: Prescribed Ambient Noise Standards.

Ambient Noise Levels Observed at Different Locations in Delhi																	
S.No.	Locations	June(2008)		July (2008)		August (2008)		Sep. (2008)		Oct. (2008)		Nov. (2008)		Dec. (2008)		Jan. (2009)	
		Noise (Day Time)	Noise (Night Time)	Noise (Day Time)	Noise (Night Time)	Noise (Day Time)	Noise (Night Time)	Noise (Day Time)	Noise (Night Time)	Noise (Day Time)	Noise (Night Time)	Noise (Day Time)	Noise (Night Time)	Noise (Day Time)	Noise (Night Time)	Noise (Day Time)	Noise (Night Time)
1	Adarsh Nagar	62.3	53	61.6	52.2	62.9	52.4	62.7	55.1	63.4	55.8	59.1	47.1	61.2	52.5	60.5	51
2	Anand Vihar	63.1	57.5	62.5	55.9	63	56	64.3	54.4	62.7	53.9	62	56	61.6	52.7	60.4	53.3
3	Ashok Vihar	61.7	52.6	61.3	62.2	60.2	51.5	61.4	55.1	**	**	61.3	50.9	60.4	51.9	60.1	50.1
4	Badli	58.7	49.1	57.1	50.9	57.4	50.6	63	55.8	**	**	61.4	57.2	59.6	51	60.6	54
5	Braham Puri	59.6	54	57.7	53.6	56.6	51.5	59	54.2	**	**	59.6	52.2	60.4	54.6	59.9	53.7
6	Daryaganj	64	57.4	62.3	52.5	63.7	56.8	62.2	53.4	**	**	62.1	52.5	62.8	56.2	60.6	55.8
7	Defence Colony	60.1	53.8	60.9	55.2	60	54.3	63	57.1	64	57.4	61.6	55.6	60.3	54.3	59.8	53.7
8	Dwaraka	60.9	52.3	59.2	51.3	61.2	52.1	62.9	55.9	**	**	59	51.1	59.3	55.8	58.1	54.5
9	Greater Kailash	63.1	62.2	61.8	56	63.9	62.6	62.7	57	61.5	55.9	61.7	53.1	62.8	55.5	59.2	49.7
10	Inder Puri	59.4	55.9	59.1	53.8	59.6	54.6	62	57.9	**	**	60.6	55.2	61.7	53.3	60.2	53.1
11	Janak Puri	62.7	55.1	61.9	55.6	61.2	53.9	62.9	56.1	**	**	62.5	60.5	62.8	57.6	59.4	53.1
12	Karawal Nagar	62.2	53.2	62.4	52.9	61.4	52.5	63.9	57.7	62.9	56.3	60.5	54.7	63	61.2	61.2	60.8
13	Karol Bagh	62.9	61.3	62.4	60.6	62	61	62.9	54.4			61.8	56.4	62.8	54.9	64	57.4
14	Kondli	60	50.3	60.1	51.1	60.4	54.2	62.4	56.8	62.2	54.7	62.2	54	64.4	54	60.8	48.3
15	Lajpat Nagar	63.6	61.8	64.6	62.3	63.6	61.5	62.5	55.9	61.9	55.5	63.1	53.1	61.3	55.1	61.2	51.9
16	Lawrence Road	59	50.9	59.7	52.2	59.1	52.6	62.4	53.2	**	**	61.4	56.8	62.3	56.5	62.4	49
17	Mandawali	61.7	56.5	63.2	56.6	62.4	55.1	62	57.2	61.6	54.2	63	56.9	59.3	51.3	60.9	52.7
18	Mangol Puri	62.8	56.2	61.6	55.9	62.5	55.9	63.6	56.8	**	**	61.4	56.8	61.3	54.3	62.6	57.6
19	Meera Bagh	60	52	59.4	51.6	60.2	52	61.4	54.8	**	**	61	56.9	62.8	56.2	60.5	52.5
20	Mehrauli	61.3	55.1	62.3	58	62.7	53.4	63.9	54.3	61.1	51.2	60.5	56.8	60.9	57.8	62.7	55.4
21	Moti Bagh	59.3	52.4	58.2	52.2	58.7	51.8	62.1	53	61.6	52.9	62.4	51.3	58.7	52.2	58.6	47.7
22	Moti Nagar	61.2	57.8	60.9	54.2	61.9	57.9	61	52.5			62.9	54.8	62.9	54.8	59.5	53.5
23	Mukherji Nagar	61.7	55.5	61	56.2	62.2	55.9	64.8	56.4	61.6	50.7	61.8	53.8	61.1	55.6	62.8	56.2
24	Nand Nagri	60.6	55.8	59.7	55	60.3	55.4	61.9	53.9	61.4	56.1	62.4	55.7	60.6	55.8	59.4	55.9
25	Narauji Nagar	60.5	52.6	60.5	55.6	60.9	53.7	61.9	56.1	62.6	51.6	62.9	56.6	60.7	52.8	59.6	51.6
26	New Friends Col	60.1	53.2	62.8	56.5	62.2	53.5	62.9	55.2	63.1	55.6	61.8	56.7	61.3	56.2	59.2	53.5
27	Pahar Ganj	63.6	60.4	63.1	57.6	67	59.1	63.8	59.2	**	**	61.9	55.4	62.7	60.1	62.6	57.6
28	Paschim Vihar	57.4	51.7	57.9	54.1	59.2	51.8	61.3	53.9	**	**	62.2	54.7	57.8	51.4	59.9	48.4
29	Patel Nagar	57.6	48.7	59.6	52.3	58	48.6	61.7	55.4	**	**	62.1	55.5	56.8	48.3	60.2	50.5
30	Prehladpur	63	59.1	59.4	54.5	62.4	57	61.9	56.1	61.6	52.9	62.8	52.8	60.5	57.6	61.7	56.5
31	R.K. Puram	60.2	55.7	60.4	57.1	60.6	55.5	62	55.6	63.1	55	59	51.6	59.6	53.4	58.7	49.1
32	Rajpura Road	62.1	52.5	60.2	52.3	62.4	52.8	63.8	57.2	63.3	53	59.2	52.7	60.2	51.6	57.6	48.7
33	Rana Pratap Bag	61	51.4	60.3	50.8	61.8	52.9	63.6	56.8	**	**	62.4	52.1	60.6	51.2	59.3	52.4
34	Rohini	64	54.3	61.1	53.5	62.3	53.4	63.5	54.7	**	**	61.7	56.8	63.3	53.9	64	57.4
35	Sarita Vihar	69	59.1	60.4	51.7	67.2	58	62.8	54.3	63.3	56.5	63	55.5	60.5	52	63.6	54.3
36	Shalimar Bagh	62.6	57.6	63.3	57.6	61.7	54.8	63.8	54.3	**	**	62	54.8	62.4	55.2	61.7	55.7
37	Shanti Vihar	61.3	55.1	65.9	56	59.7	48.3	63.1	59.2	**	**	63	55.5	58.6	47.7	59.1	47.5
38	Tilak Nagar	62.1	54.9	61.5	54.5	62.2	54.9	65	55.6	**	**	60.5	53.9	59.4	53.5	59.2	48.4
39	Tughlakabad	**	**	**	**	**	**	**	**	**	**	62.2	52.6	61	52.5	61.3	48.5
40	Vasant Kunj	62.9	58.6	63.5	58.9	61.7	56.6	61.8	56.8	61.6	55.2	63.5	58.9	61.9	54.9	59.5	55.8
41	Yamuna Vihar	59.6	51.6	59.9	51.3	60.1	52.5	62.7	51.8	63	53.9	63.8	51.3	58.6	51.2	59.9	51.1
	Min	57.4	48.7	57.1	50.8	56.6	48.3	59	51.8	61.1	50.7	59	47.1	56.8	47.7	57.6	47.5
	Max	69	62.2	65.9	62.3	67.2	62.6	65	59.2	64	57.4	63.8	60.5	64.4	61.2	64	60.8
	Average	61.473	54.96	61.02	54.81	61.413	54.47	62.6625	55.53	62.38	54.42	61.69	54.5	60.9	54.1	60.54	60.54

****Data not available**

Table 8: Delhi Pollution Control Committee, Government of N.C.T. Delhi.

**Data not available

Table 8: Delhi Pollution Control Committee, Government of N.C.T. Delhi.

the drains falling out in Yamuna. Interceptor drains should be made to process waste water reaching Yamuna. Any wastewater reaching Yamuna should be processed beforehand so that sanctity and water quality of Yamuna improves. Recreational models should be developed near Yamuna which will help build connection of Yamuna with residents of Delhi. Conclusively, joint efforts need to be made on part of government machinery and citizenry which will enable overcome the environmental concerns of Delhi.

References

- Central Pollution Control Board (2006) Water quality status of Yamuna River (1999-2005), Ministry of Environment & Forests, Government of India: New Delhi, India.
- Department of Planning (2013) Economic Survey of Delhi, 2012-13, Government of India: New Delhi, India.
- Chelani, AB, Devotta S (2007) Air quality assessment in Delhi: Before and after CNG as fuel. Environ Monit Assess 125: 257-263.
- Ravindra K, Wauters E, Tyagi SK, Mor S, Grieken RV (2006) Assessment of air quality after the implementation of Compressed Natural Gas (CNG) as fuel in public transport in Delhi, India. Environmental Monitoring and Assessment 115: 405-417.
- Sindhwan R, Goyal P (2014) Assessment of traffic-generated gaseous and particulate matter emissions and trends over Delhi.
- Department of Planning, Economic Survey of Delhi, 2014-15, Government of India: New Delhi, India.
- Aenab AM, Singh SK (2014) Critical Assessment of River water Quality and Wastewater Treatment Plant (WWTP), IOSR Journal of Environmental Science, Toxicology And Food Technology (IOSR-JESTFT) 8: 44-48.
- Forest Survey of India, State of Forest Report; Ministry of Environment & Forests: Dehradun, India 2013.
- Department of Planning (2011) Delhi Human Development Report, Government of India: New Delhi, India.
- Aenab AM, Singh SK (2012) "Evaluation of Drinking Water Pollution and Health Effects in Baghdad", Iraq. Journal of Environment Protection 533-537.
- Department of Environment and Forests (2010) State of environment report for Delhi, Government of NCT of Delhi, India.
- Singh RB, Grover A (2015) Sustainable Urban Environment in Delhi Mega City: Emerging Problems and Prospects for Innovative Solutions.
- Mallick J, Kant Y, Bharath BD (2008) Estimation of land surface temperature over Delhi using Landsat-7 ETM+ J Ind Geophys Union 12: 131-140.
- McGeehin MA, Mirabelli M (2001). The potential impacts of climate variability and change on temperature-related morbidity and mortality in the United States. Environ Health Perspectives 109: 185-189.
- Sharma JN, Kanakiya RS, Singh SK (2015) Characterisation Study and Correlation Analysis For Water Quality of Dal Lake, India. International Journal of Lakes and Rivers 8: 25-33.
- Deepika, Singh SK (2015) Water Quality Index Assessment Of Bhalswa Lake, New Delhi. International Journal of Advanced Research 3: 1052-1059.
- Singh SK, Katoria D, Mehta D, Sehgal D (2015) Fixed Bed Column Study and Adsorption Modelling on the Adsorption of Malachite Green dye from wastewater using Acid Activated Sawdust. International Journal of Advanced Research 3: 521-529.

Gene Prioritization by integrated analysis of protein structural and network topological properties for the protein-protein interaction network of neurological disorders.

Yashna Paul, Yasha Hasija*

Department of Biotechnology, Delhi Technological University, Shahbad Daulatpur, Main Bawana Road, New Delhi, Delhi 110042, India.

*Corresponding Author Email: yashahasija@gmail.com

ABSTRACT

Neurological disorders are known to show similar phenotypic manifestations like anxiety, depression and cognitive impairment. There is a need to identify shared genetic markers and molecular pathways in these diseases, which lead to such comorbid conditions. Our study aims to prioritize novel genetic markers that might increase the susceptibility of patients affected with one neurological disorder to other diseases with similar manifestations. Identification of pathways involving common candidate markers will help in the development of improved diagnosis and treatments strategies for patients affected with neurological disorders. This systems biology study for the first time integratively uses 3D- structural protein interface descriptors and network topological properties that characterize proteins in a neurological protein interaction network; to aid the identification of genes that are previously not known to be shared between these diseases. Results of protein prioritization by machine learning have identified known as well as new genetic markers which might have direct or indirect involvement in several neurological disorders. Important gene hubs have also been identified that provide an evidence for shared molecular pathways in the neurological disease network.

INTRODUCTION

Seizures, comorbid conditions like anxiety, depression, and cognitive impairment are some of the shared symptoms in patients with neurological disorders. This observation implies that these neurological disorders have certain shared genetic markers and molecular pathways that lead to their common clinical manifestations. There might be genetic markers associated with one disease, the mutations in which result into over or under expression of associated genes and interconnected molecular pathways. Such aberrations can cause similar observable symptoms in patients with different neurological disorders. For example, there are reports that suggest, that epilepsy occurs in approximately 8 to 20% of children with autism spectrum disorders with an increasing prevalence of seizures occurring in the late adulthood [1]. Also, as compared to general population, in which the incidence/probability of developing bipolar disorder is 0.07, the same in patients with epilepsy is 1.69 cases per 1000 persons-year, which is significantly high [2]. There have been reports of episodic attacks in chronic disorders: epilepsy and migraine. The diseases commonly occur together and share overlapping pathophysiological mechanisms and common clinical features. Recently identified common genetic markers and molecular substrates for epilepsy and migraine include mutations in genes like CACNA1A, ATP1A2, SLC1A3 and POLG. However, both conditions also have several distinct and important differences. Hence, the diagnosis and treatment of each of these diseases must take into consideration a potential presence of the other [3].

Keeping this in mind, we implement a strategic systems biology approach for structural and functional analysis of neurological protein interaction network. We aim to identify novel putative genetic markers through network analysis that could be the cause of comorbid conditions in neurological disorders. The approach followed for network analysis of neurological disorders in this study is unique and novel in several ways.

We have targeted the human neurological proteome for this study. Proteins function by interacting with one another and also with other molecules of the cell like, DNA and RNA; and mediate vital metabolic pathways, signalling cascades, cellular processes and organismal systems. The unique function that each protein interaction confers to the system, determines its affinity and specificity. Protein interactions therefore have a central role in the biological functioning of an organism and a perturbation of such interactions that might include gain of an inappropriate interaction or the loss of an important association controls the healthy and diseased state of an organism. Disease mutations affect the protein's binding interface causing biochemically dysfunctional allosteric changes in the protein's binding site. Studying protein interactions provides insights into the molecular basis of the disease, and this information can be used to devise better methods for prevention, diagnosis and treatment of diseases [4].

The prioritization of novel candidates by machine learning in our study, takes into consideration the structural descriptors of proteins in an interaction network. Machine learning techniques have been successfully used to find informative genes and mining critical information from raw data supplied to the machine. These prediction models have an increased interpretability and retain high accuracy to exploit the supplied data and figure out the required information effectively. Our work specifically deals with prioritizing novel gene products, that is, proteins that are previously not known to be associated with neurological disorders. This was done by identifying the characteristic protein network topological properties and 3-dimensional protein interface structural properties that are inherent of proteins that are known to be associated with neurological disorders. Protein interactions take place through protein interfaces. And differences in the structure of protein interface can lead to varied interactions. Hence, the structural properties of the protein interface play an important role in determining its interactions in a network. A similar study in which binding

site structural characteristics were used to describe cancer associated human protein-protein interfaces in a cancer network; shows that cancer protein interfaces have characteristic interface properties as compared with interfaces of normal proteins. Interface structural properties like accessible surface area (ASA), planarity, gap volume index, interface surface area, percent polar residues in the interface, percent non polar residues in the interface, and percent charged residues were used to describe cancer protein interfaces [5]. Our study used the same set of properties, calculated through the web tool 2P2I inspector (see methods), to characterize interfaces of proteins involved in neurological disease network. Two additional properties are used, namely; Gap Index and Interface size- that are calculated from the above mentioned seven properties.

To understand the global behaviour of proteins, the network graph representation with characteristic properties that define the participating proteins has been used previously. These are called network topological properties and include degree, betweenness, closeness, centrality, shortest path length etc. The inclusion of protein interface structure and using network topological properties to describe their effect on the interacting proteins has been shown to identify essential hub proteins with better accuracy than before [6]. We have taken into consideration ten network topological properties that were calculated by the network analyser plug-in of cytoscape (see methods).

Studies have shown that these protein descriptors (protein interface structural properties and network topological properties), individually, are optimal features of prioritizing novel candidates [7]. We have therefore considered both these structural descriptors together for the first time to describe and characterize known and novel potential neurological proteins under study. It was also observed that there was a decline in performance and accuracy of the classifiers at the cost of eliminating some of these features.

And therefore, all the 19 descriptors together were considered optimally fit to be included in the study.

Machine learning classifiers were trained on these parameters and subjected on known set of neurological gene products to identify their unique underlying patterns and relationship in a network and then use these to identify previously unknown markers of neurological disorders from a list of human proteins that are not known to be associated with such disorders. This structural level analysis provides important clues about the affinity and specificity of protein interactions, and hence only the proteins whose 3D structure is available, were considered. Identified risk markers could be considered important to determine patient prognosis for neurological diseases. Identifying such markers by taking into consideration the properties of known genes and proteins involved in the disorders under study is known as gene prioritization [8].

Further, from the prioritized gene list, we identified proteins hubs that have highest number of interacting partners in the network, and can be thought to participate simultaneously in most neurological pathways.

METHODOLOGY

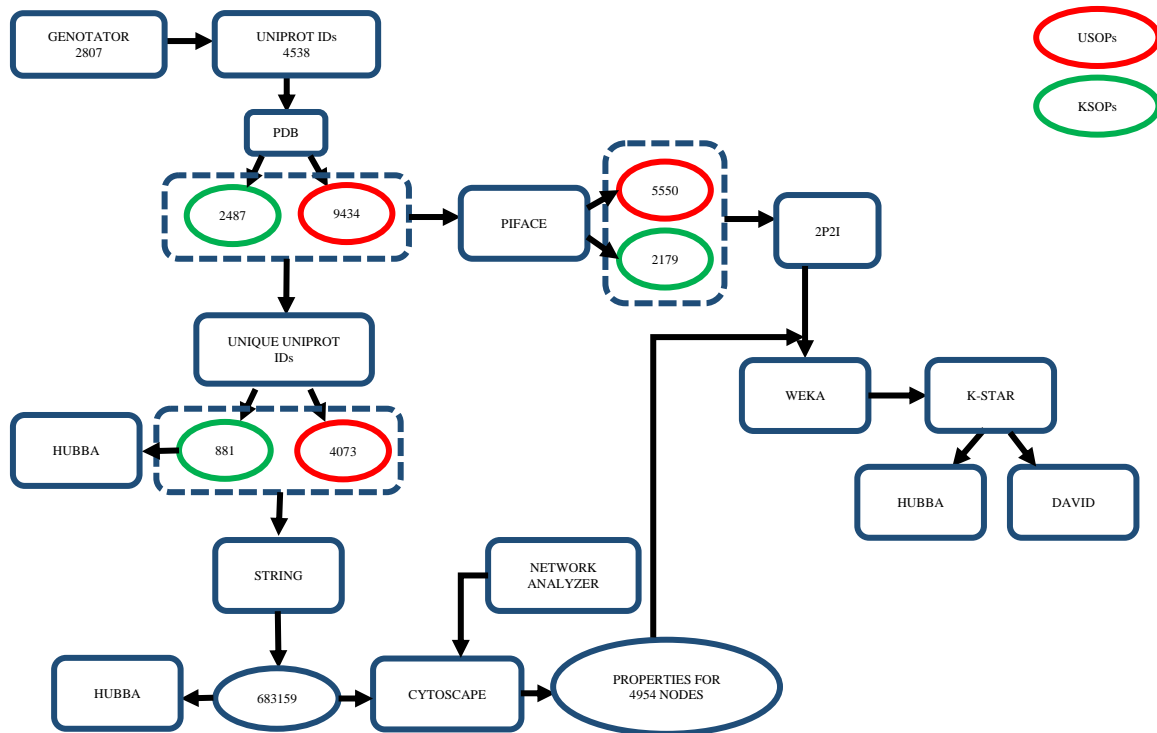


Figure 1. Flowchart of the methodology followed. KSOPs is the Known Set Of Proteins, and USOPs is the Unknown Set Of Proteins.

Screening of genes under study

Gene sets known to be associated with several neurological disorders namely Epilepsy, Alzheimer's, Parkinson's, Autism, Schizophrenia, Bipolar Disorder, and Migraine were downloaded from Genotator (<http://genotator.hms.harvard.edu/>) [9], which is an online available real-time aggregation tool that has a multi-query engine. It automatically integrates data from 11 external clinical genetics resources to provide reliable ranking of genes in order of disease relevance and covers both historical genetics research and recent advancements and discoveries in disease genetics. Total number of unique genes associated with these disorders was 2,807. A list of 4,538 proteins corresponding to these genes was downloaded from Uniprot (<http://www.uniprot.org/>) [10]. For gene prioritization one of the parameters

into consideration was interface structural properties of the interacting proteins in neurological disease network. To calculate the structural properties, the three-dimensional structures of all the proteins were downloaded from RCSB Protein Data Bank (PDB) (www.rcsb.org) [11]. Therefore the PDB Id list for 4,538 proteins was extracted from a total number of 47,532 available human protein structures on PDB. 17,457 3D-protein structures corresponded to our list 4538 proteins associated with the group of neurological diseases under study. This was considered as the known set of proteins (KSOPs). Remaining 30,075 protein structures from PDB were listed as the unknown set of proteins (USOPs), that is, the proteins not considered to be associated with the group of diseases under study. The list of 17,457 KSOPs included a number of structural variants associated with each protein. Hence this list was then manually sorted and only the protein structure with highest resolution was considered. Each protein chain structure was taken into account, as the protein structural interface that takes part in interacting with other proteins can be an assemblage of any combination of the available chains of a protein. Also, mutant and recombinant structures were avoided. If multiple structures were available for each chain, a single high resolution structure was considered specific to the protein chain. This is mainly because, high resolution crystal structures of proteins enable understanding of their associated molecular mechanisms with high degree of precision and accuracy. Such accurate structures help in addressing biological questions of fundamental importance, as well as aid in the study of drug designing and pharmacological research. Increase in the resolution of a structure increases the confidence about positions of atoms in the respective conformation. Accurate positions of atoms in a high resolution structure would help in specific and physiologically relevant interactions with other proteins in an interaction network. However, considering high resolution has minimum effect on the errors arising from multiple conformations of the protein. Therefore, taking the high resolution structure of all the conformations of each

protein into consideration is important [12]. Excluding the independent chain structures would mean losing out information on any putative protein interface structure. This left us with a list of 2,487 KSOPs, each associated with its available chain structure. Similarly, 30,075 USOPs were sorted and screened for available high resolution chain structures of all proteins, and the final list reduced to 9,434 proteins. The unique set of proteins from 2,487 KSOPs and 9,434 USOPs was used for construction of a protein-protein interaction network that was further used to analyse network topological properties of these proteins. And, the entire set of 2,487 KSOPs and 9,434 USOPs was used to fetch the structural properties of each possible interface that could be formed by different combinations of protein chains for each protein.

Protein-protein Interaction network and analysis of protein network properties

881 and 4,073 unique set of total 2,487 KSOPs and 9,434USOPs respectively were used as input for STRING (<http://string-db.org/>) to identify the potential protein-protein interactions that might have been predicted experimentally, computationally or published in literature [13]. A total of 683,159 interactions for all the proteins were extracted from STRING. The interactions were subsequently used as input to visualise and analyse a network using cytoscape (v 3.1.0) [14]. The final network had 4,954 nodes (corresponding to number of proteins in the network) and 683,159 edges (number of interactions between proteins).The Network analyser, a well-known cytoscape plugin was used to compute specific network topological properties of the protein-protein interaction (PPI) network [15]. The 10 network properties that were analysed for 4,954 proteins by this tool are listed in Table 1. The functional protein interactions extracted from STRING, were also used as input for web based tool-HUBBA (<http://hub.iis.sinica.edu.tw/Hubba/index.php>) that analyses potential hubs in the network [16]. Also, the set of 881 KSOPs was used as a separate input for STRING, and the resulting interactions were subject to HUBBA analysis, in order to

identify known protein hubs, that is, the proteins that have the maximum number of interactions in the known neurological protein-protein interaction network.

Inclusion of protein interface structural properties

Protein-protein interactions take place through the binding site of the proteins contained in the protein interface. Multiple conformations of particularly the key residues in the binding sites make these interactions possible. However, in contrast to the numerous protein-protein interactions that are possible, there are only limited and specific binding site conformations that favour protein binding. Protein interface properties are therefore useful to describe the preference of protein interaction that could take place through that surface of the protein. A protein interface is formed from a couple of protein chains that provide the most favourable binding conformation to the protein. Only certain possible combinations of a couple of the number of protein chains associated with a single protein can form the protein interface. The list of favourable protein chain combinations that were involved in forming the interface of each protein, was extracted from PIFACE (<http://prism.cccb.ku.edu.tr/piface/>) [17]. The input for this included the PDB Id of the protein and any associated two protein chains at a time. PIFACE combinations were extracted for 2,487 PDB Ids corresponding to KSOPs and 9,434 PDB Ids corresponding to USOPs. The number of favourable protein chain combinations was 2,179 and 5,550 for KSOPs and USOPs respectively. The favourable chain combinations were used for calculating interface structural properties-to be used as protein structural descriptors, with the help of an online available tool 2P2I inspector (http://2p2idb.cnrs-mrs.fr/2p2i_inspector.html) [18]. Input to this tool is a PDB Id and a combination of protein chains known to form a potential binding interface from PIFACE. The 9 protein structural descriptors that were assessed using 2P2I, are listed in Table 1.

Protein network properties	Protein interface structural properties
Average shortest path length	Total accessible surface area
Clustering coefficient	Average interface surface area
Closeness centrality	Percent average neutral residues
Eccentricity	Percent average polar residues
Stress	Percent average non-polar residues
Degree	Percent average charged residues
Betweenness	Gap index
Neighbourhood Connectivity	Interface size
Radiality	
Topological Coefficient	

Table 1. Protein structural descriptors considered for machine learning.

Gene Prioritization by machine learning

The network properties and interface properties for the KSOPs and USOPs were combined together to prepare files for machine learning using WEKA. Altogether there were 19 descriptors for all the proteins. WEKA (<http://www.cs.waikato.ac.nz/ml/weka/>) is a data mining software that includes a collection of machine learning algorithms [19]. For preparing the training file, the list of 2,179 KSOPs was divided into half after random shuffling. And same number of protein entries was taken from the unknown set after randomly shuffling it. The resulting training file had 1,090 KSOPs and 1,090 USOPs. Various available algorithms from WEKA like Bagging, Naïve Bayes, Random Forest, Rotation Forest and K*star, were trained upon a specific set of features (network topological properties and interface descriptors) associated with the KSOPs using ten-fold cross validation. Building more than one model helps explain how different classifiers make varied predictions on the training set. The models predict the Recall, ROC area, accuracy, precision, true positive rate and the false

positive rate for the training set. The models were individually applied to the test file to identify proteins that had features similar to those of KSOPs. The test file included 1,089 remaining KSOPs and 4,460 USOPs. The model that made predictions on the test set with highest precision, recall, ROC area, and accuracy was considered as the best fit model. The predictions of this model were taken for further analysis.

The combined list of resulting putative neurological candidates from the test set and the list of KSOPs from the training and test sets were used as input for STRING to identify corresponding protein-protein interactions. These interactions were then used to identify hub proteins using HUBBA. This gave a list of important proteins with most interacting partners in the new network, which includes additional identified protein candidates.

The three identified hub protein lists are compared to understand the essentiality of common hubs in all the three protein networks, namely, human structural protein interaction network, neurologically associated structural protein interaction network, and the final network of known and putative neurologically associated proteins. DAVID (<http://david.abcc.ncifcrf.gov/>) analysis of hub protein list from the third network which includes neurologically associated and newly predicted protein candidates was performed, to identify common pathways between new candidates and existing neurological pathways [20, 21].

The strategic systems biology approach to identify novel neurological candidates followed by applying the above methodology also extends the machine learning predictions for analysing hubs protein candidates and has been illustrated in Figure 1.

RESULTS AND CONCLUSIONS

Results for gene prioritization by machine learning

WEKA classifiers were used to build models on the training set. The training set was built by random selection of 1,090 KSOPs and equal number of USOPs. Known proteins were the ones that are associated with neurological disorders. The unknown list consists of all other known human proteins whose 3-Dimensional structures were available on the Protein Data Bank (PDB). There are 19 training features in both the training set and test set, for quantified description of the proteins. The features used for describing known proteins and evaluating novel candidates were an integration of protein network properties and interface structural properties. Five machine learning classifiers from WEKA, were applied to the training set, to obtain five corresponding models. These include: Naïve Bayes, Random Forest, Bagging with J48, Rotation Forest, and K-star. After 10 fold cross-validation, the predictions of the above classifiers on the training set are shown in Figure 2a. Machine learning performance metrics show that the classifier random forest has the best predictions of precision, that is, the number of instances that have been predicted correctly as known proteins. Receiver operating characteristic (ROC) curve is a graph that illustrates the performance of a classifier as its discrimination threshold varied and random forest has the maximum value for the same. Maximum recall and accuracy has been achieved by Bagging combined with J48. Sensitivity/recall is the number of known proteins that have been predicted correctly as being known. Accuracy is the proportion of true results, that is, the known proteins, and the unknown proteins classified as known. The performance of a single test/ classifier prediction can be calculated using the precision and the recall. The F-score is a single measure of the performance of the prediction, where,

$$F = 2(\text{PRECISION} * \text{RECALL} / (\text{PRECISION} + \text{RECALL}))$$

The performance/F-score for all the classifiers on trainings set were calculated by the above formula, and are depicted in Figure 2c [22]. The graph shows that the classifier Bagging_J48 has the best performance.

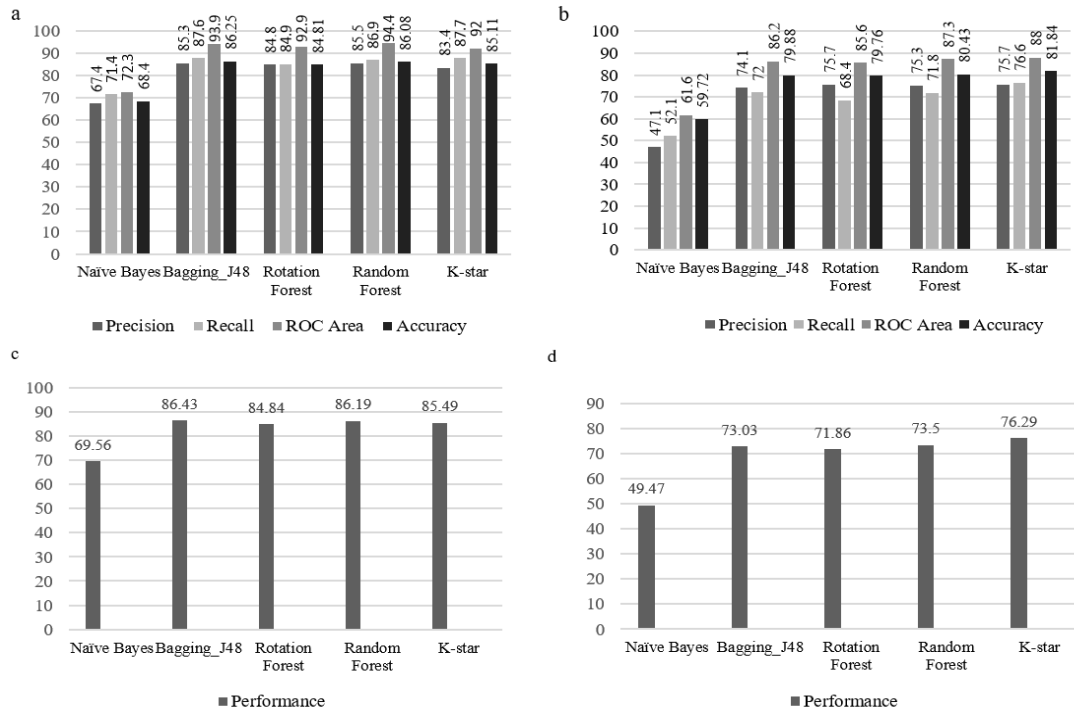


Figure 2 a. Comparative representation of the performance metrics of five model for their predictions on the training dataset. b. Comparative representation of the performance metrics of five model for their predictions on the test dataset. c. Comparison of performance/F-score values for five models on training set. d. Comparison of performance/F-score values for five models on test set.

The models that were built on training set after 10 fold cross were applied on the test dataset individually to obtain the results. The following result predictors like precision, accuracy, recall, and area under ROC curve describe how successful the models have been to mine candidate proteins involved in neurological disorders, from a set of proteins that are previously not known to be associated with neurological disorders. The test file included 1,089 remaining KSOPs and 4,460 USOPs. Values of all the four performance metrics on the

test set data for the 5 classifiers used is shown in Figure 2b. Amongst the five models used for predictions on test set data, the K-star algorithm gave best result for precision, recall, area under ROC curve as well as for the accuracy of predictions. Performance/ F-score was calculated for all the models, and is depicted in Figure 2d. Different models might perform variedly depending upon the dataset and the information contained. For the present test set, the model that gave best results was K-star. However, it can be noted that Bagging_J48 has better overall performance on the training set; whereas K-star has the third best performance in the same dataset after Bagging_J48 and Random Forest. From these results it can be concluded that K-Star algorithm makes a better discretion of noise and signal; whereas other algorithms have overfitted in the present data leading to inclusion of random error/noise. K-star specifically learns the heterogeneity and relatedness/relationship of training set data more accurately than any other algorithm; and gives the best performance in test set data by identifying maximum true positives.

The best predicted putative candidate proteins from the results of K-star algorithm are used for further analysis. Table 2 shows the list of best 10 predictions of putative protein candidates from the unknown test set as obtained from the WEKA results of all five classifiers. Many putative candidate protein predictions were found to be common in all five model results. However, they have different prediction probabilities in all results. The fact that some proteins were commonly predicted by all the classifiers increases the probability of those proteins as potential candidates, as they got mined by all classifiers. Since in certain classifier results, they might have lower prediction probabilities, they will not be taken as putative markers. Best prediction probabilities describe how accurately the previously not considered a neurological disorder candidate protein is predicted to be associated with neurological disorders.

Naïve Bayes	Bagging-J48	Rotation forest	Random forest	K-star
1HRK	1S18	1ZT4	1CC0	1G82
1MR8	1J1J	1MR1	1CI4	2GJX
1WNT	1OPL	2K03	1CKS	1MR1
1Z6X	1WMH	1L9X	1CZZ	1NR4
2B2Y	2ARY	1I3O	1DZA	1ZSV
2J4E	1I3O	1X86	1GWQ	1S18
2NN6	2B5N	1XV9	1HLO	1WPQ
1H28	1H4O	1ZT4	1HYN	1CKS
1IYI	1YBO	2PO6	1IRJ	1NLW
1Z6U	2DSQ	2EWY	1KHU	1KN0

Table 2. Ten best putative candidate predictions with a probability of 1, from all five machine learning algorithms used.

Results from Hub-Object Analyser

The Hub Object analyser (HUBBA) is a web based tool that finds hub proteins from the input protein interaction data. Hub proteins have characteristic greater number of interactions in a network, than other non-hub proteins. In other words these proteins have more interaction partners, making them physiologically important for the individual. Hub proteins are essential elements, and are indispensable for an individual's survival [23].

The first set of analysed hub proteins is from the human protein interaction network. All the protein interactions that were used for hub identification include proteins partners that have an available 3D structure in PDB. The HUBBA results for the same are shown in Figure 3a.

a	Rank	Node	Rank	Node	Rank	Node	Rank	Node
	1	GSTA	26	GPIX1	51	CCR2	76	CERU
	2	CSF2	27	TNR1A	52	IC07	77	RAGE
	3	IL8	28	EDNRB	53	ITA4	78	NMS
	4	TPA	29	INHBE	54	APAF	79	AREG
	5	TIMP1	30	IL2RA	55	TNR1B	80	IL5
	6	VCAM1	31	IBP3	56	PGH1	81	IL13
	7	IL10	32	MMP3	57	CD38	82	FA5
	8	BAX	33	ADML	58	GHRL	83	TIMP3
	9	CCL2	34	SOMA	59	CXCL7	84	NTF4
	10	PAI1	35	IL1RA	60	FOSB	85	IL9
	11	LYAM2	36	FA8	61	CCR3	86	MK
	12	NOS2	37	LYAM3	62	IL1R1	87	DSC3
	13	LIF	38	TSP1	63	BDH	88	SSR2
	14	SDF1	39	GRP	64	IL6RA	89	ITA2
	15	HGF	40	MET	65	IL4RA	90	HUTH
	16	IL1A	41	BCL2	66	ASM	91	ITAL
	17	MMP2	42	LEPR	67	GNRHR	92	MUC1
	18	IL4	43	VIP	68	PYY	93	PRLR
	19	IGF1R	44	MMP1	69	BKRB2	94	PLF4
	20	FRIL	45	ARY1	70	TLR9	95	UCN1
	21	PDGFB	46	GA45A	71	ANTR2	96	CADM1
	22	HMOX1	47	ANPRA	72	ALK	97	BKRB1
	23	EGR1	48	PA24A	73	MOG	98	HMGB1
	24	SCR2	49	FOXO1	74	TGFB2	99	TKNK
	25	IL18	50	RETN	75	ONCM	100	PDR

b	Rank	Node	Rank	Node	Rank	Node	Rank	Node
	1	BGH3	26	TPA	51	EDN1	76	FOXO1
	2	INSR	27	IRS1	52	THY	77	PGFRB
	3	NOS3	28	PA21B	53	SCR2	78	ADML
	4	ACE	29	CBP	54	ANF	79	CNR1
	5	MMP9	30	PPARA	55	GPIX1	80	NFKB1
	6	PRL	31	BAX	56	FGFR2	81	PPAP
	7	MK14	32	MBP	57	ANGT	82	CO3
	8	ICAM1	33	PAI1	58	ESR2	83	MMP1
	9	GSTA3	34	HGF	59	IL2RA	84	ITB2
	10	GSTA1	35	SDF1	60	TNR1A	85	SOMA
	11	GSTA4	36	PDGFB	61	TLR2	86	MP2K1
	12	CASP8	37	NOS2	62	CALC	87	ARY1
	13	FGF1	38	IGF1R	63	CCR5	88	CD38
	14	PDE4A	39	MMP2	64	TNR16	89	CCL5
	15	PERM	40	CCL2	65	MMP3	90	PA24A
	16	THRB	41	PRGR	66	TSP1	91	GSTP1
	17	CP2C1	42	LIF	67	FA8	92	IL1R1
	18	IL8	43	IL18	68	BCL2	93	CP1A1
	19	TF65	44	IL4	69	HSP71	94	CTLA4
	20	TNLF6	45	LYAM2	70	FGFR1	95	APAF
	21	TLR4	46	FRIL	71	RARA	96	IC07
	22	PARP1	47	HMOX1	72	LYAM3	97	CASP9
	23	CRP	48	TKN1	73	CSF1R	98	ITA4
	24	VCAM1	49	RE	74	MET	99	IL6RA
	25	TIMP1	50	CATD	75	ERBB3	100	FAS

Figure 3a. Hub proteins identified in the human structural protein interaction network. b. Hub proteins identified in the human neurological protein interaction network. The hubs are ranked in the decreasing order of priority.

The hubs are ranked on the basis of decreasing order of priority, marked by the color coding. We then find out how many of these hubs are common to hubs in the protein interaction network of neurological disorders. That is, the list of KSOPs involved in neurological disorders. The list of hub proteins from KSOPs is given in Figure 3b. There are 21 neurologically important hub proteins that are present in the first 100 hub protein list of the human interaction network. The third hub proteins list is predicted from protein interaction data of known proteins and candidates prioritized by K-star algorithm of machine learning. K-star has been shown to predict novel neurological candidates with maximum accuracy; therefore the list of genes prioritized by this algorithm can be relied on with more confidence and has been used for prediction of hub proteins in the neurological network. Therefore in addition to known neurological disease candidates, this list includes previously unknown putative neurological candidates. Their interaction data is extracted from STRING,

and the same is used as input for HUBBA. This analysis informs if any of the previously unknown neurological candidates act as hub proteins in human neurological protein interaction network. The network and list of first 100 hub proteins from this analysis is shown in Figure 4a and 4b respectively. Out of these 100 protein hubs, 44 are the predicted putative neurological candidates by machine learning, that tend to play important role in neurological protein network and are highlighted in Figure 4b.

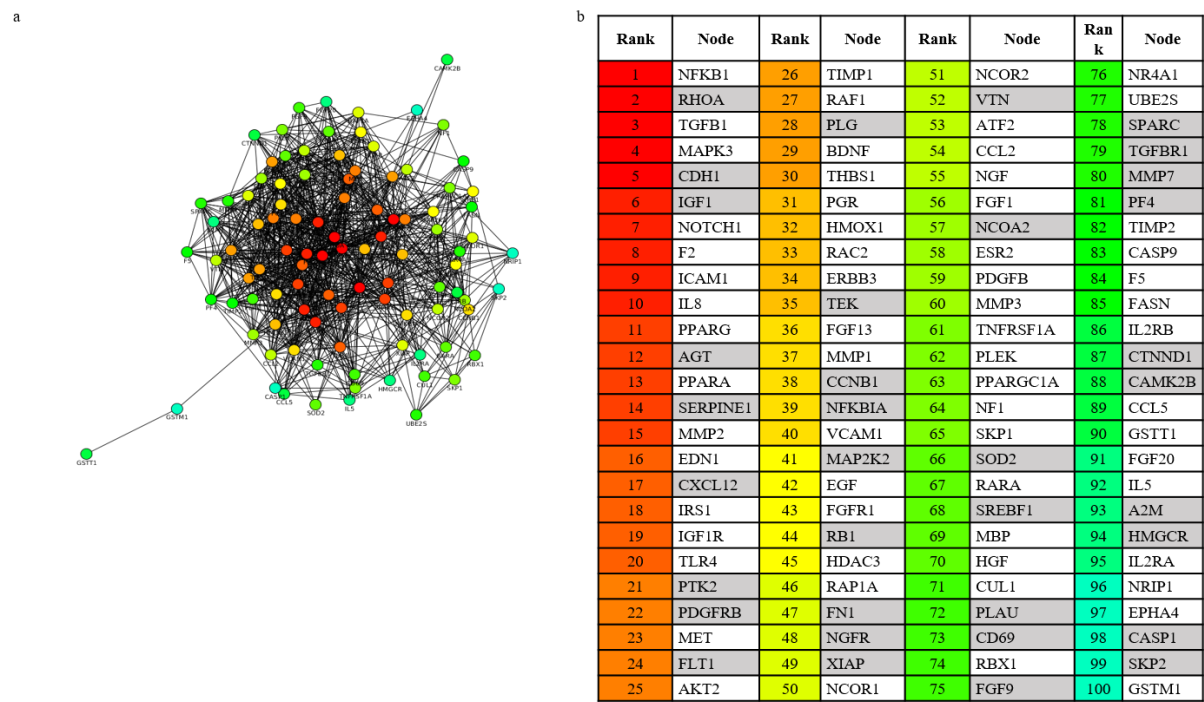


Figure 4a. Hub network of KSOPs and putative candidates. The proteins at the centre of the network are the ones that form most interactions with other proteins. b. Hub proteins identified in the human neurological protein interaction network that includes newly identified gene products. The predicted gene candidates that are behaving as hubs have been highlighted.

The identified 100 high ranking hubs from the third hub protein list were used as input for DAVID for pathway and gene ontology analysis. The most enriched pathways,

biological processes, cellular components and molecular functions are represented in Figure 5.

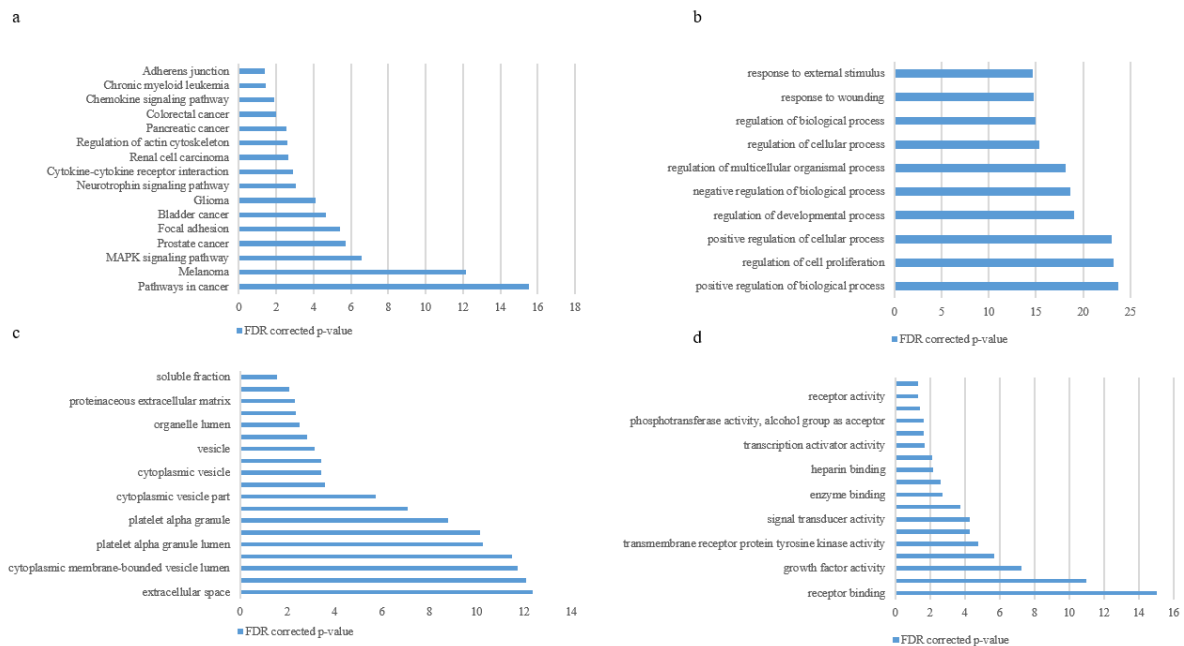


Figure 5a. Most enriched KEGG pathways from DAVID analysis. b. Enriched biological processes. c. Enriched cellular components. d. Enriched molecular functions.

DISCUSSION

The present study describes a structural systems biology approach for gene prioritization of novel protein candidates involved in neurological protein interaction networks. We have considered neurological disorders like epilepsy, Alzheimer's, Parkinson's, bipolar disorder, autism, migraine and schizophrenia for building a neurological protein network. These disorders share symptoms like depression, cognitive impairment, and anxiety. Experimental studies have shown that aberrations in the same gene or genomic area could increase the risk of acquiring several complex neuropsychiatric disorders owing to the fact that there a number of underlying mechanisms and complex pathways associated with multiple diseases [24].The interplay of numerous specific and non-specific risk factors that

result incoexistence of psychiatric and medical conditions makes diagnosis and treatment difficult that often results in other abnormalities, as in case of schizophrenia [25].

Gene prioritization for neurological disorders is an important area of research. Several studies that identify putative candidates in disorders like autism and epileptic encephalopathy have been carried out [26,27]. Scoring systems have been developed previously, using gene prioritization based on human population genetics data to identify common *de novo* functional variants across four neuropsychiatric disorders; namely epileptic encephalopathies, severe intellectual disability, schizophrenia and autism spectrum disorders. The authors in this paper have identified hot zone *de novo* mutations in these disorders that occur in the most intolerant genes [28].

In our study we use structural protein descriptors for prioritizing novel shared genetic markers in several neurological disorders owing to the specificity and characteristic structural properties of genes involved in similar phenotypic expression.

Exome sequencing studies on over thousand patient samples have identified the importance of *de novo* and gene-disruption events in neurological disorders. Deciding on potential candidates for study is dependent on many factors including recurrence of mutation and involvement of the gene in the disease protein network [29]. For example, recurrent microdeletion at the locus 1q21.1 has been associated with numerous phenotypic abnormalities including of the brain, the heart, and the eye. This emphasizes the relevance of a genotypic approach to clinically manage the treatment of different patients [30]. The method used for gene prioritization is machine learning, and the features that are used to train the machine are structural descriptors of proteins. Therefore, only the proteins whose 3D structure is available on the Protein Data Bank are used for the study. The structural descriptors include protein network properties and protein interface structural properties.

Various studies have shown that the protein network topological properties and interface structural properties are essential features for protein prioritization [31]. This study for the first time integrates these both features for gene prioritization of novel neurological candidates. Five machine learning algorithms were used for protein prioritization by WEKA. These included Naïve Bayes, rotation forest, random forest, bagging-j48 and K-star. Maximum accuracy of 81.84%, a precision of 88% and recall of 76.6% was achieved by the K-star algorithm on the test set, making its predictions the most reliable to use for further study and analysis.

Previously also certain genetic markers and pathways have been identified that are shared in these disorders. However, a lot of scope remains. Our work identifies markers that are important in the network of these diseases. Also, previously unknown markers that might lead be involved in shared pathways of these neurological disorders have been identified using HUBBA. The hubs identified in the neurological disease network are the ones that have highest number of interactions in the network, and therefore might be involved in multiple neurological pathways. DAVID analysis identifies the involvement of novel candidates in the existing neurological interaction network, wherein multiple signalling pathways like receptor binding, pathways in cancer and cell proliferation among others, get enriched. Previous studies also suggest that there are overlapping molecular pathways implicated in neurological disorders and cancers. Genes associated with these two groups of diseases are associated with kinase signalling, control of cell cycle and cellular processes and DNA repair [32].

This comprehensive neurological disease protein network analysis has therefore identified significant candidates that could be responsible for existence of shared clinical manifestations between these diseases that makes diagnosis and treatment difficult and also leads to resistance to treatment in certain cases. We present a larger network view that takes care of multiple interactions and molecular pathways associated with such diseases of

comorbid phenotype. Novel protein hubs that have been identified are important potential candidates for studying neurological disorders. The promising pattern of observations from this study and the procedure followed sets an example to conduct such more comprehensive analysis which can then be taken to next level of experimental validation.

CONFLICT OF INTERESTS

The authors declare that there is no conflict of interest.

REFERENCES

1. Stafstrom CE, Hagerman PJ, Pessah IN. Pathophysiology of Epilepsy in Autism Spectrum Disorders. In: Noebels JL, Avoli M, Rogawski MA, et al., editors. *Jasper's Basic Mechanisms of the Epilepsies* [Internet]. 4th edition. Bethesda (MD): National Center for Biotechnology Information (US); 2012.
2. Ettinger AB, Reed ML, Goldberg JF, Hirschfeld RM. Prevalence of bipolar symptoms in epilepsy vs other chronic health disorders. *Neurology*. Aug 23 2005; 65(4):535-40.
3. Bianchin MM, Londero RG, Lima JE, Bigal ME. Migraine and epilepsy: a focus on overlapping clinical, pathophysiological, molecular, and therapeutic aspects. *Curr Pain Headache Rep*. 2010 Aug; 14(4):276-83.
4. Chen J, Sawyer N, Regan L. Protein-protein interactions: general trends in the relationship between binding affinity and interfacial buried surface area. *Protein Sci*. 2013 Apr; 22(4):510-5.
5. Kar G, Gursoy A, Keskin O. Human cancer protein-protein interaction network: a structural perspective. *PLoS Comput Biol*. 2009 Dec; 5(12).
6. Gursoy A, Keskin O, Nussinov R. Topological properties of protein interaction networks from a structural perspective. *Biochem Soc Trans*. 2008 Dec; 36(Pt6):1398-403.

7. Johnson ME, Hummer G. Interface-resolved network of protein-protein interactions. *PLoSComput Biol*. 2013; 9(5).
8. Zhang KX, Ouellette BF. CAERUS: predicting CAnCErOutcomeS using relationship between protein structural information, protein networks, gene expression data, and mutation data. *PLoSComput Biol*. 2011 Mar; 7(3).
9. Wall DP, Pivovarov R, Tong M, Jung JY, Fusaro VA, DeLuca TF, Tonellato PJ. Genotator: a disease-agnostic tool for genetic annotation of disease. *BMC Med Genomics*. 2010 Oct 29;3:50.
10. UniProt Consortium. UniProt: a hub for protein information. *Nucleic Acids Res*. 2015 Jan;43(Database issue):D204-12.
11. Berman HM, Westbrook J, Feng Z, Gilliland G, Bhat TN, Weissig H, Shindyalov IN, Bourne PE. The Protein Data Bank. *Nucleic Acids Res*. 2000 Jan 1;28(1):235-42.
12. Acharya KR, Lloyd MD. The advantages and limitations of protein crystal structures. *Trends Pharmacol Sci*. 2005 Jan;26(1):10-4.
13. Szklarczyk D, Franceschini A, Wyder S, Forslund K, Heller D, Huerta-Cepas J, Simonovic M, Roth A, Santos A, Tsafou KP, Kuhn M, Bork P, Jensen LJ, von Mering C. STRING v10: protein-protein interaction networks, integrated over the tree of life. *Nucleic Acids Res*. 2015 Jan;43(Database issue):D447-52.
14. Shannon P, Markiel A, Ozier O, Baliga NS, Wang JT, Ramage D, Amin N, Schwikowski B, Ideker T. Cytoscape: a software environment for integrated models of biomolecular interaction networks. *Genome Res*. 2003 Nov;13(11):2498-504.
15. Assenov Y, Ramírez F, Schelhorn SE, Lengauer T, Albrecht M. Computing topological parameters of biological networks. *Bioinformatics*. 2008 Jan 15;24(2):282-4.

16. Lin CY, Chin CH, Wu HH, Chen SH, Ho CW, Ko MT. Hubba: hub objects analyzer-- a framework of interactome hubs identification for network biology. *Nucleic Acids Res.* 2008 Jul 1; 36(Web Server issue):W438-43.
17. Cukuroglu E, Gursoy A, Nussinov R, Keskin O. Non-redundant unique interface structures as templates for modeling protein interactions. *PLoS One.* 2014 Jan 27; 9(1).
18. Basse MJ, Betzi S, Bourgeas R, Bouzidi S, Chetrit B, Hamon V, Morelli X, Roche P. 2P2Idb: a structural database dedicated to orthosteric modulation of protein-protein interactions. *Nucleic Acids Res.* 2013 Jan; 41(Database issue):D824-7.
19. Mark Hall, Eibe Frank, Geoffrey Holmes, Bernhard Pfahringer, Peter Reutemann, Ian H. Witten (2009); *The WEKA Data Mining Software: An Update*; SIGKDD Explorations, Volume 11, Issue 1.
20. Huang da W, Sherman BT, Lempicki RA. Systematic and integrative analysis of large gene lists using DAVID bioinformatics resources. *Nat Protoc.* 2009; 4(1):44-57.
21. Huang da W, Sherman BT, Lempicki RA. Bioinformatics enrichment tools: paths toward the comprehensive functional analysis of large gene lists. *Nucleic Acids Res.* 2009 Jan; 37(1):1-13.
22. Sokolova, Marina, and Guy Lapalme. A systematic analysis of performance measures for classification tasks. *Information Processing & Management* 45.4 (2009): 427-437.
23. Batada NN, Reguly T, Breitkreutz A, Boucher L, Breitkreutz BJ, Hurst LD, Tyers M. Stratus not altocumulus: a new view of the yeast protein interaction network. *PLoS Biol.* 2006 Oct; 4(10).
24. Zhu X, Need AC, Petrovski S, Goldstein DB. One gene, many neuropsychiatric disorders: lessons from Mendelian diseases. *Nat Neurosci.* 2014 Jun; 17(6):773-81.

25. Cosoff SJ, Hafner RJ. The prevalence of comorbid anxiety in schizophrenia, schizoaffective disorder and bipolar disorder. *Aust N Z J Psychiatry*. 1998 Feb; 32(1):67-72.
26. Wall DP, Esteban FJ, Deluca TF, Huyck M, Monaghan T, Velez de Mendizabal N, Goñi J, Kohane IS. Comparative analysis of neurological disorders focuses genome-wide search for autism genes. *Genomics*. 2009 Feb; 93(2):120-9.
27. Oliver KL, Lukic V, Thorne NP, Berkovic SF, Scheffer IE, Bahlo M. Harnessing gene expression networks to prioritize candidate epileptic encephalopathy genes. *PLoS One*. 2014 Jul 9; 9(7).
28. Petrovski S, Wang Q, Heinzen EL, Allen AS, Goldstein DB. Genic intolerance to functional variation and the interpretation of personal genomes. *PLoS Genet*. 2013;9(8).
29. Hoischen A, Krumm N, Eichler EE. Prioritization of neurodevelopmental disease genes by discovery of new mutations. *Nat Neurosci*. 2014 Jun; 17(6):764-72.
30. Mefford HC, Sharp AJ, Baker C, Itsara A, Jiang Z, Buysse K, Huang S, Maloney VK, Crolla JA, Baralle D, Collins A, Mercer C, Norga K, de Ravel T, Devriendt K, Bongers EM, de Leeuw N, Reardon W, Gimelli S, Bena F, Hennekam RC, Male A, Gaunt L, Clayton-Smith J, Simonin I, Park SM, Mehta SG, Nik-Zainal S, Woods CG, Firth HV, Parkin G, Fichera M, Reitano S, Lo Giudice M, Li KE, Casuga I, Broome A, Conrad B, Schwerzmann M, Räber L, Gallati S, Striano P, Coppola A, Tolmie JL, Tobias ES, Lilley C, Armengol L, Spysschaert Y, Verloo P, De Coene A, Goossens L, Mortier G, Speleman F, van Binsbergen E, Nelen MR, Hochstenbach R, Poot M, Gallagher L, Gill M, McClellan J, King MC, Regan R, Skinner C, Stevenson RE, Antonarakis SE, Chen C, Estivill X, Menten B, Gimelli G, Gribble S, Schwartz S, Sutcliffe JS, Walsh T, Knight SJ, Sebat J, Romano C, Schwartz CE, Veltman JA, de

Vries BB, Vermeesch JR, Barber JC, Willatt L, Tassabehji M, Eichler EE. Recurrent rearrangements of chromosome 1q21.1 and variable pediatric phenotypes. *N Engl J Med*. 2008 Oct 16;359(16):1685-99.

31. Linghu B, Snitkin ES, Hu Z, Xia Y, Delisi C. Genome-wide prioritization of disease genes and identification of disease-disease associations from an integrated human functional linkage network. *Genome Biol*. 2009; 10(9):R91.
32. Plun-Favreau H, Lewis PA, Hardy J, Martins LM, Wood NW. Cancer and neurodegeneration: between the devil and the deep blue sea. *PLoS Genet*. 2010 Dec 23;6(12).

Research Article

Hybrid Dynamic MCML Style: A High Speed Dynamic MCML Style

Neeta Pandey,¹ Damini Garg,¹ Kirti Gupta,² and Bharat Choudhary¹

¹Department of Electronics and Communication Engineering, Delhi Technological University, New Delhi 110042, India

²Department of Electronics and Communication Engineering, Bharati Vidyapeeth's College of Engineering, New Delhi 110063, India

Correspondence should be addressed to Neeta Pandey; n66pandey@rediffmail.com

Received 30 September 2015; Revised 20 December 2015; Accepted 21 December 2015

Academic Editor: Alfio D. Grasso

Copyright © 2016 Neeta Pandey et al. This is an open access article distributed under the Creative Commons Attribution License, which permits unrestricted use, distribution, and reproduction in any medium, provided the original work is properly cited.

This paper proposes hybrid dynamic current mode logic (H-DyCML) as an alternative to existing dynamic CML (DyCML) style for digital circuit design in mixed-signal applications. H-DyCML introduces complementary pass transistors for implementation of logic functions. This allows reduction in the stacked source-coupled transistor pair levels in comparison to the existing DyCML style. The resulting reduction in transistor pair levels permits significant speed improvement. SPICE simulations using TSMC 180 nm and 90 nm CMOS technology parameters are carried out to verify the functionality and to identify their advantages. Some issues related to the compatibility of the complementary pass transistor logic have been investigated and the appropriate solutions have been proposed. The performance of the proposed H-DyCML gates is compared with the existing DyCML gates. The comparison confirms that proposed H-DyCML gates is faster than the existing DyCML gates.

1. Introduction

There has been tremendous boost on the design and development of portable electronic goods in recent past [1–4]. As the battery life is critical in these systems, there has been a paradigm shift towards low power designs. Though the CMOS logic circuits consume negligible static power, the dynamic power consumption increases sharply as the operating high frequencies are increased [5–8]. The MOS current mode logic (MCML) is a promising alternative to CMOS logic, in both reducing power consumption at high frequencies and providing high performance for mixed-signal applications [9–14]. Due to the presence of static current source, the power consumption of these circuits is high. Therefore, a new logic family called dynamic CML [15, 16] is suggested in literature which used dynamic current source and operate on precharge evaluate method prevailing in dynamic CMOS logic. The multiple input logic realization requires stacking of transistors leading to significant delay.

In this paper, a new method to realize the logic function in DyCML gate for reducing the stacking of transistors is presented. A dynamic logic style employing the complementary pass transistor logic (CPL) for implementing the logic

functions is proposed. This new logic style is named hybrid dynamic CML logic and is abbreviated as H-DyCML style. The paper first briefly describes the existing DyCML style and highlights its advantages over the MCML style in Section 2. Thereafter, the architecture of the proposed H-DyCML style is presented and investigated in Section 3. The power consumption of the proposed style is formulated in Section 4. The functionality of the proposed H-DyCML gates and the performance comparison with the existing DyCML gates are carried out in the simulation Section 5. Lastly, the conclusions are drawn in Section 6.

2. Dynamic Current Mode Logic (DyCML) Style [15, 16]

A DyCML gate uses dynamic current source, instead of constant current source employed in conventional CML, and achieves low power consumption. It operates on precharge and evaluate logic wherein in the output node capacitance is first precharged and subsequently evaluated according to the applied inputs. It has a pull-down network (PDN) to realize the logic function, a precharge circuit operating in

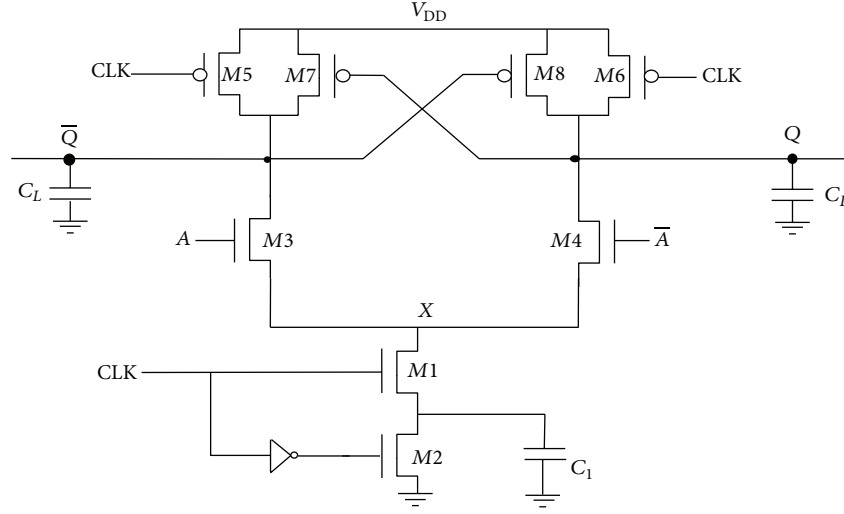


FIGURE 1: DyCML inverter [15, 16].

the precharge phase, a dynamic current source working in the evaluation phase, and a latch circuit for maintaining the voltage levels at the output.

The schematic of the DyCML inverter ($M1-M8$) is shown in Figure 1. In the circuit diagram, the transistors ($M1, M2$) and capacitor C_1 form the dynamic current source and the transistors ($M3, M4$) constitute the PDN, while the transistors ($M5, M6$) and ($M7, M8$) make the precharge and the latch circuit, respectively. During the precharge phase, the CLK is low, the transistors $M2, M5$, and $M6$ are On, and the transistor $M1$ is Off. Both the output nodes Q and \bar{Q} are precharged to the high voltage level ($V_{OH} = V_{DD}$) through the transistors $M5$ and $M6$, respectively. Also, the capacitor C_1 is discharged to the ground potential via transistor $M2$. In the precharge phase, the differential input A is applied and does not cause any change in the output level as the precharge transistors $M5, M6$ are On and the transistor $M1$ is Off. The circuit enters in the evaluation phase for high value of the CLK signal. The transistor $M1$ is On in this phase and output is evaluated according to the input.

The DyCML gates offer significant power saving and are able to achieve smaller delays in comparison to the basic MCML gates. Also DyCML gates inherit the advantageous features such as high performance, noise immunity, and robustness to supply voltage scaling of MCML gates due to the fact that these are derived from the MCML gates [15, 16]. The circuit diagrams for different DyCML gates are shown in Figure 2. It can be observed that the PDN consist of multiple levels of source-coupled transistor pair arranged in accordance with the series-gating approach which adds to the delay of the gate. In this paper, an alternate arrangement to reduce the delay of the DyCML gates is proposed. The new gates are built with an aim of reducing the number of source-coupled transistor pair levels in the PDN. To accomplish this, the complementary pass transistor logic is introduced in DyCML style and nomenclature hybrid dynamic CML (H-DyCML) gates are used for the resulting logic style.

3. Proposed Hybrid Dynamic CML (H-DyCML) Style

The basic architecture of a H-DyCML gate is shown in Figure 3. The precharge, dynamic current source, and the latch circuits are similar to those of the existing DyCML gate. The only difference is in the way of realizing the logic function. The complementary pass transistor logic (CPL) is used to realize a part of functionality while the remaining part is implemented in the PDN. To illustrate the concept, the implementation of two- and three-input XOR gates in H-DyCML style is considered and is shown in Figure 4. In the two-input H-DyCML XOR gate (Figure 4(a)), the CPL implements the XOR functionality and whose output is given as the input to the DyCML inverter. The realization of the three-input XOR gate consists of two levels of stacked source-coupled transistor pair in contrast to the three levels in existing DyCML XOR gate. The input to the lowest level is provided by the CPL logic that realizes the XOR of two inputs and the upper level is then formed by applying the series-gating approach as followed by DyCML gate. The resulting implementation is shown in Figure 4(b). Another implementation of the three-input XOR gate can be obtained by realizing the complete XOR functionality in the CPL network and then connecting its output to the DyCML inverter. This implementation of the three-input XOR with only single level of source coupled transistor is drawn in Figure 4(c).

The operation of a H-DyCML gate in general can be divided into the precharge and the evaluation phase. The operation of the two-input XOR gate is elaborated as an example. In the precharge phase, when the CLK is low, both the output nodes Q and \bar{Q} are precharged to the high voltage level ($V_{OH} = V_{DD}$) through the transistors $M5$ and $M6$, respectively. Also, the output of the complementary pass transistor logic is applied to input A but it does not cause any change in the output level as the precharge transistors

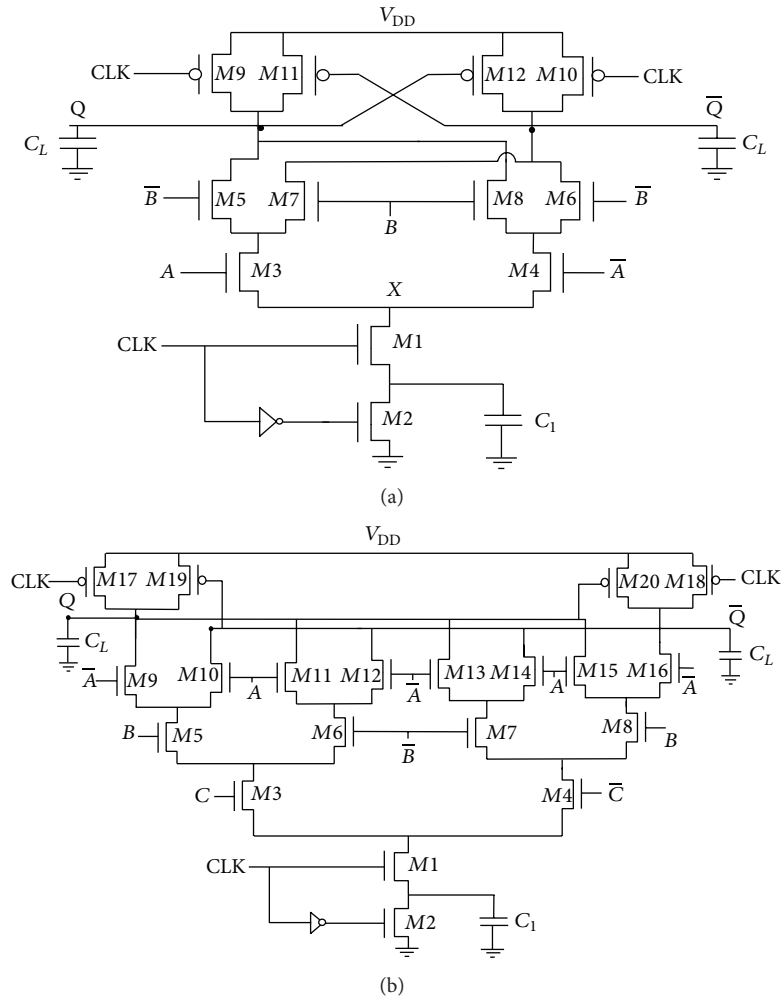


FIGURE 2: DyCML gate: (a) two-input XOR; (b) three-input XOR.

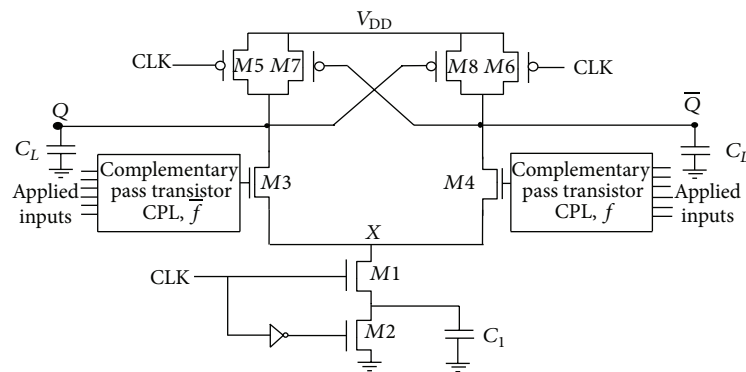


FIGURE 3: Basic architecture of H-DyCML gate.

$M5$, $M6$ are On and the transistor $M1$ is Off. For high value of the CLK signal, the circuit enters in the evaluation phase and the transistor $M1$ is On. The output of the CPL is now evaluated and is appropriately reflected at the output node. The reduction in the source coupled level reduces the resistance offered by the transistors for charging the capacitor C_1 and in turn reduces the delay of the gate.

It may be noted that the implementation of the logic function through the CPL approach involves the use of NMOS transistors. As already known the maximum voltage obtained from an NMOS transistor is one threshold voltage less than the gate voltage. Therefore, if a high input (V_{DD}) is applied to an NMOS transistor having its gate connected to high potential (V_{DD}) then the output can attain maximum

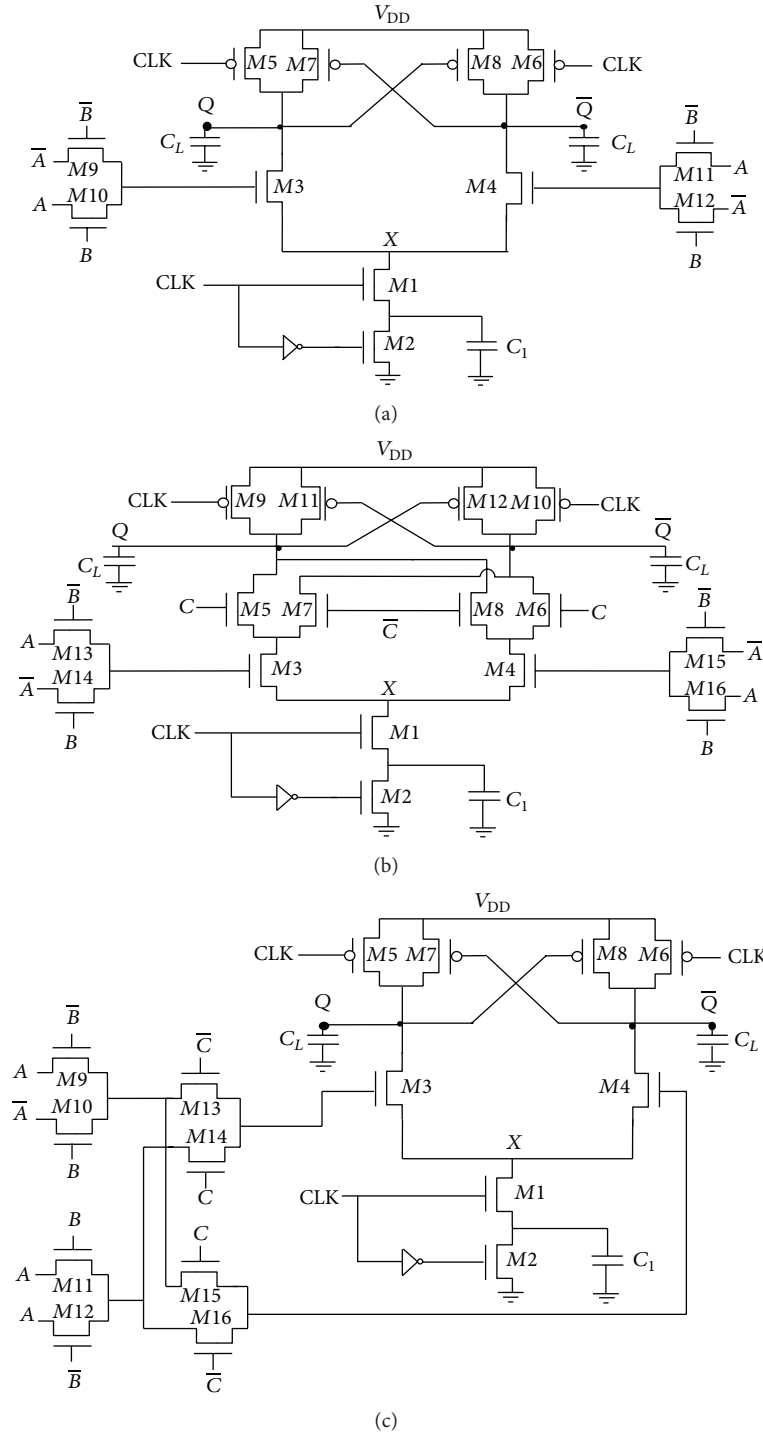


FIGURE 4: Proposed H-DyCML gates: (a) 2-input XOR gate; (b) 3-input XOR gate with two levels of source-coupled transistor pair in the PDN; (c) 3-input XOR gate with single level of source-coupled transistor pair in the PDN.

voltage (V_{OH}) of $V_{DD} - V_{T,n}$, where $V_{T,n}$ is the threshold voltage of NMOS transistor. This reduction in output voltage may lead to erroneous operation of dynamic gate. So three techniques to address the problem are proposed.

Technique 1: Use of Level Restorer. The maximum voltage obtained from the CPL can be raised by using cross-coupled

PMOS transistors operating as level restorer. To illustrate the operation of a level restorer, the CPL implementation of a two-input XOR gate with inputs A and B is considered and is shown in Figure 5. Consider that the input A is high (V_{DD}) and the input B is low ($V_{DD} - V_{SWING}$) where V_{SWING} is the voltage swing of the CML gate. For this input condition, the output of the branch representing XOR functionality (f)

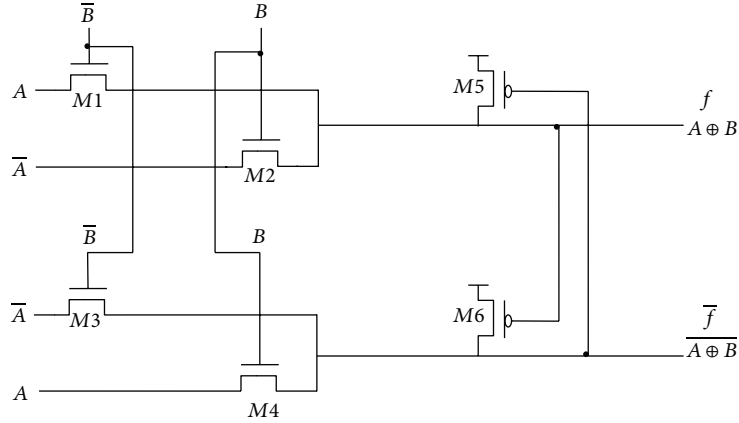


FIGURE 5: CPL with level restorer.

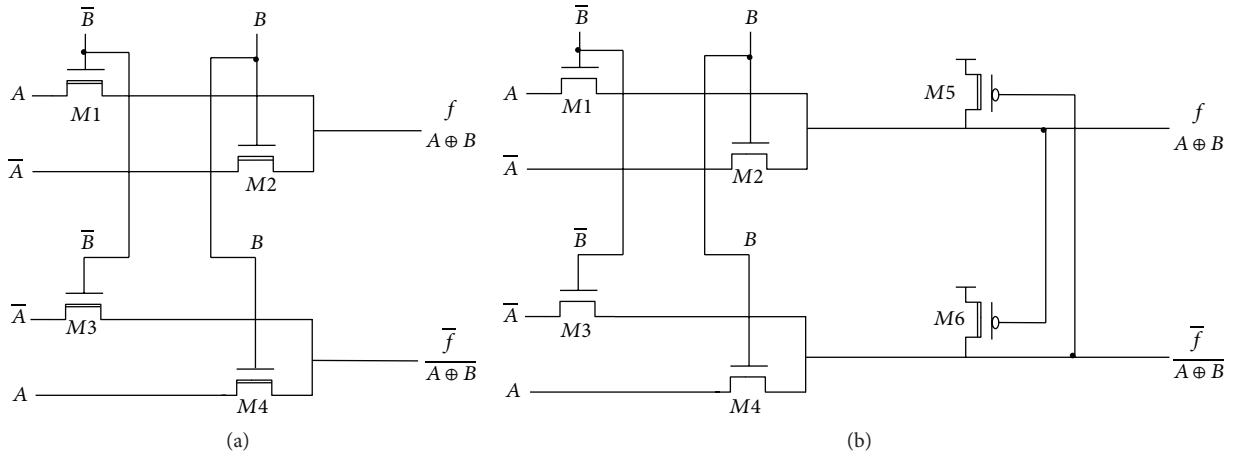


FIGURE 6: CPL logic with multiple threshold voltage transistor: (a) NMOS transistors; (b) PMOS transistors.

will be high ($V_{DD} - V_{T,n}$) whereas the other branch (\bar{f}) is low ($V_{DD} - V_{SWING}$). If the gate-source voltage of the PMOS transistor $M5$ ($V_{SG} = V_{SWING}$) is less than the threshold voltage (V_T), it gets turned On and raises the voltage level of the XOR function (f) to V_{DD} . The other PMOS transistor $M6$ will not conduct and the output of the other branch (\bar{f}) will remain low ($V_{DD} - V_{SWING}$).

It may be noted that this technique poses a restriction on the voltage swing V_{SWING} of the gate. This can be explained from the fact that the cross-coupled PMOS transistor $M5$ will be On only if gate-source voltage is less than the threshold voltage (i.e., $V_{SG} < V_T$). In other words, the voltage swing of the gate should be greater than the threshold voltage ($V_{SWING} > V_T$). Therefore for the CML gate having lower voltage swing, this technique is not suitable. Another technique to handle the lower CML gates is presented in the following.

Technique 2: Use of Multiple Threshold Voltage Transistor. The above technique has the limitation on the voltage swing of the CML gate due to the threshold voltage of the transistor. Therefore, this technique suggests the use of lower threshold voltage transistors in the circuit. This can be implemented in two ways either by using lower threshold voltage NMOS

transistors in the CPL network or by employing lower threshold voltage PMOS transistors in the level restorer. The same is depicted in Figure 6 for the two-input XOR gate. The transistors with bold lines denote low threshold voltage transistor. Thus, the H-DyCML gates with low voltage swing can also be implemented.

An alternate approach which neither having any limitations on the voltage swing of the gate nor putting any constraint on threshold voltage is also possible and is elaborated further.

Technique 3: Use of Transmission Gates. The drop in the high voltage level at the output of the CPL network can be overcome by realizing the logic function through transmission gates. An implementation of the XOR gate by using transmission gate is shown in Figure 7. Though this technique will increase the number of transistors it does not pose any restrictions on the voltage swing of the H-DyCML gate.

4. Power Consumption of H-DyCML

In the proposed H-DyCML gate, the transistor pairs $M1$ and $M2$ (Figure 3) never turns On simultaneously. As a consequence, a direct path between the power supply

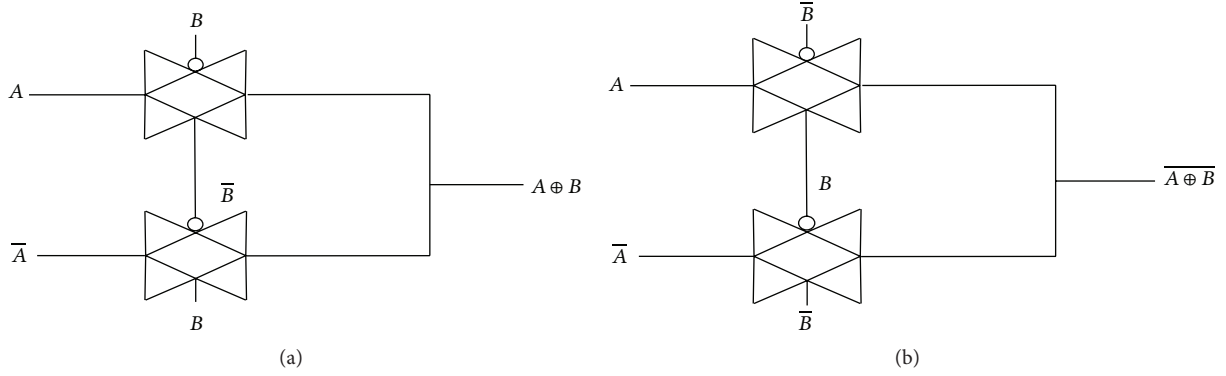


FIGURE 7: XOR function realization for H-DyCML gate.

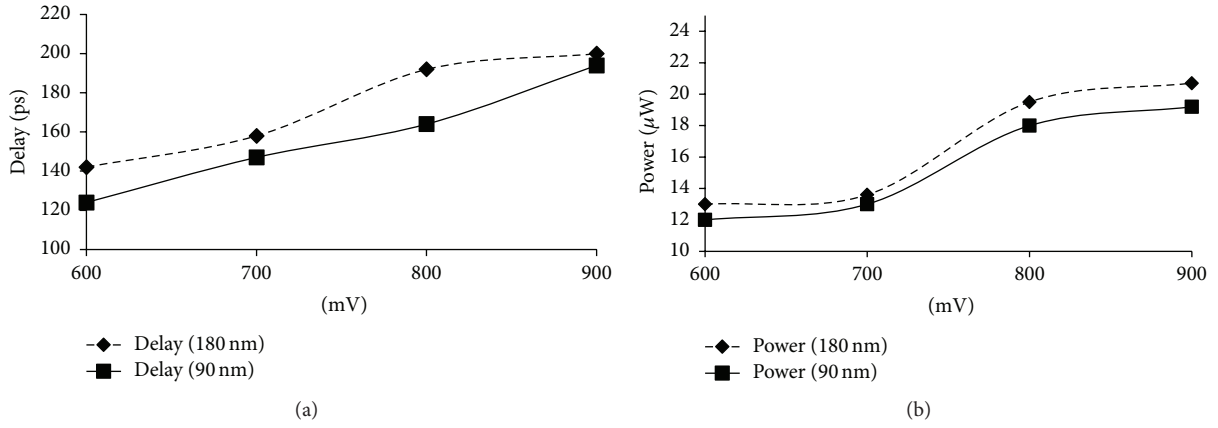


FIGURE 8: Performance of the two-input H-DyCML XOR gate by varying the voltage swing: (a) delay results: (b) power results.

and the ground is not established resulting in negligible static power consumption. The proposed H-DyCML gate however consumes dynamic power due to the presence of the load capacitors. In general, the dynamic power is given by

$$P_{\text{dyn}} = \alpha C_{\text{OUT}} V_{\text{DD}} V_{\text{SWING}} f_{\text{CLK}} \quad (1)$$

where C_{OUT} is the total load capacitance at the output node which includes the parasitic capacitances of the transistors and the external load capacitance C_L , f_{CLK} represents the frequency of the CLK signal, V_{DD} is the power supply, and V_{SWING} and α correspond to the voltage swing and switching activity of the circuit, respectively.

In H-DyCML gates, due to the inherent differential nature of the inputs, it may be noted that one of the output nodes will make a high-to-low transition which requires subsequent precharging to V_{DD} . This observation indicates that the power consumption of the H-DyCML gate is data-independent. In other words, irrespective of the differential inputs, in every clock cycle one of the output nodes will be charged. This signifies that, for a H-DyCML gate, the switching activity is unity. Equation (1) reduces to (2) for power consumption of H-DyCML gates as follows:

$$P_{\text{dynH-DyCML}} = C_{\text{OUT}} V_{\text{DD}} V_{\text{SWING}} f_{\text{CLK}} \quad (2)$$

5. Simulation Results

Different H-DyCML gates such as two-input AND, two-input OR, two-input XOR, and three-input XOR are simulated by using 180 nm and 90 nm CMOS technology parameters with a supply voltage of 1.8 V. The three techniques to realize H-DyCML gates are considered. So for the sake of fair comparison all the gates are designed to operate with a voltage swing greater than the threshold voltage of the transistor. A voltage swing of 700 mV is chosen. The other simulation settings are $C_{\text{OUT}} = 40$ fF, $f_{\text{CLK}} = 333$ MHz. The values of performance parameters such as power, delay, and power-delay product are noted and are summarized in Tables 1–5. The theoretical value of power consumption in H-DyCML gate is computed using (2) which is found to be $16.78 \mu\text{W}$ and is very close to the values reported in Tables 1–5.

It may be noted in Tables 1 and 2 that the maximum delay reduction of 37.87% is observed for the proposed H-DyCML gates in comparison to the existing DyCML gates. Analogously, the H-DyCML two-input and three-input XOR gates show a delay reduction of 48.23% and 49.4%, respectively, as compared to existing DyCML XOR gate counterparts.

To include design choices as per the suggestion, the performance of the proposed H-DyCML gates is investigated through simulations for different voltage swing and aspect

TABLE 1: Performance comparison of the existing DyCML and the proposed H-DyCML AND gate.

Parameter	Style				
	DyCML	H-DyCML (Technique 1)	H-DyCML (Technique 2)		H-DyCML (Technique 3)
			PMOS	NMOS	
Technology node 180 nm					
Delay (ps)	192.31	176.01	167.92	162.13	180.54
Power (μ W)	20.31	15.57	15.58	15.02	15.58
PDP (fJ)	3.90	2.69	2.61	2.43	2.81
Technology node 90 nm					
Delay (ps)	180	156	129	164	168
Power (μ W)	14.2	13.36	13.1	13.9	13.4
PDP (fJ)	2.55	2.08	1.68	2.27	2.25

TABLE 2: Performance comparison of the existing DyCML and the proposed H-DyCML OR gate.

Parameter	Style				
	DyCML	H-DyCML (Technique 1)	H-DyCML (Technique 2)		H-DyCML (Technique 3)
			PMOS	NMOS	
Technology node 180 nm					
Delay (ps)	236.24	172.28	162.12	219.03	170.25
Power (μ W)	32.11	13.762	13.83	13.88	13.94
PDP (fJ)	7.58	2.37	2.24	3.04	2.37
Technology node 90 nm					
Delay (ps)	180	156	129	164	168
Power (μ W)	14.2	13.36	13.1	13.9	13.4
PDP (fJ)	2.55	2.08	1.68	2.27	2.25

TABLE 3: Performance comparison of the existing DyCML and the proposed H-DyCML 2-input XOR gate.

Parameter	Style				
	DyCML	H-DyCML (Technique 1)	H-DyCML (Technique 2)		H-DyCML (Technique 3)
			PMOS	NMOS	
Technology node 180 nm					
Delay (ps)	237.93	160.63	160.00	171.31	158.33
Power (μ W)	29.28	14.84	14.84	13.23	15.20
PDP (fJ)	6.96	2.37	2.37	2.26	2.4
Technology node 90 nm					
Delay (ps)	201	143	140	145	147
Power (μ W)	24	14.8	14.8	14.91	13
PDP (fJ)	4.84	2.11	2.07	2.16	1.91

TABLE 4: Performance comparison of the existing DyCML and the proposed H-DyCML 3-input XOR gate with two levels of source-coupled transistors in the PDN.

Parameter	Style				
	DyCML	H-DyCML (Technique 1)	H-DyCML (Technique 2)		H-DyCML (Technique 3)
			PMOS	NMOS	
Technology node 180 nm					
Delay (ps)	326.39	211.02	180.00	191.31	199.05
Power (μ W)	26.54	14.84	14.84	13.23	12.32
PDP (fJ)	8.66	7.35	5.56	5.69	6.37
Technology node 90 nm					
Delay (ps)	226	175	163	169	190
Power (μ W)	23	16.2	16.8	18.4	16.7
PDP (fJ)	5.2	2.83	2.73	3.1	3.17

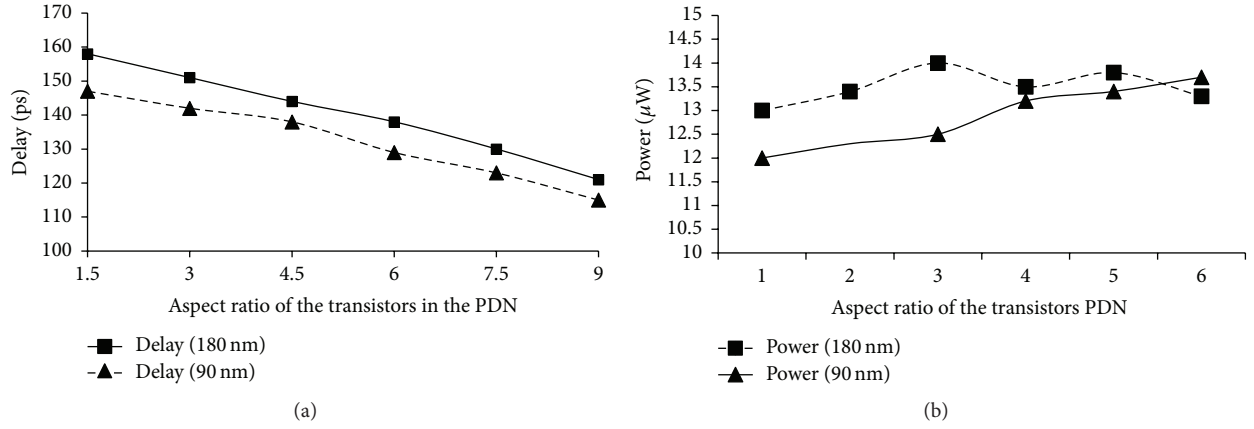


FIGURE 9: Performance of the two-input H-DyCML XOR gate by varying the aspect ratio of the transistors in the PDN: (a) delay results; (b) power results.

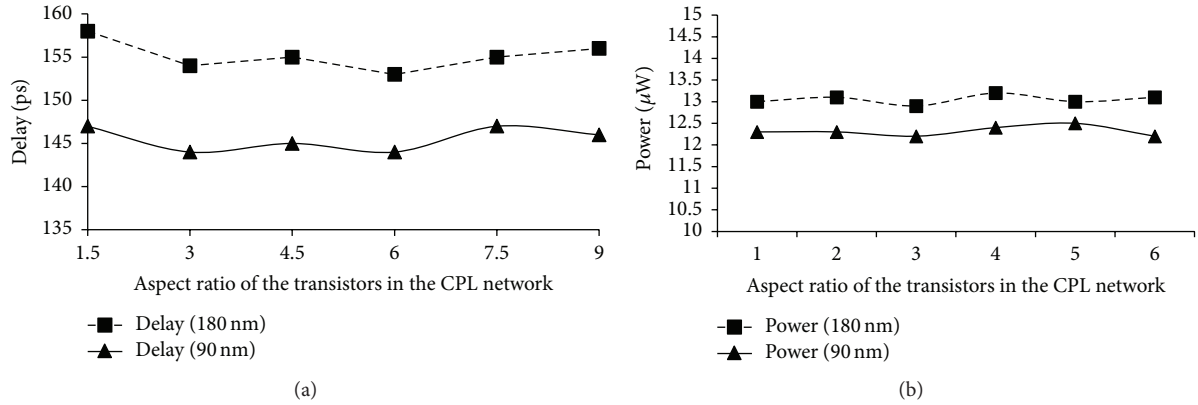


FIGURE 10: Performance of two-input H-DyCML XOR gate by varying the aspect ratio of the transistors in the CPL network: (a) delay results; (b) power results.

TABLE 5: Performance comparison of the existing DyCML and the proposed H-DyCML 3-input XOR gate with single level of source-coupled transistors in the PDN.

Parameter	Style				
	DyCML	H-DyCML (Technique 1)	H-DyCML (Technique 2)		H-DyCML (Technique 3)
			PMOS	NMOS	
Technology node 180 nm					
Delay (ps)	326.39	166	170	187	193
Power (μ W)	26.54	18	17.5	19	17.6
PDP (fJ)	8.66	2.9	2.9	3.5	3.3
Technology node 90 nm					
Delay (ps)	226	125	141	176	187
Power (μ W)	23	16.2	16.8	18.4	16.7
PDP (fJ)	5.2	2.0	2.3	3.2	3.1

ratio values. The results have been summarized for a two-input XOR gate based on technique 3 in Figures 8–10. Following are the observations:

- (i) In Figure 8, the power consumption increases with the increase in voltage which is supported with the theoretical formulations discussed in Section 4. Also, an increase in voltage swing requires more charge

to be transferred from the output load capacitance making a corresponding increase in the delay as indicated in Figure 8.

- (ii) Figure 9 shows the dependence of the delay on the aspect ratios of the transistors in the PDN network. There is a decreasing trend in delay with aspect ratio increase. To explain this, the transistors in the PDN

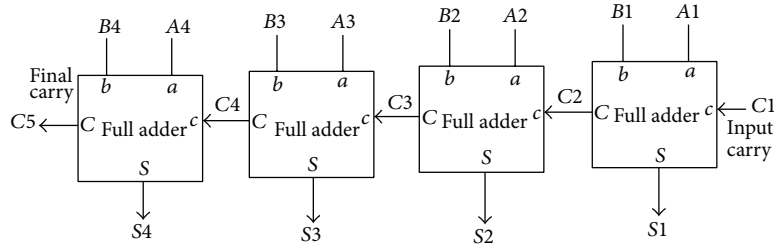


FIGURE 11: Block diagram of a 4-bit RCA.

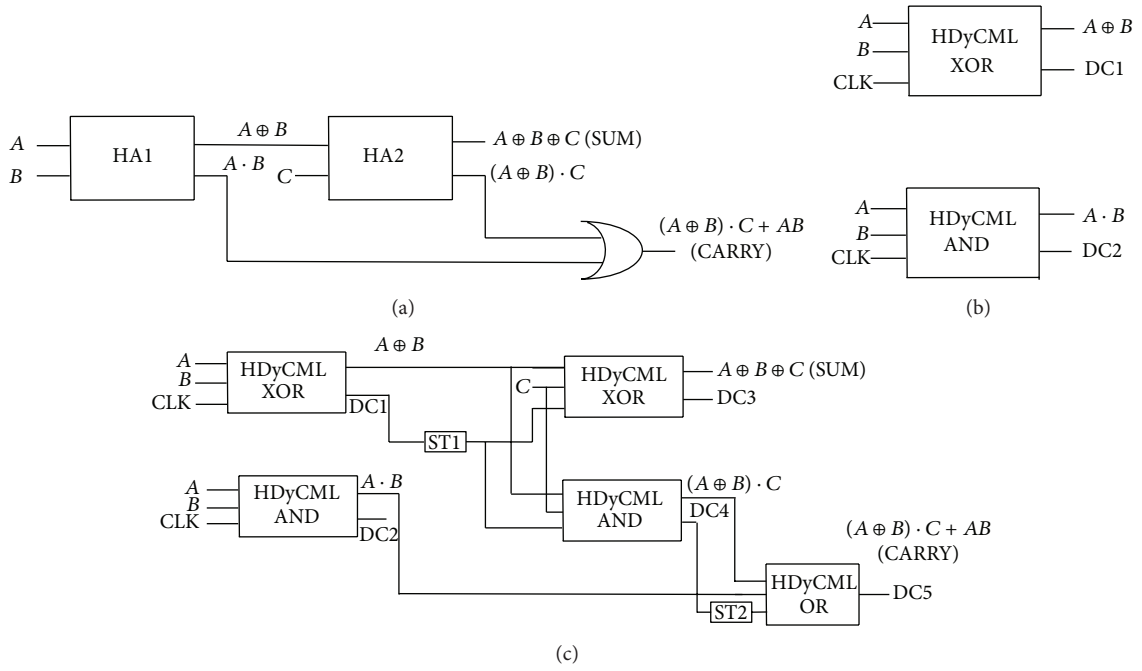


FIGURE 12: (a) Full adder schematic; (b) H-DyCML half adder schematic; (c) complete schematic of D-HyCML full adder.

can be viewed as resistor. When aspect ratios of transistors in PDN are increased it results in smaller resistance and lower delay values.

- (iii) Lastly, the power and the delay of the proposed H-DyCML gate remain almost constant for different values of aspect ratio of the transistors in the CPL network (Figure 10). This is due to the fact that the changes in the CPL network occur in the precharge phase which has no effect in determining the performance of the H-DyCML gate.

In order to present an application of the proposed style, a 4-bit RCA (Figure 11) implementation is considered. The implementation requires cascading of four full adder (FA) circuits wherein the full adder is realized by cascading two half adders (HA) and an OR gate as shown in Figure 12(a). The realization of half adder uses the schematic in Figure 12(b) and its H-DyCML realization is placed in Figure 12(c). The signals DC_i ($i = 1, 2$) represent voltage across capacitor C_1 of H-DyCML XOR and AND gates. In dynamic CML style, the direct cascading of various gates is not possible [16]; therefore self-timed buffers (STs) [16] are placed intermittently.

The operation of ST is to trigger the evaluation process in subsequent stages upon receiving a completion signal from preceding stage via DC_1 .

The performance parameters such as power, delay, and PDP are noted for the 4-bit RCA using different techniques and are noted in Table 6. It may be noted that the delay is almost the same for all the proposed topologies which may be attributed to the same number of total cascaded stages used for realization. Further, there is significant reduction in delay and power consumption in comparison to the existing DyCML style. The delay reduces by 63.43% in the proposed H-DyCML based design in comparison to existing DyCML RCA design.

6. Conclusion

In this paper, a new hybrid dynamic current mode logic (H-DyCML) is presented as an alternative to the existing DyCML style. The use of complementary pass transistors in logic function realization is proposed in H-DyCML style. This is done to reduce source-coupled transistor pair levels

TABLE 6: Performance comparison of the existing DyCML and the proposed H-DyCML 4-bit RCA.

Parameter	Style			
	DyCML	H-DyCML (Technique 1)	H-DyCML (Technique 2)	H-DyCML (Technique 3)
Delay (ps)	967.74	339.57	326.39	357.08
Power (μ W)	250.88	130.362	129.52	131.11
PDP (fJ)	242.78	44.354	42.27	46.82

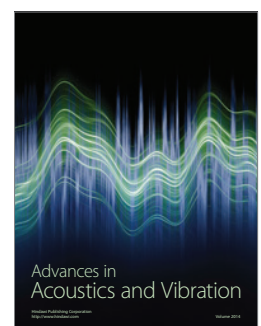
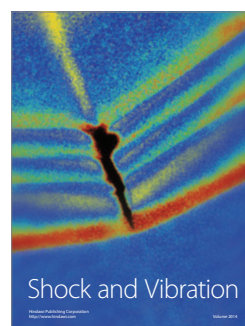
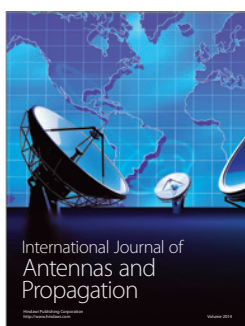
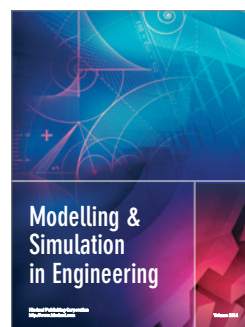
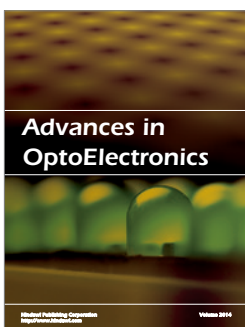
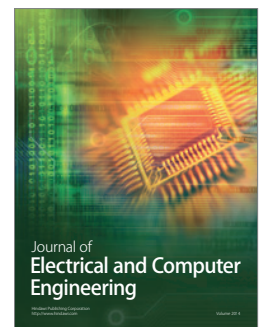
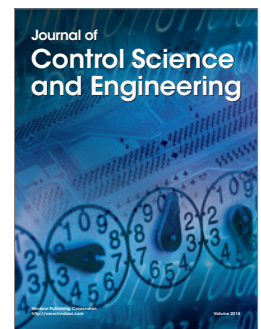
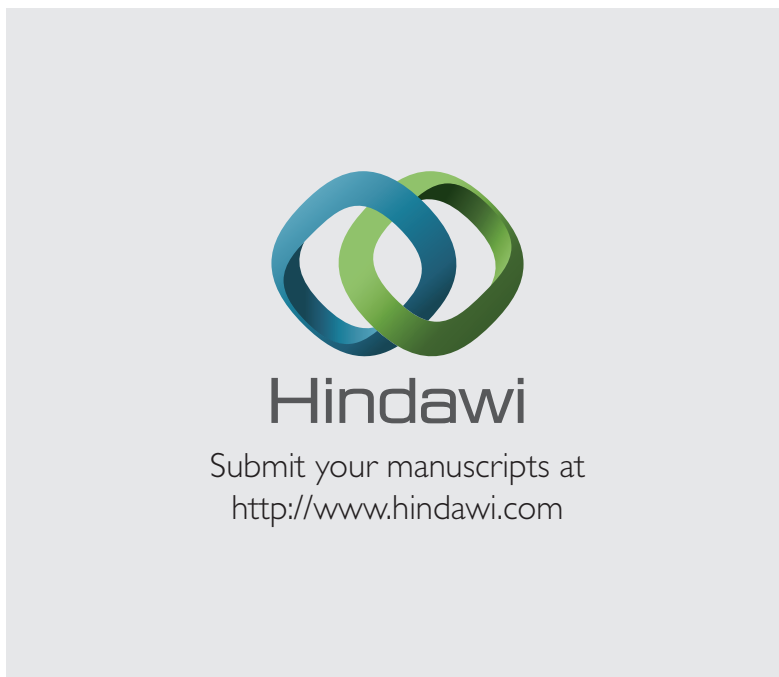
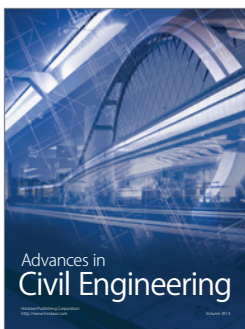
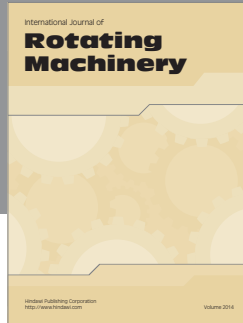
in the PDN of the gate which results in an improvement of delay of the gate. Different gates in H-DyCML style are implemented and simulations are performed to compare their performance with the existing DyCML gates. The TSMC 180 nm and 90 nm CMOS technology parameters are used. The issues related to the compatibility of the complementary pass transistor logic with CML gates are identified and appropriate solutions have been proposed. An application example is also taken to demonstrate the benefit of employing proposed H-DyCML gates over the existing DyCML gates. A maximum improvement of 63.43% was observed in delay by employing proposed H-DyCML gates. Hence, it is confirmed that the proposed H-DyCML gates offer significant speed advantage over the existing DyCML gates.

Conflict of Interests

The authors declare that there is no conflict of interests regarding the publication of this paper.

References

- [1] B. Davari, R. H. Dennard, and G. G. Shahidi, "CMOS scaling for high performance and low power—the next ten years," *Proceedings of the IEEE*, vol. 83, no. 4, pp. 595–606, 1995.
- [2] International Technology Roadmap for Semiconductors, "Radio frequency and analog/mixed signal technologies for wireless communications," Tech. Rep., ITRS, 2005.
- [3] A. P. Chandrakasan, S. Sheng, and R. W. Brodersen, "Low-power CMOS digital design," *IEEE Journal of Solid-State Circuits*, vol. 27, no. 4, pp. 473–484, 1992.
- [4] P. Ng, P. T. Balsara, and D. Steiss, "Performance of CMOS differential circuits," *IEEE Journal of Solid-State Circuits*, vol. 31, no. 6, pp. 841–846, 1996.
- [5] N. H. E. Weste and D. Harris, *Principles of CMOS VLSI Design: A System Perspective*, Addison-Wesley, 3rd edition, 2004.
- [6] R. H. Krambeck, C. M. Lee, and H.-F. S. Law, "High-speed compact circuits with CMOS," *IEEE Journal of Solid-State Circuits*, vol. 17, no. 3, pp. 614–619, 1982.
- [7] P. van der Meer, A. van Staveren, and A. van Roermund, *Low-Power Deep Sub-Micron CMOS Logic: Sub-Threshold Current Reduction*, The Springer International Series in Engineering and Computer Science, Springer, New York, NY, USA, 2004.
- [8] S.-M. Kang and Y. Leblebici, *CMOS Digital Integrated Circuits*, Tata McGraw-Hill Education, 2003.
- [9] M. Alioto and G. Palumbo, "Power-aware design techniques for nanometer MOS current-mode logic gates: a design framework," *IEEE Circuits and Systems Magazine*, vol. 6, no. 4, pp. 40–59, 2006.
- [10] M. Alioto and G. Palumbo, "Design strategy for source coupled logic gates," *IEEE Transactions on Circuits and Systems I: Fundamental Theory and Applications*, vol. 50, no. 5, pp. 640–654, 2003.
- [11] M. Alioto and G. Paulumbo, "Model and design of bipolar and MOS current-mode logic," *IEEE Transactions on Circuits and Systems—Part I: Fundamental theory and Applications*, vol. 46, pp. 1330–1341, 1999.
- [12] J. M. Musicer and J. Rabaey, "MOS current mode logic for low power, low noise CORDIC computation in mixed-signal environments," in *Proceedings of the Symposium on Low Power Electronics and Design (ISLPED '00)*, pp. 102–107, IEEE, Rapallo, Italy, July 2000.
- [13] M. Mizuno, M. Yamashina, K. Furuta et al., "A GHz MOS, adaptive pipeline technique using MOS current-mode logic," *IEEE Journal of Solid-State Circuits*, vol. 31, no. 6, pp. 784–790, 1996.
- [14] M. Yamashina and H. Yamada, "An MOS current mode logic (MCML) circuit for low-power sub-GHz processors," *IEICE Transactions on Electronics*, vol. E75-C, pp. 1181–1187, 1992.
- [15] M. W. Allam and M. I. Elmasry, "Dynamic current mode logic (Dynamic CML): a new low-power high performance logic family," in *Proceedings of the IEEE Custom Integrated Circuits Conference (CICC)*, pp. 421–424, Orlando, Fla, USA, 2000.
- [16] M. W. Allam and M. I. Elmasry, "Dynamic current mode logic (DyCML): a new low-power high-performance logic style," *IEEE Journal of Solid-State Circuits*, vol. 36, no. 3, pp. 550–558, 2001.





IMPACT OF PROMOTIONAL TOOLS ON STUDENTS DECISION-MAKING: STUDY OF PRIVATE ENGINEERING INSTITUTIONS IN DELHI NCR

Ms. Antra Singh

*Research Scholar, Department of Humanities
Delhi Technological University, Delhi*

Dr. (Mrs.) Seema Singh

*Associate Professor in Economics, Department of Humanities
Delhi Technological University, Delhi*

ABSTRACT

Selecting a college to pursue higher education (especially professional) is a highly complex process, especially when one has not been able to secure a position in the elite institutions of the country. The decision is very crucial as career of the individual is at stake and at the same time it sweeps lump-sum amount, for some it does not matter much but for some it is their life time savings. Every student aspires for the best institution, but is disheartened when he/she is not able to secure a seat there. As a result, they seek for other available avenues; they experience varied sources of inputs like influence of family, peer group, alumni, influence of institutional factors like infrastructure, quality of faculty, past placement records and influence of promotional tools like advertisements, direct marketing, public relations and sales promotion tools. So it is imperative for the administration of these private engineering institutions to comprehend students' expectations from them and accordingly strategise their usage of promotional tools to reap out maximum benefit through quality enrolment. The objective of the study is to ascertain the influence of promotional tools on student consideration sets during selecting a private engineering college in Delhi NCR. Four thousand and forty first year students enrolled in ninety-five private engineering colleges participated in this study. Questionnaire was used comprising selective demographical data and various promotional tools ministering to selection of a college. The result indicated that promotional tools have significant influence on selection of a private engineering college along with other factors. These findings will enable private colleges to formulate effective promotional strategies to provide them competitive advantage over other players, in terms of brand value as well as quality enrolment.

Keywords: *Promotional Tools, Students, Selection, Private Engineering College*

1. Introduction

Higher education (especially technical education) plays an impertinent role in economic growth and social development of the nation by spawning innovative knowledge and raising the standard of living. Despite of the fact higher education is facing predicament like shortage of funds, quality of teachers, staffs, research and infrastructure there is an upsurge in demand. This amelioration in demand for higher education has led to an unplanned expansion of private higher education. The proliferation in private engineering education has led to an intense competition among the private players to tantalize quality enrolment. They embraced themselves with numerous promotional tools to entice the potential students and their convoy.

Individual behaviour is largely influenced by the incentive structure consequent to the institutional structure (Dhesi, 1998). So it is required to inspect the expectations of benefits associated and factors influencing decision regarding college selection. These private engineering colleges lack behind from their government counterparts, in terms of number of applications. As a consequence to get their seats filled on time with good quality stuff, these private engineering colleges employ a miscellany of promotional tools to communicate and beguile the potential students and other prospects like family, relatives and many more. Thus the objective of the study is to understand the role of promotional tools in the selection of private engineering education with special reference to Delhi NCR.

1.1. Statement of the Problem

In the past couple of decades, India has remarkably advanced in the field of engineering and technical education. Engineering has contributed significantly in the growth of the nation and has improved the living standards of the masses contributing to the country's economical development. There has been a significant increase in the number of colleges and with it has increased competition.

Due to intense competition prevailing among these private engineering colleges, past several years have seen a tremendous growth in college marketing through the media (Ming, 2010). Both traditional (print) as well as modern (electronic) media, in form of newspaper and magazine advertisements, advertisements on billboards on roads and important buildings, advertisements on the display panel of some important events like cricket, hockey or other sports events, advertisements in metro train coaches, shopping malls, cinema halls and other available spaces have been beleaguered by all possible advertisements mediums. Hefty budgets are allotted to these advertising campaigns in order to grab the attention of the potential consumers. In the initial years of set up of these private colleges, heavy budgets were limited to advertisements both traditional and electronic but it was observed (Kitchen, 2003) that the marketing budgets had moved from mass media and traditional advertising to more direct consumer and trade promotions.

The current study therefore is based on the objective to investigate advertising as an influential factor in the choice of private engineering college in Delhi NCR. There are 260 private engineering colleges in Delhi NCR with the total enrolment of 156000 as per 2014-15 and for the purpose of study 4040 students in their first year are considered as respondents. First year Bachelor in Technology (B. Tech) students were considered for study under the assumption that they had gone through this process and it must be fresh to recollect the answers. The above assumptions were used to obtain the accurate result.

1.2. Purpose of Study

The purpose of the study was to determine the impact of promotional tools on the choice of private engineering college in Delhi NCR. The trends in the past are a witness to increase in enrolment which indicates that there are factors behind increase in enrolment that will help the concerned stakeholders.

1.3.Objectives of the Study

The objectives of the study were:

- a. To understand the demographic profile of the respondents opting for private engineering college
- b. To study the impact of promotional tools used by college to communicate with the potential stakeholders in selection of a college.

1.4. Significance of the Study

Since the research was concerned with engineering students pursuing their bachelor degree and the setting of the study was in Delhi NCR, it would be beneficial to the following viz.:

- a. Management of the college would benefit from the study as they will get an idea as to what are the tools influencing students decision-making so that they are able to utilise the resources (monetary as well as non-monetary) in the best possible manner.
- b. Stakeholders will also benefit from the study as there will be clarity in information.
- c. The study will be of help to the marketing department as they can lay more emphasis on those tools which are having more influence as compared to those that have less influence, thus saving the expenses also.

2. Literature Review

2.1.Marketing of Education

Marketing of education started way back in 1990s but with an increase in the competition most educational institutions, especially private have fiercely got into the arena of intensive marketing. In the competitive environment in which higher education institutions operate, enhanced customer satisfaction may be one of the ways in which institutions can create and sustain a competitive advantage. This can be achieved with effective application of the marketing mix elements.

Kotler and Armstrong (2006) provided the following marketing model: (a) Understanding the marketplace and customer needs and wants; (b) Design a customer-driven marketing strategy; (c) Construct a marketing program that delivers superior value; (d) Build profitable relationships and create customer delight; and (e) Capture value from customers to create profits and customer quality. This study focused on the need to understand the marketplace, more specifically the variables students use to choose to attend a small, Midwest private college. Research in the areas of college choice, academic major, and market conditions was used to provide the theoretical framework and aid in determining the variables that were used in this study.

2.2.Students Choice and Decision-making Process

Every person is constantly affected by a complex totality of social relations. A number of authors in various fields of science (psychology, sociology, economics) emphasize why the school-leaver views the studies as an investment into the future, what expectations drive the school-leaver to choose studies granting status in the society, what is the impact of the environment.

Student college choice is defined as “a complex, multistage process during which an individual develops aspirations to continue formal education beyond high school, followed later by a decision to attend a specific college, university or institution of advanced vocational training” (Hossler, Braxton & Coopersmith, 1989)

Research studies on college choice have primarily been categorized according to four models of college choice (Hossler et al., 1989): econometrics, sociological, consumer and combined. The econometrics model is derived from the human capital theory (Schultz, 1963; Thurow, 1972), which views college choice as a result of an

investment decision in the hopes of a higher rate of return on future earning and social capital. The sociological model focuses on the factors of socioeconomic status and personal predispositions, such as family background, parental education, educational aspirations, and preparation for attaining a higher socioeconomic status (Jackson, 1982; Litten, 1982). The consumer model views college choice as a value added, decision-making process. This model considers the cost and risk of alternatives of attending college and which college will provide the most benefits (Kotler, 1995).

The combined model takes a multi-stage and multi-discipline approach rather than a single decision-making process (Hossler, Braxton, & Coopersmith, 1989), which includes predispositions, search and choice. McDonough, Antonio, Walpole, and Perez (1998) used education, business, marketing and economic theories to examine the college choice process. Chapman (1981) suggested that student college choice is influenced by a set of student characteristics (level of educational aspiration, high school performance, socioeconomic status and aptitude) combined with a series of external influences (influences of significant people, general characteristics of an institution, and an institution's effort to communicate with prospective students). Research by Jackson (1982) concluded that economic variables, such as future income and costs associated with attending college, impacts the college choice process more than social factors. A recent conceptual model proposed by Perna (2006) assumes that an individual's college-choice decisions are shaped by four contextual layers: (1) the individual's habitus; (2) school and community context; (3) the higher education context; and (4) the broader social, economic, and policy context.

It is not easy to understand the pupil's decision-making process because it process encompasses plenty of factors which affect the school-leaver at one time. This paper will present groups of factors affecting the school-leaver's choice of studies.

2.3.Factors Influencing choice of College

In the late 1970s and early 1980s, colleges were faced with a declining pool of traditional age college students, increased competition, growing demand for state and federal financial aid and a decline in public confidence concerning the value of higher education (Hossler, Braxton, & Coopersmith, 1989). These factors resulted in an increased focus on college choice in higher education research. Research on student choice of a college is diverse in both methodology and focus. Studies on college choice tend to focus on several broad categories: (a) students' predispositions, such as high school GPA, socioeconomic status, parental income, educational aspiration, and others (Alba & Lavin, 1981); (b) institutional attributes, such as geographic location, distance from home, size, program of study (Chapman, 1981); and (c) economic factors, such as financial aid, tuition, career services (Welki & Navartil, 1987).

(Hooley and Lynch, 1981) conducted a study on the selection process of a university by students with high prospects in the higher institutions of United Kingdom and came across the following influential factors viz.: appropriateness of study program, location of university, academic reputation, distance/ proximity from home, type of university and advice from parents and teachers

(Krampf and Heinlein, 1981) are among the first to pursue research on marketing the university among prospective students at the university in United States. Using the factor analysis method, the study found that respondents gave high importance to the following factors viz.: attractive campus atmosphere, informative visit to the campus, influence of family members, field of studies that are comprehensive and attractive, distance/ Proximity from home and a peaceful study environment

There are numerous factors that students consider when determining their preference for a particular university (Soutar and Turner, 2002), including: type of course, academic reputation of the institution, atmosphere inside the campus, quality of teaching staff and type of university.

Other than the above stated factors, there are other personal factors like proximity to home, access to public transport, availability of parking space, influence of family members and peer groups.

(Maringe, 2006) conducted a study on Southampton students regarding the dominant factors affecting the decision-making for selection of a particular university among the respondents and the findings stated the influential factors in terms of percentage. Most influential factor was type of study program (7.8%) followed by price value in terms of fees and flexibility in payment (7.5%), location (6.2%), reputation of the university and website of the university (6.1%), promotional/ marketing communication tools (4.8%), corporate literature and exhibition material (4.6%) and the last was alumni and counsellors (4.5%).

(G. Sudha & D. Ashok, 2012) questionnaire was circulated among public relations officers/ administrative officers/ principals of 50 schools, colleges, industrial training institutes and management institutes in and around Vellore, Karnataka to study the factors influencing marketing communication related to six important aspects, viz.: age of institutions, ownership of institutions, intake of students, frequency of advertisements, nature of media and quantum of money spent. Data analysis tools like percentage analysis, chi square test and weighted average method was used to derive to the following conclusion: 70% of the institutions are using only “print media” and 30% are using other broadcasting media like television and radio commercials; 45% of the institutions participated in inter and intra institutional activities; 50% of the institutions used these marketing communication tools to achieve their goals i.e. to get their seats filled to the maximum capacity and 53.33% respondents admitted that integration of old and new system harmoniously is a major challenge along with others like financial constraints and continuity and consistency in the usage. With the help of chi-square test at (0.05 level of significance) there was no significant relationship between age of the institution and frequency of advertisement, intake capacity, turnover of the institution, quantum of money spend on promotional activities and nature of media chosen, Along with other conclusions like there was no significant relationship between ownership of the institution and frequency of advertisement as well as on quantum of money spend on promotional activities.

(K.Usha & Sheena, 2015) Management of the college uses email moderately (mean 4.00 ± 0.63) but students found to give low importance to these emails in the selection criteria. Also it is found that students consider employees, faculties and existing students of college and their recommendation as very important factor in the college choice decision but management occasionally uses (mean 2.83 ± 1.83) this as the promotional tool. College website (mean 5.00 ± 0.00) and social media (mean 4.17 ± 0.41) are highly used by management as a promotional tool but students gave neutral opinion (mean 3.26 ± 1.20 and 2.95 ± 1.33) to both these tools in making decision and overall management gives moderate importance for publicity and promotion (mean 3.50 ± 0.44) but students give low importance (mean 2.87 ± 0.81) to these promotional tools.

3. Research Methodology

The current study is a part of a bigger study conducted on promotional tools in education institutions. The objective of the study is to understand the influence of marketing factors in choice of private engineering college in Delhi NCR. The data was collected using survey method and it was distributed in the private engineering colleges in Delhi NCR comprising of NCT of Delhi, parts of Uttar Pradesh (Ghaziabad, Noida, Greater Noida), parts of Haryana (Faridabad and Gurgaon) and parts of Rajasthan (Alwar).

Stratified random sampling method was executed to ensure sufficient, balanced and unbiased data collection. The instrument used in the study was a structured questionnaire, developed on the basis of past research and concentrated on the demographic profile of the students as well as promotional tools as an influential factor comprising of major tools. These tools/ factors were print advertisements, digital advertisements, press release, counselling sessions, direct conversation with institute representatives, fees waiver and free laptops and institutes websites.

4. Analysis and Discussion

4.1. Demographic Profile of respondents

The (table. 1) below depicts that majority of respondents belonged to the age group of 17 to 19 years, 72.7% respondents were male and 27.3% were female respondents. Major portion comprising of 46.3% respondents hailed from Delhi NCR and Uttar Pradesh and Bihar were the states from where 28.2% and 11.8% respondents migrated to pursue their engineering education respectively and 91.7% respondents used Hindi as their mother tongue. 67.8% respondents scored more than 70% in their twelfth standard, 99.1% respondents attended English medium school and 78.2% respondents attended private schools as compared to 17.9% respondents attending government school.

(Table 1.) Demographic profile of respondents

Particulars		Frequency	Percentage (in%)
Age of respondents	< 17 years	61	1.7
	>= 17 years to < 18 years	1511	41.5
	>= 18 years to < 19 years	1856	51
	>= 19 years to < 20 years	209	5.7
	>= 20 years	3	0.1
Gender	Male	2646	72.7
	Female	994	27.3
Hometown	Delhi NCR	1685	46.3
	Uttar Pradesh	1027	28.2
	Bihar	429	11.8
	West Bengal	83	2.3
	Haryana	167	4.6
	Punjab	33	0.9
	Rajasthan	48	1.3
	Any North-eastern State	7	0.2
	Any South Indian State	46	1.3
	Any other State or Union Territory	115	3.2
Mother Tongue	Hindi	3338	91.7
	English	6	0.2
	Any other	296	8.1
Management of previous school attended	Private	2847	78.2
	Government	651	17.9
	Not sure	142	3.9
Marks scored in twelfth	Less than 49%	1	.0
	50- 59%	87	2.4
	60-69%	1083	29.8
	70-79%	2112	58
	80% and above	357	9.8
Medium of previous school attended	Hindi	32	0.9
	English	3608	99.1

(Source: Compilation by author based on a survey)

4.2. Respondents college preference

67.9% respondents considered management of the college as an important factor of which 47.8% preferred government aided college as compared to 20% respondents whose first choice was private college. IIT Delhi ranked first among other institutes with 49.7% preferring it over the others followed by other IITs (32.8%). The most sought after discipline among the respondents were Information Technology followed by Environmental Engineering opted by 22.4% and 17.6% respondents respectively. 82% respondents preferred IIT Delhi on the basis of institutions rank followed by good infrastructure (3.6%), 3.2% respondents preferred a large variety of

courses offered, 2.4% preferred the above institutions due to visibility of its advertisement in various media, 2% preferred because of good faculty, 1.4% preferred the above institution due to memorandum of understanding or other collaborations with world class universities, 0.9% preferred the above institution because of institution's publicity through news and newspapers others being college popularity in social media and information provided at counselling sessions.

(Table 2.) Respondents college preference

Particulars		Frequency	Percentage (in %)
Institute's Management as an important factor	Yes	2472	67.9
	No	1168	32.1
Institute's management preferred	Private	728	20
	Government	1739	47.8
	Management did not matter	1173	32.2
Top Institute preferred	IIT Delhi	1810	49.7
	Other IITs	1194	32.8
	NIT Delhi	216	5.9
	Other NITs	96	2.6
	BITS (Pilani, Hyderabad & Goa)	106	2.9
	Other government-aided institute	88	2.4
	Other private institutes	70	1.9
	Current institute	60	1.6
Reason for preferring the above institute	Ranking of the institute	2989	82.1
	Information provided at counselling sessions	13	0.4
	College popularity on social media	20	0.5
	Best faculty	73	2
	Good infrastructure	132	3.6
	Collaboration with foreign universities	52	1.4
	Variety of courses	118	3.2
	Advertisement in various media	89	2.4
	Institutes work or events always in news	32	0.9
	Institutes website	119	3.3
	Any other	3	0.1
Preferred discipline	Computer Science	511	14
	Environmental Engineering	642	17.6
	Information Technology	817	22.4

	Electrical Engineering	475	13
	Polymer Technology	417	11.5
	Mechanical Engineering	272	7.5
	Electrical & Instrumental Engineering	287	7.9
	Civil Engineering	118	3.2
	Automobile Engineering	60	1.6
	Automotive Engineering	33	0.9
	Chemical Technology	4	0.1
	Any other	4	0.1

(Source: Authors compilation based on survey)

4.3.Factors Influencing choice of college

4.3.1. Promotional Tools effect on choice of college

The promotional tools effecting choice of college were identified based on previous research and current trends as print advertisements, digital advertisements, press release, counselling sessions, direct conversation with institute representatives, fees waiver and free laptops and institutes websites.

(Table 3. Promotional Tools influencing choice of college)

Promotional Tools	Mean	Standard Deviation
Print Advertisement	3.97	0.81
Digital Advertisement	3.89	0.75
Press release	3.95	0.75
Counselling sessions	4.27	0.71
Direct conversation with institutes representative	4.01	0.73
Monetary incentives like fees waiver and free laptops	4.06	0.76
Institutes websites	4.06	0.73

(Source: Authors compilation based on a survey)

The popular influential factor was counselling sessions with the score of (mean 4.27 ± 0.71), followed by monetary incentives (like fees waiver and free laptops) (mean 4.06 ± 0.76), institute websites (mean 4.06 ± 0.73), print advertisements (mean 3.97 ± 0.81), press release (mean 3.95 ± 0.75) and digital advertisement (mean 3.89 ± 0.75).

Pearson correlation was carried out on all the internal/ institutional, external and marketing factors generated positive and modest results. These findings were in synchronisation with the earlier findings score of mean and standard deviations.

4.3.2. Other factors effect on choice of college

(Table 4) below depicts other factors influencing the choice of private college.

(Table 4.) Other factors influencing choice of college

Influential Factors	Mean	Standard Deviation
Vicinity to hometown	3.68	0.82
Location advantage	2.99	0.63
Fees structure	4.04	0.59
Hostel facility	3.27	0.59
International collaboration	2.46	0.59
Past placement	4.69	0.53
Overseas placement	1.62	0.55
Reputation of the institute	4.12	0.76
Variety of courses available	2.03	0.59
Student faculty ratio	1.93	0.50
Good infrastructure	4.08	0.70
Educational background of faculty	1.73	0.62
Father	4.14	0.80
Mother	2.37	0.59
Siblings	1.64	0.86
Friends/ Peer Group	3.87	0.84
Coaching Institute	1.97	0.72
Relatives	2.33	0.72
Alumni	3.21	1.97

(Source: Authors compilation based on a survey)

The most popular institutional/ internal factor was past placement record (mean 4.62 ± 0.53) followed by reputation of institute (mean 4.12 ± 0.76) and father (mean 4.14 ± 0.80) preceding factors are good infrastructure (mean 4.08 ± 0.70), fees structure (mean 4.04 ± 0.59), friends/ peer group (mean 3.87 ± 0.84), vicinity to hometown (mean 3.68 ± 0.82), hostel facility (mean 3.27 ± 0.59), alumni (mean 3.21 ± 1.97), location advantage (mean 2.99 ± 0.63), international collaboration (mean 2.46 ± 0.59), influence of mother (mean 2.37 ± 0.59) and relatives (mean 2.33 ± 0.72), variety of courses available (mean 2.03 ± 0.59). The least popular factors were influence of coaching institute (mean 1.97 ± 0.72), student-faculty ratio (mean 1.93 ± 0.50), educational background of faculty (mean 1.73 ± 0.62), siblings influence (mean 1.64 ± 0.86) and overseas placement (mean 1.62 ± 0.55).

5. Recommendations and Conclusion

Government colleges were the preferred choice of the respondents surveyed. But private colleges need not be disheartened that students prefer government colleges over private ones because their still subsist a substantial

fragment of students preferring private colleges. Reputation of academic strength can be maintained if more stress is laid on the quality of faculty, pedagogy and fees structure.

The study also revealed that there was enormous influence of father in the decision making regarding the choice of private college. Institutions should frequently interact with the present family members of the current students as it will develop faith and would thus carry positive word of mouth in the society.

Promotional tools like print advertisements, press release and digital advertisements were rated higher than other counterparts thus inflicting the importance of promotional tools in influencing the decision of selection of private college. This implies that promotional tools are dominant medium that can be used by private colleges to attract potential students. The private engineering colleges should review, reformulate and communicate their marketing strategies in synchronization with the demand of the market in order to maximize the impact of the factors on students decision making.

6. References

- G. Sudha & D. Ashok (2012), Factors influencing marketing communication in service sector: A study on educational institutions in Vellore, *International Journal of Marketing, Financial Services & Management Research*, Vol.1 Issue 10, pp 171- 185
- Hooley, G.J. and Lynch, J.E. (1981), Modelling the student university choice process through the use of conjoint measurement techniques, *European Research*, Vol. 9 (4), pp. 158-170.
- Hossler, D., Braxton. J., and Coopersmith, G. (1989). Understanding student college choice. *Higher Education Handbook of Theory and Research*, 5, 231-288
- Hossler, D., and Gallagher, K. (1987). Studying student college choice: A three-phase model and the implications for policymakers. *College and University*, 62, 207-221
- Kitchen, P.J. (2003). Critical times; an integrated marketing communication perspective. Paper presented at the First International Conference on Business Economics, Management and Marketing, Athens.
- Kotler, P. and Keller, K. L. (2009), *Marketing Management*, 13th edition. New jersey: Pearson Education, Inc.
- Krampf, R.F. and Heinlein, A.C. (1981), Developing Marketing Strategies and Tactics in Higher Education Through Target Market Research, *Decision Sciences*, Vol 12 (2), pp. 175-193.
- Maringe, F. (2006), University and course choice, Implications for positioning, recruitment and marketing, *International Journal of Educational Management*, Vol. 20 (6), pp. 466-479.
- Ming, J. S. K. (2010). Institutional Factors Influencing Students' College Choice Decision in Malaysia: A Conceptual Framework. *International Journal of Business and Social Science* Vol. 1 No. 3 pp.53-58.
- Sheena & Usha. (2015), Implication of Branding Initiatives in engineering colleges -An empirical study. *IOSR Journal of Business and Management (IOSR-JBM)*, Volume 17, Issue 11 .Ver. I (Nov. 2015), pp 04-11
- Soutar, G.N. and Turner, J.P.(2002), Students' preferences for university: a conjoint analysis, *The International Journal of Educational Management*, Vol 16 (1), pp. 40-45.

Authors Profile

Dr. (Mrs.) Seema Singh

The author is Associate Professor in Economics and Head of the Department of Humanities, Delhi Technological University since 2006. Largely, interested in issues related to gender, engineering education, employment and labour market, she has published and presented number of papers in journals and seminars & conferences. She has completed successfully several research projects sponsored by national organisations and international organisations. She received All India Council for Technical Education (AICTE) Career Award for Young Teacher in 2000. She has penned text book entitled, "Economics for Engineering Students" (2009 and 2014) and edited book entitled, "Women and Work: Changing Scenario in India" with Prof. Alakh Sharma in 1992. She is editor of MS 93- Management of New and Small Enterprises, IGNOU, Delhi, paper reviewer of the Journal of Business and Economics, USA, Academic Star Publishing Company, ISSN: 2155-7950 and member of the editorial board of the International Journal of Humanities and Social Sciences (IJHSS). She is Convenor of the publication Committee of the University Women Association of Delhi in 2014, Joint Secretary of the Indian Society of Labour Economics since 2006 and Vice-President of the Women in Science & Engineering (WISE)-India since 2011.

Antra Singh

The author is currently pursuing PhD in Department of Humanities, Delhi Technological University under the supervision of Dr. (Mrs.) Seema Singh. She has published and presented numerous papers in journals, seminars and conferences. The author also has experience of corporate and academics in teaching marketing and economics subjects.

Mathematical modeling insight of hetero gate dielectric-dual material gate-GAA-tunnel FET for VLSI/analog applications

Jaya Madan¹ · R. S. Gupta² · Rishu Chaujar¹

Received: 26 August 2015 / Accepted: 2 February 2016
© Springer-Verlag Berlin Heidelberg 2016

Abstract This paper presents a mathematical modeling insight for the novel heterogate dielectric-dual material gate-GAA TFET (HD-DMG-GAA-TFET) and validating the results with TCAD simulation. By using the appropriate boundary conditions and continuity equations, the Poisson's equation is solved to obtain the potential profile. The developed model is used to study the analog performance parameters such as subthreshold swing (SS), threshold voltage (V_{th}), transconductance (g_m), drain conductance (g_d), device efficiency (g_m/I_{ds}), intrinsic gain (g_m/g_d), channel resistance (R_{ch}) and output resistance (R_o). Further, to optimize the effect of metal work function on analog performance, three different combinations of DMG configurations has been studied. The results demonstrated that for a difference of 0.4 eV, the analog performance of the device is optimized. Low off current and high value of on current resulting into a higher I_{ON}/I_{OFF} ratio has been obtained, which is appropriate for sub-nanometre devices and low standby power applications. The analytical results obtained from the proposed model shows good agreement with the simulated results obtained with the ATLAS device simulator.

1 Introduction

Continuously scaling down the MOSFETs dimensions to sub-nanometer region lead to escalation in the power consumption (active and passive) in modern microelectronic circuits. Reducing the applied bias (according to the scaling factor) to solve this dilemma leads to reduction in gate overdrive. Along with higher power density, the fundamental limit of kT/q (due to thermal process) which corresponds to a subthreshold swing (SS) of 60 mV/dec also hindered further scaling of threshold voltage (V_{th}) and off current. To overcome these limitations, there is a renewed interest in exploring new devices that uses a new current mechanism, and that does not involve carriers traveling over a potential barrier. Among various new devices Tunnel FET has been studied extensively in the past few years. TFET uses BTBT mechanism at the tunneling junction (the source channel junction) and normal drift diffusion mechanism away from the tunneling junction (Cho et al. 2011).

TFET has the potential to lower the SS beyond the 60 mV/dec limit of conventional MOSFETs along with the extremely low OFF-current. Therefore, TFET seems to be a well adaptive candidate for ultimately scaled switches and low power devices with excellent immunity to short channel effects (SCEs) (Bhuwalka et al. 2006; Born et al. 2006; Nirschl et al. 2006; Mookerjee et al. 2009). The major roadblock with the planar TFETs is its lower ON-state current (I_{ON}), which results in lower operating speed. In order to resolve this issue, numerous kinds of TFETs with various structures and materials such as double-gate, delta layer, SiGe, and PNP structures have been proposed (Toh et al. 2007; Boucart and Ionescu 2007a, b; Toh et al. 2008; Malik and Chattopadhyay 2011; Jhaveri et al. 2010; Cho et al. 2011; Lee et al. 2010; Noguchi et al. 2015). To enhance the I_{ON} , Silicon nanowire TFET has already been fabricated

✉ Rishu Chaujar
rishu.phy@dce.edu

Jaya Madan
jayamadan.2012@gmail.com

R. S. Gupta
rsgupta1943@gmail.com

¹ Microelectronics Research Lab, Department of Engineering Physics, Delhi Technological University, Bawana Road, Delhi 110042, India

² Maharaja Agrasen Institute of Technology, Rohini, Delhi 110086, India

(Gandhi et al. 2011). Further, a high-k material has been locally inserted (near the source side) in the gate dielectric to form heterogate-dielectric (HD) TFETs (Choi and Lee 2010; Mallik and Chattopadhyay 2011). The presence of high-k dielectric results into a higher band bending due to increase in surface potential (at a constant gate bias) (Jha-vari et al. 2010; Lee et al. 2012; Madan et al. 2015a, b). This higher band bending leads to reduction in tunneling barrier width, which further increases the generation rate and hence the I_{ON} .

Another major problem with TFET is ambipolarity. The ambipolarity in the device is the conduction for both high positive and high negative V_{gs} while keeping the V_{DS} only in one direction (negative for p-type devices and positive for n-type devices) (Cho et al. 2011; Conde et al. 2014; Hraziia et al. 2012; Lee et al. 2010; Shaker et al. 2015). Ambipolarity can be reduced by using a HD structure, in which the gate dielectric is split into two regions; high-k dielectric near the source side and low-k dielectric near the drain side. The higher value of dielectric improves the electrical coupling between the gate and the tunneling junction and hence, increases the tunneling rate. The DMG further helps in the improvement of ON and OFF current characteristics. Lower work function metal near the source side increases the band overlap and hence reduces the tunneling barrier width. This reduced tunneling barrier increases the tunneling probability, and the generation rate which results in higher I_{ON} and the higher value of work function near the drain side increases the tunneling barrier width and hence helps in reducing the I_{OFF} . So an optimum value of metal work function value at source and drain side should be chosen to trade-off between ON and OFF characteristics. In this work, a heterogate dielectric, Dual material gate, gate-all around (GAA) structure has been applied to TFET to enhance analog performance of the device (Madan et al. 2014).

The paper is structured as follows: Sect. 2 describes the device structure, parameters and simulation models used in this work, Sect. 3 describes the model formulation for the device Sect. 4 describes the results verification and discussions in which the effect of DMG configuration on the analog performance of the device has been studied. Finally, the conclusions are drawn in Sect. 5.

2 Device structure, parameters and simulation models

The device structural parameters used in both simulations and analytical model are fixed: channel length is 50 nm, with L_1 (20 nm) and L_2 (30 nm), gate oxide thickness (t_{ox}) = 3 nm and radius (R) = 10 nm. Further, the source (p+), drain (n+) and channel doping (p) are 10^{20} , 5×10^{18} and 10^{16} cm^{-3} respectively. To reduce ambipolarity effect

source and drain are doped asymmetrically. In this analysis the analog performance is studied for the three different cases of DMG scheme to optimize the device for better analog performance and the cases are as stated below.

Case 1. $\Phi_{M1} = 4.1 \text{ eV}$ and $\Phi_{M2} = 4.8 \text{ eV}$

Case 2. $\Phi_{M1} = 4.3 \text{ eV}$ and $\Phi_{M2} = 4.8 \text{ eV}$

Case 3. $\Phi_{M1} = 4.4 \text{ eV}$ and $\Phi_{M2} = 4.8 \text{ eV}$

Region 1 consists of dielectric constant $\epsilon_1 = 21 \text{ HfO}_2$ (near the source) and region 2 consists of $\epsilon_2 = 3.9 \text{ SiO}_2$ (near the drain) for all the cases. The source and drain junctions are abruptly doped for an effective band to band tunneling and the interface of high-k and SiO_2 is abrupt. The simulation device structure i.e. HD-DMG-GAA-TFET consisting of heterogate dielectric and Dual material gate is shown in Fig. 1. All simulations have been performed using the ATLAS device simulator. The most important model for TFET simulations is the band-to-band tunneling (BTBT) model. Non-local models have a more physical basis and don't depend on the electric field at the individual mesh points in the simulated device structure, but rather on band diagrams calculated along cross-sections through the device. According to BBT.NONLOCAL, the tunneling happens through the 1D slice, at the tunnel junction, where each slice and the tunnel junction are perpendicular to each other. These slices are parallel to themselves. For nonlocal BTBT model, the quantum tunneling meshing has been used at the source-channel junction. In n-TFET, the electrons tunnel through the valence band of the source to conduction band of the channel by BTBT mechanism and then the carriers drift from channel to drain. Thus, to incorporate the transport away from the tunneling junction drift diffusion model is used (Boucart and Ionescu 2007a, b). The bandgap narrowing model is used in the simulations to incorporate the effect of heavily doped source and drain regions (as tunneling current is a sturdy function of bandgap). Instead of Boltzmann statistics, Fermi–Dirac statistics have been used for the same reason (heavily source and drain doping). The models activated during simulation

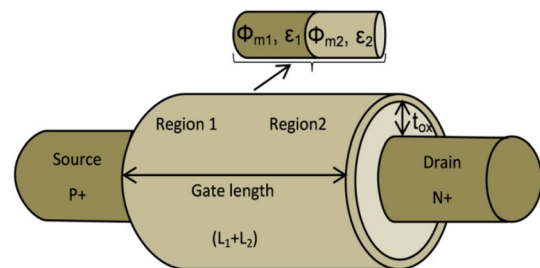


Fig. 1 Structure of n-type heterogate dielectric-dual material gate-all around-tunnel FET (HD-DMG-GAA-TFET)

Table 1 Model parameters used in simulation

Physical model	Parameter	Value
Shockley–Read–Hall for carrier recombination (SRH)	TAUN0	1.0×10^{-7} s
	TAUP0	1.0×10^{-7} s
Bandgap narrowing (BGN)	BGN.E	6.92×10^{-3} V
	BGN.N	1.3×10^{17} cm ⁻³
Nonlocal band to band tunneling model (BBT. NONLOCAL)	BB.A	4.0×10^{14} V ⁻² s ⁻¹ cm ⁻¹
	BB.B	1.9×10^7 V cm ⁻¹
	γ	2

are as follows: concentration and field dependent mobility model, Shockley–Read–Hall for carrier recombination, non-local band to band tunneling, band gap narrowing, Fermi–Dirac statistics and drift diffusion (Fukuda et al. 2013; Atlas User’s Manual 2014). The parameters used in simulation along with their values are listed in Table 1.

3 Model formulation for HD-DMG-GAA-TFET

Assuming that the influence of the charge carrier and fixed carriers are uniform in the channel, it can be neglected. The parabolic potential profile along the radial direction is assumed and based on the following boundary conditions, the Poisson’s equation is solved.

1. The surface potential is only z-dependent

$$\Phi_{si}(R, z) = \Phi_{si}(z) \quad (1)$$

2. The Electric field at the center of the channel is zero

$$\left. \frac{d\Phi_{si}(r, z)}{dr} \right|_{r=0} = 0 \quad (2)$$

3. Electric field at Si/SiO₂ interface is continuous

$$\left. \frac{d\Phi_{si}(r, z)}{dr} \right|_{r=R} = \frac{C_{fi}}{\epsilon_{si}} [V_{GS} - \Phi_{si}(z) - V_{FBi}] \quad (3)$$

where; $V_{FBi} = \phi_{mi} - \phi_s$ is the flatband voltage. i = 1 and 2 for region 1 and 2 respectively and ϕ_s is the semiconductor work function.

$$\phi_s = \chi_{si} + E_g/2q + \phi_F \quad (4)$$

and $\phi_F = k_B T / q (\ln(N_{Ch}/n_i))$ is the fermi potential. Where the parameters, symbols and their values are as listed in Table 2.

C_{f1} and C_{f2} are the capacitances per unit area of the gate dielectric for region 1 and 2 respectively and are given by

$$C_{f1} = \frac{\epsilon_1}{R \ln(1 + \frac{t_1}{R})} \text{ and } C_{f2} = \frac{\epsilon_2}{R \ln(1 + \frac{t_2}{R})} \quad (5)$$

Table 2 List of constant parameters

Parameters	Symbol	Value and unit
Electron affinity	χ_{si}	4.17 eV
Permittivity of silicon	ϵ_{Si}	11.8
Bandgap of silicon	E_g	1.08 eV
Temperature	T	300 K
Boltzmann constant	k_B	1.38066×10^{-23} J K ⁻¹
Elementary charge	q	1.60219×10^{-19} C
Plank’s constant	h	6.63×10^{-34} J s

where $t_1 = t_2 = t_{ox}$, is the gate oxide thickness.

Solving Eqs. (1)–(5) we can obtain

$$\frac{\partial^2 \Phi_{si}(z)}{\partial z^2} - k_i^2 \Phi_{si}(z) = \eta_i \quad (6)$$

The general solution of (6) is

$$\Phi_{si}(z) = A_x \exp(k_i z) + A_y \exp(-k_i z) - \eta_i / k_i^2 \quad (7)$$

$$\text{where } k_i^2 = \frac{2C_{fi}}{R\epsilon_{Si}} \text{ and } \eta_i = \frac{qN_i}{\epsilon_{Si}} - k_i^2 [V_{gs} - V_{FBi}]$$

Now using the following boundary conditions at the interface of each region, coefficients A_x and A_y can be determined.

At the source end

$$\Phi_{s1}(0) = -\frac{k_B T}{q} \ln \left(\frac{N_{source}}{n_i} \right) = V_{bi1} \quad (8a)$$

And at the drain end

$$\Phi_{s2}(L_g) = \frac{k_B T}{q} \ln \left(\frac{N_{Drain}}{n_i} \right) + V_{DS} = V_{bi2} + V_{DS} \quad (8b)$$

At the interface of region 1 and region 2,

$$\Phi_{s1}(L_1) = \Phi_{s2}(L_1) \quad (8c)$$

$$\left. \frac{d\Phi_{s1}}{dz} \right|_{z=L_1} = \left. \frac{d\Phi_{s2}}{dz} \right|_{z=L_1} \quad (8d)$$

The lateral electric field (2D) is given by

$$E_z(r, z) = -\frac{d\Phi_{si}(r, z)}{dz} \quad (9)$$

The lateral surface electric field is given by

$$E_{sz}(r, z) = A_x K_1 e^{K_1 z} - A_y K_2 e^{K_2 z} \quad (10)$$

Transverse electric field (2D)

$$E_r(r, z) = 2rP_2(z) \quad (11)$$

The tunneling generation rate determined by Eq. (13) is integrated over the volume ($\pi r^2 w_T$) to obtain the drain

current. Where w_T is the tunneling barrier width defined as the shortest distance between the valence band of the source and conduction band of the channel. It is determined from the surface potential profile, by taking the difference between the points where the surface potential falls by an amount equal to E_g/q below the surface potential and where the potential is Φ_s and is calculated as:

$$w_T = \frac{1}{K_1} \left[\ln \left[\frac{\Phi_s(z) + \frac{E_g}{q} + \frac{\eta_1}{K_1^2} + \sqrt{\left(\Phi_s(z) + \frac{E_g}{q} + \frac{\eta_1}{K_1^2}\right)^2 - 4C_1C_2}}{\Phi_s(z) + \frac{\eta_1}{K_1^2} + \sqrt{\left(\Phi_s(z) + \frac{\eta_1}{K_1^2}\right)^2 - 4C_1C_2}} \right] \right] \quad (12)$$

The tunneling generation rate can be evaluated as

$$G_{BBT} = AE^\gamma e^{-B/E} \quad (13)$$

where A, B and γ are the parameters dependent on the effective mass of electron and hole.

$$A = \frac{q^2 \sqrt{2m_{\text{tunnel}}}}{h^2 \sqrt{E_g}}, B = \frac{\pi^2 E_g^{3/2} \sqrt{m_{\text{tunnel}}/2}}{qh} \text{ and } \gamma = 2 \quad (14)$$

where m_{tunnel} is the effective mass $= 0.25m_0$ and m_0 is the rest mass of an electron. The values of A (BB.A) and B (BB.B) are listed in Table 1. The average electric field E_{avg} is calculated by integrating the total electric field E_{Tot} over the barrier width w_T as:

$$E_{\text{Tot}} = \sqrt{|E_z|^2 + |E_r|^2} \text{ and } E_{\text{avg}} = \frac{\int E_{\text{Tot}} dz}{w_T} \quad (15)$$

The expression for drain current (I_{ds}) is obtained as:

$$I_{\text{ds}} = q\pi R^2 w_T G(E_{\text{avg}}) \quad (16)$$

4 Result verification and discussion

Figure 2 shows the comparison of proposed device i.e. HD-DMG-GAA-TFET with the gate all around tunnel FET as reported by Ying et al. (2014). As evident from Fig. 2 that the V_{th} of GAA-TFET is high as compared to the proposed device. Moreover, the I_{ON} of proposed device is 219 times enhanced in comparison to the GAA TFET. Both the lower V_{th} and higher drain current makes the DMG scheme beneficial for VLSI/analog applications. Therefore in this work, critical analog parameters such as transconductance g_m , output conductance g_d , early voltage V_{EA} , device efficiency g_m/I_{ds} , intrinsic gain A_v , channel resistance R_{ch} and output resistance R_{out} has been studied to analyze the effect of DMG on the device performance.

The effect of gate bias and metal work function on electric field near source and drain side is shown in

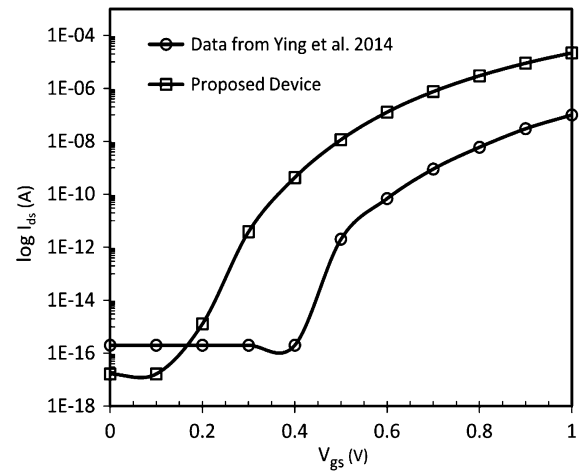


Fig. 2 Drain current–voltage comparison of proposed device HD-DMG-GAA-TFET with gate all around tunnel FET data from Ying et al. (2014)

Fig. 3a. As expected, the electric field is enhanced (near both source and drain side) with an increase in gate bias. Further, as the metal near drain side is constant; hence, the electric field near the drain is almost same for each case. With the increase in the difference in metal work function, the electric field near the source side enhances, which results in an additional lowering of barrier width and thus an increase in tunneling rate is obtained, which eventually leads to greater tunneling current and sought out the primary obstruction of TFET. Further, the SS is the amount of gate voltage required for one decade change in the drain current. In order to reduce the switching power of CMOS circuits, SS of the device should be as low as possible. Moreover, to accurately predict the circuit behavior, the V_{th} is an important parameter. The influence of metal work functions on the SS and V_{th} of the device is shown in Fig. 3b.

According to the previously reported work (Choi and Choi 2013), the I_{ON} can be enhanced by using a gate metal of lower work function near the source in comparison with metal used near drain side and to reduce the I_{OFF} , metal work function near drain should be high as compared to the metal used near the source. So in order to achieve an optimum device performance, metal near drain is kept constant ($\Phi_{\text{M2}} = 4.8$ eV) and the metal near source side is varied. As we increase the work function of metal near source side from 4.1 to 4.4 eV, the SS of the device is decreasing, but the V_{th} of the device is increasing. So the metal work function should be chosen such that the device is optimized in terms of both SS and V_{th} .

The transfer characteristics ($I_{\text{ds}}-V_{\text{gs}}$) are shown in Fig. 4a in both log scale and linear scale for each case. The graph shows the I_{OFF} of the order of 10^{-17} A and I_{ON} of the order

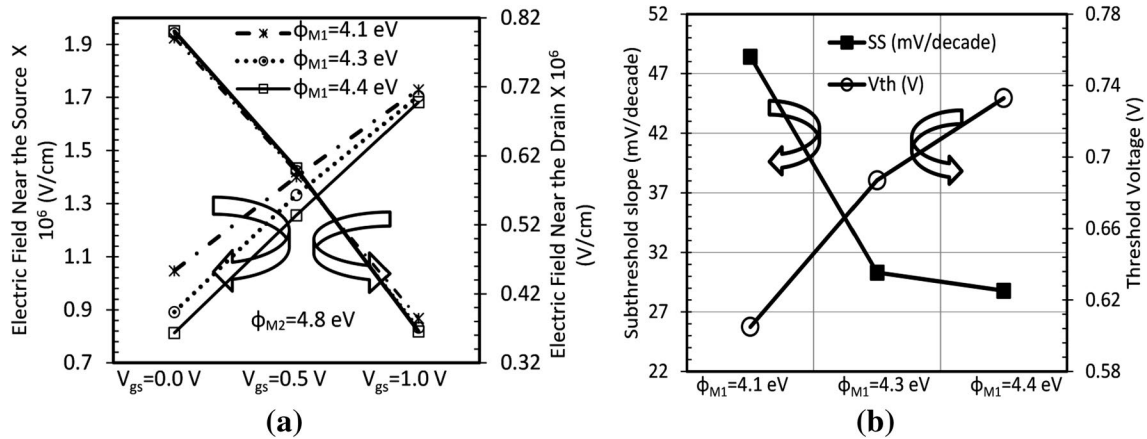


Fig. 3 **a** Electric field near source and drain side at constant $V_{ds} = 1.0$. **b** SS and V_{th} for different metal work function of HD-DMG-GAA-TFET

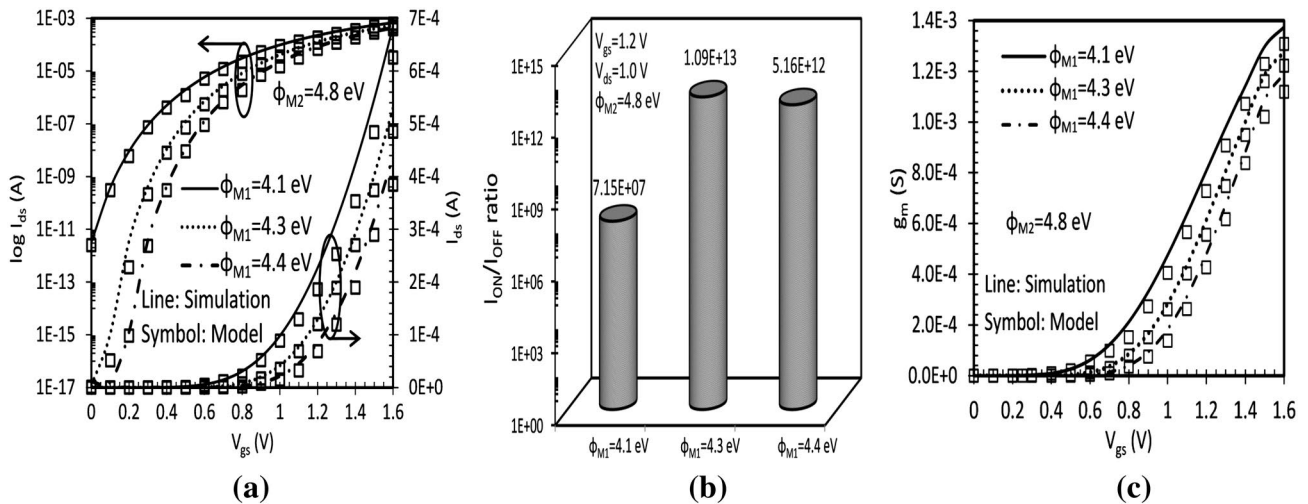


Fig. 4 **a** Transfer characteristics (I_{ds} - V_{gs}) in log and linear scale, **b** I_{ON}/I_{OFF} ratio, **c** transconductance as a function of V_{gs} for different metal work function for HD-DMG-GAA-TFET at constant $V_{ds} = 1.0$ V

of 10^{-4} A, which results in I_{OFF}/I_{ON} ratio of the order of 10^{13} . The lower value of I_{OFF} leads to a lower value of static power dissipation. Again, an increase in difference in metal work function leads to enhancement of I_{ON} by 1.5 times in case 1 as compared to case 3, but simultaneously I_{OFF} has also been increased significantly. So we need to optimize the values of metal work function to obtain an optimum value of I_{ON}/I_{OFF} ratio depending on the application. The increase in I_{ON} is the main advantage of heterogate dielectric and dual material gate. Also, it can be clearly seen from the graph that the model prediction and ATLAS device simulation are in good agreement. Figure 4b shows the variation of I_{ON}/I_{OFF} with different metal work function configurations of DMG. It is apparent from the bar graph that as work function of metal 1 increases from 4.1 to 4.3 eV the I_{ON}/I_{OFF} ratio enhances by

an order of 10^5 times. Moreover for $\phi_{M1} = 4.4$ eV, the I_{ON}/I_{OFF} ratio reduces by 0.47 times w.r.t. case 2 and increases w.r.t. case 1. The reduction in I_{ON}/I_{OFF} ratio in case 3 w.r.t. case 2 is mainly attributed to enhanced I_{OFF} as shown in Fig. 4a. Transconductance g_m , which is basically the first order derivative of the drain current with respect to the gate voltage at constant drain voltage, is shown in Fig. 4c. Transconductance decides the current driving capability of the device for a given input voltage swing. It is clear from Fig. 4c that among the three cases, the higher value of transconductance is achieved for case 1. In each case, the transconductance of the device is very much higher in the case of on state as compared to off state. So for enhanced tunneling current and transconductance, the difference of metal work function should be possibly large.

The output characteristic (I_{ds} - V_{ds}) for each case is shown in Fig. 5a. The saturation mechanism of output characteristics in the case of TFET is mainly attributed to the saturation of tunneling barrier width for higher drain bias at a constant gate bias (Boucart and Ionescu 2007a, b, Madan et al. 2015a, b). It is evident from the figure that the device predicts a qualitative agreement in linear regime and also shows a good saturation in drain current for higher drain voltages. Among the three cases, the tunneling current is enhanced by 2.7 times in case 1 with respect to case 3; thus makes it suitable for analog applications. Figure 5b illustrates the effect of DMG configurations on drain/output conductance g_d . Further, in order to achieve high gain, transistors should have low output conductance for analog applications. The output conductance is increasing with

an increase in drain bias and then attains maxima and further increase of drain bias reduces the drain conductance because of higher drain resistance at higher drain bias. As we reduce the metal work function difference, output conductance decreases, as is evident from Fig. 5b.

Figure 6a illustrates comparison of the device efficiency g_m/I_{ds} for each case. Device efficiency is the ability to convert dc power into ac gain performance at a particular drain bias. For each case, the highest value of g_m/I_{ds} is obtained for the weak inversion region and then a linear decrease is obtained with an increase in gate bias. Among the three cases, case 3 has higher device efficiency. For each case, the device efficiency has reached a value greater than 40 V^{-1} (the fundamental limit of conventional MOSFET) in the subthreshold region. Intrinsic gain is a valuable analog

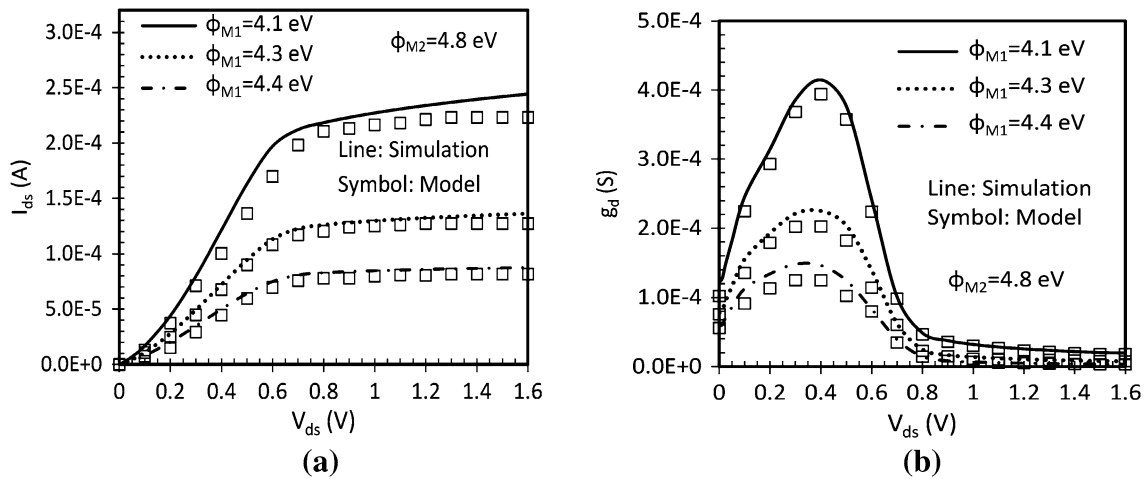


Fig. 5 **a** Output characteristics (I_{ds} - V_{ds}) and **b** output conductance for different metal work function of HD-DMG-GAA-TFET at constant $V_{gs} = 1.2 \text{ V}$

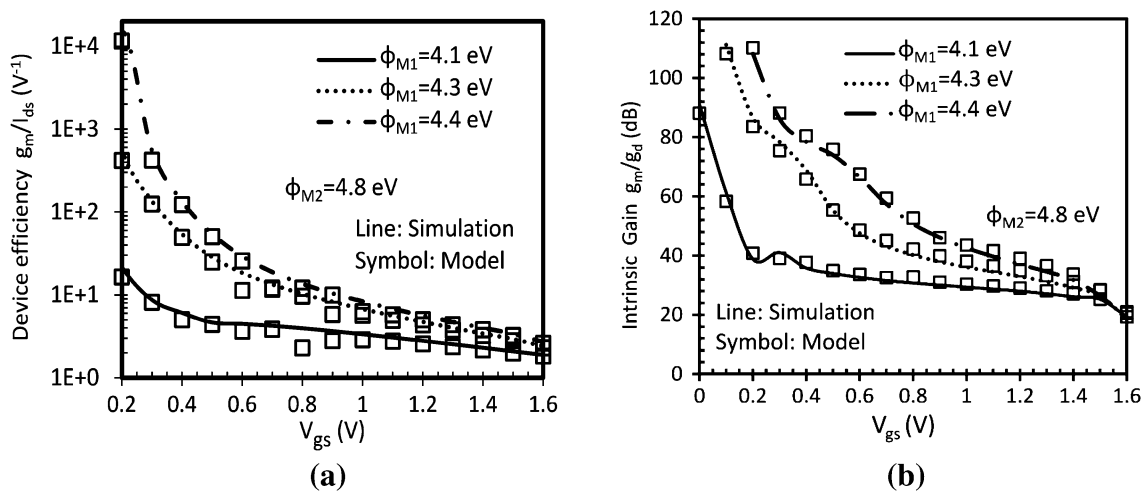


Fig. 6 **a** Device efficiency and **b** Intrinsic gain as a function of gate voltage V_{gs} for different metal work function for HD-DMG-GAA-TFET at $V_{ds} = 1.0 \text{ V}$

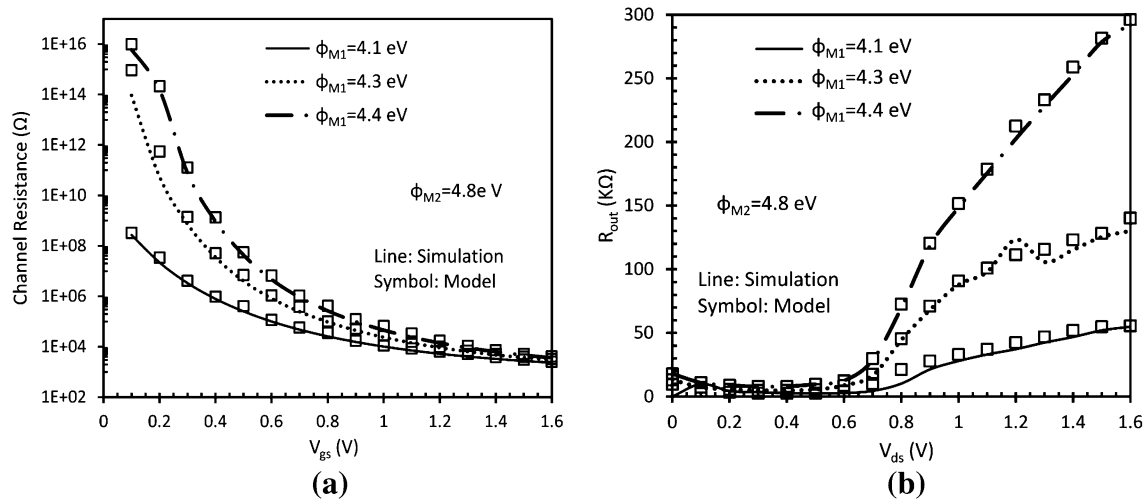


Fig. 7 **a** Channel resistance and **b** output resistance for different metal work function of HD-DMG-GAA-TFET

circuit design parameter used for designing amplifiers such as an operational transconductance amplifier (OTA). For better analog performance, an intrinsic gain of the device should be as high as possible. Comparison between of the intrinsic gain for different metal work function configuration with respect to gate bias is presented in Fig. 6b. The intrinsic voltage gain is obtained at the constant drain bias $V_{ds} = 1.0$ V, making use of the relation $A_v = g_m/g_d$. Highest intrinsic gain for a metal work function difference of 0.4 eV is attributed to the dominated decrease in output conductance in comparison with the increase in transconductance.

The influence of gate voltage and dual material gate configurations on channel resistance R_{ch} is demonstrated in Fig. 7a. For $V_{gs} = 0$ V, no band bending is there, ensuring into higher tunneling barrier width at the tunneling junction, resulting into very high R_{ch} of the order of $10^{15} \Omega$. As the gate bias increases, bands in the channel move downwards resulting in lowering of the tunneling barrier width as if a conductive channel is formed and thus drops the R_{ch} to a value of several $K\Omega$'s. Moreover, at lower gate bias, higher R_{ch} has been obtained for the case when metal work function difference is 0.4 eV, which shows a better OFF state characteristics for this configuration in comparison with the rest of the cases when the metal work function difference is 0.7 and 0.5 eV. Another important parameter for analog application is the output resistance or the drain resistance R_o . Drain resistance is numerically equal to the inverse of the output conductance. The variation of output resistance with the drain to source voltage is shown in Fig. 7b. It is clearly shown in the figure that in the linear region, the output resistance is very small, because of strong dependence of the drain current on drain voltage. But as the drain current saturates for the higher drain bias, R_o increases monotonically. It is

evident from the figure that for the case when metal work function difference is 0.4 eV, R_o is found to be extremely high due to the better output saturation current as shown in Fig. 7b.

5 Conclusion

The present work is the detailed mathematical modeling insight for the analog performance of HD-DMG-GAA-TFET. The results obtained by simulations and analytical modeling are in good agreement. The tuning of metal work functions has been done to optimize the effect of Dual metal gate on the analog performance, which shows that both device efficiency and device gain are improved for a metal work function difference of 0.4 eV. Decrease in SS and increase in V_{th} is found on decreasing the difference between work functions of two metal used near source and drain junction. Moreover, I_{OFF}/I_{ON} ratio of the order of 10^{13} has been obtained for the same DMG configuration, making it suitable for low power applications. Enhancement of channel resistance and output resistance is obtained as we decrease the difference of the metal work functions. Moreover, it has been evaluated that SS is less than 60 mV/decade in each case, and device efficiency is more than $40 V^{-1}$ in the subthreshold region. This indicates that the developed model also validates with the fact that TFET overcomes the fundamental limit of MOSFET.

Acknowledgments Authors would like to thank Microelectronics Research Lab, Department of Engineering Physics Delhi Technological University to carry out this work. One of the authors (Jaya Madan) would like to thank University Grants Commission, Govt. of India, for providing the necessary financial assistance during the course of this research work.

References

- ATLAS User's Manual (2014) SILVACO Int., Santa Clara, CA
- Bhuwalka KK, Born M, Schindler M, Schmidt M, Sulima T, Eisele I (2006) P-channel tunnel field-effect transistors down to sub-50 nm channel lengths. *Jpn J Appl Phys* 45:3106–3109. doi:[10.1143/JJAP.45.3106](https://doi.org/10.1143/JJAP.45.3106)
- Born M, Bhuwalka KK, Schindler M, Abelein U, Schmidt M, Sulima T, Eisele I (2006) Tunnel FET: a CMOS device for high temperature applications. In: *Proceedings of 25th international conference on microelectronics*, Belgrade, Serbia and Montenegro, pp 124–127. doi:[10.1109/ICMEL.2006.1650911](https://doi.org/10.1109/ICMEL.2006.1650911)
- Boucart B, Ionescu AM (2007a) Length scaling of the double gate tunnel FET with a high-K gate dielectric. *Solid-State Electron* 51(12):1500–1507. doi:[10.1016/j.sse.2007.09.014](https://doi.org/10.1016/j.sse.2007.09.014)
- Boucart K, Ionescu AM (2007b) Double gate tunnel FET with high-k gate dielectric. *IEEE Trans Electron Devices* 54(7):1725–1733. doi:[10.1109/TED.2007.899389](https://doi.org/10.1109/TED.2007.899389)
- Cho S, Sun MC, Kim G, Kamins TI, Park BG, Harris JS (2011) Design optimization of a type-I heterojunction tunneling field-effect transistor (I-HTFET) for high performance logic technology. *J Semicond Technol Sci* 11(3):182–189. doi:[10.5573/JSTS.2011.11.3.182](https://doi.org/10.5573/JSTS.2011.11.3.182)
- Choi KM, Choi WY (2013) Work-function variation effects of tunneling field-effect transistors (TFETs). *IEEE Electron Device Lett* 34(8):942–944. doi:[10.1109/LED.2013.2264824](https://doi.org/10.1109/LED.2013.2264824)
- Choi WY, Lee W (2010) Hetero-gate-dielectric tunneling field-effect transistors. *IEEE Trans Electron Devices* 57(9):2317–2319. doi:[10.1109/TED.2010.2052167](https://doi.org/10.1109/TED.2010.2052167)
- Conde AO, Garcia-Sanchez FJ, Muci J, Sucre-Gonzalez A, Martino JA, Agopian PGD, Claeys C (2014) Threshold voltage extraction in tunnel FETs. *Solid-State Electron* 93:49–55. doi:[10.1016/j.sse.2013.12.010](https://doi.org/10.1016/j.sse.2013.12.010)
- Fukuda K, Mori T, Mizubayashi W, Morita Y, Tanabe A, Masahara M, Yasuda T, Migita S, Ota H (2013) A compact model for tunnel field effect transistors incorporating nonlocal band to band tunneling. *J Appl Phys* 114(14):144512. doi:[10.1063/1.4824535](https://doi.org/10.1063/1.4824535)
- Gandhi R, Chen Z, Singh N, Banerjee K, Lee S (2011) CMOS-compatible vertical-silicon-nanowire gate-all-around p-type tunneling FETs with ≤ 50 -mV/decade subthreshold swing. *IEEE Electron Device Lett* 32(11):1504–1506. doi:[10.1109/LED.2011.2165331](https://doi.org/10.1109/LED.2011.2165331)
- Hraziia Vladimirescu A, Amara A, Anghel C (2012) An analysis on the ambipolar current in Si double-gate tunnel FETs. *Solid-State Electron* 70:67–72. doi:[10.1016/j.sse.2011.11.009](https://doi.org/10.1016/j.sse.2011.11.009)
- Jhaveri R, Nagavarapu V, Woo JCS (2010) Effect of pocket doping and annealing schemes on the source-pocket tunnel field-effect transistor. *IEEE Trans Electron Devices* 58(1):80–86. doi:[10.1109/TED.2010.2089525](https://doi.org/10.1109/TED.2010.2089525)
- Lee DS, Yang HS, Kang KC, Lee JE, Lee JH, Cho S, Park BG (2010) Simulation of gate-all-around tunnel field-effect transistor with an n-doped layer. *IEICE Trans Electron* 93-C(5):540–545. doi:[10.1587/transle.E93.C.540](https://doi.org/10.1587/transle.E93.C.540)
- Lee JS, Choi WY, Kang IM (2012) Characteristics of gate-all-around hetero-gate-dielectric tunneling field-effect transistors. *Jpn J Appl Phys* 51:06FE03. doi:[10.1143/JJAP.51.06FE03](https://doi.org/10.1143/JJAP.51.06FE03)
- Madan J, Gupta RS, Chaujar R (2014) Influence of heterogeneous gate dielectric on hetero-dielectric-DMG-GAATFET for improved tunneling current. *Int J Adv Technol Eng Sci* 2(1):41–47
- Madan J, Gupta RS, Chaujar R (2015a) Analytical drain current formulation for gate dielectric engineered dual material gate-gate all around-tunneling field effect transistor. *Jpn J Appl Phys* 54:094202. doi:[10.7567/JJAP.54.094202](https://doi.org/10.7567/JJAP.54.094202)
- Madan J, Gupta RS, Chaujar R (2015b) Threshold voltage model of a hetero gate dielectric dual material gate GAA Tunnel FET. *Advanced manufacturing, electronics and microsystems: techconnect Briefs 2015*, pp 254–257. doi:[10.13140/RG.2.1.3081.2003](https://doi.org/10.13140/RG.2.1.3081.2003)
- Mallik A, Chattopadhyay A (2011) Drain-dependence of tunnel field-effect transistor characteristics: the role of the channel. *IEEE Trans Electron Devices* 58(12):4250–4257. doi:[10.1109/TED.2011.2169416](https://doi.org/10.1109/TED.2011.2169416)
- Mookerjee S, Krishnan R, Datta S, Narayanan V (2009) Effective capacitance and drive current for tunnel FET (TFET) CV/I estimation. *IEEE Trans Electron Devices* 56(9):2092–2098. doi:[10.1109/TED.2009.2026516](https://doi.org/10.1109/TED.2009.2026516)
- Nirschl T, Henzler S, Fischer J, Fulde M, Bargagli-Stoffi A, Sterkel M, Sedlmeir J, Weber C, Heinrich R, Schaper U, Einfeld J, Neubert R, Feldmann U, Stahrenberg K, Ruderer E, Georgakos G, Huber A, Kakoschke R, Hansch W, Schmitt-Landsiede D (2006) Scaling properties of the tunneling field effect transistor (TFET): device and circuit. *Solid-State Electron* 50:44–51. doi:[10.1016/j.sse.2005.10.045](https://doi.org/10.1016/j.sse.2005.10.045)
- Noguchi M, Kim SH, Yokoyama M, Ichikawa O, Osada T, Hata M, Takenaka M, Takagi S (2015) High Ion/Ioff and low subthreshold slope planar-type InGaAs tunnel FETs with Zn-diffused source junctions. *J Appl Phys* 118:045712-1–045712-15. doi:[10.1063/1.4927265](https://doi.org/10.1063/1.4927265)
- Shaker A, Ossaimee M, Zekry A, Abouelatta M (2015) Influence of gate overlap engineering on ambipolar and high frequency characteristics of tunnel-CNTFET. *Superlattices Microstruct.* doi:[10.1016/j.spmi.2015.08.008](https://doi.org/10.1016/j.spmi.2015.08.008)
- Toh EH, Wang GH, Samudra G, Yeo YC (2007) Device physics and design of double-gate tunneling field-effect transistor by silicon film thickness optimization. *Appl Phys Lett* 90(26):263507–263510. doi:[10.1063/1.2748366](https://doi.org/10.1063/1.2748366)
- Toh EH, Wang GH, Chan L, Sylvester D, Heng CH, Samudra GS, Yeo YC (2008) Device design and scalability of a double-gate tunneling field-effect transistor with silicon-germanium source. *Jpn J Appl Phys* 47(4S):2593–2597. doi:[10.1143/JJAP.47.2593](https://doi.org/10.1143/JJAP.47.2593)
- Ying L, He Jin, Mansun C, Cai-Xia D, Yun Y, Wei Z, Wen W, Wan-Ling D, Wen-Ping W (2014) An analytical model for gate-all-around silicon nanowire tunneling field effect transistors. *Chin Phys B* 23(9):097102-1-6. doi:[10.1088/1674-1056/23/9/097102](https://doi.org/10.1088/1674-1056/23/9/097102)

Mechanical and Thermal Properties of Castor Oil-Based Polyurethane Adhesive: Effect of TiO₂ Filler

MANJEET MALIK

Delhi Technological University, New Delhi 110 042, India

RAMINDER KAUR

Department of Polymer Science and Chemical Technology, Delhi Technological University, New Delhi 110 042, India

Correspondence to: Raminder Kaur; e-mail: rkwalidtu@gmail.com.

Received: June 18, 2015

Accepted: October 29, 2015

ABSTRACT: Polyurethane (PU) production with the use of vegetable oils is greatly appreciated by researchers due to their low cost, easy availability, and nontoxic nature. The addition of TiO₂ in castor oil-based PU adhesive led to a remarkable enhancement in its mechanical and chemical resistance, an increase in T_g value, and the adhesion. TGA analysis was done to study the thermal stability of prepared adhesive. The adhesive was also characterized by differential scanning calorimetry (DSC) and FT-IR spectroscopy. Influence of various factors such as the NCO/OH molar ratio, hydroxyl value of polyols, and the amount of filler on the properties of adhesive were studied in detail. The adhesive with a mole ratio of NCO/OH equaling to 1.2, filled with 3 wt% TiO₂, was found to be much better than the commercial adhesive used for bonding wood, when tested for single lap shear strength in various environmental conditions. © 2016 Wiley Periodicals, Inc. *Adv Polym Technol* 2016, 00, 21637; View this article online at wileyonlinelibrary.com. DOI 10.1002/adv.21637

KEY WORDS: Castor Oil, adhesives, polyurethanes, thermal properties, Titanium dioxide

Introduction

Polyurethane (PU) adhesives are well known for their properties such as excellent adhesion, flexibility, good performance at low-temperature conditions, and cure speeds that can be varied according to need of manufacturer.¹ PU is synthesized by reacting isocyanates with compounds containing active hydroxyl groups like polyols.² Considering this reactivity factor, the adhesive industry has taken benefit, thus leading to the fast cure two-component adhesives. By enhancing the functionality of the polyols and isocyanates, branching or cross-linking can be increased in an organized way leading to the materials with improved mechanical properties.^{1,3} PU adhesives, both waterborne and solvent based, are reported to be the high-performance adhesives due to their excellence in adhesion properties, heat and chemical resistance, fast curing time, early green strength, high bond strength, and low shrinkage. PU adhesives made from petrochemicals are costly and nonbiodegradable. To avoid these problems, biomaterial-based PU adhesives have attracted much attention of researchers.^{2–6} Castor oil, a naturally occurring triglyceride of ricinoleic acid, can be employed for the synthesis of PU.^{7,8}

Mechanical properties of castor oil-based adhesive shows a high dependency on the NCO/OH molar ratio due to higher or

lower cross-linking achieved during a reaction.⁹ Somani et al. studied the properties of PU adhesives from three different polyester polyols, obtained by reacting a castor oil derivative and diols (glycols) with diisocyanate adducts in different NCO/OH ratios.¹⁰ They reported that the NCO/OH ratio 1.3 gave excellent lap shear strength. Silva et al. prepared solvent-less castor oil-based PU adhesives to evaluate the influence of the NCO/OH molar ratio and the chemical nature of the substrates (wood/wood and foam/foam) on the adhesive force.⁹ They reported that resulted PU adhesive foam joints showed peeling strength values 75% and wood joints showed lap shear strength values 20% higher than that of a commercialized solvent-based adhesive. The physicochemical and mechanical properties of adhesives can also be altered by the incorporation of the fillers.¹¹ Fillers are reported to impart improved adhesion, improved resistance to ageing, and reduce cost. Commonly used fillers in PU are talc, calcium carbonate, silica, titanium oxide, carbon fiber, clay, etc. In the recent past, research has been focused on the development and incorporation of nanosized fillers, which can uniformly disperse in organic matrix.¹²

The influence of nanosized TiO₂ filler on various properties of PU adhesive has been taken into account in the present study. The TiO₂ had been reported to improve surface adhesion, solar reflectance, and crack resistance in PU adhesives.¹³ In the present study, PU adhesive was synthesized by the

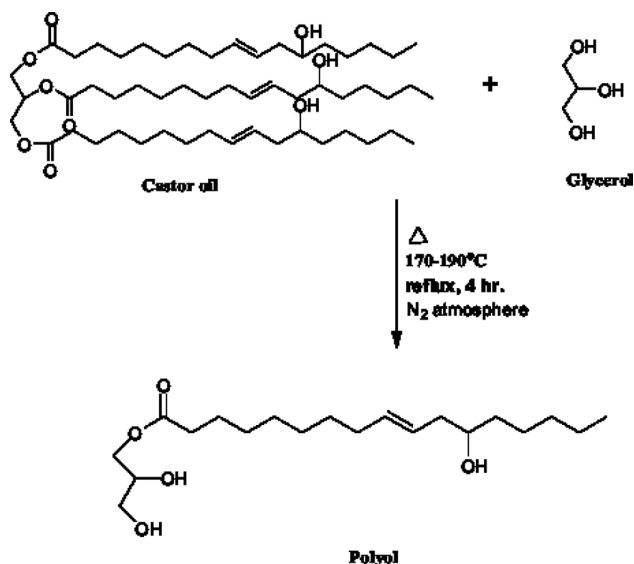


FIGURE 1. Scheme of polyol synthesis.

reaction of glycerol-modified castor oil with diphenylmethane-4,4'-diisocyanate (MDI). The main focus and aim is to improve the overall performance of adhesive by the addition of nano-sized TiO_2 as filler, and it was found to have direct influence on mechanical, physical, and chemical properties of the resulted adhesive. The adhesive formulation was characterized by FT-IR, thermal gravimetric analysis (TGA), differential scanning calorimetry (DSC), and single lap shear testing. In addition, tests for impact strength, viscosity change, and chemical resistance under various test condition had been carried out.

Experimental

MATERIALS

For the synthesis of PU adhesive, castor oil having a hydroxyl value of 160 (CDH, India) was heated in an oven for 24 h at 100°C to remove the moisture, if any. MDI (Sigma-Aldrich) was supplied by Shivathene Linopack (Parwanoo, India). Catalyst dibutyltin dilaurate (HMEDA, India) and methyl ethyl ketone (CDH, India) were used as received. Nanosized TiO₂ (particle size 15–18 nm) was synthesized in our research laboratory by the method reported in the literature.¹⁴ Commercial adhesive, FevicolTM (PU resin), was purchased from local market for the comparison purpose.

Methodology

SYNTHESIS OF POLYOL

Polyol was obtained by the modification of the castor oil, as reported in the literature^{15,16} (Fig. 1). The polyols with hydroxyl values of 500, 400, 300, and 200 were prepared using the castor oil

to glycerol ratios of, respectively, 1:1, 2:1, 3:1, and 4:1. The acetic anhydride-pyridine method was used to find out the hydroxyl value of polyols.¹⁷

PREPARATION OF ADHESIVE

The calculated amounts of polyol and MDI were added and stirred continuously for 30 min under nitrogen atmosphere at room temperature. The solutions of different NCO/OH ratios were prepared by following the same procedure. Methyl ethyl ketone was added to adjust the adequate flow of the resulted solutions. In another flask, a mixture of polyol along with requisite amount of TiO₂ and DBTDL (0.05 w/w%) was prepared. Both the mixtures (as prepared above) were mixed in a separate clean beaker and stirred for 1 min, before applying to the substrate.

SUBSTRATE PREPARATION

Teak wood without knot, decay, insect, or fungal infection, was cut into $300 \times 25 \times 3 \text{ mm}^3$ strips. Surfaces of wood strips were cleaned with sandpaper grit no. 60 (to ensure good quality of adhesion). Strips of wood were retained at $50 \pm 5\%$ relative humidity for 7 days at room temperature.

BONDING OF SUBSTRATES

The prepared adhesive solution was spread over an area of $25 \times 30 \text{ mm}^2$ on both pieces of wood that to be joined with the help of a glass rod. After keeping the adhesive joint undisturbed for 1 min, a load of 2.5 kg was applied over it and was maintained for next 24 h.

CHARACTERIZATION

The wood specimens glued by castor oil-based PU adhesive as mentioned in the section Substrate Preparation, were subjected for lap shear strength after 5 h, 10 h, 1 day, 2 days, and 4 days (for green strength). Specimens were retained at $50 \pm 5\%$ relative humidity at room temperature and were tested for lap shear strength at particular intervals (days). The measurement of adhesive strength was carried out using a universal testing machine Instron 3369 in accordance with ASTM D 906–82(1987), with a crosshead speed of 5 mm/min. Five samples for each formulation were tested, and visual observation was done for the kind of locus failure at adhesive joints. Impact strength of specimens was calculated by obtaining average of 10 samples before and after TiO_2 doping as per ASTM D-256 using a digital impact tester (International Equipments, Mumbai, India).

FTIR spectra of solid PU adhesive were recorded on a Nicolet 380 FT-IR spectrophotometer at 25°C by crushing the sample with KBr. Polyol characterization was done using a liquid assembly by putting a drop of it on the crystal surface. Thermogravimetry analysis (TGA) of resulted a PU-based adhesive was done on a Perkin-Elmer instrument (Diamond SDTA; Shelton, CT, USA) from 25 to 800°C at a heating rate of 10°C/min in inert atmosphere by taking 1 mg of sample. Calorimetric analysis was done on a DSC (TA Instruments) analyzer. Aluminum pans containing 10–12 mg of samples were subjected to a temperature range of 70 to 100°C at a heating rate of 10°C/min under inert

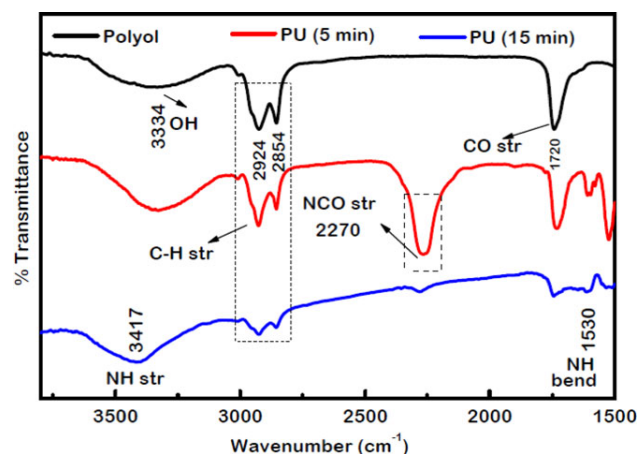


FIGURE 2. FT-IR spectrum of polyol and PU adhesive at different time durations.

atmosphere. The viscosity change with addition of TiO_2 nanoparticles was examined using a Brookfield viscometer using spindle no. 2 at 100 rpm. Morphology of TiO_2 -doped PU was analyzed using a scanning electron microscope (S-3700N; Hitachi, Japan) and for elemental characterization of TiO_2 -doped sample, the sample was examined with the EDXS analyzer unit attached to the scanning electron microscope. TEM images were obtained using a F 30 S twin 300 HRTEM at 300 kV after preparing a sample on copper grid for HRTEM.

For chemical resistance testing, specimens of wood adhered with PU adhesive were kept in water (30°C) for 24 h and then tested for lap shear strength after drying at room temperature (30°C) for 1 day. Similarly, another sets of bonded wood pieces were tested after keeping in hot water (100°C) for 1 h, in acid solution of pH = 2 at 80°C for 1 h, and in basic solution of pH 12 at 80°C for 1 h. The weight loss and dimensional changes in PU specimens with and without TiO_2 were also observed in above-mentioned conditions.

Result and Discussion

IR SPECTRA

IR spectra of the castor oil-based polyol and PU samples after 5 and 15 min (Fig. 2) showed a broad band at 3334 cm^{-1} due to the OH group. IR bands at 2924 and 2854 cm^{-1} are due to alkyl C-H stretching of aliphatic segment of fatty chain as discussed in previous studies.¹⁸ It was observed that the reaction was not taking place spontaneously after the addition of isocyanate and catalyst, but some significant changes were observed. IR spectra taken after 5 min indicated the presence of free available NCO by showing stretching frequency at 2270 cm^{-1} . The intensity of this signal decreased with time, but some amount of NCO remained unreacted, even after a reaction with polyol was completed (as MDI was taken in excess), which is desirable for a reaction with the hydroxyl group of wood substrate. The IR spectra of solidified PU adhesive (after 15 min) had shown a characteristic peak at 3417 cm^{-1} due to NH stretching, peak at 1530 cm^{-1} due to

TABLE I
Effect of Hydroxyl value on Adhesion

Hydroxyl Value (mg of KOH/g)	Avg. Lap Shear Strength MPa (± 5)	Locus of Failure
160	18	Cohesive
200	39	Cohesive
300	43	Cohesive + adhesive
400	51	Cohesive + adhesive
500	56	Substrate failure

TABLE II
Effect of Isocyanate-Hydroxyl (NCO/OH) Ratio on Adhesion

NCO/OH Ratio (Polyol with Hydroxyl Value of 400 mg of KOH/g)	Average Lap Shear Strength (MPa)(± 5)	Type of Failure
1.0	23	Cohesive
1.1	41	Cohesive
1.2	51	Adhesive + cohesive
1.3	47	Adhesive + cohesive
1.4	43	Adhesive

NH bending of the urethane group, and at 1720 cm^{-1} due to the carbonyl stretching. The addition of nanosized TiO_2 had no effect on IR spectra of PU adhesive.

EFFECT OF HYDROXYL VALUE

It is evident from the results shown in Table I that as the hydroxyl value of polyol increases, the lap shear strength of bonded wood joints also increases. This increase in strength of prepared adhesive might be because of an increase in cross-linking density due to more linkage between the hydroxyl group and isocyanate moiety. As castor oil has low hydroxyl value (160), adhesive containing more amount of castor oil, resulted in weak adhesion strength whereas the polyols with higher glycerol content showed a rapid increase in adhesive strength along with their increase in the hydroxyl value.

EFFECT OF NCO/OH RATIO ON ADHESION PROPERTIES

It is evident from Table II that the value of lap shear strength increased with an increase in the NCO/OH ratio upto 1.2. After further increasing the NCO/OH ratio, a reverse effect on bonding strength of adhesive was observed. This trend showed that a slight excess of isocyanate is favorable, as free NCO can react with hydroxyl groups present on the wood surface, thus leading to higher bond strength. However, the lower value of lap shear strength at low NCO/OH ratio is due to complete consumption of isocyanate by hydroxyl group of polyol, showing cohesive type of failure. Nevertheless, the higher NCO/OH

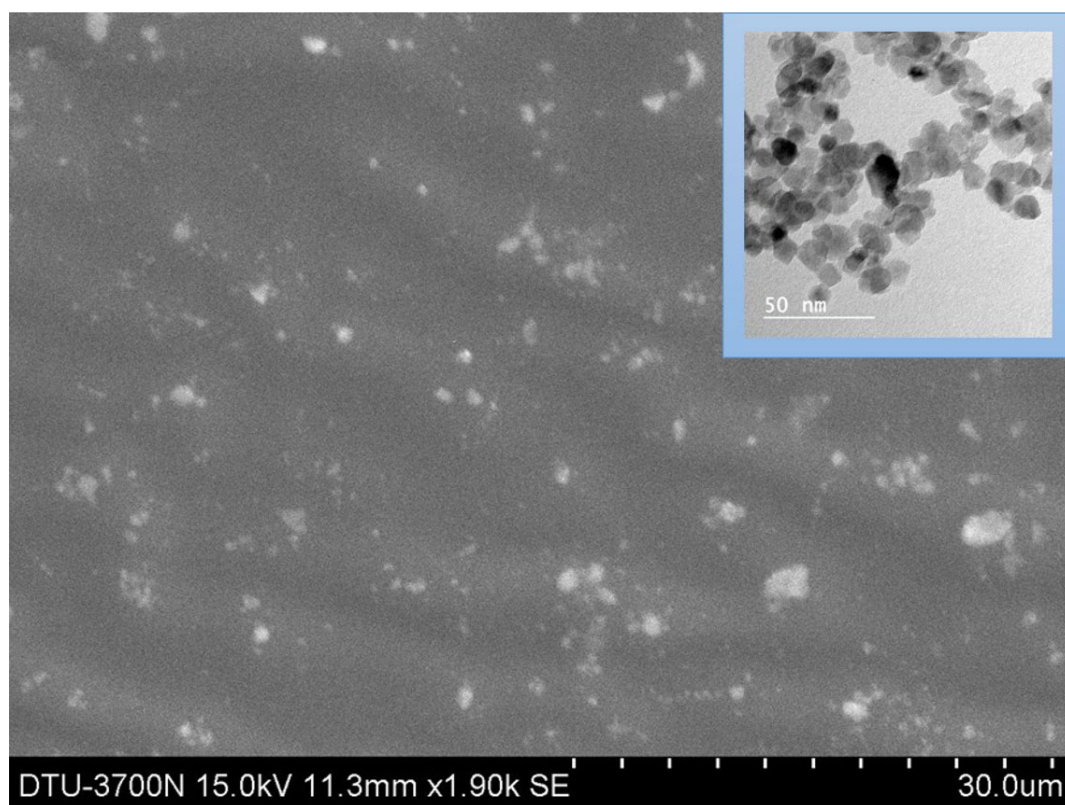


FIGURE 3. SEM and TEM (inset image) micrograph of TiO_2 -filled PU.

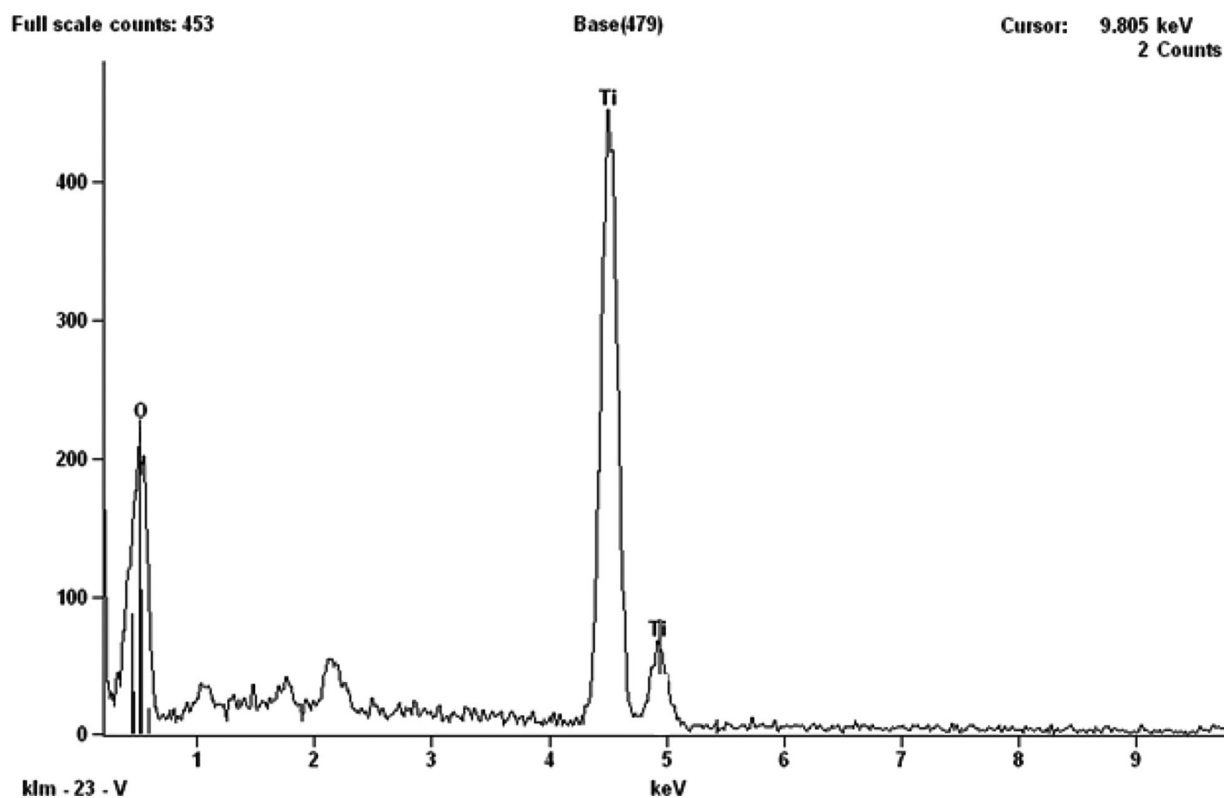


FIGURE 4. EDXS of TiO_2 -filled PU.

TABLE III
Effect of Amount of filler on Adhesion

Filler(wt%) in Polyol (Hydroxyl Value 300 mg of KOH/g)	Average Lap Shear Strength (MPa)(±5)
1	43
2	44
3	46
4	45
5	39

ratio, beyond a critical value resulted in an increase in brittleness of adhesive resulting, in a mixed mode, i.e., cohesive as well as adhesive type of failure.

MORPHOLOGICAL STUDY

The particle size of TiO₂ nanoparticles and morphology of TiO₂-doped PU were examined from micrographs obtained from HRTEM and SEM as shown in Fig. 3. It is clearly seen that TiO₂ nanoparticles of size ranging from 15 to 18 nm were uniformly distributed in the adhesive sample. From SEM images, no bubble formation or nanocracks were observed on the adhesive surface. The TiO₂ doping in adhesive was confirmed by chemical composition study using EDXS analysis (Fig. 4).

EFFECT OF THE ADDITION OF THE FILLER

The lap shear strength of adhesive filled with nanosized TiO₂ in different amounts ranging from 1 to 5 wt% was measured, and the results of the adhesion strength of each composition are shown in Table III. The results reported in Table III are the average of adhesion strength of five samples tested for each composition. It had been observed that, by incorporating TiO₂ upto a concentration of 3%, adhesion strength of bonding wood sample was found to be increased. This might be due to effective transfer of stress between polymer matrix and filler. Furthermore, with increased filler content, i.e. upto 4%, no improvement in lap shear strength was observed. On further addition of filler (5%), the lap shear strength had shown a declining trend, also evident from increased brittleness of adhesive at joint. It was found nearly impossible to disperse more filler uniformly in the adhesive sample.

No significant change was observed in impact strength of adhesive before and after doping of TiO₂ nanoparticles when an average of 10 samples was taken for both. The viscosity of system was found to increase with the addition of TiO₂ as shown in Table V.

CURING TIME AND GREEN STRENGTH

Green strength is an important property of adhesive, which shows the capability of adhesive to grip the substrates together when brought into contact at time when it is not fully cured, i.e. before achieving its full strength. For determining the green strength of prepared adhesive, polyols of different hydroxyl values were selected with the NCO/OH ratio 1.2. Bonded wood specimens were subjected to the lap shear test at different time

TABLE IV
Green Strength

Time after Adhesive Application	Average Lap Shear Strength (MPa)(± 5) (without TiO ₂)	Average Lap Shear Strength (MPa)(±5) (3% TiO ₂)
5 h	14	12
10 h	31	35
1 day	38	43
2 day	47	50
4 day	51	51

TABLE V
Viscosity Change and Weight Loss Data before and after Doping with TiO₂

Type of Adhesive System	Viscosity (mPa·s) (25° C)	Weight Loss (%) (±1)			
		In Acid	In Alkali	Cold Water	Hot Water
PU without TiO ₂	190	2.30	2.90	1.20	1.50
PU filled with 3% TiO ₂	220	2.20	2.43	1.10	1.40

TABLE VI
Chemical Resistance of Different adhesive Formulations

Hydroxyl Value (mg of KOH/g)	Average Lap Shear Strength (MPa)(±5) (Before Exposure)	Average Lap Shear Strength (MPa) (± 5) (After Exposure)			
		Cold Water	Hot Water	Acid, pH 2	Alkali, pH 10
200	39	39	36	33	31
300	43	42	40	39	37
400	51	51	47	46	45
400 (TiO ₂ -3%)	52	51	49	47	47
Commercial adhesive	34	28	24	22	19

intervals, and the results obtained are as given in Table IV. From these results, it is evident that the curing speed of adhesive varies linearly with hydroxyl values of polyol and filled PU adhesive showed a little slow curing rate as compared to corresponding adhesives without any fillers. Prepared adhesive exhibits excellent curing speed, attained 29% of its ultimate strength within just 5 h of bonding and 70% of its final strength in 1 day. Adhesive is found to be fully cured in 4 days; thereafter, no significant change in bonding strength occurred with time.

CHEMICAL RESISTANCE

Prepared adhesive was tested in different conditions such as cold water and hot water, alkali, and acid. The results of variation in bonding strength of adhesive after treatment are shown in Table VI. Adhesive exhibit good resistance to both hot and

TABLE VII**Gel Time**

Hydroxyl Value of Polyol (mg of KOH/g)	Gel Time (min)
160	65
200	58
300	45
400	39
500	26

cold water, whereas acid and alkali have some deteriorating effect on adhesive strength. This might be due to penetration of these solutions in the sample. Result of lap shear strength in the filled PU adhesive sample showed lesser loss in adhesion strength in different test conditions. No major changes in dimensions of specimen were observed (i.e., less than 2%) in all the samples. Visual inspection showed more dimensional stability in the TiO₂-doped PU sample as compared to undoped PU. It might be due to the high thermal coefficient of expansion after the addition of nanostructured TiO₂ filler, which was reported in previous studies,²¹ for the incorporation of nanostructured inorganic fillers in epoxy adhesives. The percent weight change in samples under different chemical environments is presented in Table V. The results showed that hot and cold water has very little effect on prepared PU, but in comparison with acid and alkali environment it resulted in slightly higher weight loss in specimens. The TiO₂-filled sample showed comparatively higher resistance in all chemical environments.

GEL TIME

The pot life or gel time specifies the maximum time throughout which an adhesive still available in fluid state for use with

respect to its application on the substrate. The gel time of prepared adhesive was found to be decreased with the increase in the hydroxyl value of polyol. This might be due to the increased ability of polyols for forming cross-links with isocyanate groups, as shown by results in Table VII.

COMPARISON WITH COMMERCIAL ADHESIVE

The performance of synthesized PU adhesive was compared with commercially available PU adhesive (Fevicol™) in India. In accordance with the result shown in Table VI, the synthesized PU adhesive had much better performance in terms of adhesion strength as well as against different deteriorating conditions than commercial adhesive.

THERMAL CHARACTERIZATION

Thermogravimetric analysis of castor oil-based PU adhesive is shown in Fig. 5. It can be seen from the curve that synthesized PU adhesive is stable upto 250°C as evident from no degradation in weight below this temperature. It was found that adhesive degrades in two stages, the first degradation starts at 270°C due to breaking of urethane bonds, results in the formation of carbon dioxide, carbon monoxide, amines, and aldehydes whereas the decomposition at higher temperature around 470°C is due to breaking of high energy double bonds and single bonds such as C=O, C=C, C-O, C-H bonds. These results are similar to the results shown by the studies of Somani et al.¹⁰ for stage I and that of Callister¹⁹ for stage II. The TGA curve showed that the onset of decomposition of both unfilled and filled PU adhesive was nearly same, but difference lies in the amount of residue left which is much higher in case of filled adhesive. It is also noticed in the curves that unfilled adhesive showed decomposition in three steps but the filled PU had shown the two-step decomposition,

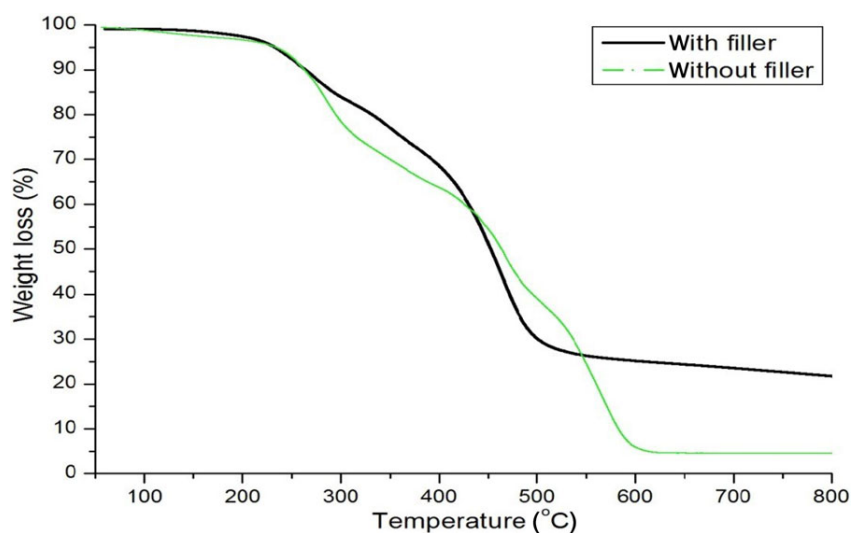


FIGURE 5. TGA of unfilled PU adhesive and TiO₂ filled adhesive.

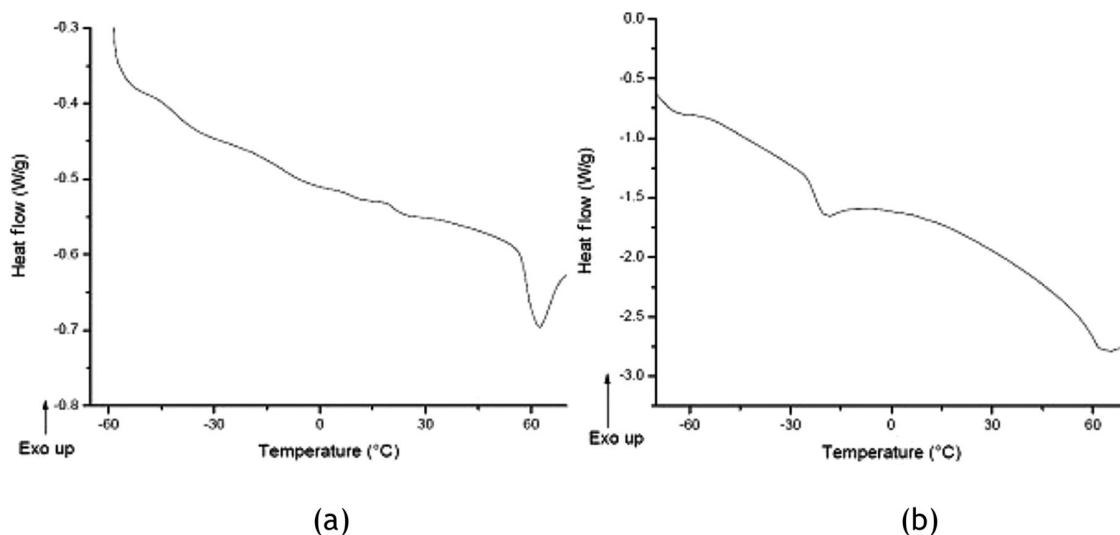


FIGURE 6. DSC Thermograms of the unfilled (a) and 3 wt% TiO₂-filled PU s (b).

indicating a better stability at midrange temperature (around 350°C).

It is apparent from DSC thermograms (Fig. 6) of unfilled and TiO₂-filled (3 wt%) castor oil-based PU adhesive that there are two glass transition temperatures, one is around -55°C and second is around -20°C, which correspond to transitions due to soft segment of PU adhesive. It has also been found that addition of TiO₂ filler increased the glass transition temperature slightly, which indicated that the filler has some interaction with polymer chains, thus favoring the phase separation between the hard and soft segments of PU, as previously studied in case of other fillers reported in the literature.²⁰

Conclusions

In this research work, nanosized TiO₂ was added to castor oil-based PU adhesives. These resulted adhesives were used for bonding wood substrates and the following conclusions were drawn:

- The isocyanate-hydroxyl ratio (NCO/OH) of 1.2 and 4 days for curing is required to develop the best performing adhesive.
- The castor oil-based PU adhesive had showed better performance than commercially available adhesive with respect to adhesion strength and long-term performance in different conditions.
- The introduction of TiO₂ upto 3 wt% to PU adhesive led to a remarkable increase in the lap shear strength and chemical resistance.
- Thermal analysis showed that the addition of TiO₂ increased the T_g values of PU adhesive, resulting in an increase in thermal stability of adhesive.

Conflict of Interest

The studies presented in article had been carried out for research purpose only, and there is no involvement of any kind of financial gain.

References

1. Cranley, P. E. In *Reaction Polymers*, Gum, W. F.; Riese, W.; Ulrich, H. (Eds.); Oxford University Press: New York, 1992; pp. 692.
2. Szycher M., *Szycher's Handbook of Polyurethanes*; Boca Raton, FL: CRC Press, 1999; Chapt. 2.
3. Petrovic, Z. S. *Polym Rev* 2008, 48, 109–155.
4. Dunky, M.; Pizzi, A.; Mittal, K. L. *Handbook of Adhesive Technology*; CRC Press: New York, 2003; pp. 887–956.
5. Desai, S. D.; Patel, J. V.; Sinha, V. K., *Int J Adhes Adhes* 2003, 23(5), 393–399.
6. Desai, S. D.; Emanuel, A. L.; Sinha, V. J *Polym Res* 2003, 10(4), 275–281.
7. Conceicao, M. M.; Candeia, R. A.; Dantas, H. J.; Soledade, L. E. B.; Fernandes, V. J., Jr.; Souza, A. G. *Energy Fuel* 2005, 19, 2185–2188.
8. Scholz, V.; Silva, J. N. *Biomass Bioenergy* 2008, 32, 95–100.
9. Silva, B. B. R.; Santana, R. M. C.; Forte, M. M. C. *Int J Adhes Adhes* 2010, 30, 559–565.
10. Somani, K.P.; Kansara, S. S.; Patel, N. K.; Rakshit, A. K. *Int J Adhes Adhes* 2003, 23, 269–275.
11. Rodriguez, R.; Perez, B.; Florez, S. J *Adhes* 2014, 90, 848–859.
12. Calpena, E. O.; Ais, F.A.; Palau, A.M.T.; Barcelo, C. O. J *Adhes* 2013, 89,174–191.
13. Hamaviriyapornwattana, N.; Sombatsompop, N.; Markpin, T.; Kositchaiyong, A.; Wimolmala, E. J *Vinyl Additi Technol* 2012, 18(3), 184–191.
14. Su, C.; Hong, B. Y.; Tsang, C. M. *Catal Today* 2004, 96, 119–126.
15. Kumar, M.; Kaur, R. *Int J Sci Res Rev* 2013, 2(1, Suppl.), 29–42.
16. Kaur, R.; Kumar, M. J *Polym Eng* 2013, 33(9), 875–880.
17. Cocks, I. V.; Vanredew, C. *Laboratory Handbook for Oil and Fat Analysis*; Academic Press: London, 1976.
18. Mishra, D.; Sinha, V. K. *Int J Adhes Adhes* 2010, 30, 47–54.
19. Callister, W. D. *Material Science and Engineering—An Introduction*; Wiley: New York, 1991.
20. Robles, J. D.; Martin-Martinez, J. M. *Int J Adhes Adhes* 2011, 31(8), 795–804.
21. May, M.; Wang, H.M.; Akid, R. *Int J Adhes Adhes* 2010, 30, 505–512.

MITIGATING CREDIT RISK: AN EMPIRICAL STUDY OF INDIAN PUBLIC SECTOR BANKS

Renu Arora, Archana Singh

Abstract

The purpose of this paper is to study the core credit risk management processes and procedures of the Indian public sector banks and identify the grey areas to improve effectiveness of these systems for risk mitigation. Credit risk management is a key banking system to control non-performing loans, and the banks need efficient alignment of credit strategy, credit policy and processes, and efficient channels of sharing risk information to mitigate credit risk. Through factor analysis, ANOVA and post-hoc studies, the managerial perceptions on credit risk management practices of these banks have been analyzed for three groups of credit and risk managers – managers in large and small banks, managers with different lengths of banking experience, and managers at different levels of management. The research finds that key areas which need improvement are HR potential development through risk trainings, data management, integration across credit departments, increasing consistencies in risk rating approaches, reducing subjectivity in credit ratings, reducing loan processing time, and increasing focal attention on problem loans.

Keywords: *India, Risk infrastructure, System disintegration, Risk-based appraisals, Inconsistencies in risk-ratings.*

Introduction

A Credit asset quality problem is one of the obstacles limiting the further development of commercial banks (JIN, 2011). Indeed, the large number of non-performing loans is the main cause of bank failure (Lin & Mei, 2006). Driven by RBI (Reserve Bank of India) pressures and profitability thrust, it is imperative for Indian banks especially for public sector banks to focus on core credit risk management processes and procedures to determine problem areas. Successful credit risk management (CRM) requires understanding the issues which credit and risk managers at different levels deem important and providing the mechanisms by which maximum participation in risk management can be undertaken in a productive manner. There may be different perceptions of credit risk conceptualization, on risk factors, during risk analysis, assessments, collateral valuation, loan reviews and risk control processes. In CRM processes, it is highly essential to ensure the highest standards of risk communication and coordination namely; the content and process of sharing of risk information among different hierarchy levels meeting certain

ments. This will ensure maximum participation and confidence in CRM systems and processes and should ultimately be very effective and efficient in achieving good quality credit assets and minimizing credit losses. While there are many studies on determinants of credit risk, risk and productivity changes in Indian banks, little has been written about perceived obstacles by different categories of risk managers to improve effectiveness of these systems.

This research aims to understand how the existing CRM systems and procedures for business loans in Indian public sector banks (PSBs) are perceived by their credit and risk managers and to find the grey areas which need improvement and control. For this purpose the three-dimensional managerial perceptions of 337 credit and risk managers of these banks on a set of 23 CRM practices for commercial loans have been gathered. An attempt has been made to examine how these practices may be managed for credit risk mitigation.

The research article has been organized

introduction of the study, section two reviews the literature, section three identifies the research objectives, section four discusses the data and research methodology, section five presents the empirical analysis and results, section six concludes and defines the managerial implications of the study.

section six concludes and defines the managerial implications of the study.

Review of literature

Commercial banks are mainly faced with credit risk, and loans are the largest and the most obvious source of credit risk (Al-Tamimi & Al-Mazrooei, 2007). Many theoretical and empirical studies have verified that internal organizational management and strategies are the determinants of a business's profitability (Lin & Mei, 2006), and the banks shall have a 'differential treatment, differential control' loan policy to reduce credit risk (JIN, 2011).

According to Lepus (2004), the key components of effective credit risk management are robust technology, defined business processes, detailed policies, and sophisticated analytics. Information Technology (IT) is a key productive factor in the banking and finance industry (BFI) as almost the entire production and delivery of services can in principle be digitized (Gewald et al., 2006). Njanike (2009) highlighted the potential obstacles to the successful implementation of effective credit risk management systems by banks namely, lack of resources, disintegration of systems across departments, inconsistency in risk-rating approaches, data management, and stringent regulatory requirements.

According to Lau (2006), the level of effectiveness (of risk analysis) does not always have to be expressed in terms of level of risk (or in terms of either risk components). For instance, merely indicating that a security control is inadequately implemented is sufficient to inform a managerial decision-maker that

something needs to be done to lower the level of risk involved (Lau, 2006). Oesterreichische (2004) suggested an optimal design of credit approval processes which shall minimize substantive and procedural errors by incorporating all possible risk mitigation measures. Lehmann (2003) found that the disadvantages of credit rating systems that rely heavily on expert judgments and subjective information are the difficulties in objectively comparing and re-examining past credit assessments. On integration and standardization, Lepus (2004) observed that many banks have yet to integrate the disparate components of their credit risk systems, for a consistent framework. Greuning and Bratanovic (2009) favored setting and enforcing clear assignment of responsibilities, decision making authority, and accountabilities appropriate for the bank's selected risk profile.

Das and Ghosh (2007), Thiagarajan et al. (2011), and Ghosh (2011) studied the problem loans of the Indian PSBs for the period from 1997-2010 and had diverse views about relationship between the size of banks and their credit risk. Kumar and Kotreshwar (2005) suggested that the Indian banks must develop a competitive early-warning system (EWS) which combined strategic planning, competitive intelligence, management action. Bhavaniprasad and Veena (2011) stressed upon the need for organizational restructuring, improvement in the managerial efficiency to assess the credit worthiness of borrowers in Indian banks. RBI reports (2011-14) had maintained that economic slow-down is not the sole reason for deteriorating asset quality but also the inadequate appraisal and monitoring of credit proposals by banks.

Thus, there is an immediate challenge before Indian public sector banks to improve their internal CRM systems and procedures to track credit delinquencies and build asset quality.

Managerial decision-making and rationality are impacted and influenced by perceptual processes, and perception causes people to make wrong choices based on false information, and incorrect decisions result in a great deal of negative effects (Cheah, 2012). The risk management institutions must institute a broad-based participatory process of high quality (MacGregor, 1994) as risk managers may be sensitive to loss of control, unfairly bearing risk for which someone else receives benefit (MacGregor, 1994).

The review of literature shows that there is not much work on how bank managers perceive the adequacy, efficiency and effectiveness of CRM strategies and processes in their organizations and there is little empirical work to directly address this issue in the context of credit risk decision making process for commercial loans in Indian public sector banks (PSBs). Since most of the credit risk management is influenced by subjectivity and experiential factors, understanding managerial perceptions on bank's credit risk management systems will help enhance goal alignment, risk sensitivity and potential development among risk managers.

Research objectives

The research objective of the study is to understand the managerial perceptions in Indian public sector banks towards various credit risk management practices in commercial credit and to delineate the problem areas for risk mitigation.

Data and research methodology

The managerial perceptions on CRM obstacles and risk mitigation measures in business loans in Indian public sector banks (PSBs) have been studied for three groups of credit and risk analysts – credit managers in large and small PSBs, credit managers with different lengths of banking experience, and credit managers at different levels of management, through a survey polled on 337 such

managers. For understanding perceptual differences between and within groups, the data has been subjected to statistical analysis to find out the most prominent obstacles and most effective or ineffective risk mitigation measures in these banks.

4.1 Sample

The study empirically examines the problems and obstacles in credit risk mitigation and control in grant of commercial loans by Indian public sector banks through a sample of their 337 credit and risk managers, 172 from large PSBs and 165 from small PSBs. Both banks and respondents were selected through non-probability convenience sampling method. Large banks' respondents were from the State Bank of India, Punjab National Bank, Bank of Baroda, Oriental Bank of Commerce, IDBI Bank, the Syndicate Bank, and the small banks' respondents were from the Vijaya Bank, Dena Bank, United Bank of India, Punjab and Sind Bank, Andhra Bank, and the State Bank of Bikaner and Jaipur, covering 46 per cent of 26 Indian PSBs. One more PSB, Bhartiya Mahila Bank has also started functioning (November, 2013), but not made part of the study for want of audited annual reports and credit results. The banks in large and small categories have been divided on the basis of their share in total assets of public sector banks with 2.5 per cent as a cut-off. The respondents were primarily dealing with SME and mid-corporate business loans, and polled through a structured questionnaire, from June to December, 2013, in and around Delhi. The 39 per cent respondents had up to seven years of banking experience, 25 per cent from eight to 20 years, and 36 per cent had more than 20 years' experience. The 14.8 per cent respondents were junior managers, 53.4 per cent middle level managers, and 31.8 per cent senior level managers.

4.2 Measures

Based on the literature review and through personal discussion with respondents, a theoretical framework of CRM systems of the Indian public sector banks was modeled (Figure 1) which was the basis of a logically structured representation of 11 obstacles in implementation of various CRM systems in these banks and 12 risk mitigation measures adopted by them. Part 1 of the research instrument tested the intensity of such obstacles (responses scaled to: very much-5, somewhat- 4, cannot say- 3, a little bit- 2, not at all- 1) and part 2 tested the effectiveness of risk mitigation measures (scored as very good- 5, good-4, average-3, below average-2, bad-1).

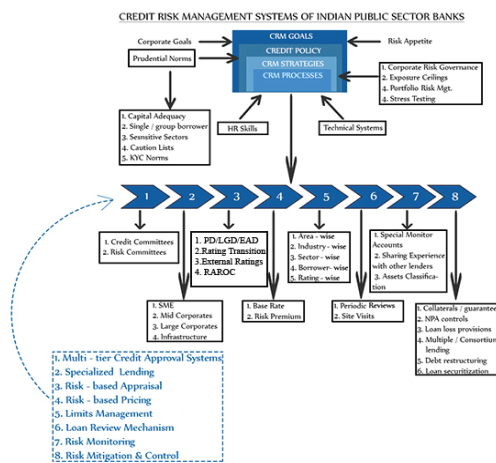


Figure 1: Modeling CRM Systems in Indian Banks.

(Source: Author's analytical studies)

4.3 Statistical Techniques Used

Data collected for the study was analyzed through Likert scale analysis, descriptive statistics, factor analysis, one-way ANOVA, and Tukey's HSD post hoc tests, using SPSS, at 0.05 level of significance. A Likert scale, a psychometric scaling technique used in structured questionnaires, was the basis of all statistical analysis in the study.

Factor analysis was used to reduce the 12 CRM obstacles into two underlying factors, and to reduce the 11 risk mitigation measures again into two factors, to

select the surrogate variables and to calculate the factor scores for each of the Data collected for the study was analyzed through Likert scale analysis, descriptive statistics, factor analysis, one-way ANOVA, and Tukey's HSD post hoc tests, using SPSS, at 0.05 level of significance. A Likert scale, a psychometric scaling technique used in structured questionnaires, was the basis of all statistical analysis in the study.

Factor analysis was used to reduce the 12 CRM obstacles into two underlying factors, and to reduce the 11 risk mitigation measures again into two factors, to select the surrogate variables and to calculate the factor scores for each of the 337 respondent on the derived factors. The derived factor scores was used in one-way analysis of variance (ANOVA) to find the significant differences in perception of three groups of credit managers and in post-hoc tests. Factor analysis is a multivariate statistical technique used primarily in data reduction and in summarizing information into a smaller number of subsets or factors. Principal component analysis has extracted principal factors explaining maximum variation in the responses.

This study used one-way ANOVA or F statistic to test the significance of various CRM variables with responses of three categories of credit managers in Indian public sector banks as independent variables. Tukey's HSD post hoc tests clarified which groups in specific had significant differences.

5. Results and discussion

For confirming the reliability of the measures, the Cronbach's α value was calculated, which came to 0.803 (23 variables), exceeding the minimum standard of 0.7. Cronbach alpha coefficient is an indicator of internal consistency in response pattern and repeatability of the measures. The analytical results for obstacles and risk mitigation measures have been explained further.

5.1 Data Analysis and Results - Part 1- Obstacles

5.1.1 Descriptives

The mean score tally among 337 respondent credit analysts (Table I) shows that most of them were feeling insufficient training (3.42), overload (3.19), lack of risk awareness (3.17), and lack of resources (3.06) as serious obstacles in implementation of credit risk management systems and processes in their banks. To analyze the responses further, data was subjected to factor analysis and ANOVA.

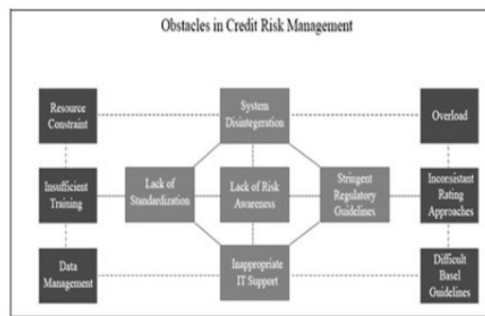


Figure 2: Obstacles in CRM Systems and Processes.
(Source: Author's analytical studies)

Table I. Descriptive Statistics-Obstacles

	N	Mean	Std. Deviation
1. Lack of resources	337	3.06	1.338
2. Lack of risk awareness	337	3.17	1.299
3. Insufficient training	337	3.42	1.213
4. Disintegration of systems across departments	337	2.98	1.234
5. Inconsistencies in risk-rating approaches	337	2.81	1.222
6. Data management	337	2.92	1.256
7. Inappropriate IT support	337	2.73	1.316
8. Lack of comprehension of Basel guidelines	337	2.69	1.270
9. Lack of standardization of risk-rating and review processes	337	2.63	1.285
10. Overload	337	3.19	1.325
11. Stringent regulatory requirements	337	2.86	1.269

5.1.2 Factor analysis

The factor analysis was applied on part 1 of the questionnaire relating to obstacles in credit risk management in sample banks. Factor analysis with principal

component extraction, was applied with varimax rotation to understand the factor loadings across the derived components. Kaiser-Meyer-Olkin (KMO) test for sampling adequacy and Bartlett's test of sphericity for examining the correlation matrix based on chi-square transformation, was conducted. The KMO measure of sampling adequacy came out to be 0.882 which was above 0.65 (the acceptable level). The chi-square value of Bartlett's test of sphericity was found to be significant, with chi square (df 55) = 1570.160 at $p = 0.000$. This showed the appropriateness of factor analysis. The varimax rotation clubbed the 11 variables on two principal factors, and using the Rotated Component Matrix, factor loadings (Table II) and Scree Plot (Figure 3) were derived. Total variance explained in two factors was 56.95% (cumulative).

The key obstacles in implementation of credit risk management systems and processes in Indian PSBs was grouped in two components for further analysis:

1. Gaps in risk infrastructure (7 variables).
2. Bottlenecks due to regulatory framework, work distribution & lack of standardization (4 variables).

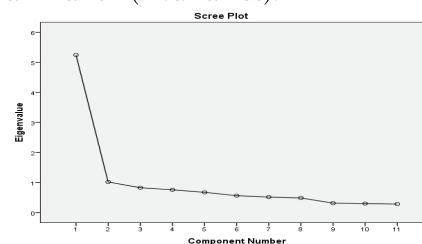


Figure 3: Scree Plot – Obstacles.

Table II. Rotated Component Matrix and Factor Loadings: CRM Obstacles

	Component	
	Gaps in risk infrastructure	Other bottlenecks
1. Lack of resources.	.690	
2. Lack of risk awareness.	.845	
3. Insufficient training.	.732	
4. Disintegration of systems across departments.	.525	
5. Inconsistencies in risk-rating approaches.	.675	
6. Data management.	.549	
7. Inappropriate IT supports.	.516	
8. Lack of comprehension of Basel guidelines.		.557
9. Lack of standardization of risk-rating and review processes.		.687
10. Overload.		.731
11. Stringent regulatory requirements.		.770

To analyze the risk perception of bank managers on these two categories of CRM obstacles, two approaches have been adopted. The first approach was to select a surrogate variable (the dependent variable) in each obstacle category and conduct ANOVA/ F test on three independent variables, managers in large or small PSBs; managers in three experience groups – ‘Up to 7 Years’, ‘8 to 20 Years’ and ‘Above 20 years’; and managers at three levels – junior, middle and senior levels. ANOVA compares the between estimates of mean variance with the within estimates. The second approach was to calculate factor scores (the dependent variable) for each respondent for two categories of CRM obstacles, and conduct ANOVA on the above three independent variables. Tukey’s HSD post hoc tests were conducted in those cases where significant differences was observed in risk perceptions to find which groups among the sample, in specific had significant perception differences.

Surrogate Variables Approach. Surrogate or substitute variable is the variable with highest factor loading in each factor category. Conducting statistical analysis on surrogate variables facilitates interpreting results in terms of original variables rather than the factor scores.

The two surrogate CRM obstacles for each of two factors were ‘Lack of Risk Awareness’ (factor loadings 0.845) and ‘Stringent Regulatory Requirements’ (factor loadings 0.770) (Table II). One-way analysis of variance (ANOVA) was conducted on surrogate obstacles to identify the significant difference in risk perceptions of three managerial groups.

The results showed statistically significant difference in managerial perception for ‘Lack of Risk Awareness’ in large and small banks, with $F(2, 334) = 3.544$, at $p = 0.030$ and the mean score for large banks was 2.97 (S.D. 1.324) against mean score for small banks is 3.38 (S.D. 1.242). Credit and risk managers in small PSBs

were perceiving lack of risk awareness as significant obstacle in managing credit risk in their banks. Though no significant difference was observed among other managerial groups viz. at different levels of management or in different experience brackets. Thus, credit managers needed more education on risk issues, to understand the risk technicalities and learn the ways of commercial borrowers, business markets, government policies and economic scenarios. There may be imbalance of risk awareness among different banks, among different ranks within banks and their risk and credit departments, and this could create problems in accurate assessment of credit risk.

Towards the second surrogate variable ‘Stringent Regulatory Requirements’, no significant difference in perception of any group of managers was observed. Any difference in groups mean scores were random or by chance. In other words, the groups were similar in their opinion. The mean score for all respondents on this variable was 2.86, signifying stringency of regulatory guidelines was not perceived as a serious problem in CRM operations in PSBs.

Factor Scores Approach. Factor scores were composite scores estimated for each respondent on each of the two derived factors - ‘Gaps in Risk Infrastructure’ and ‘Bottlenecks due to Regulatory Framework, Work Distribution & Lack of Standardization’. Factor scores were computed through SPSS, under principal component method. One way ANOVA (Tables III to V) and post-hoc tests (Table VI) was conducted on factor scores to study the differences in managerial perceptions towards two categories of CRM obstacles among the three groups.

The results of one-way ANOVA with bank size category and management levels indicated that there was significant difference in risk perception of the management in large and small public

sector banks towards ‘Gaps in Risk Infrastructure’ factor.

For large vs. small PSB credit managers, F was 12.629 (df 1,335) at $p=.000$. For different management levels, F was 6.404 (df 2,334) at $p=.002$. F statistic was not significant for differential experience groups.

Table III. ANOVA of Obstacles by Size of Bank: Large vs. Small

		Sum of Squares	df	Mean Square	F	Sig.
1. Gaps in Risk Infrastructure.	Between Groups	12.207	1	12.207	12.629	.000
	Within Groups	323.793	335	.967		
	Total	336.000	336			
2. Bottlenecks due to Regulatory Framework, Work Distribution and lack of Standardization.	Between Groups	2.343	1	2.343	2.353	.126
	Within Groups	333.657	335	.996		
	Total	336.000	336			

Table IV. ANOVA of Obstacles by Experience of Managers

		Sum of Squares	df	Mean Square	F	Sig.
1. Gaps in Risk Infrastructure.	Between Groups	3.283	2	1.641	1.648	.194
	Within Groups	332.717	334	.996		
	Total	336.000	336			
2. Bottlenecks due to Regulatory Framework, Work Distribution and lack of Standardization.	Between Groups	4.226	2	2.113	2.127	.121
	Within Groups	331.774	334	.993		
	Total	336.000	336			

Table V. ANOVA of Obstacles by Management Levels

		Sum of Squares	df	Mean Square	F	Sig.
1. Gaps in Risk Infrastructure.	Between Groups	12.409	2	6.205	6.404	.002
	Within Groups	323.591	334	.969		
	Total	336.000	336			
2. Bottlenecks due to Regulatory Framework, Work Distribution and lack of Standardization.	Between Groups	.835	2	.417	.416	.660
	Within Groups	335.165	334	1.005		
	Total	336.000	336			

Table VI. Post-hoc Multiple Comparisons

Dependent Variable: Factor - Gaps in Risk Infrastructure.

Tukey HSD

(I) Management Level	(J) Management Level	Mean Difference (I-J)	Std. Error	Sig.	95% Confidence Interval	
					Lower Bound	Upper Bound
Junior Managers	Middle Level Managers	-.46402776 [*]	.15735021	.010	-.8344632	-.0935923
	Senior Level Managers	-.59671870 [*]	.16861554	.001	-.9936751	-.1997623
Middle Level Managers	Junior Managers	.46402776 [*]	.15735021	.010	.0935923	.8344632
	Senior Level Managers	-.13269093	.12015379	.512	-.4155582	.1501763
Senior Level Managers	Junior Managers	.59671870 [*]	.16861554	.001	.1997623	.9936751
	Middle Level Managers	.13269093	.12015379	.512	-.1501763	.4155582

*. The mean difference is significant at the 0.05 level.

Tukey's post-hoc tests reveal significant differences in risk perceptions between junior credit managers with middle and senior level credit managers, but not between middle and senior level managers. Credit managers in small PSBs were given higher mean scores on all variables in ‘Gaps in risk infrastructure’ factor. Similarly, mean scores tally among different levels of management show higher scores on all variables at senior managerial positions, followed by middle level

and then by junior levels. They were thus feeling more intensely about these CRM obstacles hampering their CRM systems and procedures in mitigating and controlling credit risk. If more banks and more senior managers were perceiving these obstacles seriously in their CRM systems and processes, was cause of worry for their PSBs. F statistics are, however, not significant for any managerial group for second obstacles factor ‘Bottlenecks due to Regulatory Framework, Work Distribution & Lack of Standardization’.

5.2 Data analysis and Results - Part 2- Risk Mitigation Factors

5.2.1 Descriptives.

Mean scores analysis (Table VII) showed that most of the respondents were optimistic about the effectiveness of risk mitigation measures in their banks. They were, however, more satisfied on implementation of KYC norms (4.31), multi-tier credit approval process (4.07), risk-based appraisals and loan sanctions (4.06), and internal audit (4.0) than on reduction in processing effort per loan application (3.54) and reduction of subjectivity in credit ratings (3.56). To analyze the response patterns for underlying factors and significance tests, the data was subjected to factor analysis, ANOVA and post-hoc tests.

Table VII. Descriptive Statistics-Risk Mitigation Measures

	N	Mean	Std. Deviation
1. Regular discussions, reviews and feedback	337	3.95	.817
2. Restriction on responsibility for volume-based credit approvals and reviews	337	3.76	.816
3. Independence of credit risk assessment from credit sanctioning process	337	3.82	.952
4. Reduction in processing effort per loan application	337	3.54	.893
5. Regular rating reviews	337	3.99	.816
6. Reduction of subjectivity in credit rating	337	3.56	.878
7. Internal audits	337	4.00	.730
8. Risk-based appraisal and sanctions	337	4.06	.752
9. Independence of loan review mechanism	337	3.95	.850
10. Implementation of KYC norms	337	4.31	.801
11. Multi-tier credit approval process	337	4.07	.884
12. Focused attention on problem/weak credit exposures	337	3.87	.871

5.2.2 Factor Analysis

Factor analysis has been applied on 12 variables in part 2 of the questionnaire to test effectiveness of various credit risk mitigation measures. The KMO measure of sampling adequacy was 0.886 and above the acceptable level (0.65). The chi-square value of Bartlett's test of sphericity was found to be significant, with chi square (df 66) = 1071.289 at $p = 0.000$, signifying the appropriateness of factor analysis.

The varimax rotation has clubbed the 12 variables on two principal factors (Table VIII). Total variance explained in two factors is 47.83% (cumulative) with scree plot graphing the eigenvalues (Figure 4). The effectiveness of 12 credit risk mitigation measures in PSBs was grouped in two factors for further analysis:

1. Improving credit risk management systems (9 variables).
2. Improving internal controls (3 variables).

Table VII. Descriptive Statistics-Risk Mitigation Measures

	N	Mean	Std. Deviation
1. Regular discussions, reviews and feedback	337	3.95	.817
2. Restriction on responsibility for volume-based credit approvals and reviews	337	3.76	.816
3. Independence of credit risk assessment from credit sanctioning process	337	3.82	.952
4. Reduction in processing effort per loan application	337	3.54	.893
5. Regular rating reviews	337	3.99	.816
6. Reduction of subjectivity in credit rating	337	3.56	.878
7. Internal audits	337	4.00	.730
8. Risk-based appraisal and sanctions	337	4.06	.752
9. Independence of loan review mechanism	337	3.95	.850
10. Implementation of KYC norms	337	4.31	.801
11. Multi-tier credit approval process	337	4.07	.884
12. Focused attention on problem/weak credit exposures	337	3.87	.871

Table VIII. Rotated Component Matrix & Factor Loadings-Risk Mitigation Measures

	Component	
	Improving CRM systems	Improving internal controls
1. Regular discussions, reviews and feedback.	.439	
2. Restriction on responsibility for volume-based credit approvals and reviews.	.480	
3. Independence of credit risk assessment from credit sanctioning process.	.662	
4. Reduction in processing effort per loan application.	.722	
5. Regular rating reviews.	.550	
6. Reduction of subjectivity in credit rating.	.650	
7. Internal audits.		.642
8. Risk-based appraisal and sanctions.	.526	
9. Independence of loan review mechanism.	.686	
10. Implementation of KYC norms.		.777
11. Multi-tier credit approval process.		.776
12. Focused attention on problem/weak credit exposures.	.528	

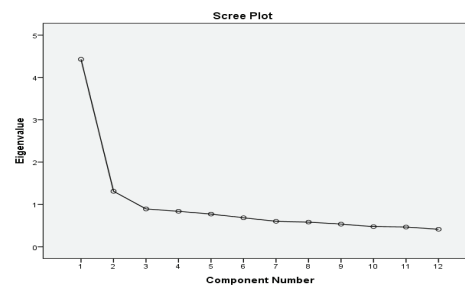


Figure 4: Scree Plot of Risk Mitigation Measures.

Again surrogate variables and factor scores approaches were adopted to analyze the risk perception of bank managers on these two components. ANOVA/F tests and Tukey's HSD post-hoc tests conducted to find the statistically significant different perceptions among managerial groups.

Surrogate Variables Approach. The two surrogate risk mitigation variables for each of the two factors are:

1. Reduction in processing effort per loan application (factor loadings 0.722).
2. Implementation of KYC norms (factor loadings 0.777).

The results of one-way analysis of variance (ANOVA) on three groups of credit managers, managers in large and small PSBs, managers with different

managers at different levels of management showed that perceptions of risk managers for 'Reduction in Processing Effort per Loan Application' were significantly different for all the three groups of managers. Whereas their perceptions for 'Implementation of KYC Norms' was not statistically significant for any group of managers. To find exactly in which managerial group, the differences for 'Reduction in Processing Effort per Loan Application' were significant, Tukey's post-hoc tests together with F test, revealed significant differences in risk perceptions:

1. Between large (mean 3.66, S.D. 0.833) and small banks' managers (mean 3.42, S.D. 0.938), showing better satisfaction in large PSBs towards effectiveness of this risk mitigation measure.

2. Between 'up to 7 years' (mean 3.35, S.D. 0.913) and 'above 20 years' (mean 3.76, S.D. 0.753) banking experience groups, but not between them with '8 to 20 years' (mean 3.53, S.D. 0.980) experience group of risk managers.

3. Between junior credit managers (mean 3.32, S.D. 0.913) and senior level credit managers (mean 3.70, S.D. 0.767), but not between them with middle level managers (mean 3.51, S.D. 0.942).

The statistical results indicated that senior positioned managers, managers with long banking experience and those working in large PSBs were more satisfied that they had been able to reduce loan processing time, may be by better risk inputs, IT networking, data management or sharing of risk information. Though their junior counterparts and managers in small PSBs were not as optimist and wanted more efforts in this regard to rationalize the credit risk assessment operations on each borrower.

Factor Scores Approach. One-way ANOVA (Tables IX to XI) and post-hoc tests (Tables XII & XIII) were conducted on 337 factor scores towards each of the

two factors of risk mitigation measures 'Improving Credit Risk Management Systems' and "Improving Internal Controls' amongst the three groups of credit managers to study the differences in management's risk perceptions. The results indicated that there were statistically significant differences in perceptions of all managerial categories towards 'Improving Credit Risk Management Systems' factor and none for the other factor 'Improving Internal Controls'.

Table IX. ANOVA of Risk Mitigation Factors by Bank Size

		Sum of Squares	df	Mean Square	F	Sig.
1. Improving Credit Risk Management Systems.	Between Groups	12.203	1	12.203	12.625	.000
	Within Groups	323.797	335	.967		
	Total	336.000	336			
2. Improving internal controls.	Between Groups	.576	1	.576	.576	.449
	Within Groups	335.424	335	1.001		
	Total	336.000	336			

Table X. ANOVA of Risk Mitigation Factors by Experience of Managers

		Sum of Squares	df	Mean Square	F	Sig.
1. Improving Credit Risk Management Systems	Between Groups	11.380	2	5.690	5.854	.003
	Within Groups	324.620	334	.972		
	Total	336.000	336			
2. Improving internal controls	Between Groups	1.054	2	.527	.525	.592
	Within Groups	334.946	334	1.003		
	Total	336.000	336			

Table XI. ANOVA of Risk Mitigation Factors by Levels of Management

		Sum of Squares	df	Mean Square	F	Sig.
1. Improving Credit Risk Management Systems	Between Groups	7.354	2	3.677	3.737	.025
	Within Groups	328.646	334	.984		
	Total	336.000	336			
2. Improving internal controls	Between Groups	1.056	2	.528	.527	.591
	Within Groups	334.944	334	1.003		
	Total	336.000	336			

Table XII. Post-hoc Multiple Comparisons

Dependent Variable: Factor-Improving Credit Risk Management Systems.

Tukey HSD

(I) Banking Experience(years)	(J) Banking Experience(years)	Mean Difference (I-J)	Std. Error	Sig.	95% Confidence Interval Lower Bound	Upper Bound
Upto 7 years	8 to 20 years	-.17425809	.1379038	.417	-.4989128	.1503966
	Above 20 years	-.42294278	.1238547	.002	-.7145230	-.1313626
8 to 20 years	Upto 7 years	.17425809	.1379038	.417	-.1503966	.4989128
	Above 20 years	-.24868470	.1405069	.181	-.5794676	.0820982
Above 20 years	Upto 7 years	.42294278	.1238547	.002	.1313626	.7145230
	8 to 20 years	.24868470	.1405069	.181	-.0820982	.5794676

*. The mean difference is significant at the 0.05 level.

Table XIII. Post-hoc Multiple Comparisons

Dependent Variable: Factor-Improving Credit Risk Management Systems.

Tukey HSD

(I) Management Level	(J) Management Level	Mean Difference (I-J)	Std. Error	Sig.	95% Confidence Interval Lower Bound	Upper Bound
Junior Managers	Middle Level Managers	-.00337565	.15857448	1.000	-.3766933	.3699420
	Senior Level Managers	-.31997956	.16992746	.145	-.7200245	-.0800654
Middle Level Managers	Junior Managers	.00337565	.15857448	1.000	-.3699420	.3766933
	Senior Level Managers	-.31660391	.12108865	.025	-.6016720	-.0315358
Senior Level Managers	Junior Managers	.31997956	.16992746	.145	-.0800654	.7200245
	Middle Level Managers	.31660391	.12108865	.025	.0315358	.6016720

*. The mean difference is significant at the 0.05 level.

For first factor 'Improving credit risk management systems', ANOVA on factor scores for each of the 337 respondents showed F was 12.625 (df 1,335) at $p=.000$ for large vs. small PSB credit managers (Table IX). For different experience groups, F was 5.854 (df 2,334) at $p=.003$ (Table X). For different management levels, F was 3.737 (df 2,334) at $p=.025$ (Table XI). ANOVA and Tukey's post hoc tests revealed significant differences in risk perceptions for this factor:

1. Between large and small PSBs.
2. Between credit managers 'up to 7 years' and 'above 20 years' banking experience groups only.
3. Between middle level and senior level credit managers, but not between them with junior level managers.

The mean scores analysis of all variables under the factor 'Improving credit risk management systems' for risk mitigation showed that except for 'Regular discussions, reviews and feedback' higher scores had been given by the large banks' managers on all variables.

Thus credit managers at large PSBs are most satisfied with their CRM systems to improve credit risk mitigation. Small banks' credit officers though feeling positive about regular discussions and feedback systems, were feeling need for improvement in other CRM systems and processes. Similarly, managers with lower banking experience and at junior managerial positions who had more operational responsibilities were feeling that higher loan processing time, more scope of subjectivity in credit ratings, and weak focus on problem loans among other things was hampering their CRM systems and procedures in mitigating credit risk, though they were more satisfied with their banks' internal audit systems than their senior counterparts. For the second factor/component, the mean score differences in managerial perceptions or opinions was not statistically significant, only random or chance differences.

Conclusions and managerial implications

The study has investigated the managerial perceptions of different categories of risk and credit managers engaged in commercial bank credit in Indian PSBs, on problems/ obstacles in credit risk management and on effectiveness of their risk mitigation measures. Understanding perceptual processes is fundamental in understanding the impact perception has on decision-making. The study provides empirical evidence that the small Indian public sector banks were facing more problems and obstacles in managing credit risk and require better risk inputs and restructuring of various credit appraisal and loan review processes.

They are feeling short on resources, training and HR development, data management and IT support, finding disintegration across departments and inconsistencies in risk rating approaches more than the large PSBs. On effectiveness of risk mitigation measures in their banks, though they are more satisfied than large PSBs regarding regular discussions and feedback systems, they are not perceiving as good on responsibility framework for loan approvals, separation of risk assessment from loan sanctions, focused attention on problem loans, on reduction in subjectivity in credit ratings and loan processing time.

The study has also observed statistically significant perceptual differences between junior and senior level credit managers, and between 'up to 7 years' and '20 years and above' categories of managers on CRM obstacles, and between middle and senior level managers on risk mitigation measures in all banks.

Further problems and obstacles in credit risk management are being felt more seriously at senior levels. Since the banks shall maintain high standards of CRM practices for achieving competitive

advantage and good asset quality, and since credit risk management is highly subjective, there is an emergent need that senior managers provide for efficient channels of communications between all operative and managerial levels, enhance consistent access to risk information, business related trainings, update data management and IT capabilities. There is also the need rigorous feedback and staff accountability framework, and continuous watch on compliance of credit risk policy and procedures. Risk audit of banks' risk management systems and procedures would also provide banks with good feedback for reduction in processing effort, subjectivity in ratings or on restructuring of risk departments. As Lepus (2004) suggested, there should be active board and senior management oversight, comprehensive internal controls and there should be strategy, policy and business processes alignment.

References

- Al-Tamimi, H., and Al-Mazrooei, F.M. (2007). Banks risk management - A comparison study of UAE national and foreign banks. *Journal of Risk Finance*, 8(2): 394-409.
- Bhavaniprasad, G.V., and D. Veena. (2011). NPA reduction strategies for commercial banks in India", *International Journal of Management and Business Studies*, 1 (3), Retrieved from [http:// www.ijmbs.com](http://www.ijmbs.com)
- Cheah, E. (2012). Managerial decision – making. *Cross-sections*, 8:19-27, Retrieved from <http://www.eview.anu.edu.au>
- Das, Abhiman., and Ghosh, S. (2007). Determinants of credit risk in Indian state owned banks: An empirical investigation. RBI, Retrieved from <http://www.mpra.uni-muenchen.de/17301>
- Gewald, H., Wullenweber, K., and Weitzel, T. (2006). The influence of perceived risks on banking managers' intention to outsource business processes – A study of the German banking and finance industry. *Journal of Electronic Commerce Research*, 7 (2):78-96.
- Ghosh, Saibal. (2011). A Simple index of banking fragility: Application to Indian data. *Journal of Risk Finance*, 12 (2):112- 120.
- Greuning, H.V., and Bratanovic, S.B. (2009). *Analysing banking risk: A framework for assessing corporate governance and financial risk*. 3rd Ed., Washington D.C: The World Bank.
- JIN, Jia-jia. (2011). Commercial bank credit risk management based on grey incidence analysis. Retrieved from <http://www.IEEE.com>
- Kumar, A. R., and Kotreshwar, G. (2005). Risk management in commercial banks :A case study of public and private sector banks. Conference paper - Ninth Capital Market Conference, December 19/20, Mumbai , Retrieved from [http:// www.ssrn.com](http://www.ssrn.com)
- Lau, M.H. (2006). Research on the relationship between risk perception, risk propensity and risk-reducing decision-making in an e-government environment. Thesis: 1-83, Erasmus University of Rotterdam, Retrieved from <http://www.jbisa.nl>
- Lehman, B. (2003). Is it worth the while- The relevance of qualitative information in credit rating", Working Paper Series, Centre of Finance and Econometrics, KANSTANZ, Germany, 17 April.
- Lepus, S. (2004). Best practices in strategic credit risk management: 1-26, October, USA:SAS.
- Lin, P. W., and Mei, A.K. (2006). The internal performance measures of bank lending: A value-added approach. Benchmarking:

An International Journal, 13(3): 272-289.

MacGregor, D.G. (1994). Risk perception, communication and community relations. Decision Research, Workshop Report no. 94-11: 1-29, Eugene, Oregon.

Njanike, K. (2009). The impact of effective credit risk management on bank survival. Economics, Annals of University of Petrosani, 9(2):173-184.

Oesterreichische National Bank, Vienna, Austria. (2004) .Guidelines on credit approval process and credit risk management. Retrieved from <http://www.oenb.at>

RBI. (2010-2014). Financial stability reports and reports on trends and progress of banking in India, Retrieved from <http://rbidocs.rbi.org.in>

Thiagarajan, S., Ayyappan., and Ramachandran. (2011). Credit risk determinants of public and private sector banks in India. European Journal of Economics, Finance and Administrative Sciences, 34:147-153.

Ms. Renu Arora
Assistant Professor in Commerce
Mata Sundri College for Women,
University of Delhi, New Delhi,
India.
e-mail: 28.renuarora@gmail.com

Dr. Archana Singh
Assistant Professor
Delhi School of Management,
Delhi Technological University, India.
e-mail: sarchana03@yahoo.co.in

Copyright of Skyline Business Journal is the property of Skyline University College and its content may not be copied or emailed to multiple sites or posted to a listserv without the copyright holder's express written permission. However, users may print, download, or email articles for individual use.

Photovoltaic effect in BiFeO₃/BaTiO₃ multilayer structure fabricated by chemical solution deposition technique

Savita Sharma, Monika Tomar, Ashok Kumar, Nitin K. Puri, Vinay Gupta



PII: S0022-3697(16)30033-6
DOI: <http://dx.doi.org/10.1016/j.jpcs.2016.02.010>
Reference: PCS7731

To appear in: *Journal of Physical and Chemistry of Solids*

Received date: 14 September 2015

Revised date: 19 January 2016

Accepted date: 11 February 2016

Cite this article as: Savita Sharma, Monika Tomar, Ashok Kumar, Nitin K. Puri and Vinay Gupta, Photovoltaic effect in BiFeO₃/BaTiO₃ multilayer structure fabricated by chemical solution deposition technique, *Journal of Physical and Chemistry of Solids*, <http://dx.doi.org/10.1016/j.jpcs.2016.02.010>

This is a PDF file of an unedited manuscript that has been accepted for publication. As a service to our customers we are providing this early version of the manuscript. The manuscript will undergo copyediting, typesetting, and review of the resulting galley proof before it is published in its final citable form. Please note that during the production process errors may be discovered which could affect the content, and all legal disclaimers that apply to the journal pertain.

Photovoltaic effect in BiFeO₃/BaTiO₃ multilayer structure fabricated by Chemical solution deposition technique

Savita Sharma^{1,3}, Monika Tomar², Ashok Kumar⁴, Nitin K. Puri³ and Vinay Gupta^{1*}

¹Department of Physics and Astrophysics, University of Delhi, Delhi, INDIA,

²Physics Department, Miranda House, University of Delhi, Delhi, INDIA,

³Department of Applied Physics, Delhi Technological University, Delhi, INDIA,

⁴CSIR-National Physical Laboratory, Dr. K.S .Krishnan Marg, Delhi, INDIA

Email: *vgupta@physics.du.ac.in, drguptavinay@gmail.com

ABSTRACT

Photovoltaic (PV) properties of bismuth ferrite (BFO) and barium titanate (BTO) multilayered ferroelectric BFO/BTO/BFO/BTO thin film structure deposited on Pt/Ti/SiO₂/Si substrates using chemical solution deposition technique are presented. X-ray diffraction analysis confirms pure phase polycrystalline nature of deposited perovskite multilayered structures. Simultaneously both distorted rhombohedral (R3c) and tetragonal phases (P4mm) of the respective BFO and BTO components are also well retained. The ferroelectric sandwiched structures grown on fused quartz substrates exhibit high optical transmittance (~70%) with an energy band gap 2.62 eV. Current-voltage characteristics and PV response of multilayered structures is determined in metal-ferroelectric-metal (MFM) capacitor configuration. Considerably low magnitude of dark current density 1.53×10^{-7} A at applied bias of 5 V establish the resistive nature of semi-transparent multilayered structure. Enhanced PV response with 40 nm thin semitransparent Au as top electrode is observed under solid-state violet laser illumination (λ - 405nm, 160 mW/cm²).

The short circuit current density and open circuit voltage are measured to be $12.65 \mu\text{A}/\text{cm}^2$ and 1.43 V respectively with a high retentivity. The results obtained are highly encouraging for employing artificial multilayered engineering to improve PV characteristics.

INDEX TERMS — Multilayered structure, chemical solution deposition, perovskite, ferroelectric photovoltaic.

Introduction

Harnessing solar energy as an alternative to compensate the depleting non renewable energy resources is a technological field with great potential. Silicon-based photovoltaic (PV) technology [1] has dominated the Solar cell Industry over the years and continues to foster till date. Photovoltaic (PV) devices converting light into electrical energy mostly employ semiconducting materials; however ferroelectric materials are equally competent owing to their internal built-in electric field [1]. Unlike PV effect in the case of conventional p-n junction based photocells, ferroelectric materials do not involve fabrication of complex p-n junction and band-gap constrained photo-voltage [1]. Ferroelectric materials exhibit unique features namely large photovoltaic voltage, photocurrent proportional to polarization magnitude and electric field controlled photovoltaic response, which make them favorable for Photovoltaic applications [2-8]. Several research groups have aimed at improving the polarization and tailoring the bandgap to harness energy in the visible wavelength range. Among various environment friendly ferroelectric materials available, BiFeO_3 (BFO) and BaTiO_3 (BTO) with perovskite structure exhibit large spontaneous polarization. BTO is one of the most exhaustively studied ferroelectric materials because of its superior dielectric and ferroelectric properties utilized for electronic and electro-optic device applications [6,9-10]. BTO in both crystal and bulk form has also been

studied for photovoltaic effect [10-11] however, not much work has been proposed for BTO thin film based devices. Furthermore, the wide band gap of BTO (~ 3.5 eV) limits its usage [6], and demands sincere efforts in the direction of tailoring its band gap for applications in the visible range. On the other side, BFO is the single-phase room temperature multiferroic material having high ferroelectric Curie temperature (~ 1120 K) and antiferromagnetic Neel temperature (~ 640 K) [12]. Although, BFO due to its narrow band gap, is an efficient photovoltaic material functional in the visible spectrum [4,7], its high leakage current poses problems for reliable device performance [13-15]. Hence, properties of both BFO and BTO need to be modified for probable photovoltaic applications. Various efforts have been made either by doping the ferroelectric materials or by using modified design structure of photovoltaic cell to overcome the mentioned issues [16-21]. A plausible multilayered structure of BFO and BTO seems to be attractive for attaining high electric polarization and accomplishing band gap narrowing. Further the interfacial strain induced between the BFO and BTO thin films may result in a high value of open circuit voltage. Prihor et al. have investigated the functional properties of $(1-x)\text{BiFeO}_3-x\text{BaTiO}_3$ solid solutions exhibiting magneto-electric coupling, with both magneto-capacitance and magneto-resistance phenomena [22]. Multiferroic studies on $(\text{BiFeO}_3)_m(\text{BaTiO}_3)_n$ superlattice structure overcoming the hindrances experienced in utilizing the individual BFO single layer thin films has been demonstrated by Ranjith et al. [23]. Enhanced values of polarization and photovoltaic parameters have been previously reported on either single crystal BFO or BFO thin films grown on epitaxially matched substrates like SrTiO_3 (STO), Fluorine-doped tin oxide $\text{SnO}_2:\text{F}$ (FTO) or SrRuO_3 (SRO) only [17,18]. Polycrystalline BTO thin film is reported to possess more depolarization field compared to polycrystalline BFO thin film. The motivation of introduction of BTO layers into BFO material is to reduce the leakage current in

the resultant multilayer structure. Negligible efforts have been made towards the realization of photovoltaic response of BFO/BTO multilayered thin film system. Thus, in the present work, BFO/BTO multilayered structure has been prepared on Pt/Ti/SiO₂/Si substrate by low cost chemical solution deposition technique and its photovoltaic properties have been investigated. Our preliminary results on enhanced photovoltaic response can be attributed to the high degree of polarization and reduced leakage current (dark current) achieved for the multilayered structure.

Experimental details

Multilayered structure of BFO/BTO were spin coated on platinized silicon (Pt(90nm)/Ti(10nm)/SiO₂/Si) substrate in ambient conditions. High purity (>99.9%) raw materials barium acetate (Ba(CH₃COO)₂), bismuth nitrate pentahydrate ((Bi(NO₃)₃·5H₂O), iron nitrate nanohydrate ((Fe(NO₃)₃·9H₂O), titanium n-butoxide (Ti(C₄H₉O)₄) as precursor and glacial acetic acid, 2-methoxyethanol as solvents with acetylacetone being chelating agent were procured from Alfa Aesar and used for preparing respective BTO and BFO solutions. To start, BTO solution was spin coated on Pt/SiO₂/Si substrate at 3000 rpm for 20 seconds. Thus, deposited BTO first layer was pyrolysed at 300°C for 5 min and subsequently annealed at 800°C for 1 hour followed by deposition of BFO thin film as second layer, is described elsewhere [24]. Similar process is repeated to get four layered structure namely BFO/BTO/BFO/BTO on Pt/Ti/SiO₂/Si substrate with total thickness 350 nm, keeping thickness of each layer approximately to 87 nm. For electrical and ferroelectric measurements, circular top electrodes of Au of 600 μm diameter and 40 nm thickness were thermally evaporated using a shadow mask on the surface of multilayered structure and subsequently in MFM capacitor configuration (Au/BFO/BTO/BFO/BTO/Pt/Si) is prepared. Figure 1 presents schematic cartoon of deposited

multilayered capacitor of BFO/BTO/BFO/BTO for better visualization, where the encircled area presents the magnified view of the capacitor configuration. The crystalline structure of prepared thin films was confirmed using X-ray diffraction (XRD) technique (Ultima 4 Rigaku). Optical transmission properties were studied by UV-Visible spectrophotometer (Lambda 35 Perkin Elmer). Precision ferroelectric workstation (Radiant Technology) was employed to determine room temperature ferroelectric behavior of prepared multilayered sample in MFM capacitor configuration at a frequency of 1 kHz and applied bias of 20 V. Current-voltage (I-V) characteristics were determined using semiconductor characterization system (4200 Keithley) with and without illumination of violet laser light (405 nm) of 160 mW/cm^2 intensity.

Results & discussion

Figure 2 plots the XRD pattern of prepared BFO/BTO/BFO/BTO multilayered structure deposited on Pt/SiO₂/Si substrate, obtained in range $2\theta = 20^\circ - 60^\circ$ under Bragg-Brentano geometry. Polycrystalline nature of both BTO and BFO component thin films in multilayered structure is clearly evident whereas perovskite structure of individual layers is also well retained. The BFO and BTO thin films in the multilayered structure crystallized respectively in distorted rhombohedral (R3c) and tetragonal (P4mm) phase [24-25] according to JCPDS/ICDD no. 01-072-0138 and 01-072-2035 respectively. All peaks in XRD pattern corresponds to either BFO or BTO, affirms the absence of parasite and secondary phase [13, 24-25], indicating the growth of single phase materials owing to optimization of temperature processing and sol preparation. Whereas, the strong XRD peaks at $2\theta \sim 40^\circ$ and 54° corresponds to underneath Pt layer and Si substrate respectively. The lattice parameters of BFO and BTO in multilayered thin film structure were calculated by Le-Bail fitting using Bruker-Topas 3 software. The lattice

parameters (a, c) of bulk and multilayered film, c/a distortion ratio along with induced strain along 'c' axis in multilayered thin film, have been summarized in Table 1. The stress modulus in the BFO/BTO multilayer structures is obtained using equation $\text{stress} = (c_0 - c)/c_0$ in %, where "c" is the respective lattice constant of BFO or BTO in deposited multilayered film and " c_0 " is the corresponding bulk value. The value of stress modulus (%) of BTO and BFO were found to be about 0.446% and 2.055% respectively for the BFO/BTO four layered thin film structure. The introduction of stress modulus in BTO and BFO increase the lattice distortion and thus lead to an improvement in ferroelectric properties.

Figure 3 shows the optical transmission spectra of BFO/BTO/BFO/BTO multilayered structure deposited on fused quartz substrate grown under similar deposition conditions. Deposited multilayered structure on quartz substrate was found to be highly transparent (>70%) in higher wavelength region (> 600 nm) depicts good optical quality. Inset in Fig. 3 shows the Tauc plot, $(\alpha h\nu)^2$ versus photon energy (h ν) calculated for multilayered structure where α is absorption coefficient, h is Planck's constant and ν is frequency of the incident photons. Thereby, extrapolation of the linear portion in Tauc plot results into optical band gap ($E_g \sim 2.62 \text{ eV} \pm 0.01 \text{ eV}$) of the multilayered structure, which is considerably lower than the reported values of optical band gap of BTO (3.5 eV) and BFO (2.67 eV) thin films available in literature [1,26]. The optical bandgap of multilayered film is determined by BFO layers with small optical gap because of the transparent BTO layers. The low value of band gap obtained for the multilayered structure in the present work is not only advantageous for photovoltaic applications in the visible region but also outlines the role of artificial multilayer engineering for successful band gap tuning. In the optical bandgap modification, major role is being played by BFO with BTO being

transparent. On the other hand, BTO is reducing the leakage current of the multilayered structure useful for obtaining enhanced ferroelectric polarization and photovoltaic response. Thus, the presence of BFO thin film has been beneficial in reducing the band gap of the multilayered structure.

Figure 4 shows the room temperature polarization-electric (P-E) hysteresis loop of multilayered structure obtained at an applied bias of 20 V and 1 kHz frequency. Multilayered structure exhibits non-lossy ferroelectric hysteresis loop with high saturation polarization ($2P_s = 100 \mu\text{C}/\text{cm}^2$), remnant polarization ($2P_r = 67.26 \mu\text{C}/\text{cm}^2$) and low coercive field ($2E_c = 13.42 \text{ kV}/\text{cm}$). Such high value of saturation polarization obtained in the multilayered thin film structure is attributed to alternative presence of highly ferroelectric BTO layer with induced interfacial strain owing to lattice mismatch and low leakage current density. Furthermore, the observed asymmetry in the hysteresis loop may ascribed to the presence of different top and bottom metal electrodes in the multilayered capacitor structure. While the hysteresis loop is asymmetric, the hysteresis loop of the multilayer capacitor begins from a negatively polarized state ~a negative polarization value in Fig. 4 with increasing a positive voltage from zero. The hysteresis loop BFO/BTO multilayer capacitor also ends at a negatively pulsed state. Since any switching voltage has not been applied to the BFO/BTO multilayer capacitor before the initial hysteresis loop measurement, we conclude that the BFO/BTO multilayer capacitor is highly polarized with the positive end of the polarization to the top electrode of the multilayer capacitor ~negatively poled state, as shown in Fig. 4. This kind of asymmetry in hysteresis loops have been shown by many other workers [27-31].

Hence, it may be inferred that the multilayered structure of BTO and BFO exhibit better ferroelectric properties with low optical band gap for better ferroelectric PV response.

Figure 5 displays the room temperature current density – voltage (J–V) characteristics of Au/BFO/BTO/BFO/BTO/Pt multilayered capacitor measured under dark and light illumination ($\lambda = 405$ nm) condition as well. Present multilayer exhibit high resistive behavior with much lower dark leakage current density 1.53×10^{-7} A at applied bias of 5 V than reported results [17]. As expected, J–V curve under light illumination ($\lambda = 405$ nm and intensity = 160 mW/cm²) shows approx. two order enhancement in current density over the entire measured range of applied bias of ± 6 V showing typical photovoltaic effect. The photovoltaic open-circuit voltage (V_{oc}) and short-circuit current density (J_{sc}) are determined from the intercepts of the horizontal and the vertical axes, respectively of Fig. 5. The values of J_{sc} and V_{oc} are measured to be about 12.65 μ A/cm² and 1.43 V, considerably larger than those reported by other workers for photovoltaic cell having single layer of ferroelectric materials [BFO (0.4 V) and BaTiO₃ (1.07 V)] [6,7]. It is well known fact that the magnitude of J_{sc} and V_{oc} , in case of ferroelectric thin films depend largely on the built-in electric field caused by the remnant polarization [1,7,24-25]. Thus, the enhanced photovoltaic response observed for multilayered structure having BFO and BTO layers is mainly credited to the higher internal depolarization field owing to large remnant polarization ($2P_r = 67.26$ μ C/cm²). The larger depolarization field separate the photogenerated electrons and holes more effectively and enhance the photovoltaic output for the multilayered structure [1,7,24-25]. It is also important to highlight the negative V_{oc} is observed due to the work function difference between BFO/BTO multilayered structures and top/bottom metal electrodes. Magnitude of photocurrent responsivity (PCR) described as ratio of the short circuit photocurrent density (Acm^{-2}) to the input optical power density ($mWcm^{-2}$) is also calculated from the J-V curve in Fig. 5 and is found to be 1.99 mA W⁻¹ at an input laser power of 160 mWcm⁻². In addition, the transient response characteristics of the photocurrent density measured

at zero bias for BFO/BTO/BFO/BTO multilayered structure in MFM capacitor configuration is plotted in Figure 6. A sharp rise in the current density and subsequently a steady state condition is achieved under the illumination of sample with laser light ($\lambda = 405$ nm) at a regular intervals of 20s (Fig. 6). When the illumination of laser is turned off, the steady state photocurrent decreases sharply and attains the initial low value of dark current (Fig. 6). The observed increase in photocurrent under light illumination is attributed to the generation of electron-hole pairs and subsequently their separation due to the depolarization field. The reproducible transient behavior of photocurrent under repeated laser On and Off cycles confirms the high retentivity of the present multilayered structure capacitor, crucial factor for device fabrication.

Conclusion

Multilayered structure of BFO/BTO prepared via chemical solution deposition technique exhibits intense polycrystalline XRD reflections with no secondary phases. Experimentally obtained optical band gap ($E_g \sim 2.62 \pm 0.01$ eV) is found to be red shifted to when compared to component BFO and BTO thin films hints the successful band gap tuning. Also multilayered structure exhibited sound ferroelectric properties showing typical P-E hysteresis loop with high ($2P_s = 100 \mu\text{C}/\text{cm}^2$) and ($2P_r = 67.26 \mu\text{C}/\text{cm}^2$) respectively. As a consequence, notable improvement in $J_{sc} \sim 12.65 \mu\text{A}/\text{cm}^2$ and $V_{oc} \sim 1.43$ V for multilayered PV cell is observed, attributed to high depolarization field assisted efficient separation of photo-generated charge carriers induced by high remnant polarization and interfacial strain between BFO and BTO layers. Our studies reveal the potential scope of multilayer engineering for future thin film PV industry.

Acknowledgement

Authors are thankful to the research grant provided by the University of Delhi for the financial support. One of the authors (SS) is thankful to the Delhi Technological University (DTU) for the teaching assistantship.

REFERENCES

- [1] Yang S Y, Seidel J, Byrnes S J, Shafer P, Yang C H, Rossell M D, Yu P, Chu Y H, Scott J F, Ager J W, III, Martin L W and Ramesh R (2010) Above-bandgap voltages from ferroelectric photovoltaic devices. *Nature Nanotech* 5:143.
- [2] Chakrabartty J P, Nechache R, Harnagea C and Rosei F (2013) Photovoltaic effect in multiphase Bi-Mn-O thin films. *Optics Express* 22: A80-A89.
- [3] Chen L, Luo B C, Chan N Y, Dai J Y, Hoffman M, Li S and Wang D Y (2014), Enhancement of photovoltaic properties with Nb modified (Bi, Na)TiO₃-BaTiO₃ ferroelectric ceramics. *J Alloys Compnd* 587:339–343.
- [4] Puli V S, Pradhan D K, Katiyar R K, Coondoo I, Panwar N, Misra P, Chrisey D B, Scott J F and Katiyar R S (2014) Photovoltaic effect in transition metal modified polycrystalline BiFeO₃ thin films. *J. Physics D: Appl phys* 47:075502.
- [5] Fan Z, Yao K, and Wang J (2014) Photovoltaic effect in an indium-tin oxide/ZnO/BiFeO₃/Pt heterostructure. *Appl Phys Letters* 105:162903.
- [6] Jiang W, Cai W, Lin Z and Fu C (2013) Effects of Nd-doping on optical and photovoltaic properties of barium titanate thin films prepared by sol-gel method. *Mater Res Bull* 48:3092-3097.
- [7] Gupta S, Tomar M and Gupta V (2014) Ferroelectric photovoltaic properties of Ce and Mn codoped BiFeO₃ thin film. *J Appl Phys* 115:014102.
- [8] Pintilie L, Dragoi C and Pintilie I (2011) Interface controlled photovoltaic effect in epitaxial Pb(Zr,Ti)O₃ films with tetragonal structure. *J Appl Phys* 110:044105.
- [9] Cai W, Fu C, Gao J, Guo Q, Deng X and Zhang C (2011) Preparation and optical properties of barium titanate thin films. *Physica B* 406:3583-3587.
- [10] Vineet S, Dharmadhikari and Grannemann W W (1982) Photovoltaic properties of ferroelectric BaTiO₃ thin films rf sputter deposited on Silicon. *J Appl Phys* 53:8988.

- [11] Chanussot G, Fridkin V M, Godefroy G and Jannot B (1977) The photoinduced Rayleigh scattering in BaTiO₃ crystals showing the bulk photovoltaic effect. *Appl Phys Lett* 31:3-4.
- [12] Ukai Y, Yamazaki S, Kawae T and Morimoto A (2012) Polarization-induced photovoltaic effects in Nd-doped BiFeO₃ ferroelectric thin films. *Jap J App Phys* 51:09LE10.
- [13] Gupta S, Tomar M, Gupta V, James A R, Pal M, Guo R, and Bhalla A (2014) Optimization of excess Bi doping to enhance ferroic orders of spin casted BiFeO₃ thin film. *J Appl Phys* 115:234105.
- [14] Gupta S, Tomar M and Gupta V (2013) Raman spectroscopy of nanocrystalline Mn-doped BiFeO₃ thin films. *J Exp Nanosci* 8(3): 261–266.
- [15] Gupta S, Sharma A, Tomar M, Gupta V and Pal M (2012) Piezoresponse force microscopy and vibrating sample magnetometer study of single phased Mn induced multiferroic BiFeO₃ thin film. *J Appl Phys* 111:064110.
- [16] Dong W, Guo Y, Liu H, Li H and Liu H (2013) Photovoltaic properties of BiFeO₃ thin film capacitors by using Al-doped zinc oxide as top electrode. *Material Letters* 91:359-361.
- [17] Dong W, Guo Y, Liu H, Li H and Liu H (2012) Enhanced photovoltaic properties in polycrystalline BiFeO₃ thin films with rhombohedral perovskite structure deposited on fluorine doped tin oxide substrates. *Mater Lett* 88:140-142.
- [18] Katiyar R K, Misra P, Sahoo S, Morell G and Katiyar R S (2014) Enhanced photoresponse in BiFeO₃/SrRuO₃ heterostructure. *J Alloys Compd* 609:168-172.
- [19] Chen B, Li M, Liu Y, Zuo Z, Zhuge F, Zhan Q F and Li R W (2011) Effect of top electrodes on photovoltaic properties of polycrystalline BiFeO₃ based thin film capacitors. *Nanotech* 22:195201.
- [20] H. Liu H, Zhao K, Zhou N, Lu H, He M, Huang Y, Jin K J, Zhou Y, Yang g, Zhao S, Wang A and Leng W (2008) Photovoltaic effect in micrometer-thick perovskite-type oxide multilayers on Si substrates. *Appl Phys Lett* 93:171911.
- [21] Fan Z, Yao K and Wang J (2014) Photovoltaic effect in an indium-tin-oxide/ZnO/BiFeO₃/Pt heterostructure. *Appl Phys Lett* 105:162903.
- [22] F. Prihor F, Lanculescu A, Mitoseriu L, Postolache P, Curecheriu L, Dragan N and Crisan D (2009) Functional Properties of the (1-x)BiFeO₃-xBaTiO₃ solid solutions. *Ferroelectrics* 391:1 76-82.
- [23] Ranjith R, Luders U, Prellier W (2010) Multiferroic studies on (BiFeO₃)_m(BaTiO₃)_n superlattice structures. *J Phys Chem Solids* 71:1140–1143.
- [24] Sharma S, Tomar M, Kumar A, Puri N K and Gupta V (2014) Photovoltaic properties of BiFeO₃/BaTiO₃ bilayered thin film. *Adv Sci Lett* 20:1316-1320.

- [25] Sharma S, Tomar M, Kumar A, Puri N K and Gupta V (2014) Multiferroic properties of BiFeO₃/BaTiO₃ multilayered thin films. *Physica B: Condensed Matter* 448:125–127.
- [26] Kamalasanan M N, Chandra S, Joshi P C, and Mansingh A (1991) Structural and optical properties of sol-gel processed BaTiO₃ ferroelectric thin films. *Appl Phys Lett* 59:3547-3549.
- [27] Lee J and Ramesh R (1996) Imprint of (Pb,La)(Zr,Ti)O₃ thin films with various crystalline qualities *Appl Phys Lett* 68:484.
- [28] Thomas R, Mochizuki S, Mihara T and Ishida T (2002) Preparation of Pb(Zr,Ti)O₃ thin films by RF-magnetron sputtering with single stoichiometric target: structural and electrical properties. *Thin Solid Films* 413:65–75.
- [29] Auciello O, Mantese L, Duarte J, Chen X, Rou S H, Kingon A I, Schreiner A F and Krauss A R (1993) Synthesis and characterization of Pb (Zr_xTi_{1-x})O₃ thin films produced by an automated laser ablation deposition technique. *Journal of Applied Physics* 73:5197.
- [30] Hu H and Krupanidhi S B (1993) Enhanced electrical properties of ferroelectric Pb(Zr_{0.5}, Ti_{0.5})O₃ thin films grown with low-energy oxygen ion assistance. *J. Appl. Phys.* 74:3373.
- [31] Meng X J, Cheng J G, Sun J L, Tan J, Ye H J, Chu J H (2000) Dependence of texture development on thickness of single-annealed-layer in sol-gel derived PZT thin films. *Thin Solid Films* 368:22-25.

Table captions :

Table 1. Lattice parameters “a” and “c”, c/a distortion ratio and stress modulus in BFO/BTO multilayer thin film structure

	BTO				BFO			
	Lattice parameter		Stress Modulus (%)	c/a distortion ratio	Lattice parameter		Stress Modulus (%)	c/a distortion ratio
	a (Å)	c (Å)			a (Å)	c (Å)		
Bulk	3.999	4.033	---	1.0085	5.876	13.867	---	2.3599
4 layers	4.229	4.051	0.446	0.9579	5.523	13.582	2.055	2.4591

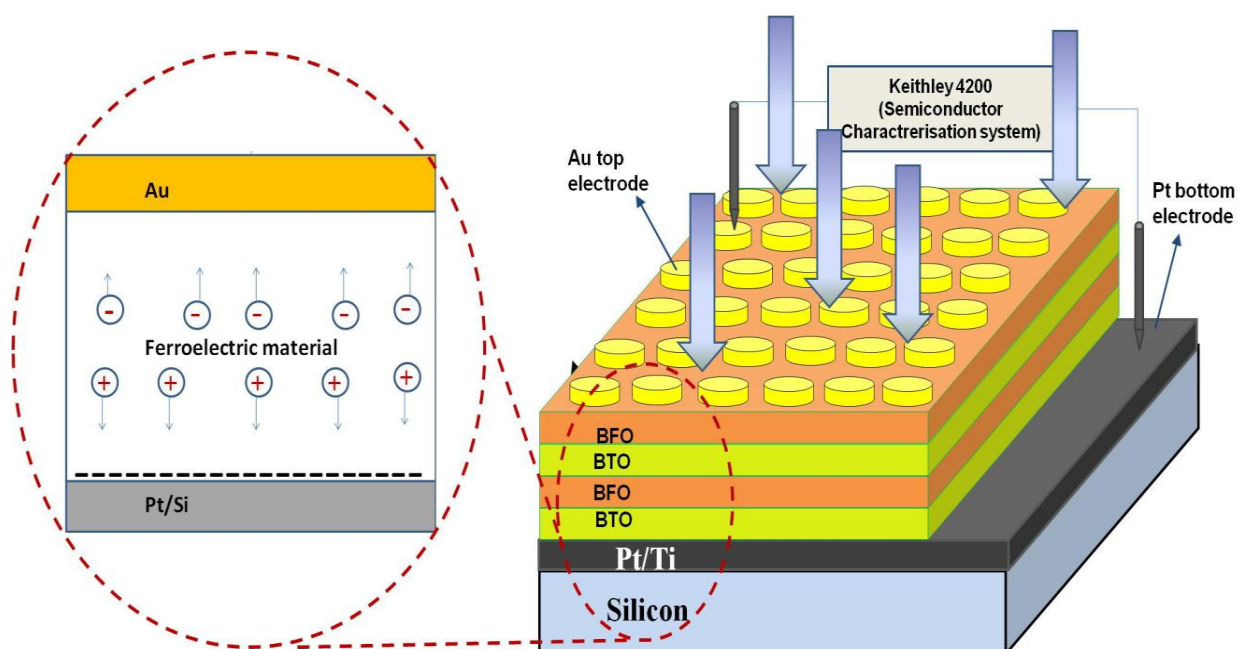


Figure 1. Schematic diagram depicting separation of charge carriers after illuminating light on BFO/BTO multilayered photovoltaic cell due to ferroelectric photovoltaic effect

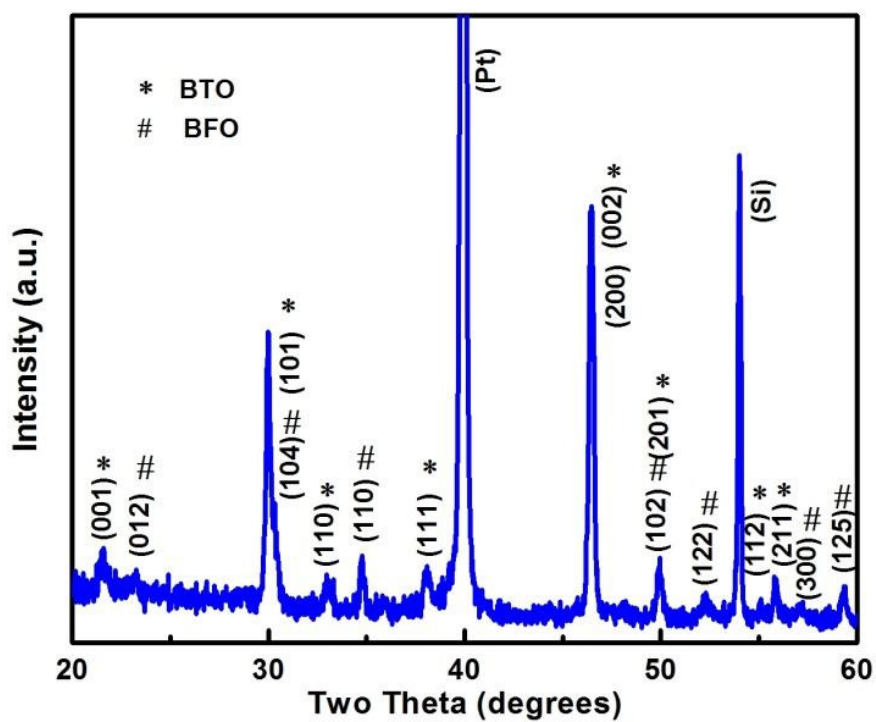


Figure 2. XRD pattern of the prepared BFO/BTO/BFO/BTO multilayered structure deposited on Pt/Ti coated Si substrate

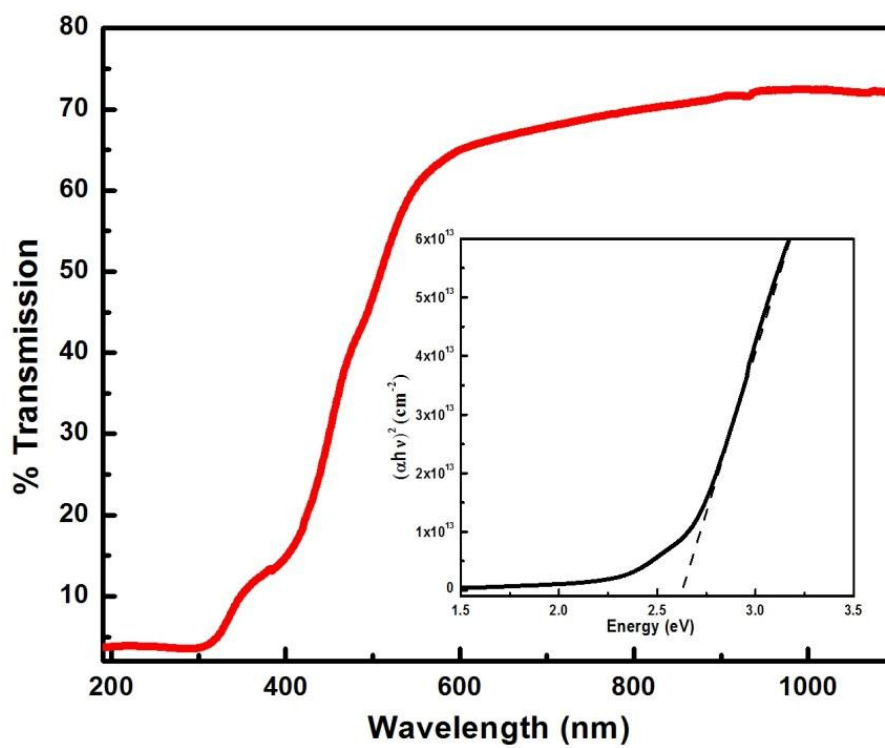


Figure 3. Optical transmission spectra of BFO/BTO/BFO/BTO multilayered structure deposited on fused quartz substrate. Inset shows the Tauc plot of the prepared multilayered system

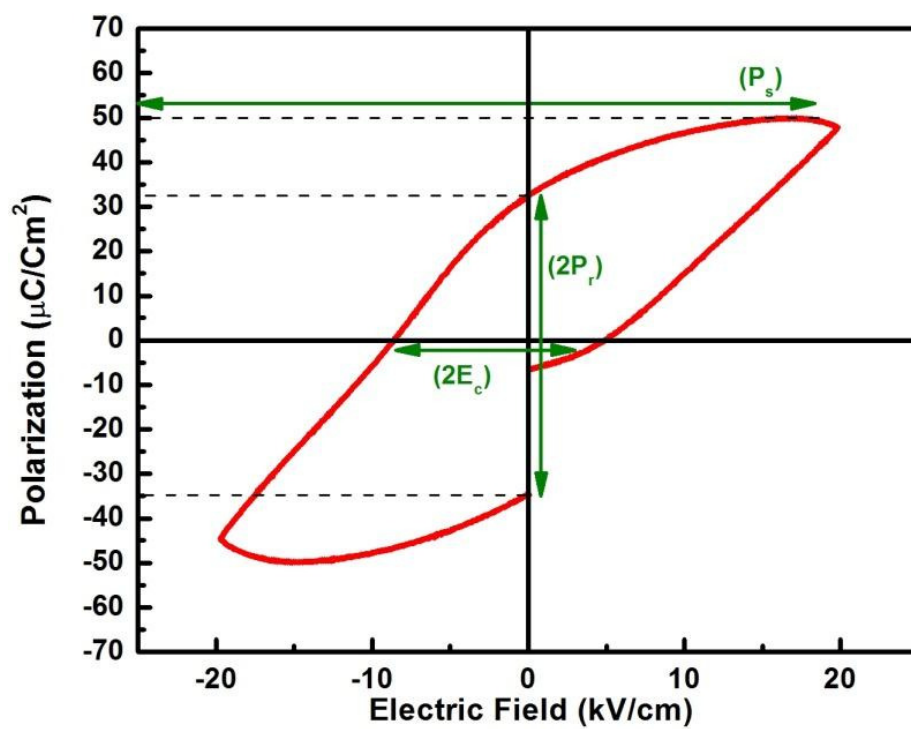


Figure 4. Room temperature ferroelectric P-E hysteresis loop of the multilayered structure in the MFM (Au/BFO/BTO/BFO/BTO/Pt) capacitor configuration

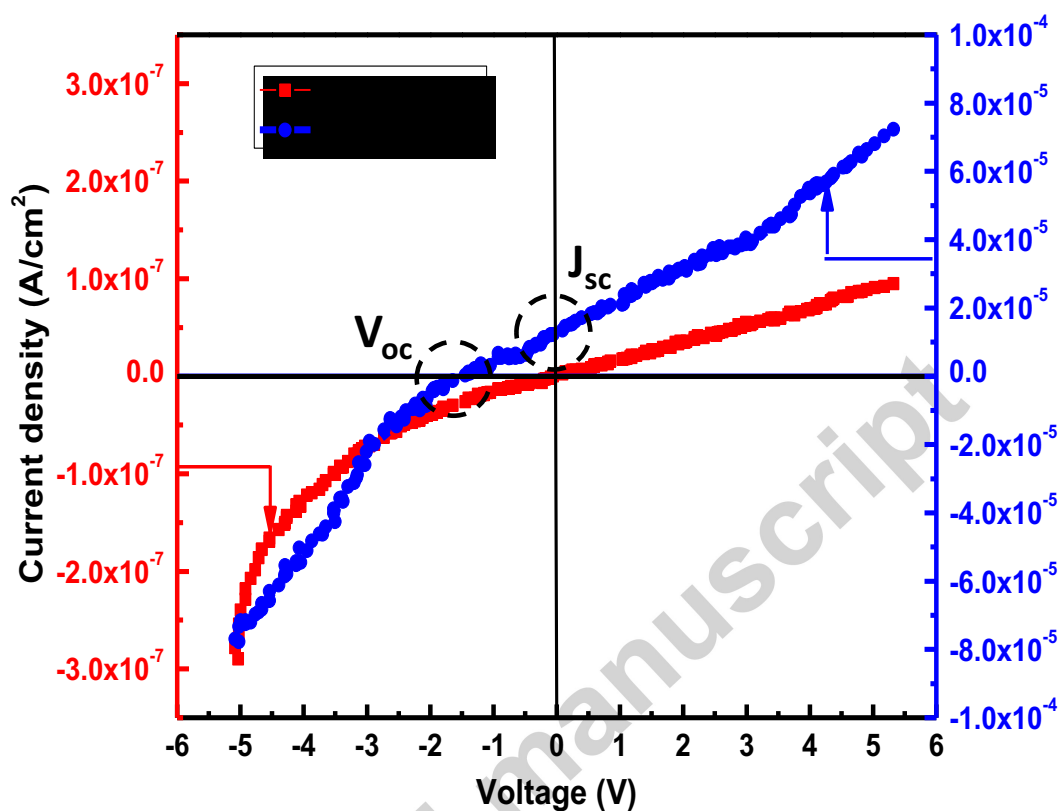


Figure 5. Current density–voltage (J–V) characteristics of the Au/BFO/BTO/BFO/BTO/Pt/Si multilayered sample under both dark condition and light illumination of $\lambda = 405$ nm and intensity = 160 mWcm⁻²

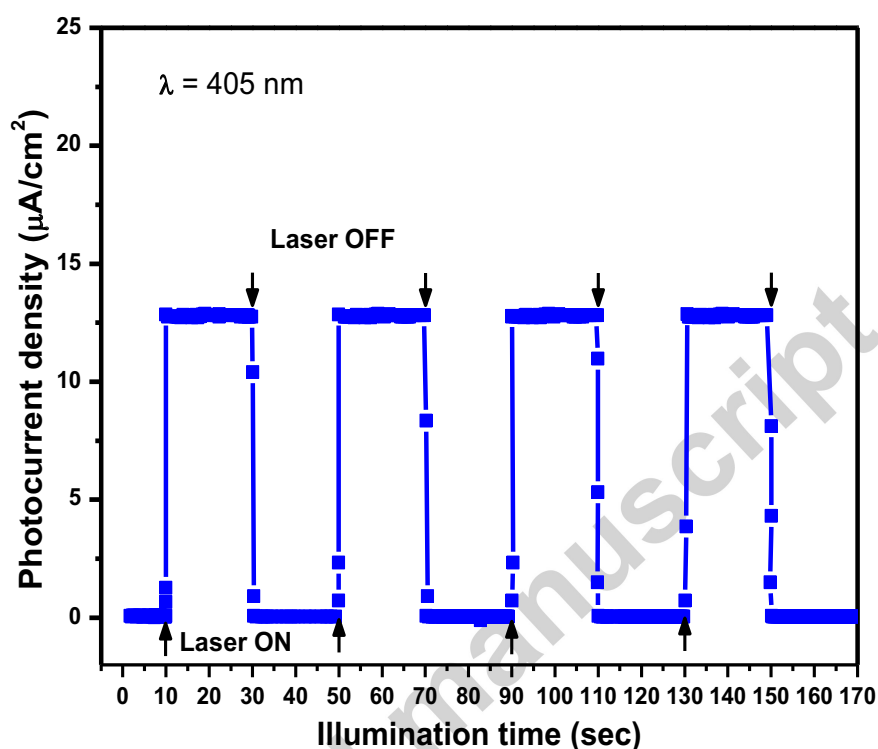
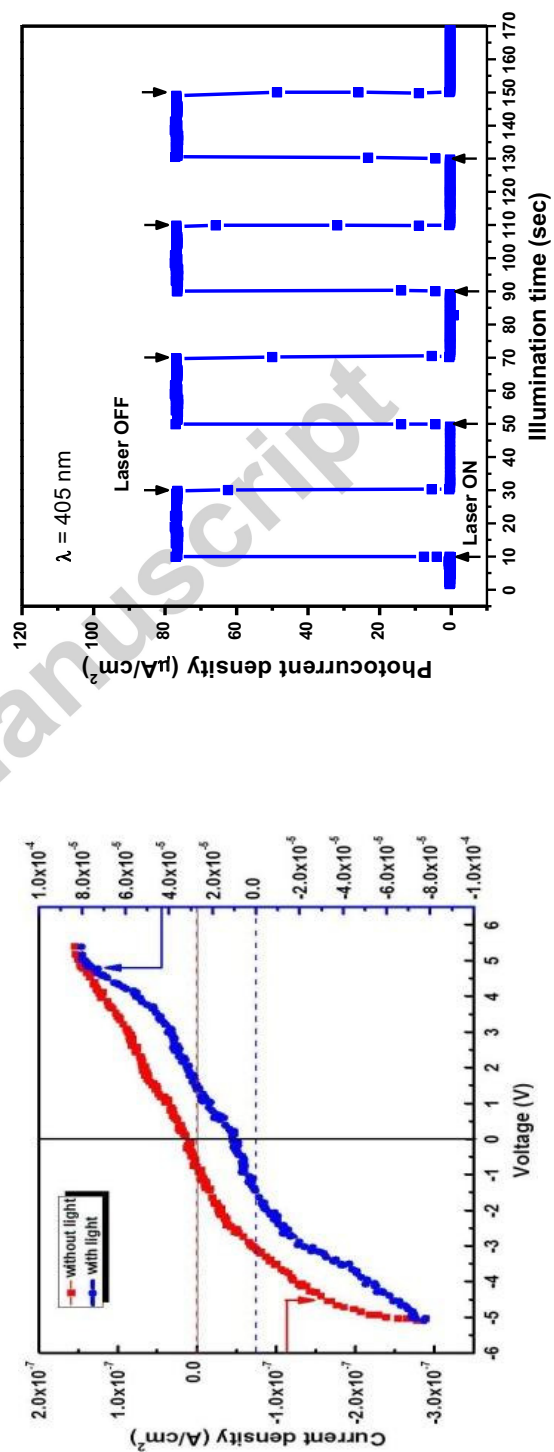
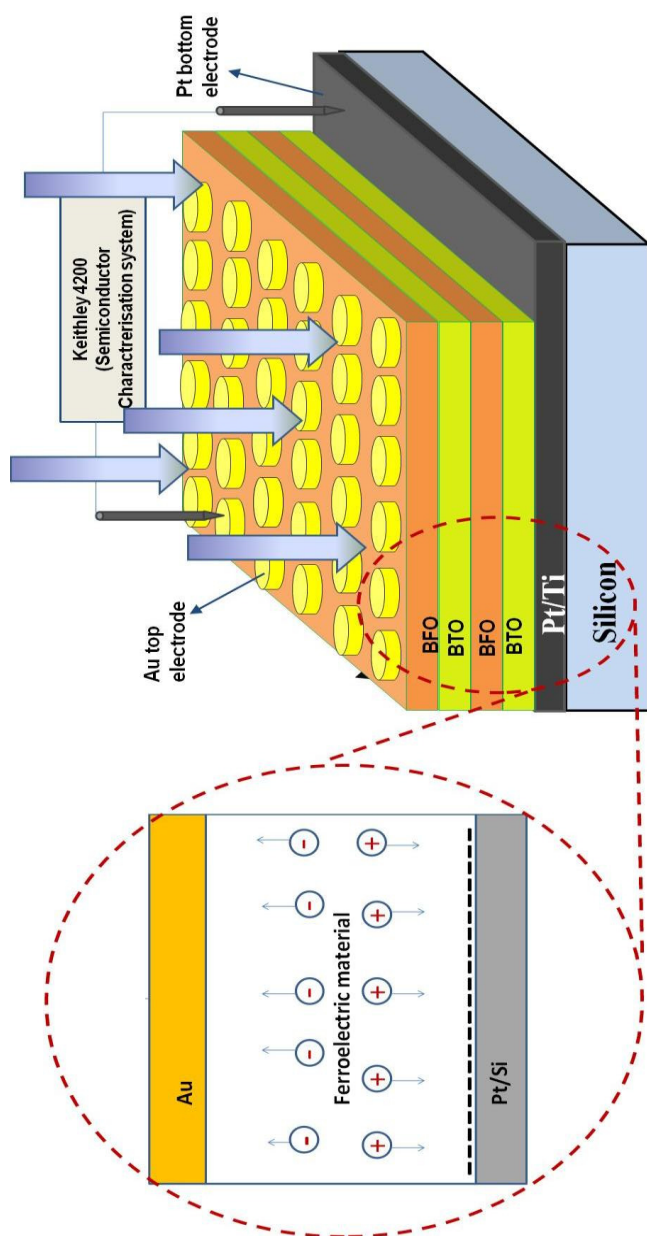


Figure 6. Transient response of short circuit photocurrent density of multilayered structure of BFO/BTO when laser beam ($\lambda = 405 \text{ nm}$ and intensity = $160 \text{ mW}/\text{cm}^2$) is switched on and off at regular intervals of 20s

Highlights

- Bismuth ferrite (BFO) and barium titanate (BTO) multilayered thin films were deposited on Pt/Ti/SiO₂/Si substrates using chemical solution deposition technique.
- The structural and optical properties were studied by X-ray diffraction (XRD) and UV-Visible Spectrophotometer respectively.
- Ferroelectric property of the prepared film was confirmed by PE hysteresis loop measurements.

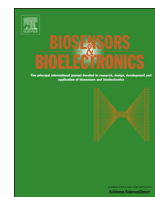
- Photovoltaic response characteristics were studied in metal-ferroelectric-metal (MFM) capacitor configuration (Au/BFO/BTO/BFO/BTO/Pt).
- Enhanced ferroelectric photovoltaic properties are attributed to efficient separation of photogenerated charge carriers due to high depolarization field.
- High depolarization field was due to higher remnant polarization and interfacial strain between BFO and BTO layers.
- The prepared multilayers exhibits enhanced photovoltaic response indicating the realization of an efficient multifunctional structure.





Contents lists available at ScienceDirect

Biosensors and Bioelectronics

journal homepage: www.elsevier.com/locate/bios

Quantum dot monolayer for surface plasmon resonance signal enhancement and DNA hybridization detection

Aditya Sharma Ghrera^a, Manoj Kumar Pandey^b, Bansi Dhar Malhotra^{b,c,*}

^a The Northcap University (Formerly ITM University), Gurgaon 122017, India

^b The DST Centre on Biomolecular Electronics, CSIR-National Physical Laboratory, Dr K S Krishnan Marg, New Delhi 110012, India

^c Department of Biotechnology, Delhi Technological University, Delhi 110042, India

ARTICLE INFO

Article history:

Received 11 December 2015

Received in revised form

27 January 2016

Accepted 5 February 2016

Available online 6 February 2016

Keywords:

Quantum dots

Cadmium selenide

Surface plasmon resonance

Langmuir–Blodgett

Nucleic acid hybridization

Chronic myelogenous leukemia

Biosensor

ABSTRACT

We report results of studies relating to the fabrication of a surface plasmon resonance (SPR)-based nucleic acid sensor for quantification of DNA sequence specific to chronic myelogenous leukemia (CML). The SPR disk surface has been modified with octadecanethiol self-assembled monolayer followed by deposition of the tri-*n*-octylphosphine oxide capped cadmium selenide quantum dots (QD) Langmuir monolayer. The deposition is performed via Langmuir–Blodgett (LB) technique. For the sensor chip preparation, covalent immobilization of the thiol-terminated DNA probe sequence (pDNA) using displacement reaction is accomplished. This integrated SPR chip has been used to detect target complementary DNA concentration by monitoring the change in coupling angle via hybridization. It is revealed that this biosensor exhibits high sensitivity ($0.7859 \text{ m}^0 \text{ pM}^{-1}$) towards complementary DNA and can be used to detect it in the concentration range, 180 pM to 5 pM with detection limit as 4.21 pM. The results of kinetic studies yield the values of hybridization and dissociation rate constants as $9.6 \times 10^4 \text{ M}^{-1} \text{ s}^{-1}$ and $2.3 \times 10^{-2} \text{ s}^{-1}$, respectively, with the equilibrium constant for hybridization as $4.2 \times 10^6 \text{ M}^{-1}$.

© 2016 Elsevier B.V. All rights reserved.

1. Introduction

Chronic myelogenous leukemia (CML) occurs in blood-forming cells of the bone marrow and is characterized by specific reciprocal translocation of chromosomes 9 and 22 (Nowell, 2007), producing BCR-ABL oncogene in the abnormal chromosome 22 (Druker et al., 2001). As BCR-ABL oncogene is tumor-specific, detection of this gene may help in the diagnosis of CML and in monitoring of the patients after bone marrow transplantation. Currently, CML diagnosis is performed via fluorescence *in situ* hybridization, flow cytometry and real-time quantitative reverse transcription polymerase chain reaction (Lee et al., 2002; Saglio and Fava, 2012). Since all these techniques are laboratory based, they require skilled clinicians and are time-consuming thereby causing delay in the therapeutic treatment. Also, the testing of the patient sample cannot be done on a regular basis. To obtain improved monitoring efficacy, there is increased interest towards the development of sensitive and miniaturized biosensors to enable the point of care diagnostics and monitoring of the disease.

For fabrication of highly sensitive biosensors that can be used

for on-line monitoring of biomolecular recognition event, surface plasmon resonance (SPR) technique has recently gained much attention (Nawattanapaiboon et al., 2015; Tahmasebpour et al., 2015; Xiang et al., 2015). Not only does it offer real-time *in situ* analysis of dynamic surface events, but it may also be used to determine rates of adsorption and desorption for a range of surface interactions. SPR sensor excites the metal/dielectric interface via mono- or polychromatic polarized light and generates propagating plasmonic waves. These plasmonic waves are highly sensitive to the refractive index (RI) changes in the sample, which can be directly correlated with the mass density changes on a metal surface, and can be used to measure real-time biomolecular interactions and target quantification. In case of the DNA biosensor, the SPR signal is produced by measuring the RI changes induced by hybridization event. SPR based detection of DNA hybridization has attracted much attention due to applications in medical diagnostics (Cennamo et al., 2015; Singh et al., 2014), biotechnology and life-science research (Huang et al., 2015), agro-food sector (Piliarik et al., 2009; Tran et al., 2013), security and environmental monitoring (Šípová and Homola, 2013).

The SPR is not limited to metals but can also be achieved in semiconductor nanocrystals with appreciable free carrier concentrations. The SPR signal enhancement of Au film has been

* Corresponding author.

E-mail address: bansi.malhotra@gmail.com (B.D. Malhotra).

reported by the electronic coupling of its surface plasmon wave with the localized plasmon of QD. Zayats et al. have employed this QD-modified Au-disk for the detection of acetylcholine esterase using SPR spectroscopy (Zayats et al., 2003). Hoa et al. have reported that patterned immobilization of QD enhances SPR signal (Hoa et al., 2007). These researchers have demonstrated that patterned immobilization of surface receptor probes, enhanced with the attachment of QD onto zero-order lamellar grating, leads to significant enhancement of the detection threshold of the SPR biosensor. Qi et al. have demonstrated a layer-by-layer surface decoration of QD on Au substrate and investigated the interactions between the QD and different proteins using *in situ* SPR technique (Qi et al., 2009). It has been revealed that QD can be used to enhance the SPR signal resulting in higher sensitivity and selectivity for detection of desired biomolecules. Ali et al. have recently reported application of the protein-conjugated QD interface to investigate the binding kinetics using antigen–antibody interaction (Ali et al., 2014) and compared the immunosensing results obtained via electrochemical and SPR techniques.

The ordered arrangement of QD with controlled thickness and interparticle spacing can be obtained through the Langmuir–Blodgett (LB) technique. We have recently reported optimized experimental conditions to obtain the stable Langmuir monolayer of CdSe QD and their LB deposition in the form of thin film (Sharma et al., 2012). These thin films are now explored for the fabrication of an SPR based nucleic acid sensor by covalent immobilization of the CML specific thiol terminated DNA as the capture probe. The change in RI value of the sensor on interaction of DNA probe with complementary target sequence identified from BCR-ABL fusion gene, single-base mismatch and non-complementary sequence has been monitored. Besides this, efforts have been made to investigate the kinetics of DNA hybridization at the sensor surface. The SPR response of this biosensor exhibits highly specific interaction with the complementary target DNA with hybridization constant of $9.6 \times 10^4 \text{ M}^{-1} \text{ s}^{-1}$ and dissociation constant of $2.3 \times 10^{-2} \text{ s}^{-1}$. To the best of our knowledge the present work is the first report on application of QD-monolayer for SPR-based detection of DNA hybridization.

2. Materials and methods

2.1. Biochemicals and reagents

All the reagents and solvents were of analytical grade and were obtained from Sigma-Aldrich, India. Buffer solutions were prepared in deionized water (Millipore, 18.0 M Ω cm) and were autoclaved prior to being used. CML specific probe oligonucleotide sequence (22 bases) identified from the BCR-ABL gene, complementary, non-complementary and one-base mismatch target sequence, were procured from Sigma-Aldrich, Milwaukee, USA. This probe corresponds specifically to the P210 kDa of BCR-ABL tyrosine kinase fusion product obtained from the reciprocal translocation of 9; 22 (Philadelphia chromosome). DNA sequences that were used for the studies are listed below.

Probe DNA:Thiol-5'-TGCCACAGCATTCGCTGACC-3' (pDNA).

Complementary:5'-GGTCAGCGGAATGCTGTGGACA-3'.

One-base mismatch:5'-GCTCAGCGGAATGCTGTGGACA-3'.

Non-complementary:5'-TACTCGCAATAACGTGATCTCC-3'.

All oligonucleotides solutions were prepared in TE buffer (1 M Tris–HCl, 0.5 M EDTA, pH 8.0) and stored at -20°C .

2.2. Characterization

Monolayer depositions were conducted using an LB trough (NIMA, UK; Model 601A). The surface chemistry measurements at

the air–water interface were conducted on an LB trough having dimensions of 10 cm \times 30 cm. The computer controlled symmetrically movable barrier was employed to regulate the surface area and constant temperature was maintained using a temperature controller (Julabo F5). The deionized water was used as the monolayer subphase and the surface pressure was measured by the immersed Wilhelmy plate. Fourier transform infrared (FT-IR) measurements were conducted in the ATR mode, with germanium waveguide, using a Perkin-Elmer Spectrum BX II spectrophotometer. The FTIR signal was obtained by averaging 64 scans at the resolution of 4 cm^{-1} . The morphological characterization was carried out using scanning electron microscope (SEM, LEO 440). The immobilization and hybridization experiments using SPR studies were recorded using an Autolab SPR, Eco Chemie (Netherlands), based on Kretschmann configuration. In the SPR experiments, linearly p-polarized light from a laser (670 nm) was directed through a prism onto the Au substrate, and the intensity of reflected light as a function of time was measured over a range of 4000 millidegrees (m^0) at 25°C . In the experiments, an Au-coated glass substrate was coupled with the plane face of the prism via an index matching fluid.

2.3. Synthesis of CdSe quantum dots

TOPO-capped CdSe nanocrystals were synthesized according to the modified Peng and Peng's method (Peng and Peng, 2000). For the preparation of trioctylphosphine selenide (TOPSe) solution, selenium powder (0.175 g) was dissolved in TOP (3 ml) and stirred for 24 h. In another reaction, cadmium oxide (CdO; 0.220 g), hexyl phosphonic acid (0.122 g) and tri-n-octylphosphine oxide (TOPO; 1.843 g) were mixed in a two-necked flask and heated to 320°C under argon atmosphere, until CdO powder was completely dissolved in the solution (Foos et al. 2006). After 6 h, the solution was cooled down to 250°C , and TOPSe solution was injected rapidly into the flask. The solution was further cooled down to 50°C , and methanol (10 ml) was added for precipitation of the CdSe nanocrystals. Thus obtained CdSe quantum dots were washed several times with methanol to remove excess residues and in the end TOPO-capped CdSe nanocrystal powders were obtained by drying in a vacuum oven.

2.4. Pre-treatment of SPR disk

Prior to their immobilization, SPR disks were treated with piranha solution followed by rinsing with de-ionized water and subsequent ultrasonication in absolute ethanol (for about 2 min) along with consecutive rinsing with de-ionized water. The SPR disk was treated with 1 mM ethanolic solution of 1-octadecanethiol (ODT) for 10 min (Ishida et al., 1997) to render it hydrophobic. The disk was again washed with ethanol to remove un-bound ODT molecules.

2.5. Langmuir–Blodgett deposition of QD monolayer

The details of optimization conditions for the CdSe Langmuir monolayer were presented in a previous report (Sharma et al., 2012). Typically, 40 μL solution of CdSe (3 mg mL^{-1} in chloroform) was vortexed with 20 μL of stearic acid (SA) solution (1 mg mL^{-1} in chloroform) for about 5 min followed by gentle spreading on the water subphase. Incorporation of SA molecules in CdSe-QD not only leads to reduction of the aggregate formation and improvement of its spreading behavior (Cheung and Rubner, 1994) but also prevents inter-digitation of the hydrophobic tails of TOPO molecules, thus acting as a spacer (Sharma et al., 2012). The solution was left for 30 min so that the chloroform could be evaporated. The pre-hydrophobized SPR disk was positioned perpendicular to

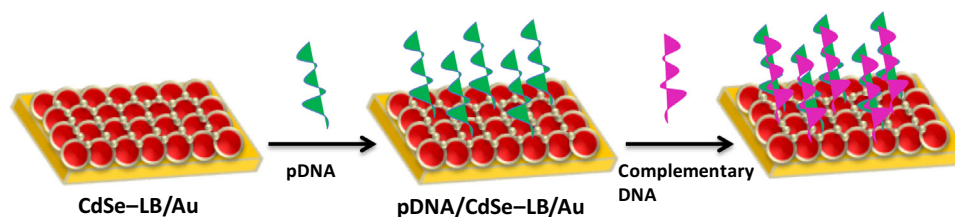


Fig. 1. Schematic showing the steps involved in the fabrication of pDNA/CdSe-LB/Au sensor disk.

air–water interface and the monolayer was subsequently deposited by vertical dipping at a rate of 10 mm min^{-1} . In order to gain insight into the CdSe-QD arrangement over the SPR disk after LB deposition, transmission electron microscopic (TEM) technique was used. Under similar experimental conditions, the QDs were deposited over the 200-mesh carbon coated Cu grid under and TEM analysis of the sample was performed. The TEM image indicates uniformly distributed particulates revealing that the ordered arrangement of CdSe-QD at the air–water interface is preserved at the solid substrate (Fig. S1).

2.6. Immobilization of DNA probe

The probe DNA molecules were immobilized on the surface of CdSe-LB/Au disk (Fig. 1) and the binding was monitored using the SPR technique. The pDNA solution (50 mM), prepared in autoclaved de-ionized water, was allowed to interact with the QD modified disk for 3 h at 25°C . The thiol terminal of the DNA probe displaced the TOPO molecules over the CdSe surface and allowed their chemisorption over the SPR disk. The pDNA/CdSe-LB/Au disk was repeatedly rinsed with water to remove any unbound pDNA on the substrate surface and the fabricated disk was utilized for CML detection using SPR technique.

2.7. Hybridization studies

For carrying out hybridization studies, the SPR experiment proceeded in triplicate phase format and the corresponding signal was monitored. Initially, before starting the experiment, the SPR signal was recorded with deionized water. The recording was performed for 300 s to obtain the baseline value. In the primary phase, the solution of target sequence was introduced into the channels and was allowed to interact with the sensor surface for the next 1800 s. The hybridization process occurs during this period and the phase is known as association (hybridization) phase. The change in the coupling angle (θ) before and after the hybridization phase corresponds to the amount of binding while keeping all other parameters constant. The next is dissociation phase, which involves the removal of un-hybridized DNA from the sensor surface. For this, the unused solution was discarded and the sensor was washed with de-ionized water through automated process. The final phase involved the regeneration phase, where the hybridized DNA strands were separated and the sensor was made ready for the next hybridization cycle. The regeneration could be achieved either by treating the sensor with strong acid or strong base. Since better regeneration results were obtained in acidic conditions (Prabhakar et al., 2008), we carried out the sensor regeneration with 5.0 mM hydrochloric acid for 120 s.

3. Results and discussion

3.1. Monitoring of probe DNA immobilization

Fig. 2 shows the SPR response before and after LB deposition of

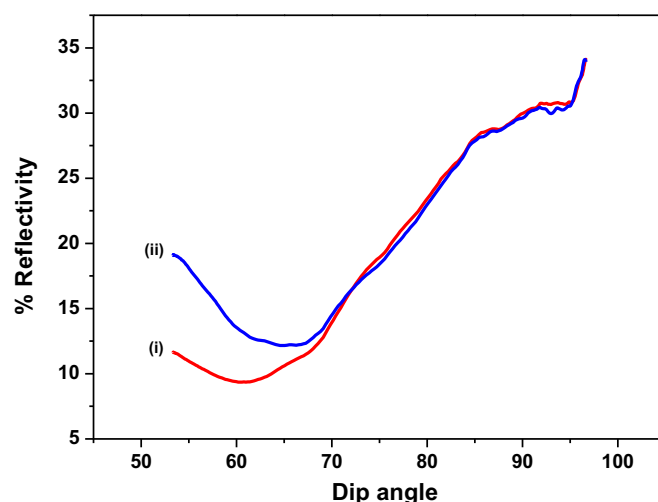


Fig. 2. Surface plasmon resonance curve for (i) the self-assembled monolayer of ODT on a Au film and (ii) same after the deposition of QD monolayer.

QD over the ODT-self assembled monolayer (SAM) modified Au disk. The SPR curve can be seen to shift to the right (increased value) as the QD are deposited at the Au surface. This is in agreement with the results reported in literature (Hoa et al., 2007; Zayats et al., 2003). The sensitivity of the SPR technique lies in the propagation of an evanescent surface plasmon wave at the boundary of metal/medium (dielectric) interface, which may be perturbed due to adsorption of the biomolecules. This is the basis of SPR spectroscopy wherein change in θ can be related to changes in refractive index (i.e., the presence of thin adlayers) at the surface of the metal. Fig. 3 shows SPR sensorgrams obtained for the thiolated DNA immobilization over the surface of SPR disk and QD modified SPR disk. It can be seen that the first phase of 120 s the baseline, after which solution of the thiolated DNA is introduced

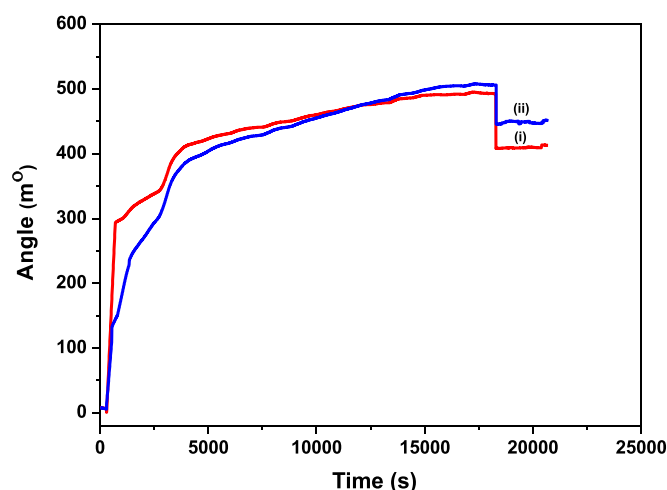


Fig. 3. SPR sensorgrams for covalent immobilization of thiolated DNA probe on the surface of (i) SPR disk and (ii) QD (CdSe-LB) modified SPR disk.

for immobilization for 10,800 s at 25 °C, followed by a washing step. The change in θ corresponds to the amount of binding of DNA at the surface. It has been found that there is a large change in θ (698 m°) during the initial 3000 s when DNA immobilization is carried out directly at the SPR disk. The change is, however, less for the QD modified disk during this period. This may be because faster immobilization occurs at the Au surface as compared to the CdSe surface. However, pDNA/CdSe-LB/Au disk yields comparable θ value as that for pDNA/Au disk after about 15,000 s.

3.2. Characterization of pDNA/CdSe-LB/Au disk

The FT-IR spectrum of pDNA/CdSe-LB/Au disk was recorded and compared with that of CdSe-LB/Au disk to confirm the pDNA immobilization (Fig. S2). The FT-IR spectrum of CdSe-LB/Au disk (Fig. S2, curve i) displays peaks at 2954 cm⁻¹, 2910 cm⁻¹, and 2844 cm⁻¹ that can be assigned to C–H stretching of the octyl chains present in TOPO and octadecyl chain in the ODT moiety, and a broad band in the range of 1420–1210 cm⁻¹ exhibits peaks corresponding to P=O and C–O stretching (von Holt et al., 2008). Further, a low intensity peak at about 1725 cm⁻¹ corresponding to carbonyl stretching vibrational mode of SA molecules is observed and this peak gets intense after immobilization of pDNA (Fig. S2, curve ii). The peaks seen at 1606 cm⁻¹ and 1448 cm⁻¹ in pDNA/CdSe-LB/Au disk are assigned to –NH bending and –CN stretching, respectively, and can be correlated with the presence of nucleoside bases (Prabhakar et al., 2011; Sharma et al., 2012). Additionally, the peaks found at 674 cm⁻¹ arising due to –CS stretching and 1086 cm⁻¹ correspond to phosphate stretching indicating successful immobilization of oligonucleotide molecules over the CdSe-LB/Au disk.

The morphological changes at the SPR disk, arising as a result of surface modification, were examined using scanning electron microscopic technique and results are displayed in Fig. S3. As can be seen (Fig. S3, panel i), the ODT-SAM on the Au surface makes it slightly rough. After LB deposition, a uniform distribution of the QD over the surface of Au-substrate can be seen (Fig. S3, panel ii). A regularly arranged globular structure in the micron scale indicates that ordered arrangement of the quantum dots onto the transducer surface provides a favorable environment for immobilization of pDNA in an oriented manner. When CdSe-LB/Au disk is incubated with pDNA, the spherical shape is found to be diminished (Fig. S3, panel iii). This change in morphology is due to the immobilization of pDNA over the QD surface.

3.3. Hybridization detection using SPR technique

Fig. 4 shows results of the SPR studies of pDNA/CdSe-LB/Au disk as a function of time for different concentrations of complementary target DNA sequence. In the SPR signal of pDNA/CdSe-LB/Au disk, 170 m° change in θ is seen after incubation with the complementary target (180 pM) for 1800 s, indicating hybridization of the immobilized pDNA with complementary DNA sequence (Fig. 4, Curve i). The change in θ is found to be less as the complementary DNA concentration is decreased (Fig. 4, Curve ii–vi). Fig. S4 shows variation in θ as a function of complementary DNA concentration. It is found that θ of pDNA/CdSe-LB/Au disk decreases linearly with decrease in complementary DNA concentration in the range from 180 pM to 5 pM. The sensitivity of the pDNA/CdSe-LB/Au biosensor has been calculated to be as 0.7859 m° pM⁻¹ from the calibration curve with a lower detection limit of 4.21 pM (3*SD/sensitivity).

Fig. 5 presents SPR curves obtained for the pDNA/CdSe-LB/Au after hybridization with the complementary, one-base mismatch and non-complementary sequences, respectively. As mentioned earlier, the change in θ of 170 m° is observed with the

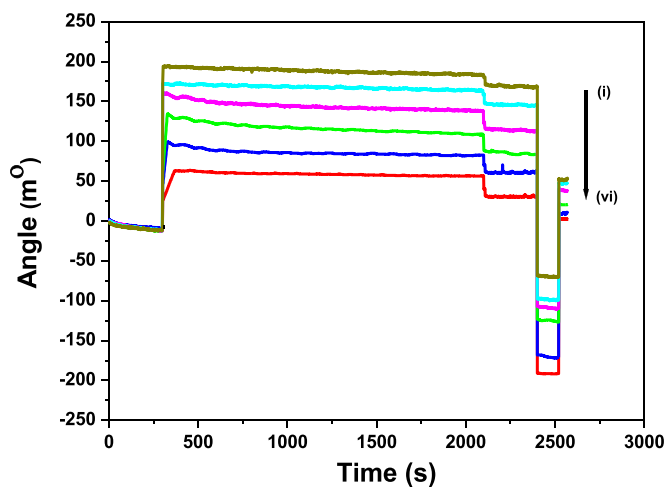


Fig. 4. SPR response of pDNA/CdSe-LB/Au as a function of time for (i) 180 pM, (ii) 150 pM, (iii) 110 pM, (iv) 75 pM, (v) 40 pM, and (vi) 5 pM concentrations of complementary DNA.

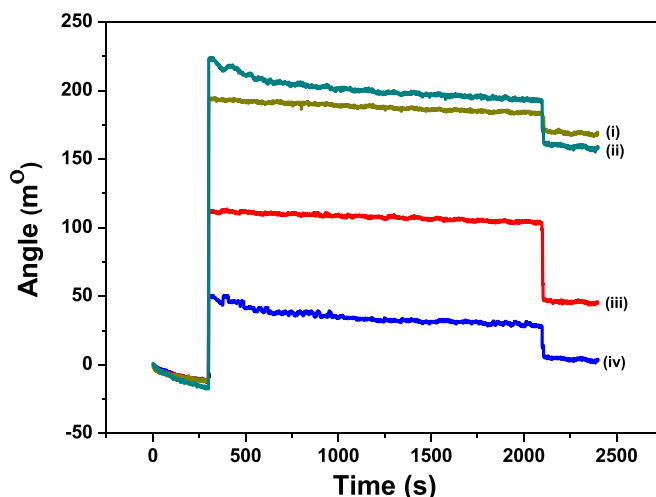


Fig. 5. SPR sensorgrams of pDNA/CdSe-LB/Au for hybridization detection with (i) complementary DNA, (ii) pool of various synthetic DNA sequences, (iii) one-base mismatch DNA and (iv) non-complementary DNA.

complementary sequence (Curve i). The change in θ of about 45 m° is seen after hybridization with one-base mismatched sequence (Curve iii) indicating some non-specific binding. However, negligible change (45 m°) in θ occurs after hybridization with the non-complementary sequence (Curve iv). This observed very small change can be attributed to non-specific adsorption of non-complementary DNA over the pDNA/CdSe-LB/Au disk. The results indicate that the fabricated DNA sensor can be used to discriminate even a single nucleotide variation in target DNA sequence. Attempts have also been made to detect the target complementary DNA sequence among a pool of different DNA sequences. For this purpose, solution containing 180 pM concentration of each of the complementary DNA, non-complementary DNA, one-base mismatch DNA and a few other synthetic DNA sequences was prepared in TE buffer. These DNA sequences were selected in a way that they do not hybridize with each other to form duplex. The solution was then introduced into the channels and the sensor chip was subjected to undergo hybridization and dissociation process. A change in 161 m° was obtained after 1800 s (Curve ii), which is comparable to that obtained with sole complementary DNA solution having 180 pM concentration. The results indicate that the sensor could quantitatively detect complementary DNA sequence among the pool of different DNA sequences.

Table 1

Comparison of response characteristics and association constant of fabricated biosensor along with those recently reported in literature for label-free SPR-based hybridization detection.

Sl. No.	Immobilization substrate	Probe modification/signal amplification substance	Detection limit	Test range	Sensitivity	Reference
1	DNA probe/straptavidin/carboxylated dextran/Au	Biotin	0.5 nM	1 μ M to 5 nM	435.51 m ⁰ nM ⁻¹	Zhang et al. (2012)
2	DNA probe/Au	Auxiliary probe/biotynalated probe/streptavidin	9 pM	1 μ M to 10 pM	Not mentioned	Ding et al. (2015)
3	DNA probe/Au	Mismatched catalytic hairpin assembly/streptavidin aptamer	1 pM	100 nM to 5 pM	174.24 m ⁰ nM ⁻¹	Li et al. (2016)
4	DNA probe/AuNP/HDT/Au	AuNp	20 Amol	100 nM to 10 pM	241.0 m ⁰ M ⁻¹	Xiang et al. (2015)
5	Hairpin DNA probe/Au	DNA-linked AuNP/reporter DNA	8 fM	150 pM to 0 pM	Not mentioned	Wang et al. (2016)
6	DNA Probe/CdSe-QD/ODT/Au	CdSe-QD	4.21 pM	180 pM to 5 pM.	0.7859 m ⁰ pM ⁻¹	This work

3.4. Determination of rate constant

Attempts were made to calculate values of the hybridization constant (k_a) and dissociation constant (k_d) for pDNA/CdSe-LB/Au electrode. The kinetic analysis of the hybridization phase was used to obtain the value of hybridization and dissociation rate constants and the equilibrium constant (Ali et al., 2014; Prabhakar et al., 2008). The binding reaction equation for the two macromolecular interactants is given as

$$[A] + [B] = [AB] \quad (1)$$

The rate of formation of complex in hybridization phase is given by:

$$\frac{d[AB]}{dt} = k_a[A][B] - k_d[AB] \quad (2)$$

and k_a and k_d follows relation given by Eq. (3).

$$k_s = k_d[C] + k_d \quad (3)$$

The values of k_s can be obtained by the integrated rate equation for association phase presented in Eq. (4).

$$R_t = E(1 - e^{-k_s t}) + R_0 \quad (4)$$

where

$$E = \frac{k_a C R_{max}}{k_d C + k_d} \quad (5)$$

Here, R_0 represents the signal at zero time, C is the complementary DNA concentration, and E is maximum change in the response. The kinetic information can be obtained from Eq. (3) and calculations have been done by nonlinear curve fitting using kinetic evaluation software. The k_a and k_d are evaluated from the plot of k_s versus C where slope of curve gives the value of k_a and intercept yields the information about k_d . The values of k_a and k_d rate constants for complementary DNA hybridization are estimated to be $9.6 \times 10^4 \text{ M}^{-1} \text{ s}^{-1}$ and $2.3 \times 10^{-2} \text{ s}^{-1}$, respectively, with the equilibrium constant for hybridization (k_a/k_d) as $4.2 \times 10^6 \text{ M}^{-1}$. This quantum dot monolayer based SPR biosensor shows higher k_a and k_s values for the complementary target DNA as compared to that obtained using direct immobilization of DNA probe on Au disk (Prabhakar et al., 2008). This shows that application of QD results in improved kinetics of the sensor. Table 1 shows results of these studies along with those reported in literature for SPR-based DNA hybridization sensors. It can be seen that the fabricated sensor presents improved or comparable detection limit and sensitivity as compared to sensors based on streptavidin either employed as a signal enhancing agent or to

support the probe DNA immobilization. However, the observed lower detection limit of this sensor as compared to sensors having gold nanoparticles as the signal enhancing agent can be attributed to the localized surface plasmon resonance phenomenon caused by the collective oscillations of surface electrons in noble metal nanoparticles.

4. Conclusions

In the present work, the SPR signal enhancement of Au film has been observed via CdSe QD. The QDs are found to excite the surface plasmons to particle plasmons when placed in close proximity to the Au film. The QD monolayer has been deposited over the Au substrate using Langmuir–Blodgett technique that provides organized assembly of QD over the substrate surface. This organized assembly of QD has led to strong optical coupling of incident light to resonance thus enhance the sensitivity ($0.7859 \text{ m}^0 \text{ pM}^{-1}$) of the SPR biosensor. The pDNA/CdSe-LB/Au electrode is found to selectively detect complementary target DNA in the concentration range from 5 pM to 180 pM with a limit of detection as 4.21 pM. The values of hybridization and dissociation rate constants for hybridization event have been found to be $9.6 \times 10^4 \text{ M}^{-1} \text{ s}^{-1}$ and $2.3 \times 10^{-2} \text{ s}^{-1}$, respectively, with the equilibrium constant for hybridization (k_a/k_d) as $4.2 \times 10^6 \text{ M}^{-1}$. The selectivity of the biosensor has been demonstrated by discrimination of single-nucleotide mismatch and non-complementary DNA sequence. The results of these studies clearly demonstrate efficacy of the QD-based SPR sensor as a high throughput device for detecting the specific DNA hybridization. The efforts should be made to utilize this SPR sensor for analysis of clinical samples.

Acknowledgments

We thank Director, NPL, New Delhi, India for the facilities. Financial support received under the Department of Science and Technology project (DST/TSG/ME/2008/18) is gratefully acknowledged.

Appendix A. Supplementary material

Supplementary data associated with this article can be found in the online version at <http://dx.doi.org/10.1016/j.bios.2016.02.013>.

References

- Ali, M.A., Srivastava, S., Pandey, M.K., Agrawal, V.V., John, R., Malhotra, B.D., 2014. Anal. Chem. 86, 1710–1718.

- Cennamo, N., Pesavento, M., Lunelli, L., Vanzetti, L., Pederzoli, C., Zeni, L., Pasquardini, L., 2015. *Talanta* 140, 88–95.
- Cheung, J.H., Rubner, M.F., 1994. *Thin Solid Films* 244, 990–994.
- Ding, X., Yan, Y., Li, S., Zhang, Y., Cheng, W., Cheng, Q., Ding, S., 2015. *Anal. Chim. Acta* 874, 59–65.
- Druker, B.J., Sawyers, C.L., Kantarjian, H., Resta, D.J., Reese, S.F., Ford, J.M., Capdeville, R., Talpaz, M., 2001. *N. Engl. J. Med.* 344, 1038–1042.
- Foos, E.E., Wilkinson, J., Mäkinen, A.J., Watkins, N.J., Kafafi, Z.H., Long, J.P., 2006. *Chem. Mater.* 18, 2886–2894.
- Hoa, X.D., Martin, M., Jimenez, A., Beauvais, J., Charette, P., Tabrizian, M., Kirk, A.G., 2007. *Lasers and Electro-Optics Society*, 2007. In: *Proceedings of the 20th Annual Meeting of the IEEE*. pp. 598–599.
- Huang, H.H., Seeger, C., Helena, D.U., Lindblad, P., 2015. *Mol. Biol. BMC Res. Notes*, 8.
- Ishida, T., Tsuneda, S., Nishida, N., Hara, M., Sasabe, H., Knoll, W., 1997. *Langmuir* 13, 4638–4643.
- Lee, W.I., Kantarjian, H., Glassman, A., Talpaz, M., Lee, M.S., 2002. *Ann. Oncol.* 13, 781–788.
- Li, J., Lei, P., Ding, S., Zhang, Y., Yang, J., Cheng, Q., Yan, Y., 2016. *Biosens. Bioelectron.* 77, 435–441.
- Nawattanapaiboon, K., Kiatpathomchai, W., Santanirand, P., Vongsakulyanon, A., Amarit, R., Somboonkaew, A., Sutapun, B., Sriksirin, T., 2015. *Biosens. Bioelectron.* 74, 335–340.
- Nowell, P.C., 2007. *J. Clin. Invest.* 117, 2033–2035.
- Peng, Z.A., Peng, X., 2000. *J. Am. Chem. Soc.* 123, 183–184.
- Piliarik, M., Párová, L., Homola, J., 2009. *Biosens. Bioelectron.* 24, 1399–1404.
- Prabhakar, N., Matharu, Z., Malhotra, B.D., 2011. *Biosens. Bioelectron.* 26, 4006–4011.
- Prabhakar, N., Arora, K., Arya, S.K., Solanki, P.R., Iwamoto, M., Singh, H., Malhotra, B.D., 2008. *Analyst* 133, 1587–1592.
- Qi, X., Bo, Z., Shan, H., Fangfang, T., Hongliang, G., Yushu, G., Xiaorong, L., Zhike, H., Yi, L., 2009. *Nanotechnology* 20, 325101.
- Saglio, G., Fava, C., 2012. *Compr. Cancer Netw.* 10, 121–129.
- Sharma, A., Pandey, C.M., Matharu, Z., Soni, U., Sapra, S., Sumana, G., Pandey, M.K., Chatterjee, T., Malhotra, B.D., 2012. *Anal. Chem.* 84, 3082–3089.
- Singh, A., Verma, H.N., Arora, K., 2014. *Appl. Appl. Biochem. Biotechnol.* 175, 1330–1343.
- Šípová, H., Homola, J., 2013. *Anal. Chim. Acta* 773, 9–23.
- Tahmasebpour, M., Bahrami, M., Asgari, A., 2015. *Opt. – Int. J. Light Electron Opt.* 126, 2747–2751.
- Tran, D.T., Knez, K., Janssen, K.P., Pollet, J., Spasic, D., Lammertyn, J., 2013. *Biosens. Bioelectron.* 43, 245–251.
- von Holt, B., Kudera, S., Weiss, A., Schrader, T.E., Manna, L., Parak, W.J., Braun, M., 2008. *J. Mater. Chem.* 18, 2728–2732.
- Wang, Q., Liu, R., Yang, X., Wang, K., Zhu, J., He, L., Li, Q., 2016. *Sens. Actuators B* 223, 613–620.
- Xiang, Y., Zhu, X., Huang, Q., Zheng, J., Fu, W., 2015. *Biosens. Bioelectron.* 66, 512–519.
- Zayats, M., Kharitonov, A.B., Pogorelova, S.P., Lioubashevski, O., Katz, E., Willner, I., 2003. *J. Am. Chem. Soc.* 125, 16006–16014.
- Zhang, D., Yan, Y., Li, Q., Yu, T., Cheng, W., Wang, L., Ju, H., Ding, S., 2012. *J. Biotechnol.* 160, 123–128.



Journal of Quality in Maintenance Engineering

Ranking of barriers for effective maintenance by using TOPSIS approach

Rajesh Kumar Singh ayush gupta Ashok Kumar Tasmeem Ahmad Khan

Article information:

To cite this document:

Rajesh Kumar Singh ayush gupta Ashok Kumar Tasmeem Ahmad Khan , (2016),"Ranking of barriers for effective maintenance by using TOPSIS approach", Journal of Quality in Maintenance Engineering, Vol. 22 Iss 1 pp. -

Permanent link to this document:

<http://dx.doi.org/10.1108/JQME-02-2015-0009>

Downloaded on: 01 February 2016, At: 20:14 (PT)

References: this document contains references to 0 other documents.

To copy this document: permissions@emeraldinsight.com

The fulltext of this document has been downloaded 7 times since 2016*

Users who downloaded this article also downloaded:

Rosângela Maria Vanalle, Wagner Cezar Lucato, Roberto Torres Rogrigues, (2016),"The utilization of ISO 9004: case study of the maintenance area of a public transportation company", Journal of Quality in Maintenance Engineering, Vol. 22 Iss 1 pp. -

Lasse Metso, Salla Marttonen, Nils Thenent, Linda Newnes, (2016),"Adapting the SHEL model in investigating industrial maintenance", Journal of Quality in Maintenance Engineering, Vol. 22 Iss 1 pp. -

Mohamed Noomane Darghouth, Daoud Ait-Kadi, Anis Chelbi, (2016),"Joint reliability based design and periodic preventive maintenance policy for systems sold with warranty", Journal of Quality in Maintenance Engineering, Vol. 22 Iss 1 pp. -

Access to this document was granted through an Emerald subscription provided by emerald-srm:544911 []

For Authors

If you would like to write for this, or any other Emerald publication, then please use our Emerald for Authors service information about how to choose which publication to write for and submission guidelines are available for all. Please visit www.emeraldinsight.com/authors for more information.

About Emerald www.emeraldinsight.com

Emerald is a global publisher linking research and practice to the benefit of society. The company manages a portfolio of more than 290 journals and over 2,350 books and book series volumes, as well as providing an extensive range of online products and additional customer resources and services.

Emerald is both COUNTER 4 and TRANSFER compliant. The organization is a partner of the Committee on Publication Ethics (COPE) and also works with Portico and the LOCKSS initiative for digital archive preservation.

*Related content and download information correct at time of download.

Ranking of Barriers for Effective Maintenance by using TOPSIS approach

1. Introduction

Due to the rapidly changing scenario of globalized market, many organizations around the globe are facing problems due to increased number of competitors and volatility in consumer requirements for quality product at the lowest cost (Chandra and Shastry, 1998). In such scenario, many firms are losing their market share to multinational firms (Khanna and Sharma, 2011). Phusavat and Kanchana (2008) and Singh and Sharma (2015) have observed that some factors to achieve competitiveness are: quality, reliability, flexibility, ability to meet demand and delivery requirements. Most of the organisations are working towards improvement of manufacturing flexibility (Singh and Sharma, 2014). Therefore it became crucial for the firms to put focus on effective maintenance systems. Alsyuf (2007) and Ahmed et al., (2005) have observed that a common strategy to cut cost is by increasing the level of automation in operations. Automation will have fewer number of employees but due to the complex machinery, the work of maintenance department becomes very important (Ahuja and Khamba, 2008; Garg and Deshmukh, 2006; Hansson and Backlund, 2003). Thus an active maintenance management department will be very essential to excel in service and consequently increase the market share. As the technical developments are growing, the influence of productivity and quality, are also moving increasingly from man to machine. The importance of maintenance becomes further important aspect in the industry with the fact that high productivity and quality can be achieved by means of well developed and organized maintenance system. Therefore difficulties faced by the organization should be actively identified, evaluated and managed by the maintenance managers (Mohamed, 2005).

In the era prior to industrial revolution in England near the mid of eighteenth century, maintenance mainly consisted of craftsman such as carpenters, smith, masons for the regular maintenance work, which was usually performed by repairing or making a new part to fit. As there was no concept of dimensional control the maintenance work used to be tedious job. But as the development grew in the maintenance field, Jefferson (1785) noted that the parts were being made accurately enough to be interchangeable. These small but accelerating developments gradually converted the maintenance work to be more diagnostic. Due to high share of maintenance system in operating budget of manufacturing firms, it has been also regarded as “necessary evil” by top management (Cooke, 2003; Eti et al., 2007). But this attitude is increasingly been replaced by the one which regards maintenance as the control of reliability and a strategic issue (Eti et al., 2006). Business leaders are increasingly realising the importance of maintenance in cost control, to save time and others resources by optimizing their productivity and maximizing the OEE. Business leaders are now using this as a competitive weapon or as a contributor to profit (Sherwin, 2000). As the production Technology is advancing too quickly, many models have come into existence like the Eindhoven University of Technology (EUT) model, Total productive maintenance (TPM), Total quality maintenance (TQM), Reliability Centred maintenance (RCM), Condition based maintenance (CBM). Further the improvements such as fewer defects and errors, reduced waste can be achieved by increasing maintainability of machines (Brah et al., 2002; Hansson and Eriksson, 2002; Hendricks and Singhal, 2001; Kaynak, 2003).

Cholasuke et al, (2004) have observed that even after adopting the appropriate maintenance models for achieving productivity goals, the organizations fail to achieve performance targets due to different barriers in implementation of maintenance systems. Cooke (2000) has identified organisational barriers in implementing TPM based on case studies but he has not ranked them. Therefore objectives of this study are to identify major barriers in effective maintenance management and then rank them using the TOPSIS methodology. Remaining part of the paper is organised as follows: Section 2 deals with literature review for identifying the barriers in maintenance management, section 3 deals with the methodology used to rank the barriers i.e TOPSIS approach, Section 4 presents the findings, finally section 5 is the concluding remark.

2. Identification of barriers in maintenance management

Now a day's all the maintenance operations are within the reach of achieving the world-class level of maintenance delivery, and its credit is awarded to the automation in the industry (Ahmed et al., 2005; O'Sullivan et al., 2011). However, human inputs are still an important factor. Skills beyond the competence of the average maintenance supervisor or worker is required for the automated and technologically advanced equipment, and importantly an appropriate and effective maintenance organization is required to use it effectively (Mohamed, 2005). According to Poduval et al. (2015), time, money, manpower, resources and commitment from all the stake holders are required for implementing maintenance work in industries. The organization as a whole should be willing to change its outlook and adapt itself to the new practices and cultural changes that are required for the successful implementation of maintenance models. There are many barriers in implementing effective maintenance in organizations. Major barriers identified from the literature are discussed in following sections and summarized in a framework (figure 1)

Insert figure 1 here

Lack of Benchmarking

Benchmarking is a continuous process to move towards best in class by achieving high maintenance effectiveness standard regularly (Åhrén and Parida, 2009; Raouf and Ben-daya, 1995). The initial benchmarking helps in bridging the gap between the prevailing equipment condition and the desired manufacturing excellence (Ahuja and Khamba, 2007). The main concern for benchmarking from maintenance point of view are unplanned downtime, defects in equipment or degradation in speed of manufacturing equipment (Raouf and Ben-daya, 1995). Effective benchmarking of different processes ensures product quality and customer satisfaction (Singh, 2011). It is possible by measuring ones performance with respect to the "Best in Class" performer (Hansson and Backlund, 2003). It helps in identifying its strengths and weaknesses and provides a sense of direction for the plan. It is five step process: planning; analysis; integration; action; and implementation and result (Rauof and Ben-Daya, 1995). Lack of benchmarking causes poor maintainability and reliability (Hansson and Backlund, 2003).

Lack of communication and Information

Communication and information in an organization implies open and meaningful communication in such a way that information flows laterally thus creating an open atmosphere in the organization (Mosadeghrad, 2014). It includes informal meetings between management and union representatives to complement formal communications that helps in increasing interest and acceptance. Lad and Kulkarni (2010a) have proposed a mechanism to link operational requirements with machine tool reliability and maintenance parameters. Where employees understanding and involvement could be achieved (Abraham et al., 1999; Pintelon et al, 1999; Tsang and Chan, 2000; Hansson and Backlund, 2003). Due to lack of communication and information not flowing laterally, members of organization are not able to identify and report the sources of maintenance and reliability; and are not able to put their valuable suggestions for improvement (Hansson and Backlund, 2003).

Lack of measurement of Overall Equipment Effectiveness (OEE)

OEE is measure of effectiveness of the equipment or machine or it is a performance indicator (Rolfesen and Langeland, 2012). It depends on three parameters i.e. System availability rate, Performance rate and Quality rate. The real goal of maintenance activities is to increase OEE and due to lack of measure of OEE the maintenance activities can't be implemented properly (Kumar et al., 2014). The progress of the company depends on these three parameters of OEE (Prickett, 1999). System availability refers to the rate of availability of machine tool. Availability depends on the system design which determines the systems reliability, maintainability with the aim that system performs all its functions throughout its life successfully (Lad and Kulkarni, 2008). Performance rate tells us about the losses incurred due to using the machine at low performance rate and the degradation of performance is mainly due to unfulfilled maintenance work (Al-Sultan, 1996). Quality rate refer to the losses occurred due to the low quality, bad quality means more rejections (Prickett, 1999). Elimination of waste such as scrap and rework can be easily achieved by quality improvement which increases productivity and thus leads to reduced cost.

Continuous improvement of these three parameters of OEE should be an important target. The analysis of these factors can be used for improvement of individual tool reliability and importantly to prevent the recurrence of similar type of failures in a machine tool (Prickett, 1999). But if the organizations fail to measure OEE then they are not able to monitor most important factors influencing the system performance. Lad and Kulkarni (2010b) have suggested parameter estimation method for the machine tool reliability analysis to overcome the problem of unavailability of a well-defined failure data collection mechanism.

Lack of Team work

Team working means involvement of entire organizations to eliminate the defects, i.e. the company wide approach to achieve quality where the role of each and every employee is crucial (Graham, 2014; Ledet, 1999). It also helps in achieving better reliability at lower cost (Ledet, 1999). Not only the maintenance department but the entire organization should ensure the reliable and dependable maintenance system (Madu, 2000). Traditional factors of maintenance management like information

system, data collection etc. are still important and are key factors to improve maintainability and reliability. These factors must be coordinated in a cohesive form (Hansson and Backlund, 2003). But many organizations have reported that team working between the production and maintenance department is not only an issue of principle but also an issue of practicability (Cooke, 2000). Many experiments have shown that proper maintenance activities can be performed when the whole business unit works toward a common goal, otherwise sub-optimization will result in unachieved goals (Rolfesen and Langeland, 2012).

Lack of effective performance measures

For maintenance systems effectiveness apart from OEE, other performance measures are also equally important. Due to the substantial cost of maintenance as compared to operational cost, measuring of effective performance becomes very important to become competitive and cost effective. Usually maintenance measures are not part of performance framework. For this structural audits can be carried out to measure productivity and to identify area of improvement (Raouf, 1994, Raouf and Ben-Daya, 1995). To monitor and to take timely decisions, the information about the performance of machine is very important and lack of this information causes ineffective and inefficient maintenance process (Parida and Kumar, 2009).

Lack of Commitment of employees towards maintenance

According to Davis (1997), many organizations failed to implement maintenance system properly due to reluctant and demoralized production department, who were in fear of losing job and were unwilling to do stressful work as they don't see the benefits of implementations due to lack of knowledge (Hardwick and Winsor, 2001; Karlsson and Ljungberg, 1995; Shin et al., 1998). This can be overcome by recognizing the employees and visibly showing them the benefits of implementations (Allen and Kilmann, 2001; Hartman, 1992). Since activities are actually implemented by the employees thus the employees who are having lack of positive attitude towards maintenance further increases the cost of maintenance (Hansson and Backlund, 2003). Due to this fewer resources are spent on other aspects of maintenance.

Lack of Training

Effective working of maintenance department requires that the managers and employees have the appropriate knowledge, skills and expertise in the field of quality management (Mosadeghrad, 2014). It helps in changing the mind set of employees from traditional maintenance approach to the new and modern approach. It further helps in reducing the maintenance crew and increases the flexibility as the small maintenance works could then be performed by the average maintenance personnel or the shop floor workers (Nembhard, 2014). It also increases the commitment and brings about the positive behavioural changes. Training is required with adequate amount of practical knowledge; otherwise employees tend to forget what they were taught (Hansson and Backlund, 2003). For example a untrained planner would not be able to determine job content, duration, number of workers required, number of spare parts required etc (Raouf and Ben-daya, 1995).

Lack of proper strategic planning and Implementation

Strategies set directions for deciding operations functions to ensure competitiveness (Singh et al. 2010). These are the functions that help in integrating the quality requirement with the business activities (Chin et al., 2002). These are the activities to develop and identify the obstacles in achieving the desired goals (Hartman, 1992; Hipkin and Lockett, 1995; Shin et al., 1998). They help in facilitating the follow-ups and monitoring the achievements like involvement of employees and understanding between management and workers by setting goals, and identifying solution (Abraham et al, 1999; Schawan and Khan, 1994). It also links maintenance programme with company's mission, vision and strategies (Bardeol and Sohal, 1999; Riis et al., 1997). It is observed that lack of proper strategic planning and implementation can prove to be a bottleneck due to the unclear picture of benefits to organization from the improvements (Abreu et al., 2013).

Lack of Top management support

Atkinson (1990) and Jaehn (2000) have observed that 80% of firms fail due to the lack of top management support. Implementation of maintenance activities in organizations requires major resources like human resources, money and time. Top management is responsible for providing these resources (Shin et al., 1998; Hansson and Backlund, 2003). It has become very important to change traditional methods and organization structure to the new and modern one (Singh et al., 2008). Therefore one of the major job of top management in today's business environment is to reorganize the traditional organization reporting system to obtain the quality maintenance and reliability information on timely basis (Hansson and Backlund, 2003). Major resources need proper implementation and clear understanding of objectiveness and methodologies of maintenance system (Clark, 1991; Hipkin and Lockett, 1995). Real goal of maintenance is to increase OEE and not to reduce the labour count. Asjad et al. (2013) have suggested supportability based contract alternatives for operating life of mechanical systems. According to them supportability for a user is the ability of the manufacturer to execute all the support activities that are required for the upkeep of the system, in the most effective, efficient and timely manner throughout the operating life of the product, whenever and wherever needed.

Lack of Empowerment

For effective maintenance management, employee empowerment for taking different decisions at own levels are very important. Empowerment means to develop the teams and to build a matured staff (Mohamed, 2005). Employees should be active participants and satisfied with their job with feeling of ownership (Hansson and Backlund, 2003; Aghazadeh, 2002; Yamashina, 2000). To use maintenance for competitive advantage, organizations should empower employees to adapt processes as per environmental changes (Douglas and Judge, 2001). Lack of empowerment

means inactive participation of employees thus there is decrement in efficiency of maintenance program.

Lack of Awareness about safety and health

For the success of any enterprise an important prerequisite is the safety of people, environment and assets (Narayan, 2012). According to survey of European Agency for safety and health at work in year 2000, 10 to 15% of fatal accidents and 15 to 20% of all accidents were associated with maintenance work. Thus maintenance is usually regarded as critical to operators. They are more exposed to variety of hazards with potential harm to their health (Grusenmeyer, 2010). Therefore one of the main works of the maintenance department should be to create a safe workplace with utmost importance of safety in the plant (Singh et al., 2013). Safety in plant refers to personal safety as well as process safety. Personal safety is important in the industries, but the more important factor is the process safety (Narayan, 2012). Therefore safety and health at work place should be everyone's concern. Barriers identified based on literature review and experts opinion are summarised table 1.

Insert table 1 here

3. Research methodology

For ranking of different barriers, multi criteria decision making (MCDM) tool i.e TOPSIS is applied in this research. MCDM is very important tool to deal with unstructured problems containing multiple and conflicting objectives (Lee and Eom, 1990). Many 'MCDM' techniques have been developed, but the TOPSIS approach is the most widely used technique. Technique for order preferences by similarity to ideal solution (TOPSIS) method was proposed by Hwang and Yoon (1981). It is considered to give very reliable solution because in TOPSIS poor performance in one criteria can be negated by good performance in other criteria. Therefore many authors have been analysing their data with the TOPSIS methodology. Jothimani and Sarmah, (2014) have used TOPSIS for measuring the supply chain performance (SCP) in the light of a real life case study. Ramezani and Lu, (2014) have used TOPSIS for identifying an optimal maintenance policy that can minimize the failures. Kumar and Singh (2012) have used this approach for evaluating 3 PL for global supply chains. Khanna and Sharma (2011) have used TOPSIS for ranking of CSFs for total quality management implementation. Strength of TOPSIS methodology over other MCDM techniques is that the both negative and positive criteria can be simultaneously used in decision making. In addition to this, it is simpler and faster than other methods such as AHP, FDAHP and SAW. In this method two artificial alternatives are hypothesized:

1. Ideal alternative: the one having the best level for all attributes considered.
2. Negative ideal alternative: the one having worst attribute values.

TOPSIS selects the alternative that is the closest to the positive ideal solution and farthest from negative ideal alternative. Thus providing a more realistic form of

modelling as compared to non-compensatory methods. Major steps in TOPSIS approach are as follows.

Step 1: On the basis of 'm' alternative and 'n' criteria, a matrix with elements x_{ij} is made, where each element denotes the rating of i^{th} decision maker (DM) with respect to j^{th} criteria.

This matrix is known as decision matrix denoted by 'D':

$$D = \begin{bmatrix} x_{11} & x_{12} & \dots & x_{1n} \\ x_{21} & x_{22} & \dots & x_{2n} \\ \dots & \dots & \dots & \dots \\ x_{m1} & x_{m2} & \dots & x_{mn} \end{bmatrix}$$

$i = 1, 2, 3, \dots, m$ is the number of alternative and $j = 1, 2, 3, \dots, n$ is the number of criteria.

Step 2: Now, the normalized matrix is calculated with elements $r_{ij} = \frac{x_{ij}}{\sqrt{\sum_{i=1}^n x_{ij}^2}}$ for i

$= 1, 2, \dots, n$; $j = 1, 2, \dots, m$. It is denoted by R.

$$R = \begin{bmatrix} r_{11} & r_{12} & \dots & r_{1n} \\ r_{21} & r_{22} & \dots & r_{2n} \\ \dots & \dots & \dots & \dots \\ r_{m1} & r_{m2} & \dots & r_{mn} \end{bmatrix}$$

Step 3: Construct the weighted normalized matrix with elements $v_{ij} = w_j r_{ij}$, where w_j = weights of different attributes. It is denoted by V.

$$V = \begin{bmatrix} v_{11} & v_{12} & \dots & v_{1n} \\ v_{21} & v_{22} & \dots & v_{2n} \\ \dots & \dots & \dots & \dots \\ v_{m1} & v_{m2} & \dots & v_{mn} \end{bmatrix}$$

Step 4: Determining the positive ideal solution v_j^+ and negative ideal solution v_j^- by finding the maximum and minimum values of weighted normalized elements in each column in the case of benefit criteria and just reverse for cost criteria.

Step 5: Calculate the Euclidean distance for each alternative.

The Euclidean distance from positive ideal solution is represented by s_i^* .

$$s_i^* = [\sum_j (v_{ij}^* - v_j^+)^2]^{1/2}$$

Where $i = 1, 2, \dots, m$; $j = 1, 2, \dots, n$

The Euclidean distance from negative ideal solution is represented by s'_i .

$$s'_i = [\sum_j (v'_{ij} - v_j^-)^2]^{1/2}$$

Where $i = 1, 2, \dots, m$; $j = 1, 2, \dots, n$

Step 6: Calculate the relative closeness to the ideal solution c_i^* . If it is closest to 1, then it depicts the best solution.

$$c_i^* = \frac{s'_i}{(s_i^* + s'_i)}, \text{ where } 0 < c_i^* < 1$$

Where s_i^* represents distance from positive ideal solution and, s'_i represents distance from negative ideal solution.

Step 7: Rank the alternatives according to the preference order of closeness ratio c_i^* . The one that have the shortest distance to the ideal solution is the best alternative. Shortest distance to the ideal solution depicts longest distance from negative ideal solution.

4. Results and Discussion

A successful Maintenance management system plays a crucial role in improving machines productivity and overall performance. It gives an edge to the company over its competitors. To successfully implement the maintenance management, the managers should be aware about the barriers of maintenance management, and should try to overcome them. For obtaining input data, a team of three experts/Decision makers (DMs) was made in this study. These three decision makers (DM1, DM2 and DM3) are Maintenance department heads from top ranked companies in NCR Delhi India, each having experience of more than 10 years. These top ranking firms are mainly from manufacturing sectors. On basis of their experience DM1 is given a weightage of '0.5', DM2 a weightage of '0.2' and DM3 a weightage of '0.3'. Barriers are given score in scale of 1-10 (1-Very low, 10-Very high). By using step 2 and 3, weighted normalized decision matrix is made as given in table 2. By using step 4, positive and negative ideal solutions are determined as given in table 3. By using step 5, separation of each CSF from the positive and negative ideal solution is determined and shown in table 4 and 5. Now, by using step 6, the relative closeness of each barrier to the ideal solution (closeness ratio) is found as given in table 6 and based on closeness ratio i.e step 7, relative ranking of these barriers is shown in table 7.

Inset tables 2 to 7 here

It is observed that lack of top management support is the biggest barriers in successful implementation of effective maintenance management. Willingness of top management can only bring about the positive changes in the culture and functioning of the company. Usually it is observed that top management especially in SMEs are not very supportive for maintenance initiatives because return is not short term and lot of changes are required (Kumar et al, 2015). It is usually observed that investing in preventive maintenance activities is considered as waste by management in many organisations. They are still following traditional breakdown maintenance systems. Next barrier as per importance is lack of awareness for OEE. As we know that the one of the main goal of maintenance system is to increase OEE therefore lack of awareness for measuring OEE is surely an unhealthy sign for a firm. Lack of OEE can cost a lot to them due to downtime and lost quality (Lad and Kulkarni, 2012). Usually organisations measures machines performance in terms of machines productivity and ignore other factors related with product rejections and speed, thus designating and using OEE helps in identifying causes of losses in manufacturing and helps in keeping a track of factors influencing the overall performance (Prickett, 1999). Next barrier for effective maintenance is lack of strategic planning and implementation. Organisations usually do not frame exclusive policies and strategies for maintenance which can help in increasing the commitment level of upper management and employees (Hansson and Backlund, 2003). It is the biggest reason for unsuccessful implementation of maintenance system (Newall and Dale, 1991). For successful maintenance systems, employees' empowerment is essential. It promotes involvement of employees, increases job satisfaction and creates a sense of ownership among employees (Aghazadeh, 2002; Yamashina, 2000). Lack of empowerment is the driving factor for the 'lack of communication' and 'lack of teamwork'. Poor communication can lead to decrease in the growth momentum of the organization. To have the high employee morale and productivity, teamwork is an important factor. When the whole organization is working as a unit then obviously the chances of getting desirable result would increase. The next major barrier is the lack of proper training which is very important as proper training not only increases the skills of the employees but also their commitment towards the maintenance work. In addition to this for successful maintenance systems, employees should be trained to perform cross functional work in addition to routine work. Safe and healthy workplace is a prerequisite for a successful maintenance programme. Ignorance of this factors can lead to serious consequences for environment, company and man. The next important barrier is the lack of performance measure as to become cost effective and competitive it's very important to know the areas of improvement. But as the activities are actually implemented by the employees' thus uncommitted staff can become a serious issue for the maintenance work. The last major barrier is the lack of benchmarking. As benchmarking is a tool to keep the goal to be become "best in class" attainable. Thus it is very important to use benchmarking on continuous basis for sustainable competitiveness of any organisation.

5. Concluding Remarks

As the competition is rising in the world market and local markets around the globe, firms are increasingly realizing the importance of effective maintenance management. It can help to increase the market share by the means of improving product quality,

decreasing rejection, reducing cost and by providing superior service to the customers. Many models such as TPM, RCM, and CBM are employed in the industry to solve maintenance related problems. Successful implementation of these models involves many difficulties. This study has identified eleven main barriers in the implementation of effective maintenance management system. These barriers are Lack of Benchmarking, Lack of Communication, Lack of empowerment, Lack of teamwork, Lack of commitment of employees towards maintenance, Lack of training, Lack of proper Strategic Planning, Lack of top management support, Lack of awareness about safety and health, Lack of effective performance measurement, Lack of proper OEE. Managers should address these barriers effectively to have a positive impact of the maintenance system on the performance.

Analysis and findings have shown that lack of top management support, lack of focus on OEE and lack of strategic planning and implementation are the biggest barrier in effective maintenance management. Whereas lack of benchmarking is relatively ranked lower than the other barriers but it cannot be ignored. These barriers can only be overcome by the willingness and strong leadership which really wants to develop a quality oriented culture in the industry. These findings will help management in formulating maintenance strategies. However before generalising these findings, some empirical and case studies may be carried out as future scope of study.

References:

1. Asjad, M., Kulkarni, M.S. and Gandhi, O.P. (2013) 'Supportability scenario-based contract alternatives for operating life of a mechanical system', *Int. J. Indian Culture and Business Management*, Vol. 6, No. 1, pp.102–114.
2. Abraham, M., Crawford, J. and Fisher, T. (1999), "Key factors predicting effectiveness of cultural change and improved productivity in implementing total quality management", *International Journal of Quality & Reliability Management*, Vol. 16, No. 2, pp. 112-32.
3. Abreu, J. and Martins, P.V., Fernandes, S. and Zacarias, M.,(2013), "Business Processes Improvement on Maintenance Management: A Case Study" *Procedia Technology*, Vol.9, pp.320 – 330
4. Adebajo, D., Abbas, A. and Mann, R. (2010). "An investigation of the adoption and implementation of benchmarking". *International Journal of Operations & Production Management*, Vol.30, No. 11, pp.1140-1169
5. Aghazadeh, S-M. (2002), "Implementation of total quality management in the managed care industry", *The TQM Magazine*, Vol. 14, No. 2, pp. 79-91.
6. Ahmed, S., Hassan, M.H. and Taha, Z. (2005), "TPM can go beyond maintenance: excerpt from a case implementation", *Journal of Quality in Maintenance Engineering*, Vol. 11, No. 1, pp. 19-42.
7. Åhrén, T., Parida, A. (2009), "Maintenance performance indicators (MPIs) for benchmarking the railway infrastructure", *Benchmarking: An International Journal*, Vol. 16, No. 2, pp. 247 - 258
8. Ahuja, I.P.S. and Khamba, J.S , (2008), "Assessment of contributions of successful TPM initiatives towards competitive manufacturing", *Journal of Quality in Maintenance Engineering*, Vol. 14, No. 4, pp. 356-374.

9. Ahuja, I.P.S. and Khamba, J.S. , (2007) "An evaluation of TPM implementation initiatives in an Indian manufacturing enterprise", *Journal of Quality in Maintenance Engineering*, Vol. 13, No. 4, 2007 pp. 338-352
10. Allen, R.S. and Kilmann, R.H. (2001), "The role of the reward system for a total quality management-based strategy", *Journal of Organizational Change Management*, Vol. 14, No. 2, pp. 110-31.
11. Al-Sultan, K. (1996), "Maintenance in Saudi Arabia: needs and recommendations for improvement" *Journal of Quality in Maintenance Engineering*, Vol. 2, No. 4, pp. 5-16.
12. Alsyouf, I. (2007), "The role of maintenance in improving companies' productivity and profitability", *International Journal of Production Economics*, Vol. 105, No. 1, pp. 70-8.
13. Aspinwall, E. and Elgharib, M. (2013), "TPM implementation in large and medium size organisations", *Journal of Manufacturing Technology Management*, Vol. 24, No. 5, pp. 688 - 710
14. Atkinson, P.E. (1990), "Creating Culture Change: The Key to Successful Total Quality Management", IFS Publications, Bedford.
15. Bardoel, E.A. and Sohal, A.S. (1999), "The role of cultural audit in implementing quality improvement programs", *International Journal of Quality & Reliability Management*, Vol. 16, No. 3, pp. 263-76.
16. Brah, S.A., Tee, S.L. and Rao, B.M. (2002), "Relationship between TQM and performance of Singapore companies", *International Journal of Quality & Reliability Management*, Vol. 19, No. 4, pp. 356-379.
17. Chandra, P. and Shastry, T. (1998), "Competitiveness of Indian manufacturing: finding of the 1997 Manufacturing Futures Survey", *Vikalpa*, Vol. 23 No. 3, pp. 15-25.
18. Chin, K.S., Pun, K.F., Xu, Y. and Chan, J.S.F. (2002), "An AHP based study of critical factors for TQM implementation in Shanghai manufacturing industries", *Technovation*, Vol. 22, No. 11, pp. 707-715.
19. Cholasuke, C., Bhardwa, R. & Antong, J. (2004), "The status of maintenance management in UK manufacturing organisations: results from a pilot survey", *Journal of Quality in Maintenance Engineering*, Vol. 10, No. 1, pp. 5-15.
20. Clark, H.J. (1991), "Totally quality management: getting started", *Total Quality Management*, Vol. 2, No. 1, pp. 29-38.
21. Cooke, F.L. (2000), "Implementing TPM in plant maintenance: some organisational barriers", *International Journal of Quality & Reliability Management*, Vol. 17, No. 9, pp. 1003-16.
22. Cooke, F.L. (2003), "Plant maintenance strategy: evidence from four British manufacturing firms", *Journal of Quality in Maintenance Engineering*, Vol. 9 No. 3, pp. 239-49.
23. Davis, R. (1997), "Making TPM a part of factory life", *TPM Experience* (Project EU 1190, Sponsored by the DTI), Findlay.
24. Ding, S.H., Kamaruddin, S. and Azid, I.A., (2014) "Maintenance policy selection model – a case study in the palm oil industry", *Journal of Manufacturing Technology Management*, Vol. 25, No. 3, pp. 415 – 435.
25. Douglas, T.J. and Judge, W.Q. (2001), "Total quality management implementation and competitive advantage: the role of structural control and

- exploration", *The Academy of Management Journal*, Vol. 44, No. 1, pp. 158-169.
26. Eti, M., Ogaji, S. & Probert, S. (2006), "Reducing the cost of preventive maintenance (PM) through adopting a proactive reliability-focused culture", *Applied Energy*, Vol. 83, pp. 1235-1248.
 27. Eti, M., Ogaji, S. & Probert, S. (2007), "Integrating reliability, availability, maintainability and supportability with risk analysis for improved operation of the Afam thermal power-station", *Applied Energy*, Vol. 84, pp. 202-221.
 28. Garg, A. and Deshmukh, S.G. (2006), "Maintenance management: literature review and directions", *Journal of Quality in Maintenance Engineering*, Vol. 12, No. 3, pp. 205-38.
 29. Graham, N.K., Arthur, Y.D. and Mensah, D.P., (2014) "Managerial role in ensuring successful total quality management programme in Ghanaian printing firms", *The TQM Journal*, Vol. 26, No. 5, pp.398 – 410
 30. Grusenmeyer, C. (2010), 'Sous-traitance et accidents', *Exploitation de la base de donnees EPICEA de l'INRS*; CARWH Conference, 'Worker health in a changing world of work', Toronto, 28–29 May 2010.
 31. Hansson, J. and Backlund, F. (2003), "Managing commitment: increasing the odds for successful implementation of TQM, TPM or RCM", *International Journal of Quality & Reliability Management* Vol. 20, No. 9, pp. 993-1008
 32. Hansson, J. and Eriksson, H. (2002), "The impact of TQM on financial performance", *Measuring Business Excellence*, Vol. 6, No. 4, pp. 44-54.
 33. Hardwick, J. and Winsor, G. (2001), "RCM – making the process more cost-effective", in, *Proceedings of International Conference on Maintenance Societies (ICOMS)*, Melbourne, Australia, pp. 1-7.
 34. Hartman, E.H. (1992), "Successfully Installing TPM in a Non-Japanese Plant", *TPM Press*, Pittsburgh, PA
 35. Hendricks, K.B. and Singhal, V.R. (2001), "Firm characteristics, total quality management and financial performance", *Journal of Operations Management*, Vol. 19, No. 3, pp. 269-285.
 36. Hipkin, I.B. and Lockett, A.G. (1995), "A study of maintenance technology implementation", *OMEGA, The International Journal of Management Science*, Vol. 23, No. 1, pp. 79-88.
 37. Hwang, C.L. and Yoon, K. (1981), "Multiple Attributes Decision Making Methods and Applications", *Springer*, Berlin, Heidelberg.
 38. Jaehn, A.H. (2000), "Requirements for total quality leadership", *Intercom*, Vol. 47, No. 10, pp. 38-39.
 39. Jefferson, T. (1785), Letter to John Jay (quoted by Durfel, W.F., *Journal of the Franklin Institute*, Vol. 137, No. 2, 1894).
 40. Jothimani, D. and Sarmah, S.P., (2014) "Supply chain performance measurement for third party logistics", *Benchmarking: An International Journal*, Vol. 21, No. 6, pp.944 – 963.
 41. Karlsson, U. and Ljungberg, O (1995), "Overcoming the difficulties of implementing TPM in Europe", *Maintenance*, Vol. 10 No. 3, pp. 19-25.
 42. Kaynak, H. (2003), "The relationship between total quality management and their effects on firm performance", *Journal of Operations Management*, Vol. 21, No. 4, pp. 405-435.

43. Khanna , H. K. and Sharma, D.D., (2011), "Identifying and ranking critical success factors for implementation of total quality management in the Indian manufacturing industry using TOPSIS", *Asian journal on quality* , Vol. 12, No. 1, pp.124-138.
44. Kodali, R., Mishra, R.P., and Anand, G. (2009) ;" Methodology and Theory Justification of world-class maintenance systems using analytic hierarchy constant sum method"; *Journal of Quality in Maintenance Engineering*, Vol. 15, No. 1, pp. 47-77
45. Kumar , J., Soni , V.K., Agnihotri , G. (2014) "Impact of TPM implementation on Indian manufacturing industry", *International Journal of Productivity and Performance Management*, Vol. 63, No. 1, pp.44 - 56
46. Kumar, P and Singh, R.K, (2012) "A fuzzy AHP and TOPSIS methodology to evaluate global 3PL", *Journal of Modelling in Management*, Vol.7, No.3, pp. 287-303.
47. Kumar, R, Singh, R.K., and Shankar, R, (2015) "Critical success factors for implementation of supply chain management in Indian small and medium enterprises and their impact on performance", *IIMB Management Review*, Vol. 27, No. 2, pp. 92–104.
48. Lad, B.K. and Kulkarni, M.S (2012), "Optimal maintenance schedule decisions for machine tools considering the user's cost structure", *International Journal of Production Research*, Vol. 50, No. 20, 5859-5871.
49. Lad, B.K. and Kulkarni, M.S. (2008), "Integrated reliability and optimal maintenance schedule design: a Life Cycle Cost based approach", *Int. J. Product Lifecycle Management*, Vol. 3, No. 1, pp.78–90.
50. Lad, B.K. and Kulkarni, M.S. (2010a) 'A mechanism for linking user's operational requirements with reliability and maintenance schedule for machine tool', *Int. J. Reliability and Safety*, Vol.4, No.4, pp.343 – 358.
51. Lad, B.K. and Kulkarni, M.S. (2010b) 'A parameter estimation method for machine tool reliability analysis using expert judgement', *International Journal of Data Analysis Techniques and Strategies*, Vol. 2, No. 2, pp. 155–169.
52. Latino, M. (1999), "Management side of engineering", *Plant Engineering*, Vol. 55, No. 2, pp. 32-5.
53. Ledet, W.J. (1999), "Engaging the entire organization key to improving reliability", *Oil & Gas Journal*, 24 May, pp. 54-7.
54. Lee,S.M. and Eom, H.B. (1990),"multiple-criteria decision support system: the powerful tool for attacking complex, unstructured decisions", *systems practice*, Vol. 3, No. 1, pp.51-65.
55. Leong, T.K., Zakuan, N. and Saman, M.Z.M., (2012), " Quality Management Maintenance and Practices- Technical and Non-Technical Approaches", *Procedia - Social and Behavioral Sciences*, Vol. 65, pp.688 – 696
56. Madu, C.N. (2000), "Competing through maintenance strategies", *International Journal of Quality & Reliability Management*, Vol. 17, No. 9, pp. 937-48.
57. Mohamed, O.A., (2005), "Identifying the Barriers Affecting Quality in Maintenance within Libyan Manufacturing Organisations"; "School of Management University of Salford", Salford, UK.
58. Mosadeghrad, A.M. (2014),"Why TQM programmes fail? A pathology approach", *The TQM Journal*, Vol. 26, No. 2, pp. 160 – 187.

59. Narayan, V. (2012), "Business performance and maintenance", *Journal of Quality in Maintenance Engineering*, Vol. 18, No. 2, pp. 183 – 195
60. Nembhard, D.A. (2014), "Cross training efficiency and flexibility with process change", *International Journal of Operations & Production Management*, Vol. 34, No. 11, pp. 1417 – 1439.
61. Newall, D. and Dale, B.G. (1991), "The introduction and development of a quality improvement process: a study", *International Journal of Production Research*, Vol. 29, No. 9, pp. 1747-1760.
62. O'Sullivan, D., Rolstada's, A. and Filos, E. (2011), "Global education in manufacturing strategy", *Journal of Intelligent Manufacturing*, Vol. 22, No. 5, pp. 663-74.
63. Parida, A. and Kumar, U. (2009), "Maintenance Productivity and Performance Measurement", *Handbook of maintenance management and engineering XXVII* page-741
64. Phusavat, K. and Kanchana, R. (2008), "Future competitiveness: viewpoints from manufacturers and service providers", *Industrial Management & Data Systems*, Vol. 108, No. 2, pp. 191-207.
65. Pintelon, L., Nagarur, N. and Puyvelde, F.V. (1999), "Case study: RCM – yes, no or maybe?", *Journal of Quality in Maintenance Engineering*, Vol. 5, No. 3, pp. 182-91.
66. Poduval, P.S, Pramod, V.R. and Jagathy Raj V P , (2015), "Interpretive structural modeling (ISM) and its application in analyzing factors inhibiting implementation of total productive maintenance (TPM)", *International Journal of Quality & Reliability Management*, Vol. 32, No. 3, pp. 308-331.
67. Pophaley, M. and Vyas, R.K. (2010) "Plant maintenance management practices in automobile industries: A retrospective and literature review"; *JIEM*, Vol. 3, No. 3, pp. 512-541
68. Prickett, P.W. (1999), "An integrated approach to autonomous maintenance management", *Integrated Manufacturing Systems*, Vol. 10, No. 4, pp. 233 – 243.
69. Ramezani, F and Lu, J., (2014) "An intelligent group decision-support system and its application for project performance evaluation", *Journal of Enterprise Information Management*, Vol. 27, No. 3, pp.278 – 291.
70. Raouf A. (1994), *Improving Capital Productivity through Maintenance*. *International Journal of Operations & Production Management*, Vol. 14, No. 7, pp. 44–52
71. Raouf, A. and Ben-Daya, M. (1995), "Total maintenance management: a systematic approach", *Journal of Quality in Maintenance Engineering*, Vol. 1, No. 1, pp. 6 – 14
72. Riis, J.O., Luxhoj, J.T. and Thorsteinsson, U. (1997), "A situational maintenance model", *International Journal of Quality & Reliability Management*, Vol. 14, No. 4, pp. 349-66.
73. Rolfsen, M. and Langeland, C., (2012), "Successful maintenance practice through team autonomy", *Employee Relations*, Vol. 34, No. 3, pp. 306 – 321
74. Schawn, C.A. and Khan, I.U. (1994), "Guidelines for successful RCM implementation", *Proceedings of ASME Joint International Power Generation Conference*, Phoenix, AZ, pp. 1-16.

75. Shaaban, M.S., Awni , A.H. (2014),"Critical success factors for total productive manufacturing (TPM) deployment at Egyptian FMCG companies", *Journal of Manufacturing Technology Management*, Vol. 25, No. 3, pp. 393 – 414
76. Sherwin, D. (2000), "A review of overall models for maintenance management", *Journal of Quality in Maintenance Engineering*, Vol. 6 No. 3, pp. 138-164.
77. Shin, D., Kalinowski, J.G. and El-Enein, G.A. (1998), "Critical implementation issues in total quality management", *SAM Advanced Management Journal*, Vol. 63, No. 1, pp. 10-14.
78. Singh, K. and Ahuja, I.S. (2014),"Effectiveness of TPM implementation with and without integration with TQM in Indian manufacturing industries", *Journal of Quality in Maintenance Engineering*, Vol. 20, No.4, pp. 415 - 435
79. Singh, R., Gohil, A.M, Shah D.B. and Desai, S.,(2013), " Total Productive Maintenance (TPM) Implementation in a Machine Shop: A Case Study" *Procedia Engineering*, Vol. 51 pp. 592 – 599.
80. Singh, R.K and Sharma, M.K (2015), "Selecting competitive supply chain using Fuzzy-AHP and Extent analysis", *Journal of Industrial and Production Engineering*, Vol. 31, No. 8, pp. 524-538.
81. Singh, R.K and Sharma, M.K (2014), "Prioritizing the alternatives for flexibility in supply chains", *Production Planning and Control*, Vol.25, No.2, pp-176-192.
82. Singh, R.K., (2011) "Analyzing the Interaction of Factors for Success of Total Quality Management in SMEs" *Asian Journal on Quality*, Vol.12, No.1, pp.6-19.
83. Singh, R.K., Garg, S.K. and Deshmukh, S.G.,(2008) "Strategy development by SMEs for competitiveness: a review", *Benchmarking: An International Journal*, Vol. 15, No. 5, pp. 525-547
84. Singh, R.K., Garg, S.K., Deshmukh, S.G., (2010) "Strategy development by Indian SSIs", *Industrial Management & Data Systems*, Vol. 110, No. 7, pp. 1073-1093.
85. Tsang, A.H.C. and Chan, P.K. (2000), "TPM implementation in China: a case study", *International Journal of Quality & Reliability Management*, Vol. 2, pp. 144-57.
86. Yamashina, H. (2000), "Challenge to world-class manufacturing", *International Journal of Quality& Reliability Management*, Vol. 17, No. 2, pp. 132-43.
87. Yongtao , T., Liyin , S., Craig , L., Weisheng ,L. and Michael , C.H.Y (2014) "Critical success factors for building maintenance business: a Hong Kong case study", *Facilities*, Vol. 32, No. 5/6, pp.208 – 225.

Ranking of barriers for effective maintenance by using TOPSIS approach

List of figures and tables



Figure1: Barriers in implementation of effective maintenance management

Table 1: Barriers in effective maintenance management

Barriers	References
Lack of Benchmarking	Adebanjo et al (2010); Singh, (2011); Shaaban and Awni , (2014)
Lack of Communication and information	Mohamed, (2005); Leong et al., (2012)
Lack of empowerment	Yongtao et al., (2014), Poduval et al., (2015)
Lack of teamwork	Rolfen and Langeland, (2012), Aspinwall and Elgharib, (2013)
Lack of commitment of employees towards maintenance	Singh and Ahuja, (2014); Mosadeghrad, (2014)
Lack of training	Singh et al., (2013); Mosadeghrad, (2014)
Lack of proper Strategic Planning and implementation	Singh et al., (2010); Abreu et al., (2013); Mosadeghrad, (2014), Ding et al. (2014)
Lack of top management support	Kodali et al., (2009); Singh et al.,(2008), Kumar et al. (2015)

Lack of awareness about safety and health	Grusenmeyer, (2010); Singh et al., (2013); Narayan, (2012)
Lack of effective performance measurement	Parida and Kumar, (2009), Lad and Kulkarni (2010a)
Lack of measurement of OEE	Pophaley and Vyas, (2010), Lad and Kulkarni (2010b)

Table 2: Weighted normalized matrix



Decision Makers 	DM1(0.5)	DM2(0.2)	DM3(0.3)
Barriers			
1. Lack of benchmarking	0.051164	0.028834	0.0305
2. Lack of communication	0.153493	0.06728	0.091499
3. Lack of employee empowerment	0.204658	0.038446	0.106749
4. Lack of team work	0.102329	0.057668	0.106749
5. Lack of commitment of employee towards maintenance	0.076747	0.057668	0.04575
6. Lack of proper training	0.127911	0.057668	0.076249
7. Lack of strategic planning and implementation	0.204658	0.06728	0.091499
8. Lack of top management support	0.23024	0.06728	0.137249
9. Lack of effective performance measures	0.076747	0.048057	0.076249
10. Lack of awareness about safety and health	0.127911	0.076891	0.04575
11. Lack of measurement of OEE	0.179076	0.076891	0.121999

Table 3: Summary of +ve ideal solution and –ve ideal solution

Positive ideal sol.	0.23024	0.076891	0.137249
Negative ideal sol.	0.051164	0.028834	0.0305

Table 4: Distance from the positive ideal solution (s_i^*)

Decision Makers 	DM1(.5)	DM2(.2)	DM3(.3)	Average
Barriers				
1. Lack of benchmarking	0.179076	0.048057	0.106749	0.111294
2. Lack of communication	0.076747	0.009611	0.04575	0.044036
3. Lack of employee empowerment	0.025582	0.038446	0.0305	0.031509
4. Lack of team work	0.127911	0.019223	0.0305	0.059211
5. Lack of commitment of employee towards maintenance	0.153493	0.019223	0.091499	0.088072
6. Lack of proper training	0.102329	0.019223	0.060999	0.06085
7. Lack of strategic planning and implementation	0.025582	0.009611	0.04575	0.026981
8. Lack of top management support	0	0.009611	0	0.003204
9. Lack of effective performance measures	0.153493	0.028834	0.060999	0.081109
10. Lack of awareness about safety and health	0.102329	0	0.091499	0.064609

11. Lack of measurement of OEE	0.051164	0	0.01525	0.022138
--------------------------------	----------	---	---------	----------

Table 5: Distance from the negative ideal solution (s_i')


Decision makers 	DM1(.5)	DM2(.2)	DM3(.3)	Average
Barriers				
1. Lack of benchmarking	0	0	0	0
2. Lack of communication	0.102329	0.038446	0.060999	0.067258
3. Lack of employee empowerment	0.153493	0.009611	0.076249	0.079785
4. Lack of team work	0.051164	0.028834	0.076249	0.052083
5. Lack of commitment of employee towards maintenance	0.025582	0.028834	0.01525	0.023222
6. Lack of proper training	0.076747	0.028834	0.04575	0.050443
7. Lack of strategic planning and implementation	0.153493	0.038446	0.060999	0.084313
8. Lack of top management support	0.179076	0.038446	0.106749	0.10809
9. Lack of effective performance measures	0.025582	0.019223	0.04575	0.030185
10. Lack of awareness about safety and health	0.076747	0.048057	0.01525	0.046684
11. Lack of measurement of OEE	0.127911	0.048057	0.091499	0.089156

Table 6: Summary of closeness ratio


Decision maker 	$c_i^* = \frac{s_i'}{(s_i^* + s_i')}$
Barriers	
1. Lack of benchmarking	0
2. Lack of communication	0.604328
3. Lack of employee empowerment	0.716883
4. Lack of team work	0.467974
5. Lack of commitment of employee towards maintenance	0.208656
6. Lack of proper training	0.453246
7. Lack of strategic planning and implementation	0.757569
8. Lack of top management support	0.971213
9. Lack of effective performance measures	0.271218
10. Lack of awareness about safety and health	0.419471
11. Lack of measurement of OEE	0.801084

Table 7: Ranking of barriers in effective maintenance management

Barriers	Ranks
1. Lack of benchmarking	11
2. Lack of communication	5
3. Lack of employee empowerment	4
4. Lack of team work	6
5. Lack of commitment of employee towards maintenance	10
6. Lack of proper training	7
7. Lack of strategic planning and implementation	3
8. Lack of top management support	1
9. Lack of effective performance measures	9
10. Lack of awareness about safety and health	8
11. Lack of measurement of OEE	2

Rectification of Corrupted Neural Networks

Prakhar Dogra

¹Delhi Technological University, Department of Computer Science and Engineering, Shahbad, Bawana Road, Delhi – 110042, India

Abstract: *Imagine if the data set provided for training an artificial neural network turns out to be corrupted. This paper presents a method that can be used to rectify the said neural network after it has been trained but on some corrupted data. In order to rectify the neural network we are provided with a replacement data set for the corrupted data. The proposed method uses the old weights of the corrupted neural network to determine the new weights of the rectified neural network model. Moreover, the proposed method is compared with the present typical method for solving the above stated problem.*

Keywords: Neural network, error, corrupted, Cost function, weights

1. Introduction

Consider a simple example of statistics. Assume that there are 10 numbers in a set that have a mean value of x . But now we are informed that a number in the set was incorrect and should have been something else. Now we need to find a new mean. There is a typical way to find way the new mean. We replace the incorrect number with the correct number. Then we find the mean. But there is a much smarter way to do it. We could use the formula below:

New mean = (Old mean*number of elements in the set – incorrect number + correct replacement number)/ number of elements in the set

Now imagine this problem in an artificial neural network. Consider that we have already trained a neural network. After that, we realize (or come to know of) that some of the outputs in the data were incorrect. Later, we are given the replacement output values and asked to find the new correct weights for the neural network model. For example, consider the MNIST database of handwritten digits that has a training set of 60,000 examples, and a test set of 10,000 examples. It is a subset of a larger set available from NIST [1]. The digits have been size-normalized and centred in a fixed-size image. Now assume that about 1000 images in the training data turned out to be incorrectly classified (the output values were incorrect or the images were incorrectly labelled). A typical way to solve this problem is to simply replace the incorrectly classified output data with correctly classified output data and then train the neural network from the beginning (re-initialize the parameters) [2].

In this paper, a method is explained where we don't need to apply the above typical method in order to get correct weights for the neural network. A new method is proposed that takes lesser computation to achieve the rectified neural network. The paper is organised as follows. Section 2 explains the typical method that is usually used to solve the above stated problem. Section 3 explains the proposed method. Section 4 gives a brief about the implementation and analysis of the proposed method explained in Section 3. Section 5 briefs about the applications of proposed method on different types of problems. Finally, section 6 compares the proposed method to the typical method used.

2. Typical Solution

Since we have already trained the artificial neural network before realizing that some of the data is corrupted, the typical method suggests that we need to train the neural network from the beginning (re-initialize the parameters) [2]. Consider an example of the MNIST data set [1] (say an image that displays the digit 7 but its output data shows that the image is a hand-written digit 1). Now this example is corrupted. Assuming that the neural network has already been trained on the data set that has some corrupted data examples (or examples with incorrect output value), we should know that our neural network has been corrupted. It means that the weights of each node of each layer have been corrupted. There is a typical way to solve this problem. After we are provided with the correct data set, we need to re-initialize the parameters (or weights) of the neural network. Then we have to apply forward propagation [3] and back-propagation [4] [5] method in order to train the neural network. In this method, the corrupted data set and the weights are discarded and replaced. This method requires the same amount of computation as required when the data set was corrupted.

The accuracy and time required for this method and the proposed method (discussed in section 3) are compared in Section 6.

3. The Proposed Method

The proposed method can be explained by taking examples from MNIST data set [1]. We have to assume that some of the examples in the data set have incorrect output values like an image of a digit 7 has output value of 1. In the previous section, we have explained that the method requires the cost function values of the corrupted neural network in order to reverse the effects of the incorrect examples with the new correct examples.

The proposed method can be explained in the following steps:

1. Storing the corrupted data

The corrupted data is the data set containing some examples that have incorrect output values (some images are

incorrectly labelled). The weights created while training the neural network with the corrupted data set are also stored so they can be used during the rectification process. Corrupted data set is compared with the new data set in order to check which examples have incorrect output values. Then these corrupt data set examples are stored along with their respective correct output values and their respective indices from the original data set (corrupt) in a separate file. This creates an incorrect-correct data set (i.e., the output values). This data set is then used further in the proposed method to reverse the effects on the corrupted neural network.

2. Modified Back Propagation

For the proposed method we have modified the back propagation algorithm. In the modified back propagation algorithm the error term for the first iteration is calculated as the difference in the incorrect and correct output values of the new (not corrupt) and corrupted dataset respectively. Then we follow the usual back propagation algorithm to update the weights. We use forward propagation to find the hypothesis term and subtract it from the output value (given) to find the error term δ . Then using the traditional back propagation algorithm we calculate the error terms of the previous layers. Then we calculate the numerical gradients of the respective layers using the respective error terms (denoted by δ). Following that we update the weights of the neural network using the respective numerical gradients.

In short we can say that we backpropagate only once with the error term as the difference in the incorrect and correct output values.[6] Then we follow the usual back propagation algorithm to update the values. Usually the data set (incorrect-correct output data set) is much smaller than the original data set it takes much lesser time to rectify the data set.[7] This can be seen from the results presented in the next section.

In the proposed method, we use the saved incorrect-correct data set to create an array of respective error terms. For example, the hypothesis predicts the image as digit 7 and the incorrect output value is 9 whereas the correct output value is 1. The error term of this example will be a vector $\delta = [-1 \ 0 \ 0 \ 0 \ 0 \ 1 \ 0 \ -1 \ 0]^T$. In the vector above, the values are assumed to be either 0 or 1 or -1. But in actual implementation, these values are usually floating-point values varying between -1 and 1 and are usually very near to either -1, 0 or 1. After that, we can run a series of back-propagation and forward propagations (as explained above) to update the old weights.[8] We would just need the last updated weights of the neural network. Here the number of iterations required need not be equal to when originally training the neural network. Since the incorrect-correct example pair data set is smaller than the original data set, we can reduce the number of iterations because the smaller data set will require less amount of tuning and hence less number of iterations.[9]

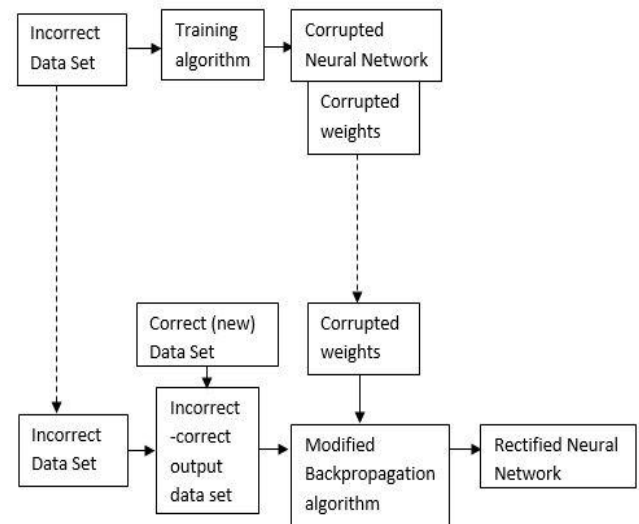


Figure 1: Proposed method

4. Implementation and Analysis

The proposed method was tested on several data sets. All the data sets were corrupted by replacing original values with random (output values within the range of the original set) values at random positions in the data sets. One of the results of our implementation have been shown below. These are the results are of the popular MNIST data set for Hand-written digit recognition problem. There were 5000 examples in the original data set and out those examples, 200 random examples were corrupted (incorrect output values). As you can see from the table below, the percentage accuracy dropped by nearly 5% when 4% examples were corrupted. It means that the weights in the neural network got corrupted. After rectification process the accuracy wasn't exactly restored when the neural network was trained on the original (no incorrect outout values) data set but the accuracy increased by nearly 4% when the corrupted neural network (corrupted weights) was tested.

Table 1: Percentage accuracies in different cases

<i>Data set</i> \ <i>Rectification</i>	<i>Before Rectification</i>	<i>After Rectification</i>
Corrupted Dataset	90.56%	94.31%
New Data set (original)	95.7%	—

As the number of corrupted examples were increased, the accuracy of the corrupted neural network also decreased. Moreover after rectification the accuracy also increased from the corrupted neural network case but not in a linear fashion as expected. The reason might be due to random examples being chosen everytime the original output values were replaced with random values in order to make corrupted data set.

Moreover, the relation between the time elapsed for the neural network to rectify and the number of examples being corrupted wasn't linear either. This might also be due to the random examples being chosen everytime the original output values were replaced with random values in order to make corrupted data set.

5. Applications

The proposed method is a solution to the problem when an artificial neural network is trained over a data set that consists of some examples that have incorrect output values. This improved backpropagation algorithm [10][11] can be applied to similar types of problems. For example, we have a data set that consists of a million images of very small number of people (say 20). And after training the network we realise that some of those images were incorrectly classified due to incorrect output values. Later we are provided with a correct data set. Rather than re-training the neural network from the beginning (re-initialising the parameters), we can simply apply the above proposed method to train the neural network. This method can be applied to almost any neural network that faces the above stated problem. Neural network can be for object images, hand-written images, data sets that require complex neural networks to learn, etc.

The proposed method can be modified and used in Software Re-Engineering and Reverse Engineering problems. Where, if we need to change the testing data, we might not actually be required to compute all the values from the scratch typically and use the new method similar to the above discussed improved back propagation [10][11] to get the new values. For example, let's take the concept of black box testing. We don't know what code lies inside the software but what we want is to test out a lot of values to see if any error comes out or not. Now assume that an error does come. What can we do in such a situation. We can use the basic approach of the above proposed method and modify the software without going too deep into the code of the software.

6. Comparison between Typical and Proposed Method

As explained in Section 2, the typical method involves the replacement of incorrect examples with correct examples and then trains the neural network from the beginning. And as explained in previous sections, the proposed method uses stored values of old neural network weights to rectify it using the new correct examples. As we can see from the explanations provided in above sections, the typical method uses slightly less memory usage because it doesn't prefer to store the old weights of the neural network (corrupted). But the proposed method requires less computation. Firstly, it doesn't calculate the cost function values of all the elements. It simply calculates cost function of the incorrect examples and the replacement correct examples. Moreover, while training the neural network, only the incorrect-correct example pairs are trained rather the complete data set. Suppose that we have a MNIST data set that consists of 60000 images for training. Out of these we have 1000 examples with incorrect output values. We can simply observe that the size of the array used for training the neural network (especially when using a vectorized implementation approach [5]). Moreover, there wasn't any relation found between the number of examples being corrupted and the percentage increase in the accuracy after rectification, probably due to the randomness of the selection process.

References

- [1] LeCun, Yann; Corinna Cortes; Christopher J.C. Burges. "MNIST handwritten digit database, Yann LeCun, Corinna Cortes and Chris Burges". Retrieved 17 August 2013.
- [2] Handwritten Digit Recognition by Neural Networks with Single-Layer Training. S. KNERR, L. PERSONNAZ, G. DREYFUS, Senior Member, IEEE. IEEE TRANSACTIONS ON NEURAL NETWORKS, vol. 3, 962 (1992).
- [3] Introduction to multi-layer feed-forward neural networks. Daniel Svozil, Vladimir Kvasnička, Jiří Pospíchal. Chemometrics and Intelligent Laboratory Systems 39 (1997) 43-62.
- [4] Rumelhart, David E.; Hinton, Geoffrey E.; Williams, Ronald J. (8 October 1986). "Learning representations by back-propagating errors". *Nature* 323 (6088): 533–536. doi:10.1038/323533a0
- [5] D. E. Rumelhart, G. E. Hinton, and R. J. Williams. *Learning Internal Representations by Error Propagation* in Rumelhart, D. E. and McClelland, J. L., *Parallel Distributed Processing: Explorations in the Microstructure of Cognition*. MIT Press, Cambridge Massachusetts, 1986.
- [6] A. Olaru, S. Olaru, L. Ciupitu, "Research of the Neural Network by Back Propagation Algorithm", *Advanced Materials Research*, Vols. 463-464, pp. 1151-1154, Feb. 2012
- [7] Kuldip Vora and Shruti Yagnik and Mtech Scholar, "A Survey on Backpropagation Algorithms for Feedforward Neural Networks", *International Journal of Engineering Development and Research*, ISSN: 2321-9939
- [8] Md Nasir Sulaiman and Maslina Darus. "An improved error signal for the backpropagation model for classification problems." *International Journal of Computer Mathematics*. 01/2001; 76(3):297-305. DOI: 10.1080/00207160108805026
- [9] Tasos Falas and A-G Stafylopatis, "The impact of the error function selection in neural network-based classifiers", *IJCNN'99. International Joint Conference on Neural Networks*, 1999. Volume 3 Pges 1799-1804.
- [10] M C Bossan, "A modified backpropagation algorithm for neural classifiers." *Proceedings of the 38th Midwest Symposium on Circuits and Systems* (1995).
- [11] J Lv, Z Yi, "An Improved Backpropagation Algorithm Using Absolute Error Function (2005)", ISBN 2005, LNCS 3496.

Author Profile



Prakhar Dogra is an undergraduate student (B.Tech) in Computer Engineering at Delhi Technological University (formerly as Delhi College of Engineering). He has till date published 2 other research papers both in the field of Computer Science and Engineering.

Synthesis of Ni filled multiwalled carbon nanotubes and study of magnetic behaviour

Reetu Kumari, Anshika Singh, Rajesh Kumar, Lucky Krishnia, Vinay Kumar, Nitin K. Puri, Pawan K. Tyagi*

Department of Applied Physics, Delhi Technological University, Delhi 110042, India

*Corresponding author. Tel: (+91) 11-27852212; Fax: (+91) 11-27871023; E-mail: pawan.phy@dce.edu

Received: 09 September 2015, Revised: 21 September 2015 and Accepted: 03 January 2016

ABSTRACT

In this report, we have illustrated the synthesis of the Ni-filled multiwalled carbon nanotubes (MWCNTs) on both metallic and non-metallic substrates, by using thermal CVD technique. Scanning Electron Microscopy (SEM) and X-ray diffraction (XRD) have been used to characterize the surface morphology and crystalline nature of the MWCNTs encapsulated with Ni nanorod. These filled MWCNTs have exhibited strong magnetic response due to encapsulation of pure phase of Ni. Magnetic Force Microscopy (MFM) study of such filled tubes reveals the pole formation in the Ni nanorod and confirms magnetization direction perpendicular to tube axis. Filling occurs in a fragmented manner confirmed by MFM and each fragment found to have north and south poles along the axis perpendicular to the tube i.e. radial direction of tube. Copyright © 2016 VBRI Press.

Keywords: Carbon nanotubes; thermal CVD; magnetic force microscopy (MFM); magnetization direction.

Introduction

Metal-filled multiwalled carbon nanotubes (MWCNTs) have potential industrial application in various fields of science and technology. The injection or filling of metal into the MWCNT may significantly amend their mechanical [1], electrical [2] and magnetic properties [3-7]. The metal-filled MWCNTs have variety of industrial applications such as catalysts [8], electronic devices [9], magnetic tape [10], and biosensors [11]. Filling of MWCNT can be accomplished either *in-situ* or *ex-situ* [12]. Among all, routes of *in-situ* filling have been preferred because of the easy way and filler exhibit high integrity in properties. *In-situ* filling can be made by various methods such as Arc discharge [13], Laser ablation [14], Plasma enhanced CVD [15] and Thermal CVD [16, 17]. Generally, in order to study the magnetic properties of ferromagnetic materials filled inside MWCNT, Fe, Co and Ni have been selected as filler in the most of published reports [17-22]. Among all metals, which have been filled to the date, filling with Fe, or Fe₃C has been reported by most of the researchers [20, 23-25]. This happens due the high solubility of carbon in Fe. However, due to low binding energy of carbon with Fe, crystalline quality of MWCNT grown by using Fe as catalyst is low as compared to MWCNT grown by using Ni or Co as catalyst. Filling of the pure phase of Fe is very difficult because of the rapid formation of Fe₃C, which dominates over Fe phase formation. The carbide formation deteriorates the magnetic properties of the filled MWCNTs. MWCNTs filled with pure phase exhibit extraordinary magnetic properties. However, very few researchers have published the CVD method to grow pure Fe, Ni, Co; Ni/Pt filled MWCNTs [20, 21, 22, 26]. For the application of nanorod filled inside

MWCNT as nanomagnet, it is important to first investigate magnetization behaviour and then pole formation in ferromagnetic nanorod filled inside the MWCNT. Another burning issue related to on-going research in area of MWCNT is to grow the MWCNT on conducting, non-conducting, magnetic or non-magnetic substrates. Among them MWCNTs grown on conducting substrate are of high importance. Reason is, if MWCNT follow root-growth mechanism depending on catalyst nature [27] then substrate-MWCNT interface has low contact resistance and substrate can be used as a one contact for the devices. Objective of present study is two folds: (1) to grow pure Ni-filled MWCNTs on various substrates, and (2) to study the magnetization behaviour in confined nanorod by using MFM.

Experimental

Materials and synthesis method

Thermal chemical vapour deposition (Thermal CVD) technique was used to grow Ni-filled MWCNTs. In the technique quartz tube of inner diameter (ID) 3.5 cm and length of 60.0 cm was used as a reactor. The system has a 10.0 cm pre-heating zone (100 - 150 °C) and 15.0 cm heating zone (800 - 900 °C). To grow samples on quartz we have taken mixture of nickelocene and benzene of ratio 0.015 gm/ml. The mixture was first introduced in pre heating zone where solution vaporized and then vapour were introduced in to hot zone by using Ar/H₂ mixture as a carrier gases. Flow of Ar/H₂ gas mixture (Ar-100 sccm, H₂-50 sccm) was optimized for growth on all substrates. After the completion of reaction, system was set to cool down to room temperature in the presence of Ar. In order to grow MWCNTs on SiO₂/Si, Copper (Cu) and Stainless Steel (SS)

temperature was set at 830 °C. When temperature of furnace reaches to reaction temperature, substrates were brought in to the hot zone in such a manner that the dense vapours immediately diffused on the substrates at set reaction temperature. After synthesis substrates were found to be fully covered by black thick layer of MWCNTs.

Characterization techniques

As-grown samples were characterized with Bruker D8 Advance X-Ray diffractometer and Hitachi S3100 Scanning Electron Microscopy. Very few amount of sample dispersed in Isopropyl alcohol (IPA) and then sonicated for 20 minutes to make a uniform dispersion. A single drop of dispersion of MWCNTs was used to make thin film on Si substrate. The thin film of MWCNTs on Si substrate was used in MFM study.

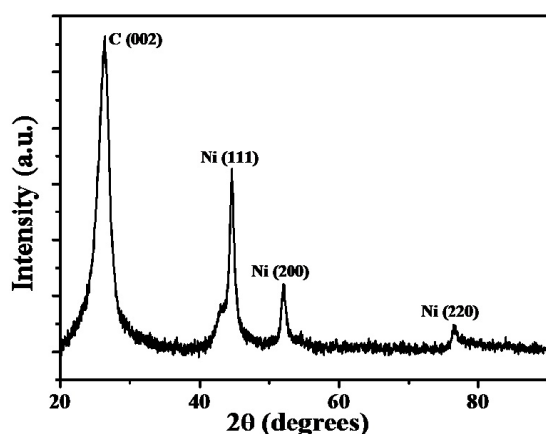


Fig. 1. XRD diffraction pattern of the as-grown Ni-filled MWCNTs, which grow on wall quartz reactor.

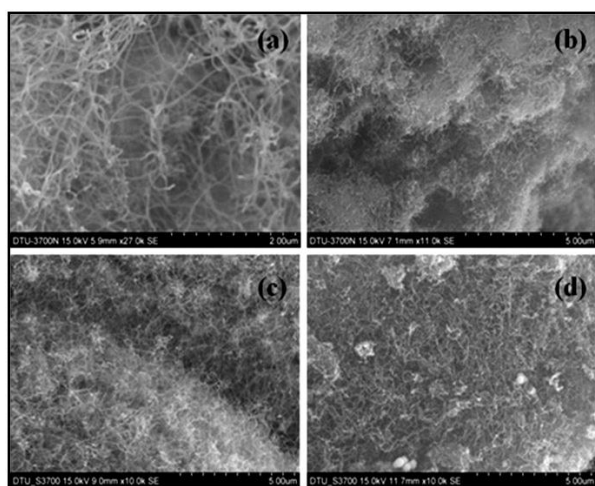


Fig. 2. SEM Images of Ni filled-MWCNTs grown on (a) Cu substrate, (b) SS substrate, (c) SiO₂/Si (300 nm/500 μm) substrate, (d) quartz.

Results and discussion

X-ray diffraction (XRD) measurement was performed on the as-grown filled MWCNTs scratched from the walls of quartz reactor. In **Fig. 1**, signature peak of MWCNT at $2\theta = 26.33^\circ$ position, reflected from (002) plane of graphite (PCPDF 75-2078) was observed. Diffraction peaks at

$2\theta = 44.62^\circ, 51.9^\circ$ and 76.50° positions are identified and found to be of (111), (200) and (220) planes of the fcc Ni (PCPDF 87-0712). Filling of fcc Ni having symmetry with intimate walls MWCNT have been also reported in Ref. [26] and reported results are matched with observed values. XRD profile confirmed that MWCNTs filled with fcc Ni have high crystalline quality. This is evident by FWHM (2°) and intensity of peak observed at ($2\theta = 26.33^\circ$) position.

Growth possibility of MWCNTs on various substrates has been demonstrated and confirmed by SEM images as shown in **Fig. 2**. Variation in density of MWCNT with morphological change clearly depicts the influence of the substrates on MWCNT growth.

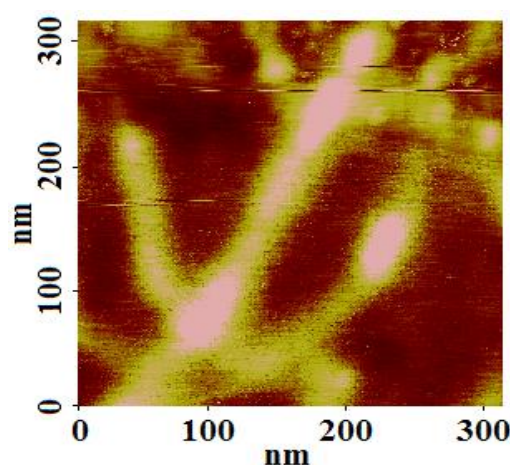


Fig. 3. MFM topography of Ni filled MWCNTs by using magnetic tip in tapping mode.

MWCNTs grown on Cu (**Fig. 2(a)**) are less curly than that grown on other substrates. MWCNTs are well separated while CNTs on SS grown in bunches of high density. On SiO₂ coated Si substrate, MWCNTs are observed to be grown more vertical and have uniform morphology. In powder samples scratched from the walls of quartz reactor, MWCNTs are found to be grown randomly. As-grown MWCNTs have shown strong magnetic interaction when they are brought close to the bar magnet. This confirms the presence of Ni as either filler or catalytic impurities. Further, fragmented filling of Ni inside the core of MWCNT have been confirmed by MFM and shown in **Fig. 3**. Detailed MFM studies of Ni-filled MWCNT have shown in **Fig. 4**. In order to corroborate tip-sample interaction, MFM studies including amplitude and phase changes have been performed for hard disk also (shown in **Fig. 5**). MFM measurement performed on Ni-filled MWCNT with the lift height of 50 nm.

Image in **Fig. 3** is the topographic image of Ni filled CNTs captured by using magnetic tip in tapping mode. Bright contrast in topographic image, if captured by using the magnetic tip in tapping mode, directly measures the dominating interaction between tip-Ni while other interaction like, between CNT and tip are minimized. So, intensity can be assumed as a direct measure of the interaction strength. Therefore, filled parts of MWCNT respond very strongly to the magnetized tip and have both vander waal and magnetic interaction. Consequently, filled

parts of MWCNT can be identified by the contrast variation. Filling inside the MWCNT was found to be fragmented as confirmed by the intensity variation along tube axis (as shown in **Fig. 3**).

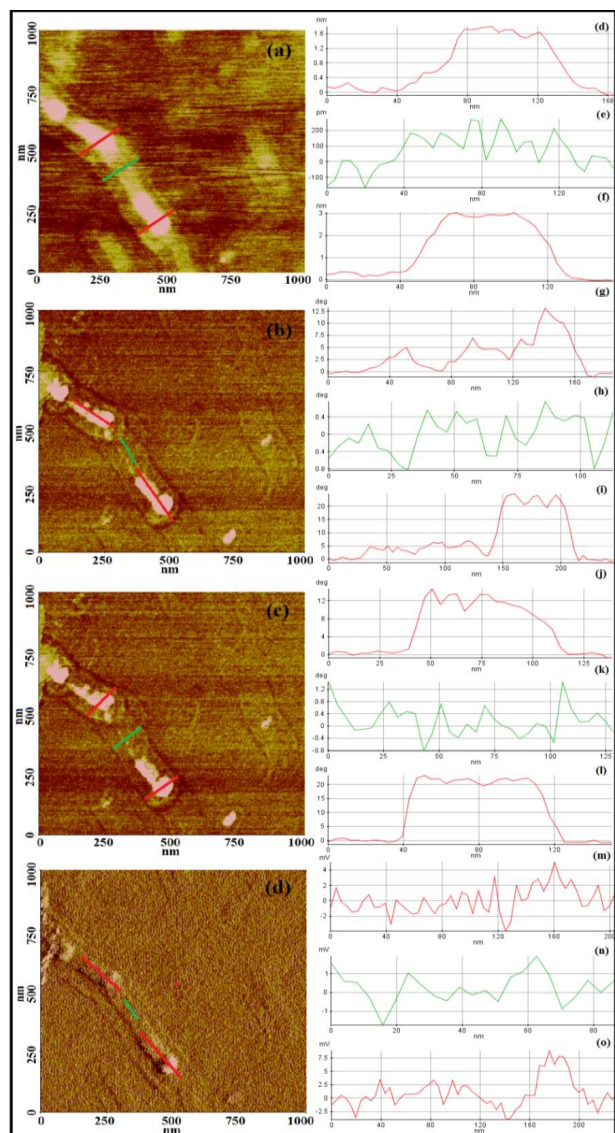


Fig. 4. MFM studies with lift height 50 nm (a) Topography, (b & c) Phase, and (d) amplitude images of Ni filled MWCNT. (e-o) corresponding profiles of filled and unfilled regions represented by lines in planes (a-c).

In the present study, MFM measurements were taken in two passes across each scan of the sample. In the first pass surface topography was scanned which is represented in (**Fig. 4(a)**). The topographical trace and retrace were performed in tapping mode of AFM. In second pass, the probe was lifted to the desirable height from the surface so that short-range forces (vander walls force) get minimize. At this height the tip was able to trace and retrace only magnetic responses. The magnetic interaction depends on the factors like: lift height, coercivity and the magnetic moment of the tip as well as magnetic stray field intensity of the sample [28]. In this scan mode, a force acts between magnetic tip and sample magnetic stray field and this force gradient results in change in phase as well as amplitude

with which cantilever vibrates [28]. The shift in phase and amplitude are exceedingly informative in analyzing magnetic response. In **Fig. 4 (b, c and d)** these shifts are explained along with their corresponding line profiles.

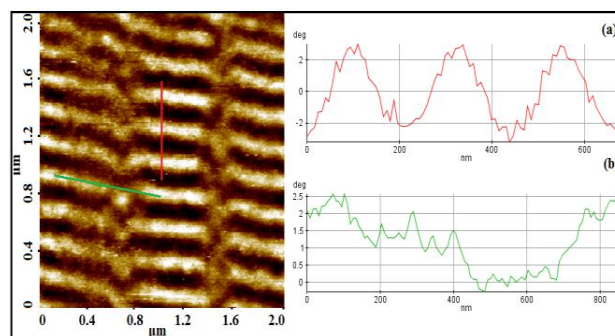


Fig. 5. MFM phase image of hard disk drive.

Fig. 4(b) represents the phase profile of Ni-filled MWCNT captured in lift mode. Remarkable, phase shifts have observed as confirmed by line profiling in filled parts as shown in **Fig. 4(g)** and (**i**). Along the tube axis bright contrasts appeared to be uniform. In line profile if we moves from darker to brighter portion the phase is shifted from 0 to 12.5° and again it goes down to 0° in darker region. The same phenomenon occurs in other filled part where phase shift goes to 20° degree and vice-versa. Importantly, there is no significant phase shift observed in unfilled part of MWCNT (**Fig. 4h**). The contrast in phase image has been reported to depend on nature of interaction which present between tip and sample, either attractive or repulsive [29]. Bright contrast is presumed due to repulsive magnetic interaction, and results in positive phase shift. Therefore, in the studied sample strong repulsive magnetic interaction was found to be acting between probe and filled parts of MWCNT. Similarly, line profiles were taken along the radial direction of the tube as shown in **Fig. 4(k, l and m)**. Nearly exact phase shifts in positive direction have been observed. Uniformity of contrast as well phase shift confirmed the existence of single domain in both radial or along the axis of Ni nanorod. Consequently, in studied sample nickel nanorod having single domain structure is confirmed. In order to study the phase shift behaviour more extensively, we have compared the MFM phase image of standard hard disk drive (**Fig. 5**). In **Fig. 5(a)** the profile shows that from darkest to brightest region the phase shifted from -2.5° to 2.5° while in darkest contrast it again fell down to -2.5°. Therefore, for each cycle (darkest to brighter contrast), phase shifted from -2.5° to 2.5°. The negative shift occurs due to attractive magnetic force while positive is due to repulsion. This confirmed that in hard disk poles were formed perpendicular to bit length. However, line profile along the length of bit area (**Fig. 5b**) the phase shift was not negative anywhere but was positive in brighter contrast area with the same value as in **Fig. 5b**. In the scanned image along length of bit area has the darker contrast with almost negligible phase shift (**Fig. 5b**) is not as dark as appeared in perpendicular to the bits length because the less darker portion does not show any pole in that direction. Therefore, it has been confirmed that

transition in the direction of magnetization is only observed along the width of the bits.

In Ni-filled MWCNT, the direction of magnetization was found to be perpendicular to the tube axis. This is evident by the result, i.e. no negative phase shift either along or perpendicular to tube axis. The line profile of MFM phase is somewhat similar to the line profile along length of bit area (in Fig. 5) of the phase image of the hard disk where only one type of interaction is observed (in bright contrast) and rest part does not seem to have magnetic responses. If direction of magnetization is along the tube axis then magnetic contrast should be bright at one end and negative at the other end because poles would be formed along the tube axis. Lutz *et al.* have reported the direction of magnetization in case of Fe and Fe₃C nanowire inside MWCNTs [29]. In their report they have mentioned the MFM images of both types of nanowires and explained the direction of magnetization taking contrast into account. However, they have reported that in case of Fe poles form along the tubes axis but in our case filling of Ni inside MWCNT causes pole formation perpendicular to the tube. The studied Ni-filled MWCNT are grown randomly and mostly found to be lying in substrate plane. So we assume that radial direction is perpendicular to substrate plane. As reported in Ref [30], a magnetic field gradient in radial direction was applied in order to maintain the temperature during growth. Instead of shape or magnetocrystalline anisotropy this gradient may be controlling the direction of magnetization in Ni nanorod.

Conclusion

We have demonstrated the growth of Ni filled MWCNTs on metallic and non-metallic both kinds of substrates. The filling of metal inside MWCNT takes place in fragmented manner which is confirmed by probing the filled MWCNTs with MFM. Positive variation in the phase in both directions along as well as perpendicular to the tube axis confirmed that in Ni nanorod poles are formed in radial direction. In magnetization shape anisotropy is not playing a decisive role. The strong magnetic interaction proposes that filled MWCNT can be used for storage devices capable of storing data for long term.

Reference

- Coleman, J.N.; Khan, U.; Gun'ko, Y.K.; *Adva. Mater.*, **2006**, *18*, 689. DOI: [10.1002/adma.200501851](#)
- Mathur, A.; Wadhwa, S.; Tweedie, M.; Hazra, K.S.; Dickinson, C.; Roy, S.S.; Mitra, S.K.; Misra, D.S.; McLaughlin, J. A.; *Physica E*, **2011**, *44*, 29. DOI: [10.1016/j.physe.2011.06.035](#)
- Shpak, A.P.; Kolesnik, S.P.; Mogilny, G.S.; Petrov, Yu. N.; Sokhatsky, V.P.; Trophimova, L. N.; Shanina, B. D.; Gavriljuk, V. G.; *Acta Mat.*, **2007**, *55*, 1769. DOI: [10.1016/j.actamat.2006.10.039](#)
- Jian-hua, L.; Ruo-yu, H.; Gua-hua, L.; Dong-guang, W.; *Ne. Carb. Mater.*, **2010**, *25*, 192. DOI: [10.1016/S1872-5805\(09\)60026-3](#)
- Wolny, F.; Mühl, T.; Weissker, U.; Lipert, K.; Schumann, J.; Leonhardt A.; Büchner B.; *Nanotech.*, **2010**, *21*, 435501. DOI: [10.1088/0957-4484/21/43/435501](#)
- Weissker, U.; Hampel, S.; Leonhardt, A.; Büchner, B.; *Mater.*, **2010**, *3*, 4387. DOI: [10.3390/ma3084387](#)
- Bao J.; Zhou, Q.; Hong, J.; Xu, Z.; *Appl. Phys. Lett.*, **2002**, *81*, 4592; DOI: [10.1063/1.1526461](#)
- Che, G.; Lakshmi, B. B.; Martin, C. R.; Fisher, E. R.; *Langmuir*, **1999**, *15*, 750. DOI: [10.1021/la980663i](#)
- Kawano, T.; Christensen, D.; Chen, S.; Cho, C.Y.; Lin, L.; *Appl. Phys. Lett.*, **2006**, *89*, 163510. DOI: [10.1063/1.2364151](#)
- Winarski, T. Y.; U. S. Patent 7976966 B2, **2011**.
- Freemantle, M.; *Chem. Eng. News*, **1996**, *74*, 62.
- Tyagi, P.K.; Singh, M. K.; Misra, D. S.; *Encycl. of Nanos. Tech.*, **2003**, *3*, 416.
- Loiseau, A.; Pascard, H.; *Chemical Physics Lett.*, **1996**; *256*, 246. DOI: [10.1016/0009-2614\(96\)00459-9](#)
- Thess, A.; Lee, R.; Nikolaev, P.; Dai, H.; Petit, P.; Robert, J.; Xu, C.; Kim, S. G.; Rinzler, A.G.; Colbert, D.T.; Scuseria, G. E.; Tománek, D.; Fisher, J. E.; Smalley, R. E.; *Science*, **1996**, *273*, 483. DOI: [10.1126/science.273.5274.483](#)
- Hayashi, Y.; Tokunaga, T.; Kaneko, K.; Henley, S. J.; Stolojan, V.; Carey, J.D.; Silva, S.R.P.; *IEEE Trans. Nanotech.*, **2006**, *5*, 485. DOI: [10.1109/TNANO.2006.880456](#)
- Huczko, A.; *App. Phys. A: Mater. Sci. Process*, **2002**; *74*, 617. DOI: [10.1007/s003390100929](#)
- Rao, C.N.R.; Govindraj, A.; Sen, R.; Satishkumar, B.S.; *Mat. Res. Innov.*, **1998**, *2*, 128. DOI: [10.1007/s100190050075](#)
- Leonhardt, A.; Ritschel, M.; Kozuharova, R.; Graff, A.; Mühl, T.; Huhle, R.; Mönch I.; Elefant D.; Schneider C. M.; *Diam. Rela. mater.*, **2003**; *12*: 790. DOI: [10.1016/S0925-9635\(02\)00325-4](#)
- Leonhardt, A.; Hampel, S.; Müller, C.; Mönch, I.; Koseva, R.; Ritschel, M.; Elefant, D.; Biedermann, K.; Büchner, B.; *Chem. Vap. Deposition*, **2006**, *12*, 380. DOI: [10.1002/cvde.200506441](#)
- Karmakar, S.; Sharma, S.M.; Mukadam, M.D.; Yusuf, S.M.; Sood A. K.; *J. Appl. Phys.*, **2005**, *97*, 054306-01-054306-05. DOI: [10.1063/1.1858878](#)
- Poswal, H. K.; Karmakar, S.; Tyagi, P. K.; Misra, D. S.; Busetto, E.; Sharma, S. M.; Sood, A. K.; *Phys. Stat. Solid. (b)*, **2007**, *244*, 3612. DOI: [10.1002/pssb.200642608](#)
- Tyagi, P.K.; Misra, A.; Singh, M. K.; Misra, D. S.; Ghatak, J.; Satyam, P.V.; Normand, F.L.; *Appl. Phys. Lett.*, **2005**, *86*, 253110. DOI: [10.1063/1.1953881](#)
- Geng, F.; Cong, H.; *Phys. B*, **2006**, *382*, 300. DOI: [10.1016/j.physb.2006.03.003](#)
- Iskhakov, R. S.; Komogortsev, S.V.; Balaev, A.D.; Okotrub, A.V.; Kudashov, A.G.; *JETP Lett.*, **2003**, *78*, 236. DOI: [10.1134/1.1622038](#)
- Weissker, U.; Löffle, M.; Woln, F.; Lutz, M.U.; Scheerbaum, N. J., *Appl. Phys.*, **2009**, *106*, 054909-5. DOI: [10.1063/1.3204495](#)
- Singh, M.K.; Titus, E.; Tyagi, P.K.; Palnitkar, U.A.; Misra, D.S.; Roy, M.; Dua, A. K.; Cojocar, C. S. ; Normand, F.L., *J. Nanosci. Nanotech.*, **2003**, *3*, 165. DOI: [10.1166/jnn.2003.200](#)
- Tyagi, P.K.; Janowska, I.; Cretu, O.; Pham-Huu, C.; Banhart, F., *J. Nanosci. Nanotechnology*, **2011**, *11*, 1. DOI: [10.1166/jnn.2011.3740](#)
- Bramowicz, M.; Kulesza, S.; Czaja, P.; Maziarz, W.; *Arch. Metall. mater.*, **2014**, *59*, 451. DOI: [10.2478/amm-2014-0075](#)
- Lutz, M.U.; Weissker, U.; Wolny, F.; Müller, C.; Löffler, M.; Mühl, T.; Leonhardt, A.; Büchner, B.; Klingeler, R., *J. Phys. Conference Series*, **2010**, *200*, 072062. DOI: [10.1088/1742-6596/200/7/072062](#)
- Kumari, R.; Krishnia, L.; Kumar, V.; Singh, S.; Singh, H. K.; Kotnala, R.K.; Juluri, R. R.; Bhatta, U. M.; Satyam, P. V.; Yadav, B. S.; Tyagi, P.K., Article in preparation. DOI: [10.1039/c0cs00136h](#)



THE DESIGN OF A HIGH SPEED NONLINEAR FEEDBACK-BASED CURRENT COMPARATOR

Veepsa Bhatia^{1*}, Neeta Pandey², Ranjana Shridhar², Asok Bhattacharyya²

¹ *Department of Electronics and Communication Engineering, Indira Gandhi Delhi Technical University for Women, New Delhi-110006, India*

² *Department of Electronics & Communication Engineering, Delhi Technological University, Shahbad Daultpur, Bawana Road, Delhi-110042, India*

(Received: September 2015 / Revised: December 2015 / Accepted: January 2016)

ABSTRACT

In this paper a new current comparator architecture is presented, which utilizes the concept of nonlinear feedback to speed up the operation. The analytical formulation for quantifying the effect of the feedback is put forward. The functionality of the proposed comparator is verified using simulations carried out on an Orcad Pspice tool using Taiwan Semiconductors Manufacturing Company (TSMC) 0.18 μm technology parameters. The resolution and delay are found to be ± 10 nA and 1.48 ns, respectively at a reference current of 1 μA . The effects of parameter variations on the performance of the proposed comparator at different design corners is also studied. The usefulness of the proposed comparator is demonstrated through a 3-bit current mode flash Analog to Digital Converter (ADC) and its performance parameters are also calculated using simulations. The simulation results show that the 3-bit current mode flash Analog to Digital Converter exhibits no missing codes and has Differential Non-Linearity (DNL) of -0.25 Least Significant Bit (LSB) and Integral Non-Linearity (INL) of -0.19 LSB.

Keywords: Current comparator; Current mode analog to digital converters; High resolution; Nonlinear feedback

1. INTRODUCTION

Amplitude comparison of signals is an essential operation in numerous applications, such as front end signal processing, Very Large Scale Integration (VLSI) neural network, quiescent supply current (IDDQ) testing, neuromorphic systems etc., (Banks et al., 2005). The overall performance of these systems depends heavily on comparator, therefore the desired features of comparator is high speed and accuracy and low power dissipation. The current comparator has received considerable attention as many sensors in System on Chip (SoC), such as temperature, Complementary Metal-Oxide Semiconductor (CMOS), Advanced Photo System (APS), etc., provide an output current signal. The current signals can be directly processed by current comparators whereas voltage comparator would require a current to voltage converters and therefore current comparator saves crucial power and area.

The current comparator provides a voltage output using a process which involves injection of two currents and distinguishing whether the difference of two currents is positive or negative. The design of current comparators has to be done keeping the need for low input impedance, quick time response and accuracy in focus. A number of current comparators are available

*Corresponding author's email: veepsa@gmail.com, Tel. +91-11-23869525, Fax. +91-11-23900261
Permalink/DOI: <http://dx.doi.org/10.14716/ijtech.v7i1.2024>

in literature which can broadly be classified on the basis of current sensing mechanism (Toumazou et al., 1990; Freitas & Current, 1993; Traff, 1992; Banks & Toumazou, 2008; Chen et al., 2001; Tang & Toumazou, 1994; Min & Kim, 1998; Ravezzi et al., 1997; Tang & Pun, 2009; Chavoshisani & Hashemipor, 2011). The first generation current comparators are based on sensing input current at a low impedance node followed by a voltage amplification mechanism (Frietas et al., 1993). This technique is known as a resistive input scheme. It has limited resolution and operational frequency. The input current sensing mechanism is capacitive in the second generation current comparators. This technique provides better resolution than that reported in Frietas et al., (1993) due to the larger voltage swing at input node, but it still suffers from low-speed characteristics. A remedy to these limitations was reported by Traff, (1992), where nonlinear feedback is introduced along with capacitive sensing, which lowers the input impedance and provides better speed. Subsequently, many structures based on concept of Traff, (1992) have been reported in various researches, (Banks et al., 2008; Chen et al., 2001; Tang et al., 1994; Min et al., 1998; Ravezzi et al., 1997; Tang et al., 2009; Chavoshisani & Hashemipor, 2011) as an improvement over it. The comparators reported in Chavoshisani and Hashemipor (2011) are also based on capacitive sensing, but employ active elements, such as a current conveyor, second generation (CCII) (Chavoshisani & Hashemipor, 2011) and a differential current conveyor, second generation (DCCII) as reported by Chavoshisani et al., (2011). As these structures accept the difference of input currents, an additional current subtraction circuit is required for complete comparison, which will cause the variation in the reported performance parameters. (Traff, 1992; Banks et al., 2008; Chen et al., 2001; Tang & Toumazou, 1994; Min & Kim, 1998; Ravezzi et al., 1997; Tang & Pun, 2009; Chavoshisani & Hashemipor, 2011). In this paper, a current comparator is proposed that has an inbuilt current differencing circuitry. It uses three stage resistive load amplifiers in the gain stage and a nonlinear feedback to reduce impedance and voltage swing at an input node, which leads to improvement in the speed and resolution of the comparator. A CMOS inverter is used as output stage to provide rail-to-rail swing for lower currents.

The paper is organized as follows: the proposed current comparator architecture along with analytical formulation to quantify the effect of feedback on the current comparator performance is presented. The performance of the theoretical proposition is verified through Pspice simulations using TSMC 0.18 μ m CMOS technology parameters. An application of the proposed current comparator is demonstrated by implementing a three bit current mode flash ADC. The functionality of the same is verified through simulations and performance parameters are calculated. Finally, conclusions are drawn.

2. CURRENT COMPARATOR

A current comparator compares an input current with a reference current and gives an output voltage. The concept of current comparator is reported by Traff, (1992), as shown in Figure 1. The current I_{in} shown in Figure 1 is the difference between input and reference currents. The output (V_{out}) is high when the input current is positive and vice versa. However, in general, a current comparator consists of a current difference stage, a gain stage followed by an output stage as reported by Chavoshisani et al., (2011) and depicted in Figure 2.

The architecture of the proposed comparator is illustrated in Figure 3 in which transistors Mc1-Mc12 form the current differencing stage, which provides output current I_{diff} as the difference of I_{in1} and I_{in2} . The gain stage of the proposed comparator consists of three resistive load amplifier cascaded stages (M1-M4, M2-M5, M3-M6), respectively and a nonlinear feedback (Mpf - Mnf) around the gain stage for performance improvement. The type of nonlinear feedback is of a shunt-shunt type i.e., output voltage is sampled and fed to the input in the form of current. This is achieved by connecting the output node C to the gates of the feedback

transistors (M_{pf}-M_{nf}), while tying their sources to input node B. The output stage (M_{z1}-M_{z2}) provides rail-to-rail swing even under low input current differences.

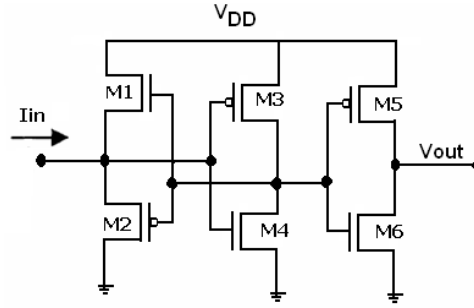


Figure 1 Current comparator concept (Traff, 1992)

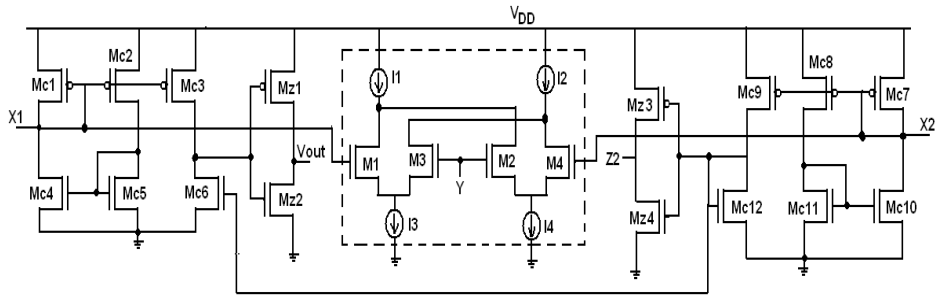


Figure 2 Differential current conveyor based current comparator (Chavoshisani et. al, 2011)

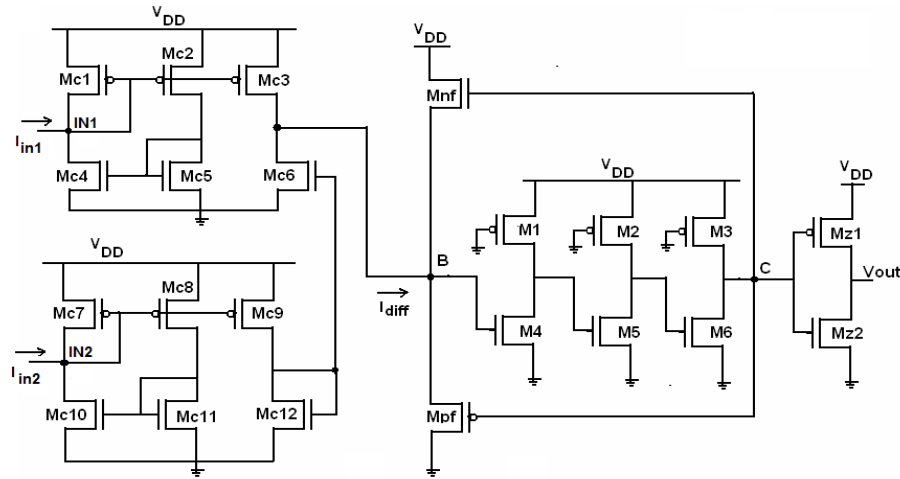


Figure 3 Proposed current comparator

The input impedance R_{in1} and R_{in2} of the terminals IN1 and IN2 are as shown in Equation 1:

$$R_{in1} = \frac{1}{g_{mc1}} \parallel r_{oc1} \parallel r_{oc4}$$

$$R_{in2} = \frac{1}{g_{mc7}} \parallel r_{oc7} \parallel r_{oc10} \quad (1)$$

where g_{mci} and r_{oci} are transconductance and output resistances of transistors M_{ci}.

The overall operation of the nonlinear feedback is explained as follows: For low current

differences the transistors M_{pf} and M_{nf} do not turn ON. Thus the node B impedance is capacitive, which causes slow charging/ discharging of the node voltage to which the gain and the output stages respond. For high positive values of current I_{diff} , node B voltage increases, which results in a reduction in node C voltage, due to inverting nature of the cascaded amplifier stage. The transistor M_{pf} switches ON as its source (node B) and gate (node C) voltages are respectively high and low. Conversely, the high negative values of current I_{diff} cause a decrease in node B voltage and a subsequent increase in node C voltage. This makes M_{nf} ON, due to a low voltage at its source (node B) and a high voltage at its gate (node C). For high values of current I_{diff} the impedance of node B turns resistive. Thus, the circuit responds to a wide range of input difference currents. Further, nonlinear feedback helps in reducing the voltage swing and input impedance at node B, as discussed in the following section.

2.1. Voltage Swing Reduction

An expression for voltage swing is formulated in this subsection. The source voltage of M_{pf} and M_{nf} (node B) for positive and negative input current differences is given respectively as shown in Equations 2 and 3:

$$V_{B+} = \frac{A_{OL}}{1 + A_{OL}} V_Q + \frac{1}{1 + A_{OL}} |V_{TP}| \quad (2)$$

$$V_{B-} = \frac{A_{OL}}{1 + A_{OL}} V_Q - \frac{1}{1 + A_{OL}} V_{TN} \quad (3)$$

where V_Q refers to Q-point voltage of the first amplifier (M1-M4) of the cascaded amplifier stage, V_{TP} , V_{TN} are the threshold voltage of the PMOS and NMOS transistors respectively and A_{OL} represents the overall open loop gain of the cascaded amplifier stages.

It may be noted from Equation 2 and Equation 3 that the voltage swing of the input node B ($V_{B+} - V_{B-}$) is reduced, due to nonlinear feedback. The smaller swing leads to faster charging/discharging of node B and speeds up the response time.

The overall open loop gain of the cascaded amplifier stages is given by Equation 4:

$$A_{OL} = \frac{A_{O1}}{1 + sR_1C_1} \cdot \frac{A_{O2}}{1 + sR_2C_2} \cdot \frac{A_{O3}}{1 + sR_3C_3} \quad (4)$$

where A_{Oi} , R_i and C_i respectively represent low frequency small signal gains, equivalent resistance and capacitance associated with the input node of the i^{th} ($i = 1,2,3$) amplifier stage. The approximate gain A_{Oi} of the i^{th} stage amplifier is product of transconductance of driver (g_{mi}) and resistance of load R_i (Razavi, 2000) and is written as shown in Equation 5:

$$A_{Oi} = -g_{mi} * R_i \quad (5)$$

for $i = 1,2,3$

The equivalent resistances R_1 , R_2 and R_3 are given by Equations 6a, 6b, and 6c:

$$R_1 = r_{o1} \parallel r_{o4} \parallel R_{p1} \quad (6a)$$

$$R_2 = r_{o2} \parallel r_{o5} \parallel R_{p2} \quad (6b)$$

$$R_3 = r_{o3} \parallel r_{o6} \parallel R_{p3} \quad (6c)$$

In Equation 6, r_{oi} represents the output resistance of the transistor M_i . The resistive load resistance of i^{th} stage (R_{pi}) ($i = 1,2,3$) is given by Equation 7:

$$R_{pi} = \frac{1}{\mu_p C_{ox} \left(\frac{W}{L} \right)_{pi} (V_{DD} - |V_{TP}|)} \quad (7)$$

The symbols used in Equation (7) have their usual meaning.

The equivalent capacitances C_1 , C_2 and C_3 are given by Equations 8, 9 and 10:

$$C_1 = \left(1 + \frac{1}{|A_{O1}|}\right) * C_{gd4} + C_{gs5} + C_{gd1} + C_{db1} + (1 + |A_{O2}|) * C_{gd5} \quad (8)$$

$$C_2 = \left(1 + \frac{1}{|A_{O2}|}\right) * C_{gd5} + C_{gs6} + C_{gd2} + C_{db2} + (1 + |A_{O3}|) C_{gd6} \quad (9)$$

$$C_3 = \left(1 + \frac{1}{|A_{O3}|}\right) * C_{gd6} + C_{gs7} + C_{gs2} + C_{gd3} + C_{db3} + (1 + |A_Z|) * (C_{gdZ1} + C_{gdZ2}) \quad (10)$$

where C_{gdi} , C_{gdZ1} , C_{gdZ2} represent gate to drain capacitances associated with transistors M_i , M_{Z1} and M_{Z2} respectively; C_{gsi} denotes gate to source capacitances associated with transistor M_i and A_Z is the gain of output stage inverter.

2.2. Reduction in Input Impedance

In this section analytical formulation for input impedance is developed. Figure 4a shows only one half of the feedback loop, as either Mnf or Mpf will be ON at a time. The corresponding small signal model of the gain stage is shown in Figure 4b where $Z_{in,ol}$ represent open loop input impedance and g_{mnf} , r_{onf} are transconductance and output resistance of transistor Mnf.

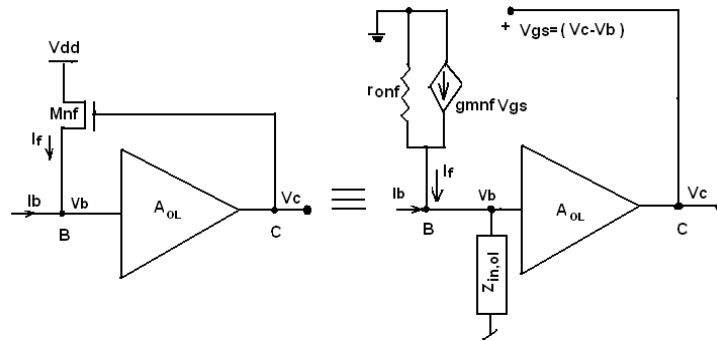


Figure 4 (a) High gain inverter stage with part of non-linear feedback; (b) its equivalent small signal model

$$V_c = [I_b + g_{mnf}(V_c - V_b)](r_{onf} \parallel Z_{in,ol})A_{OL} \quad (11)$$

$$V_c = A_{OL}V_b \quad (12)$$

where

$$Z_{in,ol} = r_{oc} \parallel (sC_{gd4}(1 + |A_{OL}|)) \parallel sC_{gs4} \quad (13)$$

where $|A_{OL}|$ represents magnitude of open loop gain A_{OL} . Solving Equation 11 and Equation 12, the input impedance is obtained as shown in Equations 14 and 15:

$$Z_{in} = \frac{V_b}{I_b} = \frac{r_{onf} \parallel Z_{in,ol}}{1 + g_{mnf}(|A_{OL}| + 1)(r_{onf} \parallel Z_{in,ol})} \quad (14)$$

with approximation $(1 + |A_{OL}|) \approx |A_{OL}|$, Equation 14 reduces as follows in Equation 15:

$$Z_{in} = \frac{V_b}{I_b} = \frac{r_{onf} \parallel Z_{in,ol}}{1 + g_{mnf}(|A_{OL}|)(r_{onf} \parallel Z_{in,ol})} \quad (15)$$

Equation 15 shows that the input impedance at node B decreases due to nonlinear feedback by a factor $|A_{OL}|$ approximately.

3. SIMULATION RESULTS

The theoretical proposition is verified through simulations performed on an Orcad Pspice tool using TSMC CMOS 0.18 μm technology parameters and a supply voltage of 1.8 V. The current I_{in} was applied as input at IN1 in the form of current pulse and reference currents (I_{ref}) was input at IN2 node. The functionality of the current comparator is shown in Figures 5a, 5b and 5c for I_{ref} of 1 μA and I_{in} of ($I_{ref} \pm \Delta I$) where $\Delta I = 50 \text{ nA}$, 500 nA and 1000 nA, respectively. The comparator output exhibits rail-to-rail swing as the output equals the supply voltage for $I_{in} > I_{ref}$ and zero for $I_{in} < I_{ref}$. The proposed circuit functions correctly for a minimum current difference of $\pm 10 \text{ nA}$, so the resolution is $\pm 10 \text{ nA}$.

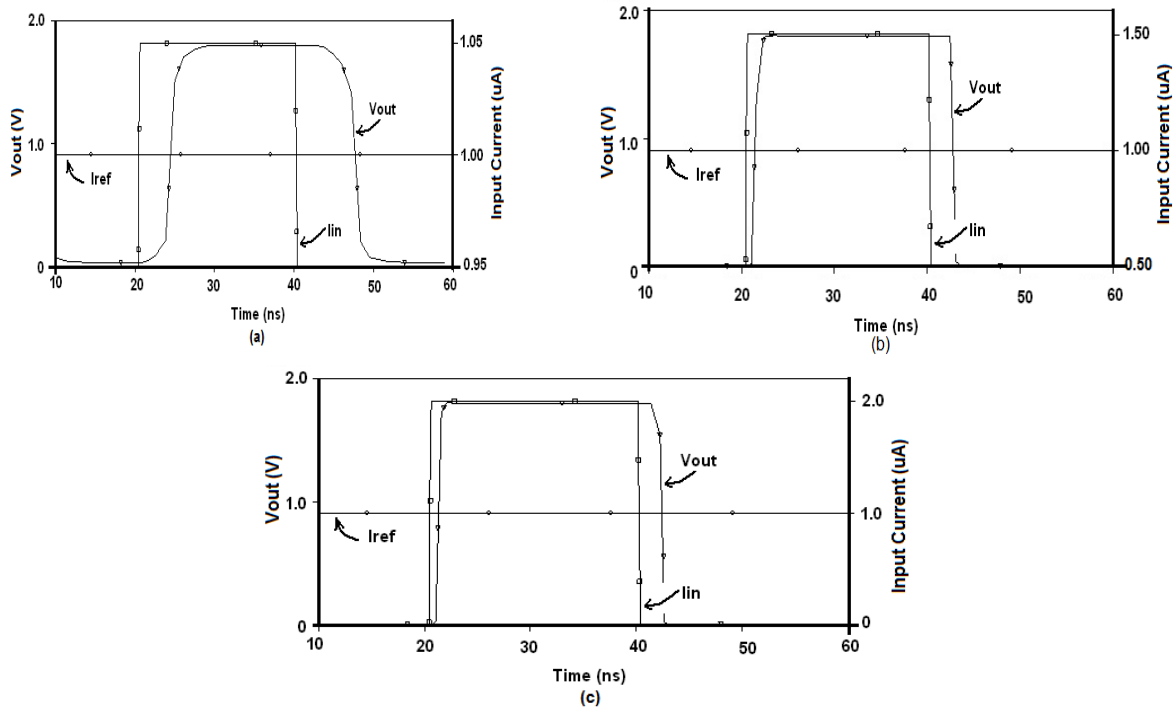


Figure 5 Comparator output for I_{ref} of 1 μA and Input current difference of: (a) $\pm 50 \text{ nA}$; (b) $\pm 500 \text{ nA}$; (c) $\pm 1 \mu\text{A}$

The variation of performance parameters namely delay, power dissipation and Power Delay Product (PDP) with input current differences (I_{in} is varied and reference current (I_{ref}) is kept at 1 μA and is studied through a number of simulation runs. To quantify the effect of nonlinear feedback on the proposed current comparator, the structure of Figure 3 was also simulated without nonlinear feedback (i.e., Mpf - Mnf) under the same simulation conditions.

Figure 6 depicts various plots for performance parameters versus input current differences, specifically variations of input current difference with respect to delay in Figure 6a, power dissipation in Figure 6b and power delay product (PDP) in Figure 6c. Figure 6a illustrates that the propagation delay reduces with increasing current differences due to faster charging/discharging of the node capacitance. It may also be noted that there is significant improvement in the delay due to nonlinear feedback. The power dissipation remains the same

for the proposed comparator with and without feedback and the former circuit gives a better PDP. To study the effect of variation in power supply on the proposed comparator's delay, simulations were carried out at supply voltages of 1 V, 1.2 V, 1.4 V, 1.6 V and 1.8 V, respectively and various current differences. Figure 7 shows the delay as a function of both power supply and the current differences.

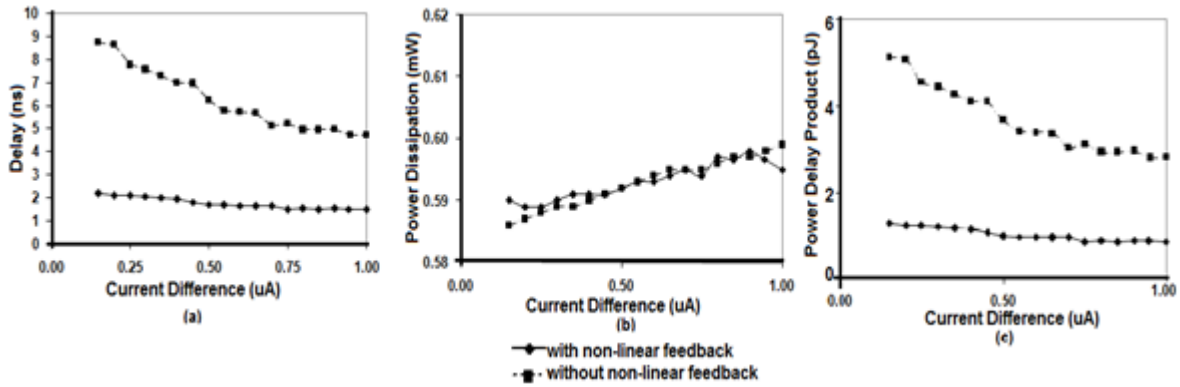


Figure 6 Variation of: (a) delay; (b) power dissipation; and (c) power delay product versus current difference

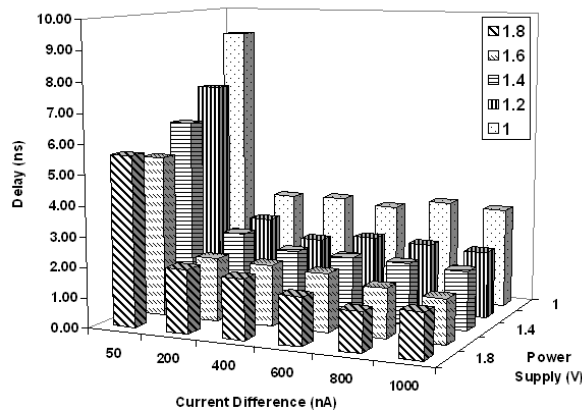


Figure 7 Delay versus variation in power supply and current difference

Process corner analysis was also carried out on the proposed comparator to study its behavior under extreme cases of process mismatch between PMOS and NMOS during manufacturing. The impact of parameter variations on the performance of the proposed comparator at different design corners is also studied and the corresponding results for delay and power dissipation are depicted in Figures 8a and 8b, respectively. In this analysis, three corners exist, namely typical, fast and slow. Slow and Fast corners exhibit carrier mobilities that are higher and lower than normal respectively. Specifically, the corner FS represents both the fast NMOS and the slow PMOS.

For the proposed current comparator, it is observed that the propagation delay is lower at the process corner FF, while the power dissipation is higher than at the process corner TT. Similarly, for process corner SS, a higher propagation delay is observed, while the power dissipation is lower than at the process corner TT.

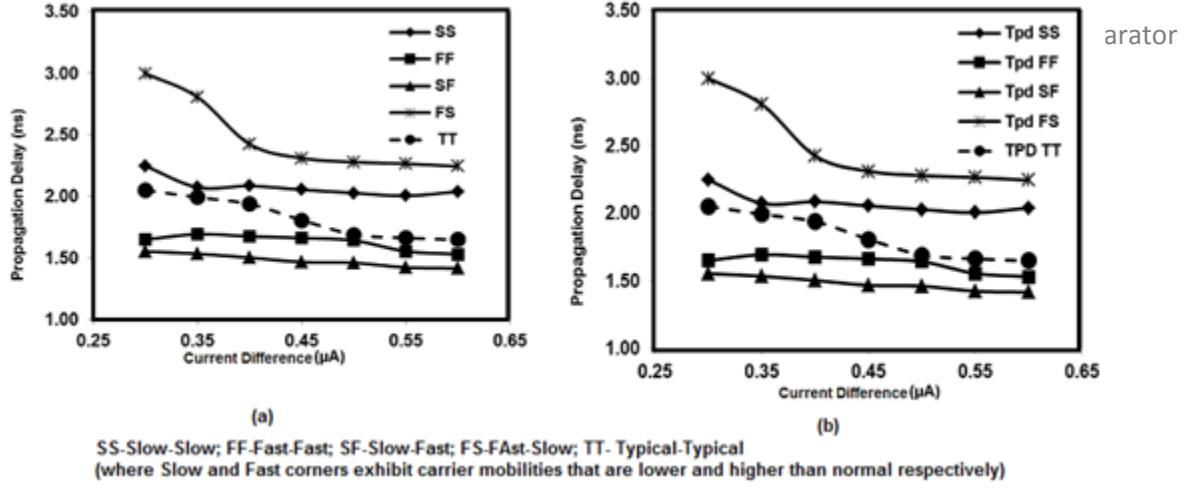


Figure 8 (a) Effect of process corner analysis on propagation delay; (b) Effect of process corner analysis on power dissipation

4. APPLICATION

In this section the proposed comparator is used to implement a 3-bit current mode flash ADC. An N bit current mode flash ADC requires $2^N - 1$ comparators, so seven current comparators are required for the 3-bit flash Analog-to-Digital Converter (ADC). The output of comparators is in the form of the thermometer code, so an encoder is needed to obtain desired binary output. The schematic of the 3-bit flash ADC is shown in Figure 9. The input range of the ADC is taken as 0 to 3.5 μA and seven reference currents $I_{\text{ref}i}$ ($i = 1$ to 7) are chosen as 0.25 μA , 0.75 μA , 1.25 μA , 1.75 μA , 2.25 μA , 2.75 μA and 3.25 μA , respectively. The comparator outputs are C_7 (MSB), C_6 to C_2 and C_1 (LSB). The encoder outputs are B_2 (MSB), B_1 and B_0 (LSB), respectively.

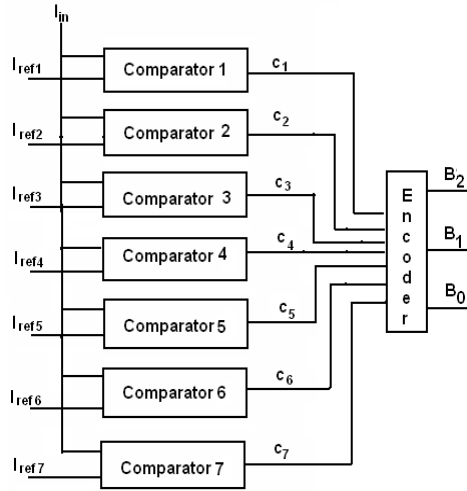


Figure 9 A 3-bit ADC

The relation between comparator and encoder output is:

$$B_0 = C_1 \oplus C_2 \oplus C_3 \oplus C_4 \oplus C_5 \oplus C_6 \oplus C_7 \quad (16)$$

$$B_1 = \overline{C_4} C_2 + C_4 C_6 \quad (17)$$

$$B_2 = C_4 \quad (18)$$

where $\overline{C_4}$ represents the complement of C_4 .

The functionality of the ADC has also been demonstrated by simulations on Pspice. The ADC response is shown in Figure 10 and Figure 11 for ramp and sinusoidal inputs respectively, which confirms the correctness of the comparator behavior. The ADC transfer characteristic of Figure 9 is shown in Figure 12a along with ideal ADC. The Differential Non-Linearity (DNL) is computed to be -0.25 LSB and was plotted as in Figure 12b. It is clear that ADC does not suffer from missing codes. To compute Integral Non-Linearity (INL), the ADC characteristics are redrawn in Figure 13a with the dotted line representing the switching point where code transitions should actually take place. The INL is calculated from Figure 13a and we get maximum INL as -0.19 LSB, as plotted in Figure 13b.

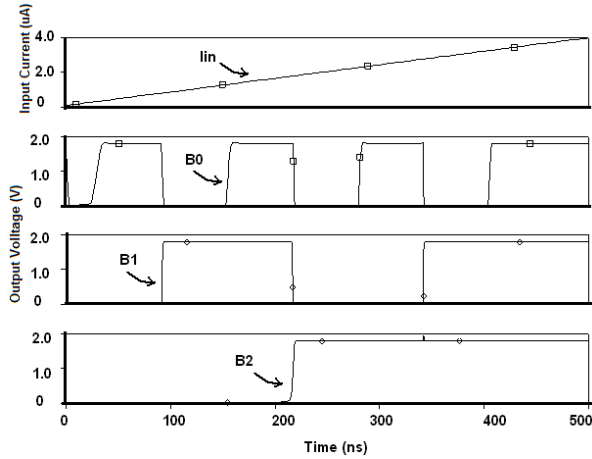


Figure 10 ADC output for ramp input

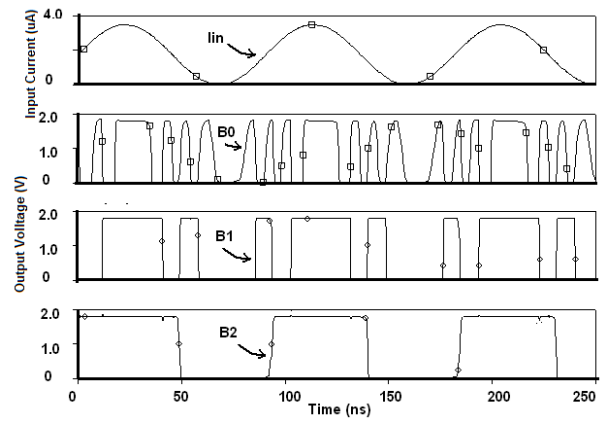
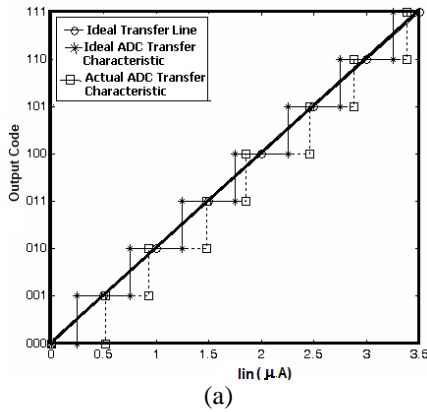
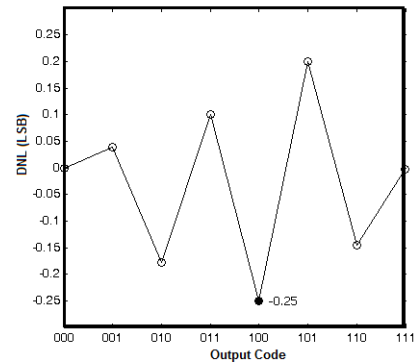


Figure 11 ADC output with sinusoidal input

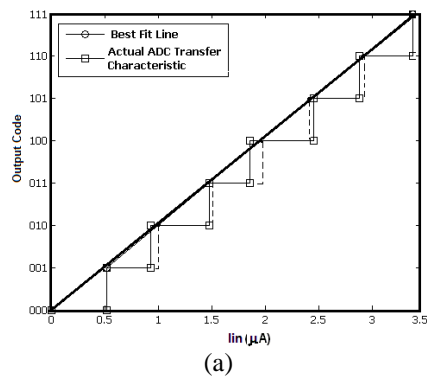


(a)

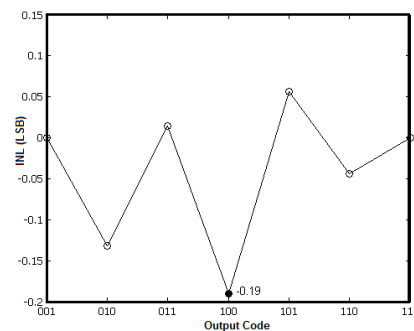


(b)

Figure 12 (a) 3-bit ADC transfer characteristic; (b) DNL versus output code



(a)



(b)

Figure 13 (a) 3-bit ADC transfer characteristic with best fit line; (b) INL versus output code

5. CONCLUSION

In this paper, new current comparator architecture is presented which utilizes nonlinear feedback around the gain stage and shown its application in a 3-bit current mode flash ADC. The analysis of the comparator around the feedback loop shows that the input impedance decreases approximately by a factor of loop gain. The proposed current mode comparator shows ± 10 nA resolution and has a delay of 1.48 ns at reference current of 1 μ A. The 3-bit current mode flash Analog-to-Digital Converter (ADC) shows no missing code and has Differential Non-Linearity (DNL) and Integral Non-Linearity (INL) of -0.25 LSB and -0.19 Least Significant Bit (LSB), respectively.

6. REFERENCES

- Banks, D., Toumazou, C., 2008. Low-power High-speed Current Comparator Design. *Electronics Letters*, Volume 44(3), pp. 171–172
- Banks, D.I., Degenaar, P., Toumazou, C., 2005. A Colour and Intensity Contrast Segmentation Algorithm for Current Mode Pixel Distributed Edge Detection, Euroensors XIX
- Banks, D.I., Degenaar, P., Toumazou, C., 2005. Distributed Current Mode Image Processing Filters. *Electronics Letters*, Volume 41, pp. 1201–1202
- Chavoshisani, R., Hashemipor, O., 2011. A High-speed Current Conveyor Based Current Comparator. *Microelectronics Journal*, Volume 42(1), pp. 28–32
- Chavoshisani, R., Hashemipor, O., 2011. Differential Current Conveyor Based Current Comparator. *Int. J. Electron. Commun. (AEÜ)*, Volume 65(11), pp. 949–953
- Chen, L., Shi, B., Lu, C., 2001. Circuit Design of a High Speed and Low Power CMOS Continuous-time Current Comparator. *Analog Integrated Circuits and Signal Processing*, Volume 28, pp. 293–297
- Freitas, O.A., Current, K.W., 1993. CMOS Current Comparator Circuit. *Electronics Letters*, Volume 19, pp. 695–697
- Min, B.M., Kim, S.W., 1998. High Performance CMOS Current Comparator using Resistive Feedback Network. *Electronics Letters*, Volume 34(22), pp. 2074–2076
- Ravezzi, L., Stoppa, D., Dallabetta, G.F., 1997. Simple High-speed CMOS Current Comparator. *Electronics Letters*, Volume 33, pp. 1829–1830
- Razavi, B., 2000. *Analog Integrated Circuit*, Tata McGraw Hill Publications
- Tang, A.T.K., Toumazou, C., 1994. High PCMOS Current Comparator. *Electronics Letters*, Volume 30(1), pp. 5–6
- Tang, X., Pun, K.P., 2009. High Performance CMOS Current Comparator. *Electronics Letters*, Volume 45(20), pp. 1007–1009
- Toumazou, C., Lidgey, F.J., Haigh, D.G., 1990. *Analogue IC Design: The Current-mode Approach*, Peter Peregrinus Ltd
- Traff, H., 1992. Novel Approach to High Speed CMOS Current Comparators. *Electronics Letters*, Volume 28(3), pp. 310–312